研究集会報告 18特1-1

移動境界まわりの強非線形流れ解析

九州大学応用力学研究所

2007年3月

Reports of RIAM Symposium
No. 18 特 1 - 1

Analyses of Strongly Nonlinear Flows around Moving Boundaries

Proceedings of the Symposium held at Research Institute for Applied Mechanics,
Kyushu University, Kasuga, Fukuoka, Japan, December 7-8, 2006

Research Institute for Applied Mechanics
Kyushu University
March, 2007

移動境界まわりの強非線形流れ解析
研究集会報告集

２００６（平成１８）年１２月７日～１２月８日
研究代表者　　青木尊之（東京工業大学学術国際情報センター）

目　　次

Intl. RIAM Symposium 2006

Fluid Simulation by Using Multi-Moment Scheme and Conservative Formulation

Takayuki Aoki

Global Scientific Information and Computing Center, Tokyo Institute of Technology

Contents

- Multi-moment Schemes
  - CIP Scheme
  - IDO Scheme
    - Staggered Grid
    - Collocated Grid + Stable Coupling
- CFD Applications
  - Compressible Flow
  - Incompressible Flow (Free Surface Flow)
- Conservative Formulation of IDO Scheme
  - Recent results
- DEM Applications

CIP Scheme

- Fractional step method

$$\frac{\partial f}{\partial t}+u\frac{\partial f}{\partial x}=g \;\Rightarrow\; \begin{cases} \dfrac{\partial f}{\partial t}+u\dfrac{\partial f}{\partial x}=0 \\ + \\ \dfrac{\partial f}{\partial t}=g \end{cases}$$

Advection Phase : CIP Scheme ($f^n \to f^*$)

Non-advection Phase : Finite Difference ($f^* \to f^{n+1}$)

CIP Scheme for advection phase

$$\frac{\partial f}{\partial t}+u\frac{\partial f}{\partial x}=0$$

Semi-Lagrangian Procedure

Using local analytic solution,

$$f(x,t)=f(x-u\Delta t,t-\Delta t)$$

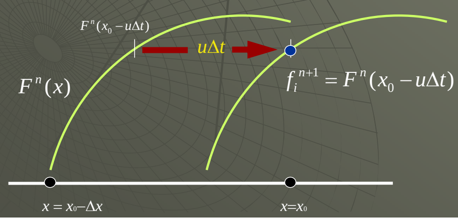

Interpolation by Multi-moment

Upwind Interpolation $u_i>0$

$$F(x)=a(x-x_i)^3+b(x-x_i)^2+f_{x,i}(x-x_i)+f_i$$

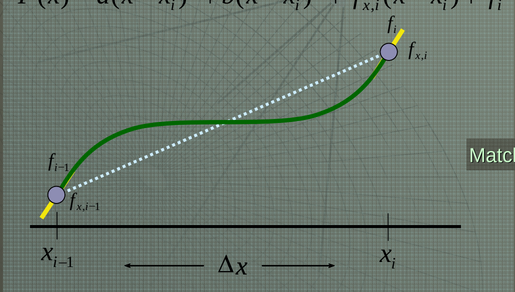

Matching Condition :

$F(x_{i-1})=f_{i-1}$

$F_x(x_{i-1})=f_{x,i-1}$

$$a=\frac{1}{\Delta x^2}(f_{x,i}+f_{x,i-1})-\frac{2}{\Delta x}(f_i-f_{i-1}),\quad b=\frac{1}{\Delta x}(2f_{x,i}+f_{x,i-1})-\frac{3}{\Delta x^2}(f_i-f_{i-1})$$

IDO Scheme Interpolated Differential Operator

T. Aoki: Comp. Phys. Comm., 102(1-3) 132-146 (1997)

Interpolation f_i f_{i+1}

$$F(x)=a_nx^n+a_{n-1}x^{n-1}+\cdots+a_1x+a_0$$

An approximate solution

Differentiation

$$\frac{\partial f}{\partial x}=F'(x)\neq\cancel{\frac{f_{i+1}-f_i}{\Delta x}} \qquad \frac{\partial^2 f}{\partial x^2}=F''(x)\neq\cancel{\frac{f_{i+1}-2f_i+f_{i-1}}{\Delta x^2}}$$

Operation

$$\frac{\partial f}{\partial t}=\Im\left(\frac{\partial f}{\partial x},\frac{\partial^2 f}{\partial x^2},\frac{\partial^3 f}{\partial x^3},\cdots\right),\quad \frac{\partial^2 f}{\partial t^2}=\Im^2 f,\quad \frac{\partial^3 f}{\partial t^3}=\Im^3 f$$

Hermite Interpolation

Center Interpolation

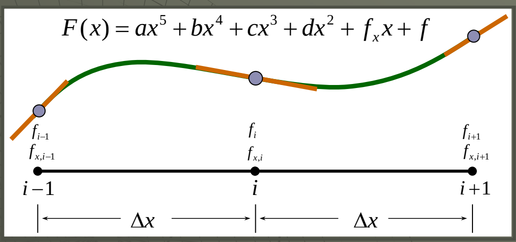

$$a = -\frac{3}{4\Delta x^5}(f_{i+1} - f_{i-1}) + \frac{1}{4\Delta x^4}(f'_{i+1} + 4f'_i + f'_{i-1}) \qquad c = \frac{5}{4\Delta x^3}(f'_{i+1} - f'_{i-1}) - \frac{1}{4\Delta x^2}(f_{i+1} + 8f_i + f_{i-1})$$

$$b = -\frac{1}{2\Delta x^4}(f_{i+1} - 2f_i + f_{i-1}) + \frac{1}{4\Delta x^3}(f'_{i+1} - f'_{i-1}) \qquad d = \frac{1}{\Delta x^2}(f_{i+1} - 2f_i + f_{i-1}) - \frac{1}{4\Delta x}(f'_{i+1} - f'_{i-1})$$

Matching Condition : $F(\Delta x) = f_{i+1}$ $\quad F'(\Delta x) = f'_{i+1}$ $\quad F(-\Delta x) = f_{i-1}$ $\quad F'(-\Delta x) = f'_{i-1}$

Time Integration

$$f(t^n + \Delta t) = f(t^n) + \Delta t \cdot \left.\frac{\partial f}{\partial t}\right|^n + \frac{1}{2}\Delta t^2 \cdot \left.\frac{\partial^2 f}{\partial t^2}\right|^n + \frac{1}{6}\Delta t^3 \cdot \left.\frac{\partial^3 f}{\partial t^3}\right|^n + O(\Delta t^4)$$

$$f_x(t^n + \Delta t) = f_x(t^n) + \Delta t \cdot \left.\frac{\partial f_x}{\partial t}\right|^n + \frac{1}{2}\Delta t^2 \cdot \left.\frac{\partial^2 f_x}{\partial t^2}\right|^n + O(\Delta t^3)$$

By replacing,

$$\frac{\partial f}{\partial t} = \Im\left(\frac{\partial f}{\partial x}, \frac{\partial^2 f}{\partial x^2}, \frac{\partial^3 f}{\partial x^3}, \cdots\right), \quad \frac{\partial^2 f}{\partial t^2} = \Im^2 f, \quad \frac{\partial^3 f}{\partial t^3} = \Im^3 f$$

By differential operation,

$$\frac{\partial f}{\partial x} \to F'(x) \qquad \frac{\partial^2 f}{\partial x^2} \to F''(x)$$

1D Linear Advection Equation

$$\frac{\partial f}{\partial t} + u\frac{\partial f}{\partial x} = 0$$

$$f_t = -uf_x \quad f_{tt} = u^2 f_{xx} \quad f_{ttt} = -u^3 f_{xxx}$$

$$f_{tx} = -uf_{xx} \quad f_{ttx} = u^2 f_{xxx}$$

Taylor expansion

$$\begin{aligned} f^{n+1} &= f^n - u\Delta t \cdot f^n{}_x + \frac{(u\Delta t)^2}{2} f^n{}_{xx} - \frac{(u\Delta t)^3}{6} f^n{}_{xxx} \\ &= f^n - u\Delta t \cdot f^n{}_x + \frac{(u\Delta t)^2}{2} F_{xx}(0) - \frac{(u\Delta t)^3}{6} F_{xxx}(0) \\ &= f^n - u\Delta t \cdot f^n{}_x + \frac{(u\Delta t)^2}{2} 2b - \frac{(u\Delta t)^3}{6} 6a \\ &= F(-u\Delta t) \end{aligned}$$

$$\begin{aligned} f_x^{n+1} &= f_x^n - u\Delta t \cdot f^n{}_{xx} + \frac{(u\Delta t)^2}{2} f^n{}_{xxx} \\ &= f_x^n - u\Delta t \cdot 2b + (u\Delta t)^2 3a \\ &= F_x(-u\Delta t) \end{aligned}$$

Fourier Series

$$f(x) = \sum_k \hat{f}(k) e^{iwx/h}$$

$$f_x(x) = \sum_k \hat{f}_x(k) e^{iwx/h}$$

$h = L/N$: grid spacing

$w = 2\pi kh/L$: scaled wavelength

Fourier Analysis for Time-evolution equation

$$\mathbf{F}_n = \mathbf{S}^n \mathbf{F}_0 \quad \Rightarrow \quad g_n(w) = |g_n(w)| e^{i\alpha_n(w)} = \frac{\hat{f}^n(k)}{\hat{f}^0(k)}$$

$|g_n(w)|$ **: Gain** $\qquad \alpha_n(w)$ **: Phase**

Fourier Analysis

for Advection Equation

Y. Imai, and T. Aoki,
J. Comp. Phys, Vol.217, pp.453-472 (2006)

$$\frac{\partial f}{\partial t} + u\frac{\partial f}{\partial x} = 0$$

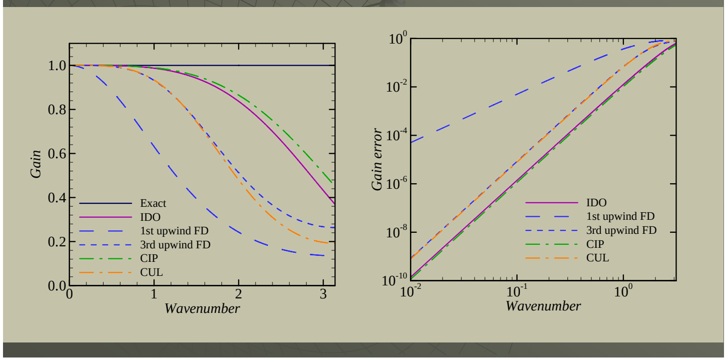

IDO Scheme on Staggered Grid

- Advection term is accurate and stable.
- Non-ddvection term ?

$$\frac{\partial \rho}{\partial t} + u\frac{\partial \rho}{\partial x} = -\rho\boxed{\frac{\partial u}{\partial x}} \qquad \frac{\partial u}{\partial t} + u\frac{\partial u}{\partial x} = -C_S^2\boxed{\frac{\partial \rho}{\partial x}}$$

- Simple Finite Difference with 2nd order

$$\left.\frac{\partial u}{\partial x}\right|_{i+1/2} = F_x(\Delta x/2) = \frac{u_{i+1} - u_i}{\Delta x}$$

$$\left.\frac{\partial \rho}{\partial x}\right|_i = F_x(\Delta x/2) = \frac{\rho_{i+1/2} - \rho_{i-1/2}}{\Delta x}$$

IDO Scheme on Collocated Grid

$$\frac{\partial \rho}{\partial t} + \cdots = -\rho \frac{\partial u}{\partial x} \qquad \frac{\partial u}{\partial t} + \cdots = -C_S^2 \frac{\partial \rho}{\partial x}$$

$$\frac{\partial \rho_x}{\partial t} + \cdots = -\rho \frac{\partial^2 u}{\partial x^2} \qquad \frac{\partial u_x}{\partial t} + \cdots = -C_S^2 \frac{\partial^2 \rho}{\partial x^2}$$

ρ_{i-1}, u_{i-1} $\qquad$ ρ_i, u_i $\qquad$ ρ_{i+1}, u_{i+1}

$$\left.\frac{\partial \rho}{\partial t}\right|_i + \cdots = -\rho_i \boxed{u_{x,i}} \qquad \left.\frac{\partial \rho_x}{\partial t}\right|_i + \cdots = -\rho_i u_{xx,i} = -\rho_i U_{xx}(x_i)$$

$$\left.\frac{\partial u}{\partial t}\right|_i + \cdots = -C_S^2 \boxed{\rho_{x,i}} \qquad \left.\frac{\partial u_x}{\partial t}\right|_i + \cdots = -C_S^2 \rho_{xx,i} = -C_S^2 F_{xx}(x_i)$$

- Poor coupling → Sometimes, unstable

Stable Coupling
on Collocated Grid

Y. Imai, and T. Aoki,
J. Comput. Phys., Vol.215, pp.81-97 (2006)

$$\left.\frac{\partial u}{\partial x}\right|_i = \frac{1}{3} u_{x,i} + \frac{2}{3} F_x(\Delta x)$$

$$= \frac{1}{3} u_{x,i} + \frac{2}{3}\left(\frac{3}{4} \frac{u_{i+1} - u_{i-1}}{\Delta x} + \frac{1}{4} \frac{u_{x,i+1} + u_{x,i-1}}{\Delta x^2} \right)$$

$u_{x,i-1}$, u_{i-1} $\qquad$ u_i $\qquad$ $u_{x,i+1}$, u_{i+1}

- Stable and 4-th Order Accuracy

2D Driven Cavity Flow

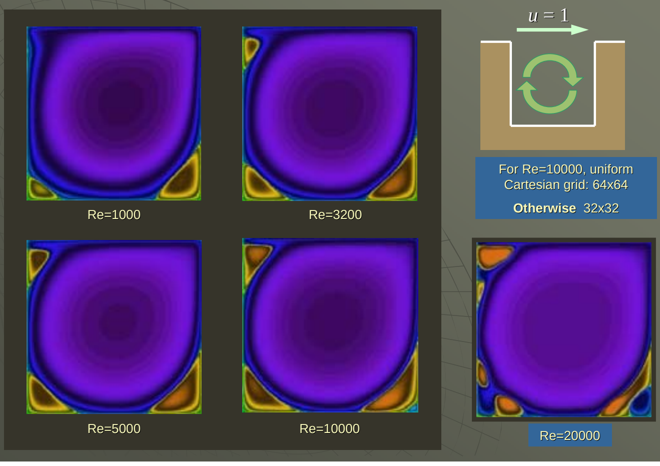

IDO-SC

Y. Imai, and T. Aoki,
J. Comput. Phys., Vol.215, pp.81-97 (2006)

Steady State of Cavity flow（Re = 3200: 40×40 mesh）

Normal IDO → IDO-SC

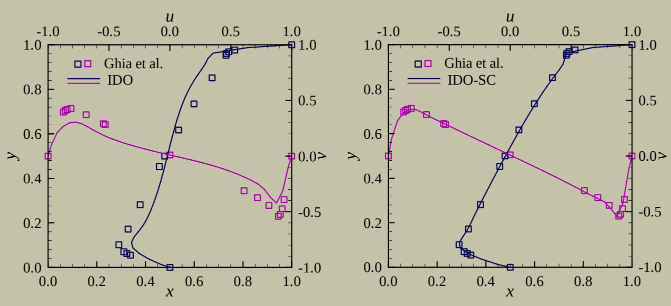

IMPORTANCE of Safety Analysis for High Explosives

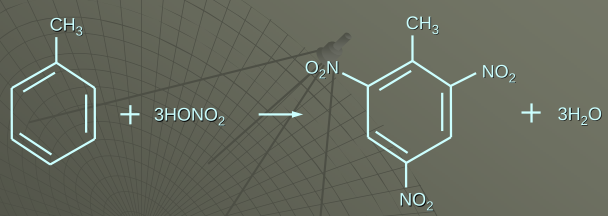

1kg-TNT explosion : 3.22 MJ
30kg-TNT explosion : 100 MJ

Dangerous and difficult experiment → Numerical Simulation

TNT Explosion

IGNITION	DETONATION	EXPANSION	SHOCK WAVE
Large Energy Release		No Energy Release	
		Blast Wave	
Drastic Pressure Change		Drastic Pressure Change	
Solid Density		Drastic Density Change	

Basic Equations of the blast wave

Compressible Fluid Equations

Continuity Equation $$\frac{\partial \rho}{\partial t} + \mathbf{u}\cdot\nabla\rho = -\rho\nabla\mathbf{u}$$

Momentum Equation $$\frac{\partial \mathbf{u}}{\partial t} + \mathbf{u}\cdot\nabla\mathbf{u} = -\frac{1}{\rho}\nabla p$$

Energy Equation $$\frac{\partial e}{\partial t} + \mathbf{u}\cdot\nabla e = -\frac{p}{\rho}\nabla\mathbf{u}$$

Equation of State $$p = p(e,\rho)$$

Density : ρ Velocity : u
Internal Energy : e Pressure : p

Rational function CIP

Monotone Interpolation Xiao, et al.: Comp. Phys. Comm., 94(2-3) 103-118 (1996)

$$F(x) = \frac{a(x-x_i)^3 + b(x-x_i)^2 + c(x-x_i) + d}{1+\alpha B(x-x_i)}$$

CIP → RCIP

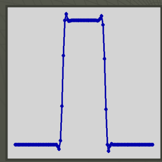

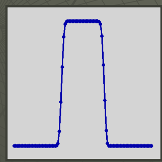

$$a = [g_i - S + (g_{i+1} - S)(1+\alpha B\Delta x)]/\Delta x^2$$
$$b = S\alpha B + (S - g_i)/\Delta x - a\Delta x$$
$$c = g_i + f_i \alpha B$$
$$d = f_i$$

$$B = [|(S-g_i)/(g_{i+1}-S)| - 1]/\Delta x$$
$$S = (f_{i+1} - f_i)/\Delta x$$

Shock Tube Problem with Extremely Large Density and Pressure Jump

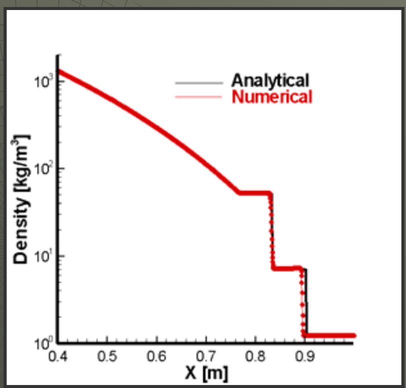

100g-Pentolite Explosion on the Table

2D Cylindrical Simulation

X4 magnify at the center

100g-TNT on the table

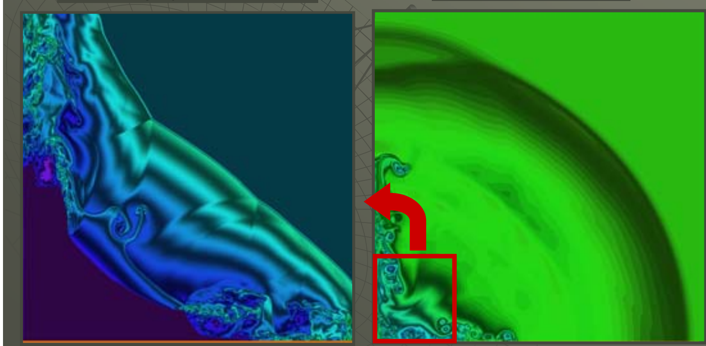

INCOMPRESSIBLE FLUID

$$\nabla\cdot\boldsymbol{u} = 0$$
$$\frac{\partial \boldsymbol{u}}{\partial t} + (\boldsymbol{u}\cdot\nabla)\boldsymbol{u} = -\nabla p + \frac{1}{\mathrm{Re}}\Delta\boldsymbol{u}$$

SMAC Algorithms

Burgers Equation

$$\frac{\partial \boldsymbol{u}}{\partial t} = -(\boldsymbol{u}\cdot\nabla)\boldsymbol{u} + \frac{1}{Re}\nabla^2\boldsymbol{u} \qquad \boldsymbol{u}^n \to \boldsymbol{u}^*$$

Poisson Equation $$\Delta p = \frac{\nabla\cdot\boldsymbol{u}^*}{\Delta t} \qquad \boldsymbol{u}^{n+1} = \boldsymbol{u}^* - \Delta t\cdot\nabla p$$

POISSION EQUATIION

$$\Delta\phi = \rho$$ ρ : given source term

1-dimensional case

- 2nd Order Center Difference Method

$$\phi_{xx} = \rho \Rightarrow (\phi_{i+1} - 2\phi_i + \phi_{i-1})/\Delta x^2 = \rho_i$$

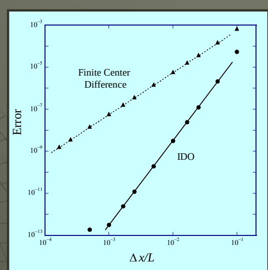

- IDO Scheme

$$\phi_{xx} = \rho \Rightarrow \frac{2}{\Delta x^2}(\phi_{i+1} - 2\phi_i + \phi_{i-1}) - \frac{1}{2\Delta x}(\phi_{x,i+1} - \phi_{x,i-1}) = \rho_i$$

$$\phi_{xxx} = \rho_x \Rightarrow \frac{15}{2\Delta x^3}(\phi_{i+1} - \phi_{i-1}) - \frac{3}{2\Delta x^2}(\phi_{x,i+1} + 8\phi_{x,i} + \phi_{x,i-1}) = \rho_{x,i}$$

Simulation for Falling Leaves

Major difficulties:
- Fluid-structure interaction
- Complex shape of leaves
- Very thin structure

Shape of the leaf :
modeled by
Geometry data
200 polygons
DXF or STL CAD format

Computational Mother Domain: 50x50x80
Computational Sub-Domain: 40x40x30

INTERGRID Method (CUT CELL)

Cartesian Grid with InterGrid

- High Accuracy and Low computation
- Special treatment for only cut-cells describing the boundary
- Suitable for physical discontinuity, i.e. multi-phase flow or extreme density jump
- Escape from BFC difficulty
- Geometry data compatibility

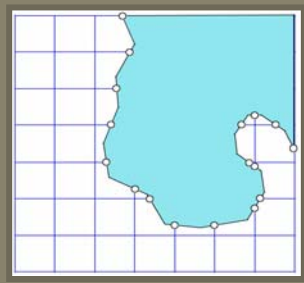

Thin Body Treatment

Two values at the same position, representing the front and the rear surface pressure.

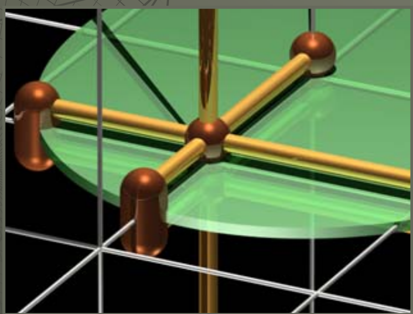

Overset Grid

Sub-domain (fine Grid)

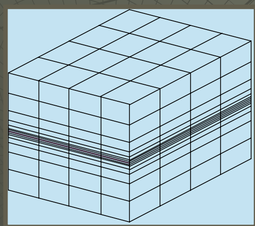

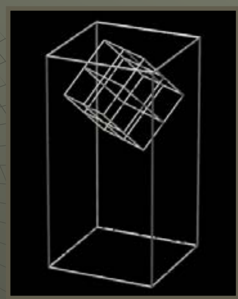

Cubic Interpolation
Mother-domain ⟷ Sub-domain

Bubbly Flow Simulation

- Channel Width (H) 10 mm
- Channel Length (L) 250 mm
- Mesh Size : 0.25 mm
- Mesh Number : 40 × 40 × 1000
- Equal grid spacing
- Incoming Flow Velocity : 0.5 m/sec
- Wall Boundary condition: non-slip
- Periodic in the gravity direction
- Room Temperature
- No thermal process
- Initial Condition
  - －Average Void Ratio : 0.1
  - －Diameter of bubble : 2 mm
  - －Number of bubbles : 594
  - (=66 stages X 9)

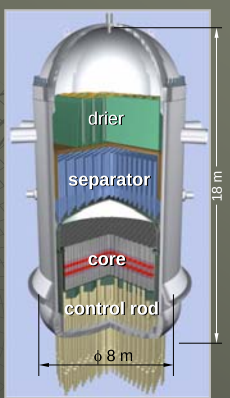

BWR

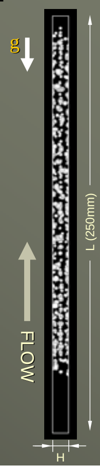

Computational Methods

- Gas – Liquid Unified Solver : CIP (CCUP) method
- 3-dimentional Compressible / Incompressible fluid
- Surface Tension : CFS model
- Contact angle between wall and bubbles
- Surface tracking method : improved VOF method

$$\frac{\partial \rho_l \phi_l}{\partial t} + \nabla \cdot (\rho_l \phi_l \boldsymbol{u}) = 0$$

$$\frac{\partial \rho_g \phi_g}{\partial t} + \nabla \cdot (\rho_g \phi_g \boldsymbol{u}) = 0$$

$$\rho = \rho_l \phi_l + \rho_g \phi_g \qquad \phi_l + \phi_g = 1$$

$$\frac{Du_i}{Dt} = -\frac{1}{\rho}\frac{\partial p}{\partial x_i} + \frac{1}{\rho}\frac{\partial \tau_{ij}}{\partial x_j} + g_i + \sigma_i$$

$$\frac{De}{Dt} = -\frac{p}{\rho}\frac{\partial u_i}{\partial x_i} + \frac{1}{\rho}\frac{\partial}{\partial x_i}\left(\lambda \frac{\partial T}{\partial x_i}\right) + q$$

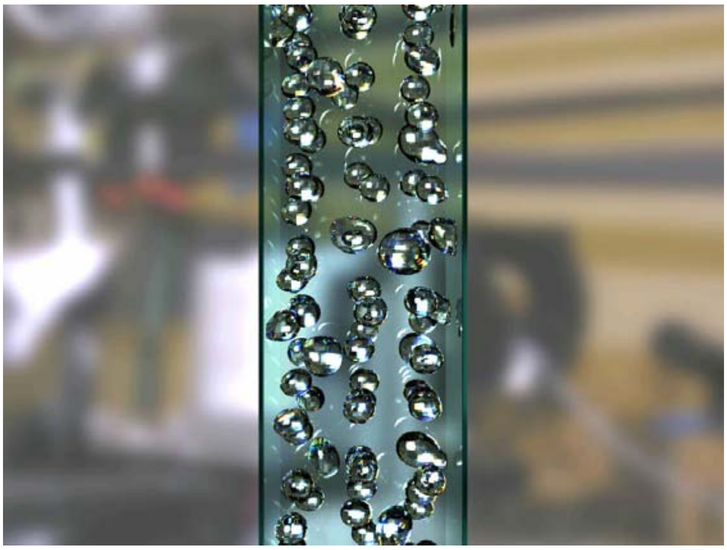

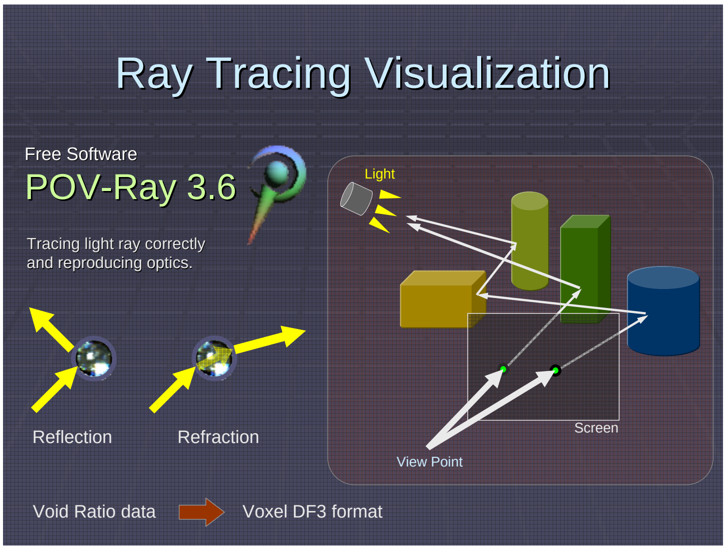

Mass Conservation with non-uniform velocity

Benchmark Test

$$\frac{\partial f}{\partial t}+u\frac{\partial f}{\partial x}+f\frac{\partial u}{\partial x}=0$$

$$u(x)=\frac{1}{1+\alpha\sin k_x x},\quad \alpha=0.5,\quad k_x=2\pi$$

- Initial Profile: $0\le x\le 1$
  $f=1 \quad for \quad 0.4\le x\le 0.6, \qquad f=0 \quad elsewhere$
- Periodic Boundary Condition
- N = 100 $(\Delta x=0.01)$
- CFL = 0.2 $\Delta t=CFL\times\Delta x=0.002$

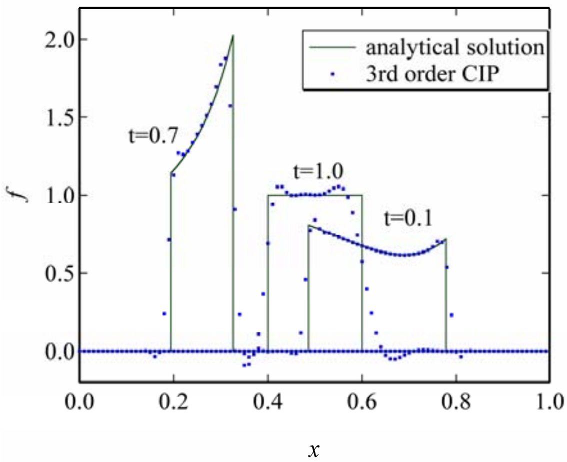

Dependent Variables for Conservative IDO

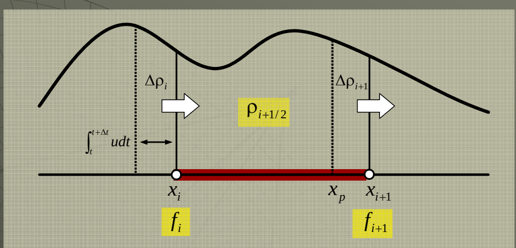

$$F(x)=a(x-x_i)^2+b(x-x_i)+f_i$$

$$a=\frac{3f_{i+1}+3f_j}{\Delta x^2}-\frac{6\rho_{i+1/2}}{\Delta x^3},\qquad b=\frac{6\rho_{i+1/2}}{\Delta x^2}-\frac{2f_{i+1}+4f_i}{\Delta x}$$

$$f_{x,i}=\frac{6\rho_{i+1/2}}{\Delta x^2}-\frac{2f_{i+1}+4f_i}{\Delta x}$$

$F(x_i)=f_i \qquad F(x_i+\Delta x)=f_{i+1}$

$\int_{x_i}^{x_i+\Delta x}F(x)dx=\rho_{i+1/2}$

Conservative Formulation

Mass continuum Eq. $\dfrac{\partial f}{\partial t}+\dfrac{\partial uf}{\partial x}=0$

Non-conservative

$$\frac{\partial f_i}{\partial t}=-uf_{x,i}-u_x f_i$$

$$\frac{\partial f_{x,i}}{\partial t}=-uf_{xx,i}-2u_x f_{x,i}-u_{xx}f_i$$

Conservative

$$\frac{\partial f_i}{\partial t}=-uf_{x,i}-u_x f_i$$

$$\frac{\partial \rho_{i+1/2}}{\partial t}=-uf_{i+1}+uf_i$$

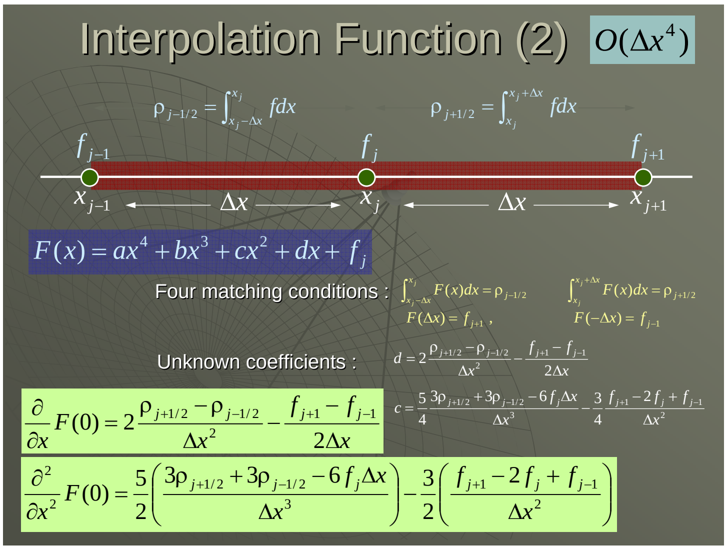
Interpolation Function (2)
$O(\Delta x^4)$
$\rho_{j-1/2} = \int_{x_j-\Delta x}^{x_j} f dx$
$\rho_{j+1/2} = \int_{x_j}^{x_j+\Delta x} f dx$
f_{j-1} f_j f_{j+1}
x_{j-1} Δx x_j Δx x_{j+1}
$F(x) = ax^4 + bx^3 + cx^2 + dx + f_j$
Four matching conditions : $\int_{x_j-\Delta x}^{x_j} F(x)dx = \rho_{j-1/2}$ $\int_{x_j}^{x_j+\Delta x} F(x)dx = \rho_{j+1/2}$
$F(\Delta x) = f_{j+1}$, $F(-\Delta x) = f_{j-1}$
Unknown coefficients : $d = 2\frac{\rho_{j+1/2} - \rho_{j-1/2}}{\Delta x^2} - \frac{f_{j+1} - f_{j-1}}{2\Delta x}$
$c = \frac{5}{4}\frac{3\rho_{j+1/2} + 3\rho_{j-1/2} - 6 f_j \Delta x}{\Delta x^3} - \frac{3}{4}\frac{f_{j+1} - 2 f_j + f_{j-1}}{\Delta x^2}$
$\frac{\partial}{\partial x}F(0) = 2\frac{\rho_{j+1/2} - \rho_{j-1/2}}{\Delta x^2} - \frac{f_{j+1} - f_{j-1}}{2\Delta x}$
$\frac{\partial^2}{\partial x^2}F(0) = \frac{5}{2}\left(\frac{3\rho_{j+1/2} + 3\rho_{j-1/2} - 6 f_j \Delta x}{\Delta x^3}\right) - \frac{3}{2}\left(\frac{f_{j+1} - 2 f_j + f_{j-1}}{\Delta x^2}\right)$

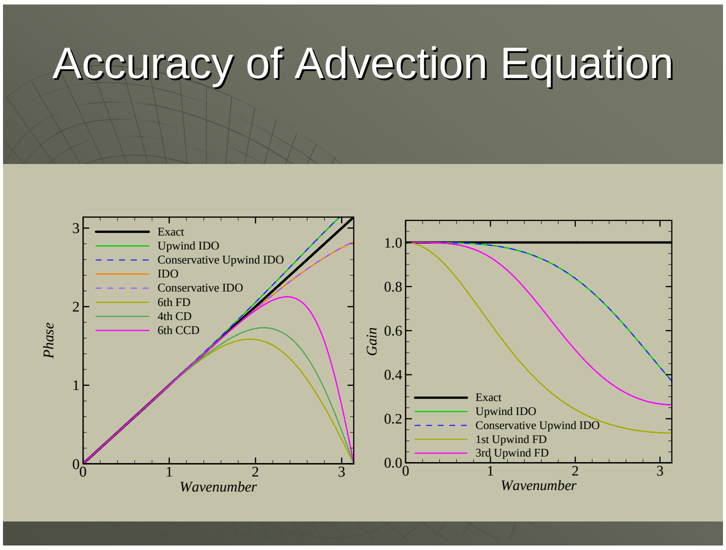
Accuracy of Advection Equation
Exact
Upwind IDO
Conservative Upwind IDO
IDO
Conservative IDO
6th FD
4th CD
6th CCD
Phase
Wavenumber
Exact
Upwind IDO
Conservative Upwind IDO
1st Upwind FD
3rd Upwind FD
Gain
Wavenumber

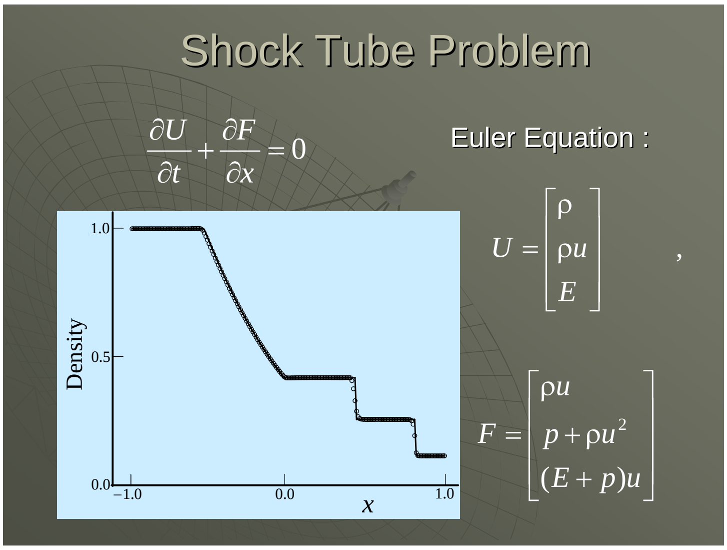
Shock Tube Problem
$\frac{\partial U}{\partial t} + \frac{\partial F}{\partial x} = 0$
Euler Equation :
$U = \begin{bmatrix} \rho \\ \rho u \\ E \end{bmatrix}$,
$F = \begin{bmatrix} \rho u \\ p + \rho u^2 \\ (E+p)u \end{bmatrix}$
Density
x

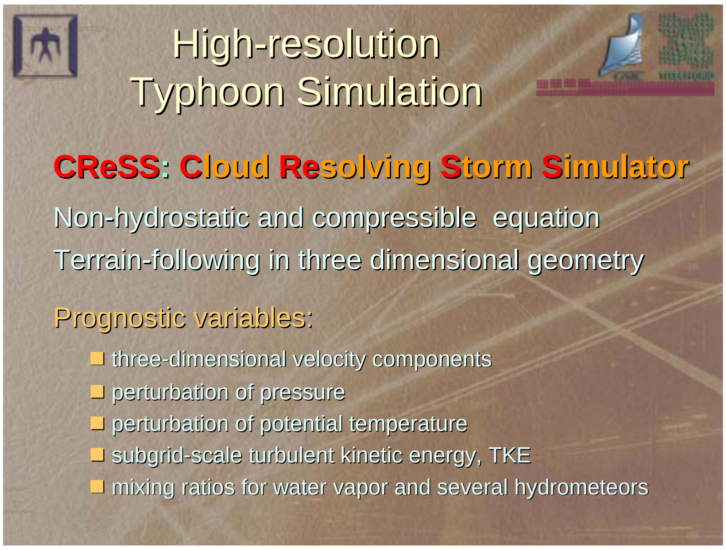
High-resolution
Typhoon Simulation
CReSS: Cloud Resolving Storm Simulator
Non-hydrostatic and compressible equation
Terrain-following in three dimensional geometry
Prognostic variables:
three-dimensional velocity components
perturbation of pressure
perturbation of potential temperature
subgrid-scale turbulent kinetic energy, TKE
mixing ratios for water vapor and several hydrometeors

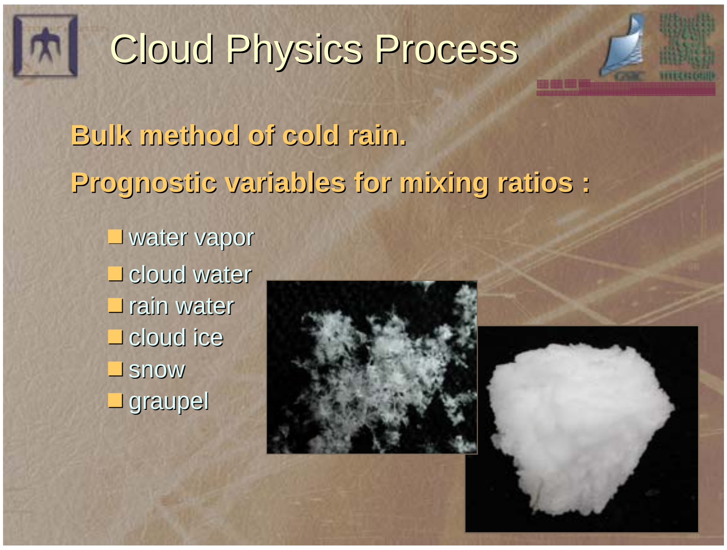
Cloud Physics Process
Bulk method of cold rain.
Prognostic variables for mixing ratios :
water vapor
cloud water
rain water
cloud ice
snow
graupel

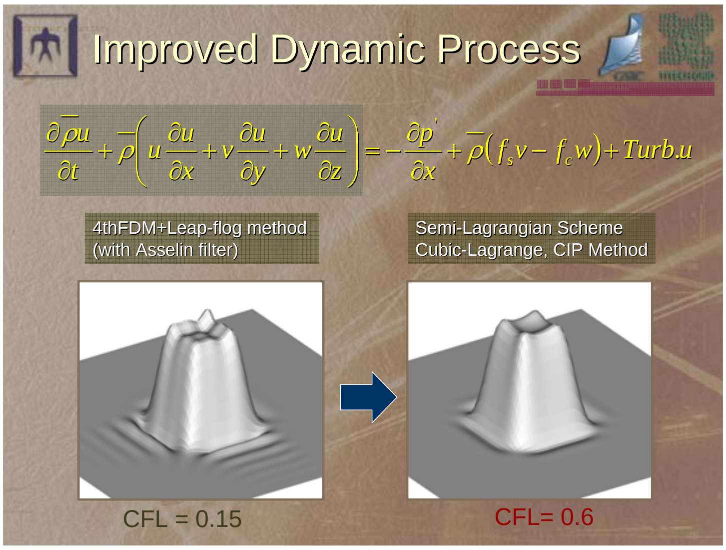
Improved Dynamic Process
$\frac{\partial \bar{\rho} u}{\partial t} + \bar{\rho}\left(u\frac{\partial u}{\partial x} + v\frac{\partial u}{\partial y} + w\frac{\partial u}{\partial z}\right) = -\frac{\partial p'}{\partial x} + \bar{\rho}(f_s v - f_c w) + Turb.u$
4thFDM+Leap-flog method
(with Asselin filter)
Semi-Lagrangian Scheme
Cubic-Lagrange, CIP Method
CFL = 0.15
CFL= 0.6

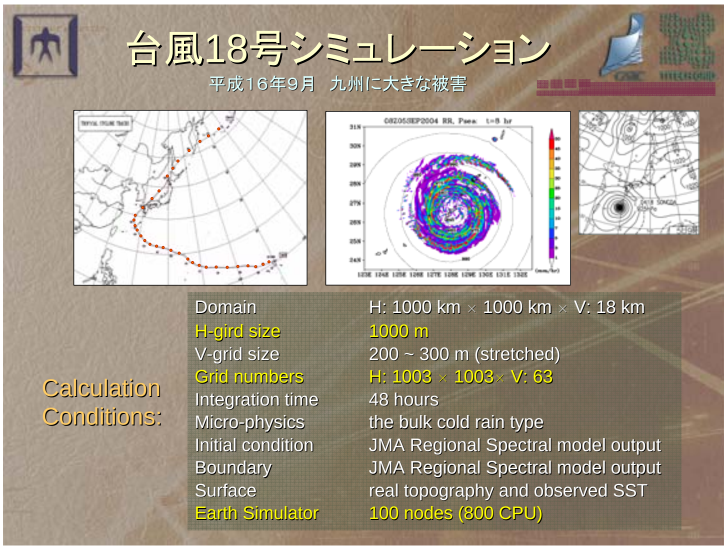

台風18号シミュレーション
平成16年9月　九州に大きな被害
Calculation Conditions:
Domain	H: 1000 km × 1000 km × V: 18 km
H-gird size	1000 m
V-grid size	200 ~ 300 m (stretched)
Grid numbers	H: 1003 × 1003 × V: 63
Integration time	48 hours
Micro-physics	the bulk cold rain type
Initial condition	JMA Regional Spectral model output
Boundary	JMA Regional Spectral model output
Surface	real topography and observed SST
Earth Simulator	100 nodes (800 CPU)

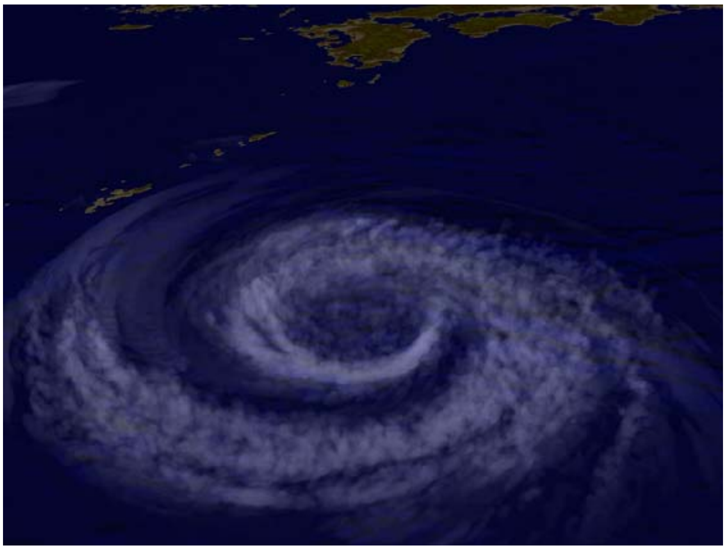

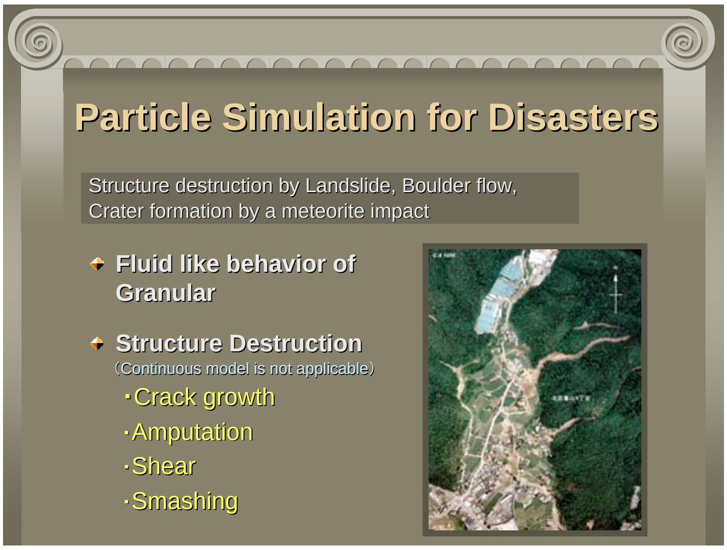

Particle Simulation for Disasters
Structure destruction by Landslide, Boulder flow,
Crater formation by a meteorite impact
Fluid like behavior of Granular
Structure Destruction
(Continuous model is not applicable)
・Crack growth
・Amputation
・Shear
・Smashing

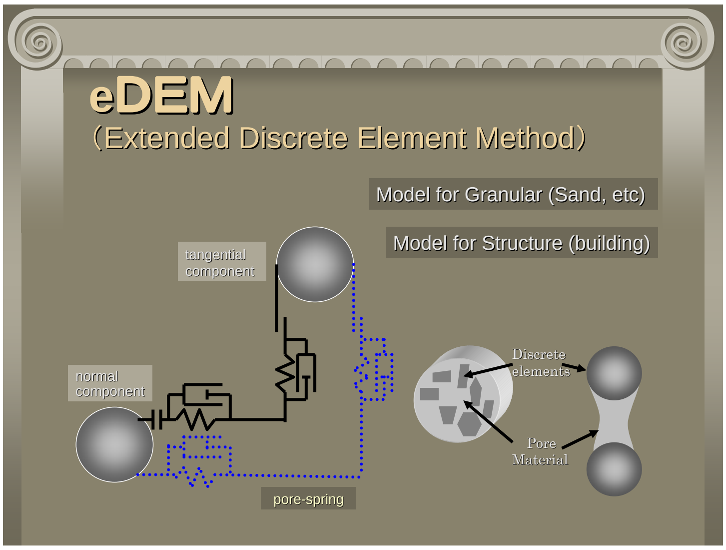

eDEM
(Extended Discrete Element Method)
Model for Granular (Sand, etc)
Model for Structure (building)
tangential component
normal component
pore-spring
Discrete elements
Pore Material

Rock Fall
Rock Fall : One of slope disasters
Prevention
Control of Sediments
exp : fence, wall, net
Improvement of Hazard Map
Numerical Simulation : effective tool

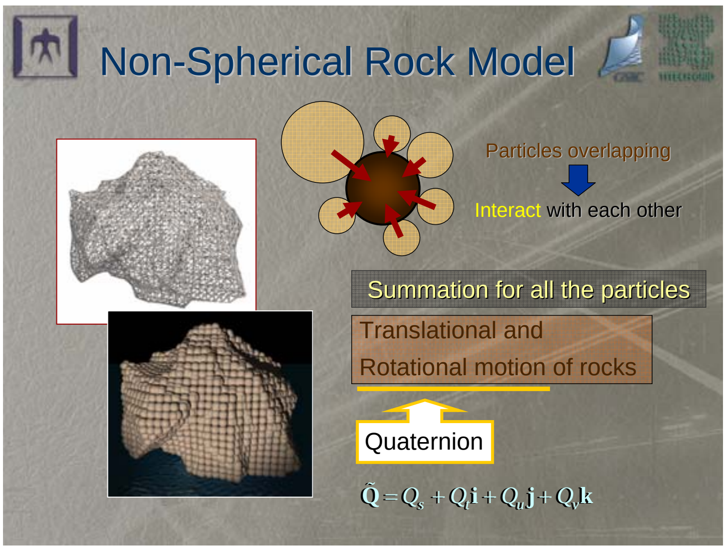

Non-Spherical Rock Model
Particles overlapping
Interact with each other
Summation for all the particles
Translational and
Rotational motion of rocks
Quaternion
$\tilde{Q} = Q_s + Q_t\mathbf{i} + Q_u\mathbf{j} + Q_v\mathbf{k}$

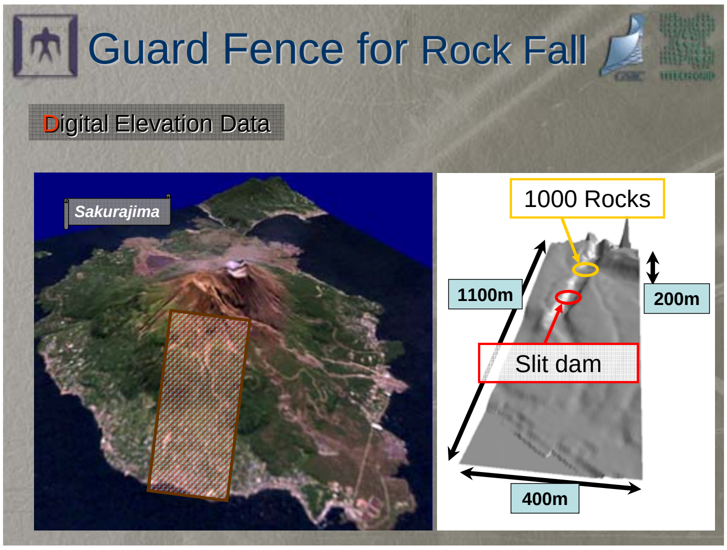
Guard Fence for Rock Fall
Digital Elevation Data
Sakurajima
1000 Rocks
1100m
200m
Slit dam
400m


九州大学応用力学研究所国際研究集会
2006 年12月7日，8日
Numerical Simulation on Turbulent Transports over Free Interface
M2 Susumu YAMASHITA,
Feng XIAO & Keiko TAKAHASHI
In collaboration with Takahashi group in the Earth Simulator center

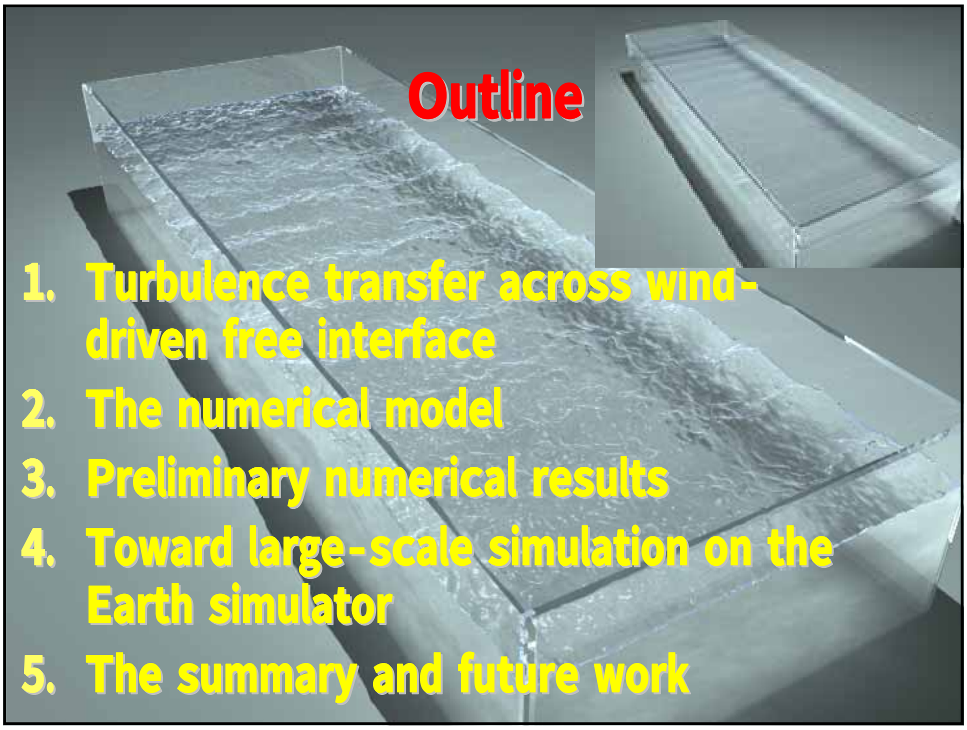
Outline
1. Turbulence transfer across wind-driven free interface
2. The numerical model
3. Preliminary numerical results
4. Toward large-scale simulation on the Earth simulator
5. The summary and future work

Turbulence transfer across wind-driven free interface

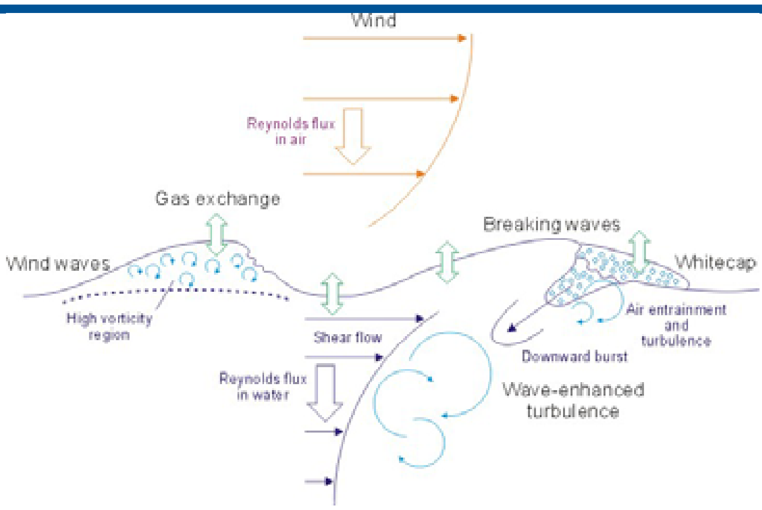

Kyusyu Univ. Environmental Fluid Science, Matunaga group

Motivation

- bulk method

Heat transfer

$$Q = h_l(T_b - T_i)$$

$$h_l = h_l(U_\infty) \ ?$$

improved

$$h_l = h_l(U_\infty, \text{wave}...)$$

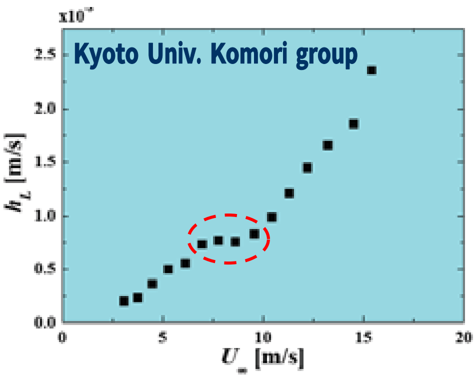

The numerical model (1/2)

- Robust solver for fluid of variable density
  - Projection method with special spatial discretisation

→ VSIAM3: a CIP/MM-FVM

(Volume/Surface Integrated Averaged Multi Moment Method)

- Explicit computations of moving interface/free boundary
  - Interface capturing methods without explicit geometrical "Reconstruction" (density capturing)

→ THINC & STAA methods

Tangent of Hyperbola for Interface Capturing

The numerical model (2/2)

- Other complexities

Dynamics and singularities at interfaces

→ Volume force formulations (Continuum Surface Force model, Brackbill et al, 1992)

- Poisson solver

→ TF Bi-CGSTAB
AMG : Algebraic Multigrid (now evaluating.)

Incompressible multi-fluid interfacial flows
--- Governing equations ---

$$\begin{cases} \dfrac{\partial u_i}{\partial t} + \dfrac{\partial (u_i u_j)}{\partial x_j} = -\dfrac{\partial p}{\partial x_i} + \nu \dfrac{\partial^2 u_i}{\partial x_j \partial x_j} + g_i + F_i \\ \dfrac{\partial u_i}{\partial x_i} = 0 \end{cases}$$

surface tension,...

$$\frac{\partial \phi}{\partial t} + \frac{\partial (\phi u_i)}{\partial x_i} = 0$$

Density Function

density & viscosity

$$\rho(x,y,z,t) = \rho_1 \phi(x,y,z,t) + \rho_2 [1 - \phi(x,y,z,t)]$$

$$\mu(x,y,z,t) = \mu_1 \phi(x,y,z,t) + \mu_2 [1 - \phi(x,y,z,t)]$$

VSIAM3: a CIP/MM finite volume method

$$\frac{\partial \overline{{}^V\phi}}{\partial t} = \oint_\Gamma \boldsymbol{F}(\phi) \cdot \boldsymbol{n} d\Gamma; \quad \boldsymbol{F}(\phi): \ \text{Flux} \quad \boldsymbol{n}: \ \text{normal vector}$$

Conventional Finite Volume Method
Using only the
Volume integrated average (VIA) $\overline{{}^V\phi}$

$\Longrightarrow$ **Single integrated moment**

VSIA Based Finite Volume Method
Using both the
Volume integrated average (VIA) $\overline{{}^V\phi}$
Surface integrated average (SIA) $\overline{{}^S\phi}$

$\Longrightarrow$ **Multi integrated moment**

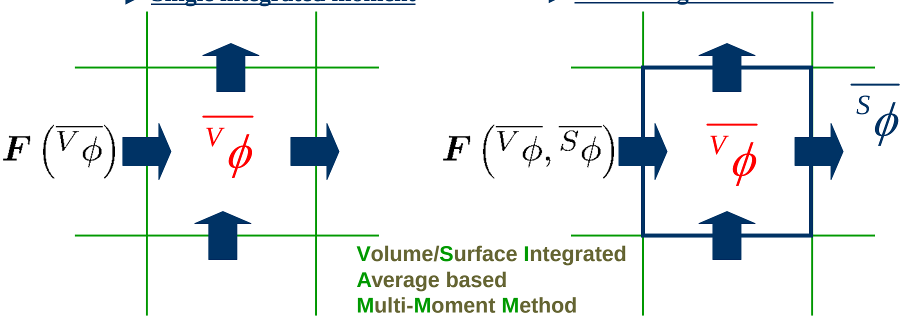

Advection scheme

CIP-CSLR (CIP-Conservative Semi-Lagrangian with Rationalfunction)

Aspects:

- Interpolation function : rational function
- Exactly conservative
- Non-oscillatory and less diffusive
- Easy to extend to multi-dimension problems

Surface advection scheme

THINC (Tangent of Hyperbola for Interface Capturing) scheme

- Algebraic-type method
- Interpolation function : hyperbolic tangent function
- Exactly conserves the advected quantity
- Oscillation-less and smearing-less solution
- Quite simple and easy to extend to 3D code

Surface advection scheme

Interpolation function of THINC scheme

$$F_i(x) = \frac{\alpha}{2}\left(1 + \gamma \tanh\left(\beta\left(\frac{x - x_{i-(1/2)}}{\Delta x_i} - \tilde{x}_i\right)\right)\right)$$

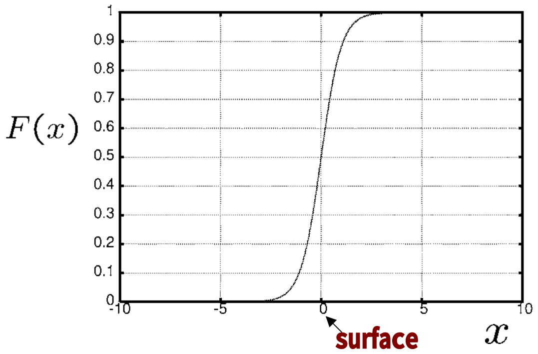

Validation of the THINC scheme

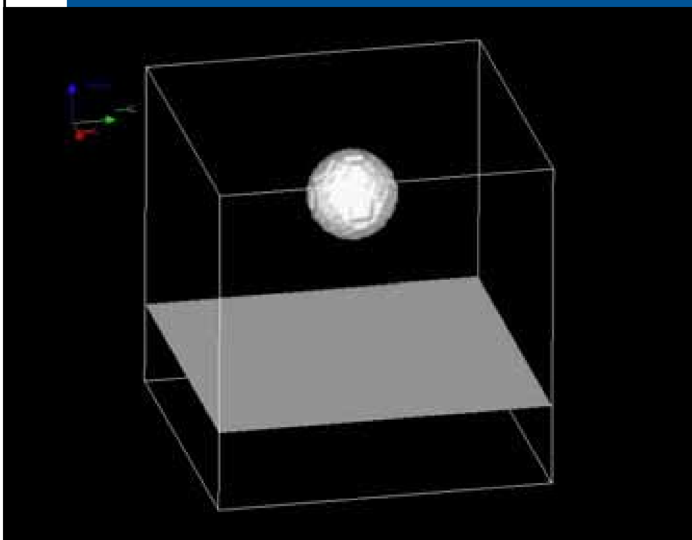

Grid 80x80x80

DEPARTMENT OF ENERGY SCIENCES, TOKYO Tech.

Validation of the THINC scheme

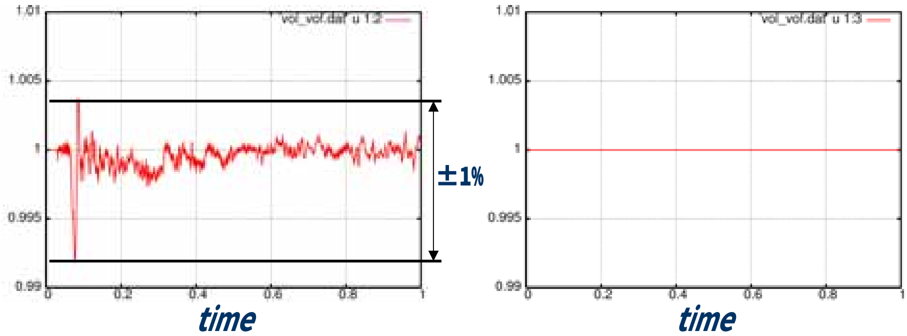

$$\frac{\sum_{ijk} Vol_{ijk}^{n}}{\sum_{ijk} Vol_{ijk}^{initial}} \qquad \frac{\sum_{ijk} f_{ijk}^{n}}{\sum_{ijk} f_{ijk}^{initial}}$$

DEPARTMENT OF ENERGY SCIENCES, TOKYO Tech.

Parallel poisson solver

Fully parallelizable preconditioned Bi-CGSTAB method

- Preconditioner : tri-diagonal preconditioner
- Single step Jacobi splitting (only partitioning direction in the calculating preconditioning matrix process.)

DEPARTMENT OF ENERGY SCIENCES, TOKYO Tech.

Available hardware

- PC clusters in the lab.
- The Earth simulator
- TSUBAME
  (Grid servers in Tokyo Tech)

Spec of hardware

PC cluster (our Lab. !!)	
Processors	5
CPU	Pen4 3GHz
Mem	10GB
Rmax	5GFlops

TSUBAME (Tokyo Tech)	
Processors	10368
CPU	Opteron 2.4/2.6GHz
Mem	21248 GB
Rmax	38180 GFlops

The Earth Simulator	
Processors	5120
CPU	NEC (vector CPU)
Mem	10240 GB
Rmax	35860 GFlops

Preliminary results

normalization

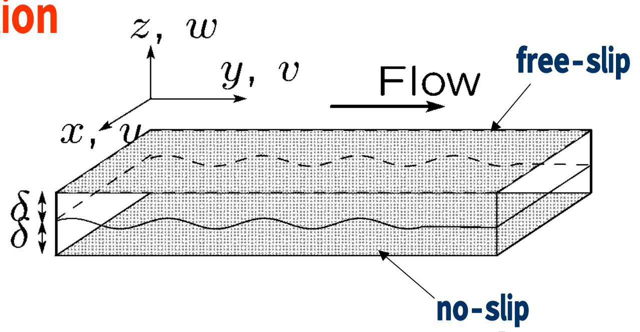

[length, velocity, time, pressure]

$$[\delta,\ U_a,\ \delta/U_a,\ \rho_a U_a^2]$$

Preliminary results

Then each normalized physical quantities are given by

$$u_i^+ = u_i/U_a, \quad x_i^+ = x_i/\delta, \quad p^+ = p/(\rho_a U_a^2), \quad (1)$$

$$\nu_a = \mu_a/\rho_a, \quad \nu_\ell = \mu_\ell/\rho_\ell, \quad (2)$$

$$R_e = \frac{U_a\delta}{\nu_a}, \quad F_r = U_a/\sqrt{g\delta}, \quad W_e = \frac{\gamma}{\rho_a \delta U_a^2}, \quad (3)$$

the density ratio and the viscosity ratio are defined as

$$\ell = \frac{\rho_\ell}{\rho_a}, \quad m = \frac{\mu_\ell}{\mu_a}. \quad (4)$$

Department of Energy Sciences, Tokyo Tech.

Preliminary results

$$\mu = \mu_a \left[m\phi + (1 - \phi) \right],$$

$$\rho = \rho_a \left[\ell\phi + (1 - \phi) \right],$$

thus we have

$$\nu = \frac{\mu}{\rho} = \nu_a \left(\frac{m\phi + (1 - \phi)}{\ell\phi + (1 - \phi)} \right)$$

$$\rightarrow \frac{\nu}{U_a \delta} \equiv \frac{1}{R_e^{\text{each}}} = \frac{1}{R_e} \left(\frac{m\phi + (1 - \phi)}{\ell\phi + (1 - \phi)} \right).$$

normalization

$$\frac{\partial u_i^+}{\partial x_i^+} = 0,$$

$$\frac{\partial u_i^+}{\partial t^+} + \frac{\partial}{\partial x_j^+}(u_i^+ u_j^+) = -\underbrace{\frac{\rho_a}{\rho}}_{(A)} \frac{\partial p^+}{\partial x_i^+} + \frac{1}{R_e^{\text{each}}} \frac{\partial}{\partial x_j^+} \left(\frac{\partial u_i^+}{\partial x_j^+} + \frac{\partial u_j^+}{\partial x_i^+} \right) + \frac{1}{F_r^2} - \underbrace{\frac{\gamma}{\rho U_a^2 \delta}}_{(B)} \frac{\partial \widehat{n}_i}{\partial x_i^+} n_j^+,$$

$$\frac{\partial \phi}{\partial t^+} + \frac{\partial (\phi u_i^+)}{\partial x_i^+} = 0.$$

(A) : $\dfrac{\rho_a}{\rho} = \dfrac{\rho_a}{\rho_a(\ell\phi + (1 - \phi)} = \dfrac{1}{\ell\phi + (1 - \phi)},$

(B) : $\dfrac{\gamma}{\rho U_a^2 \delta} \equiv \dfrac{1}{W_e^{\text{each}}} = \dfrac{\gamma}{\rho_a(\ell\phi + (1 - \phi))U_a^2 \delta} = \dfrac{1}{W_e(\ell\phi + (1 - \phi))}.$

Preliminary results

Material constants of each fluids

$$\rho_\ell = 996.62 \text{ kg/m}^3$$
$$\rho_a = 1.18 \text{ kg/m}^3$$
$$\mu_\ell = 0.001 \text{ Pa s}$$
$$\mu_a = 1.86 \times 10^{-5} \text{ Pa s}$$
$$\sigma = 0.073 \text{ N/m}$$

Parameters

$$U_a = 1 \text{ m/s}, \ \delta = 0.25 \text{ m};$$
$$R_e = 15793.5$$
$$W_e = 4.028$$
$$F_r = 0.638$$
$$\ell = 847.25$$
$$m = 53.7$$

Parameters

$$U_a = 1 \text{ m/s}, \ \delta = 1 \text{ cm};$$
$$R_e = 631$$
$$W_e = 16113.7$$
$$F_r = 3.19$$
$$\ell = 847.25$$
$$m = 53.7$$

parallelization

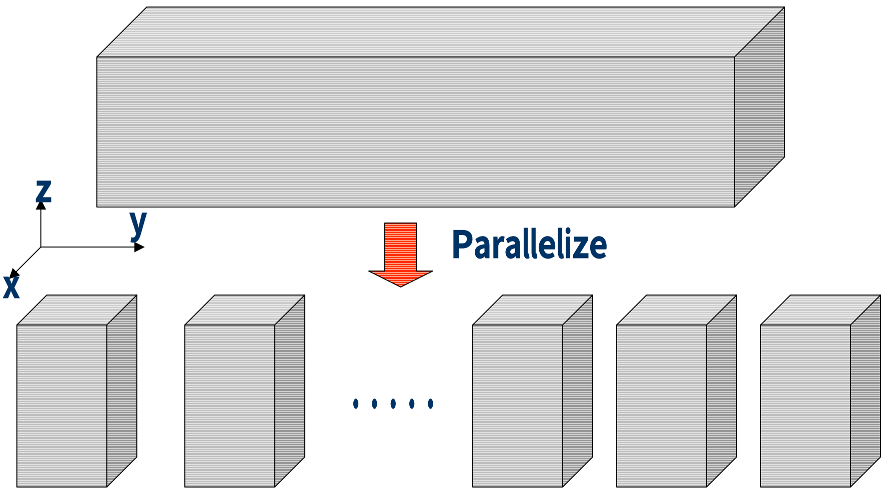

Preliminaly results (x,y,z)=2cm,8cm,2cm:64x256x64)

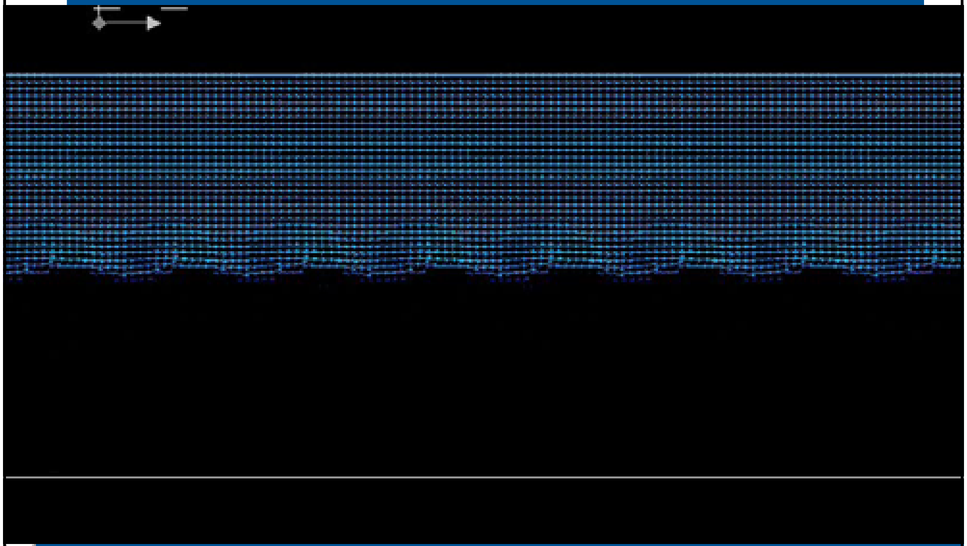

Preliminary result

Statistical analysis of turbulence near the free-surface (x,y,z) = (2cm,8cm,2cm) (64x256x64 in our Lab.)

Time spectra of the wave amplitude

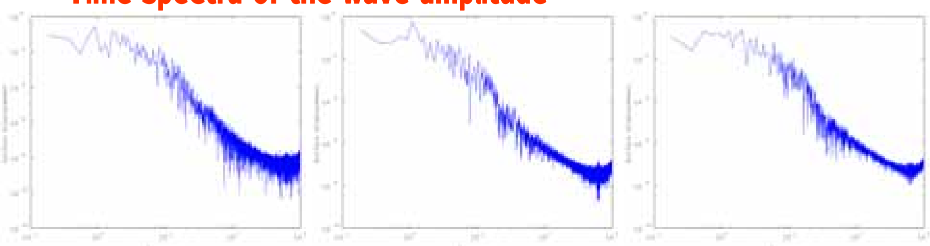

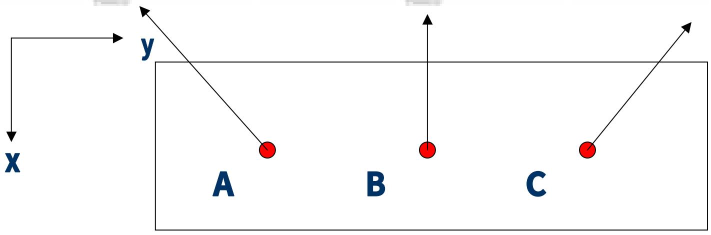

Preliminary result

Statistical analysis of turbulence near the free-surface

(x,y,z) = (2cm,8cm,2cm)
(64x256x64 in our Lab.)

Time spectrum of the wave amplitude

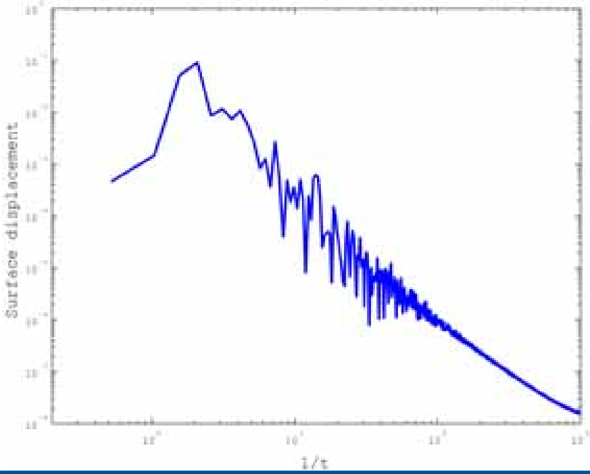

DEPARTMENT OF ENERGY SCIENCES, TOKYO Tech.

Preliminary result

Mean velocity profile ($\overline{v}$)

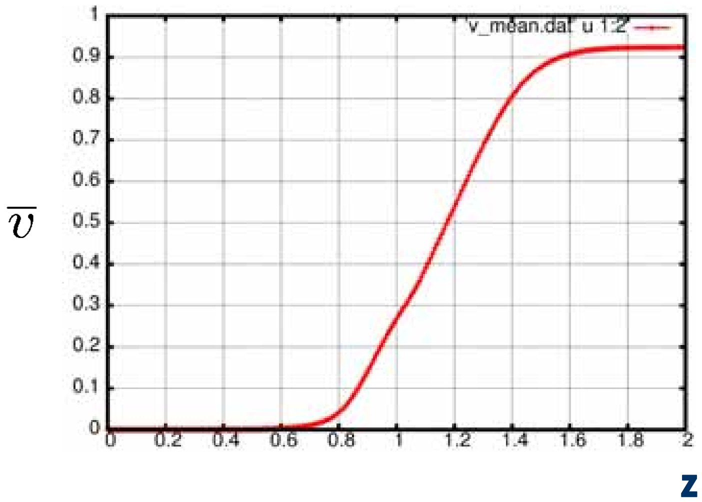

DEPARTMENT OF ENERGY SCIENCES, TOKYO Tech.

Preliminary result

Root-mean-square of the velocity components

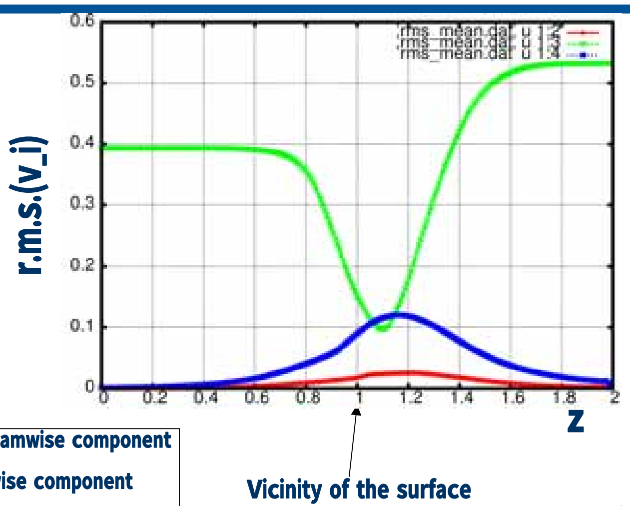

Green : Streamwise component
Red : Spanwise component
Blue : Normal component

$$\mathrm{r.m.s.}(v_i') = \sqrt{\overline{v_i'^2}}$$

DEPARTMENT OF ENERGY SCIENCES, TOKYO Tech.

Preliminary result

Root-mean-square of the velocity components

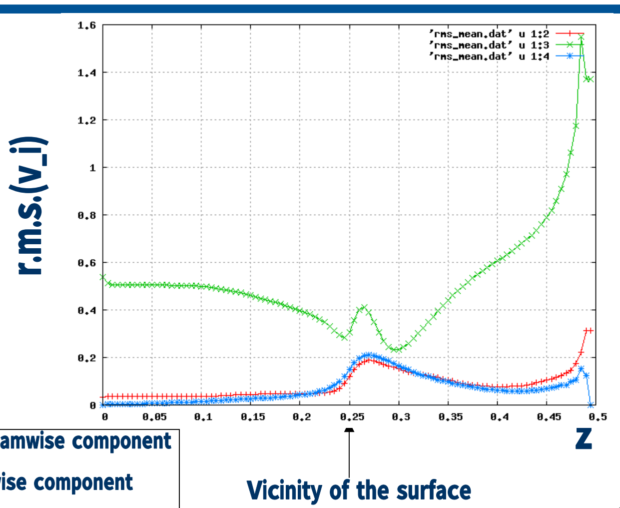

Green : Streamwise component
Red : Spanwise component
Blue : Normal component

$$\mathrm{r.m.s.}(v_i') = \sqrt{\overline{v_i'^2}}$$

DEPARTMENT OF ENERGY SCIENCES, TOKYO Tech.

Three components of the vorticity profile

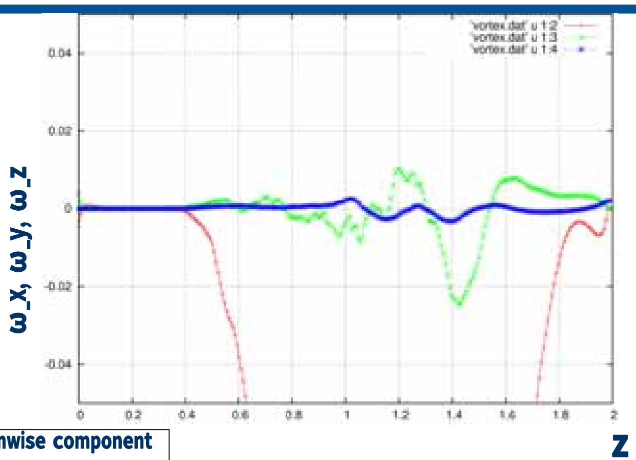

Green : Streamwise component

Red : Spanwise component

Blue : Normal component

Reynolds stress and surface displacement
point A

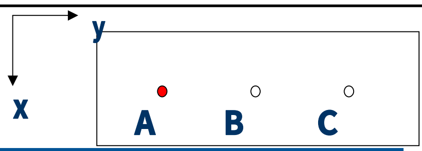

Reynolds stress

Surface displacement

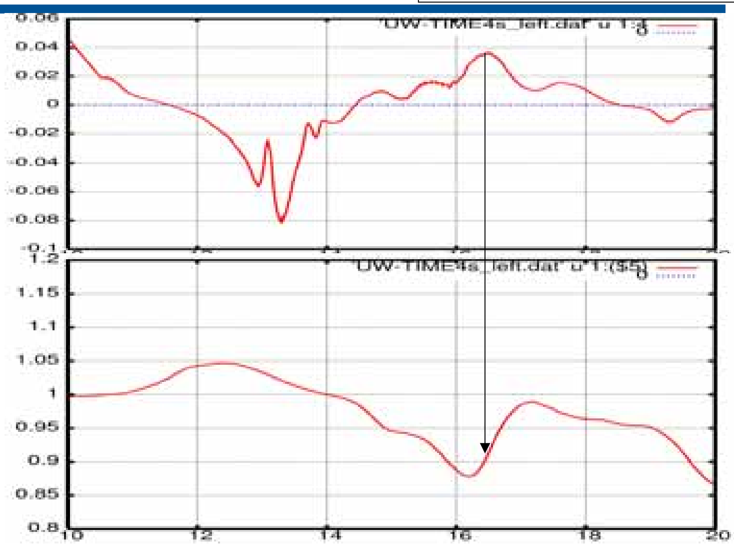

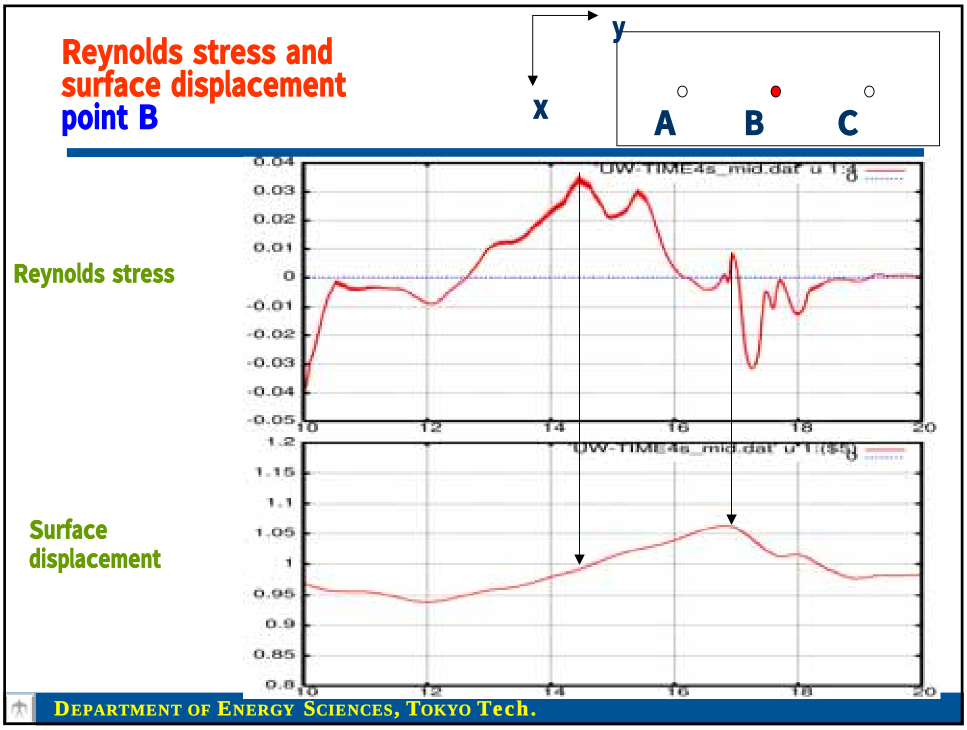
Reynolds stress and
surface displacement
point B
y
x
A
B
C
Reynolds stress
Surface
displacement
'UW-TIME4s_mid.dat' u 1:4
0
'UW-TIME4s_mid.dat' u 1:($5)
0
0.04
0.03
0.02
0.01
0
-0.01
-0.02
-0.03
-0.04
-0.05
1.2
1.15
1.1
1.05
1
0.95
0.9
0.85
0.8
10
12
14
16
18
20
DEPARTMENT OF ENERGY SCIENCES, TOKYO Tech.

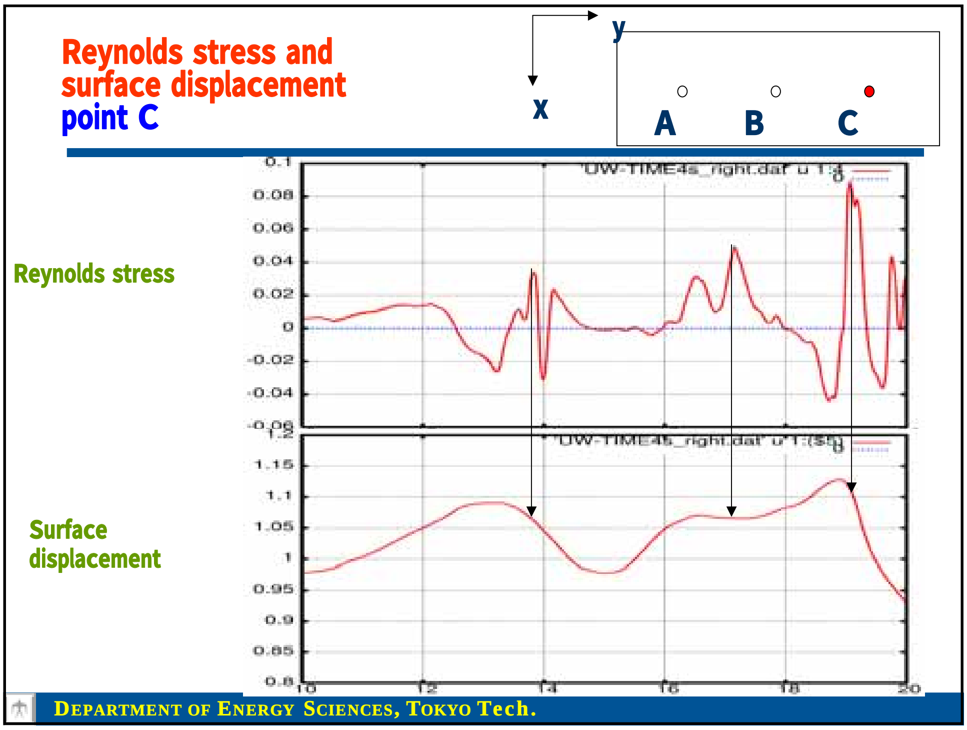
Reynolds stress and
surface displacement
point C
y
x
A
B
C
Reynolds stress
Surface
displacement
'UW-TIME4s_right.dat' u 1:4
0
'UW-TIME4s_right.dat' u 1:($5)
0
0.1
0.08
0.06
0.04
0.02
0
-0.02
-0.04
-0.06
1.2
1.15
1.1
1.05
1
0.95
0.9
0.85
0.8
10
12
14
16
18
20
DEPARTMENT OF ENERGY SCIENCES, TOKYO Tech.

Preliminary results in the ESC

open-channel flow simulation

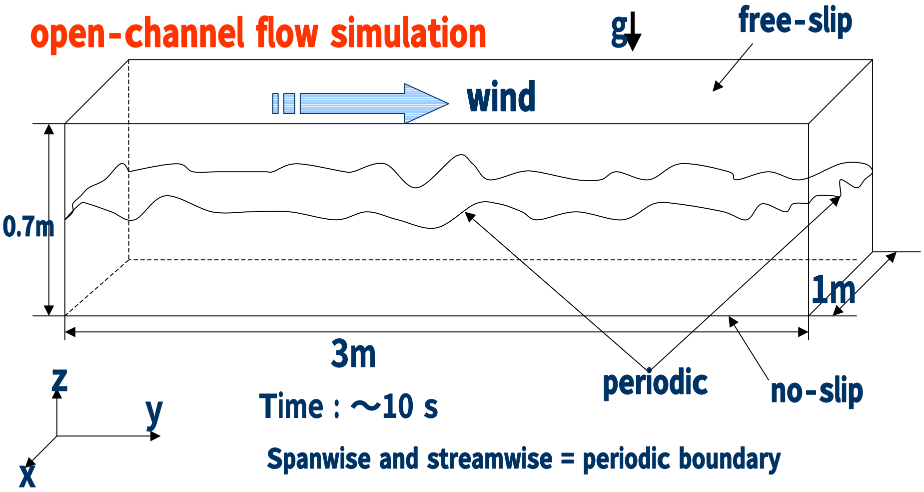

Time : ～10 s

Spanwise and streamwise = periodic boundary

Top and bottom wall = free and no-slip boundary

3D view (257x513x129, calculated in the Earth Simulator)

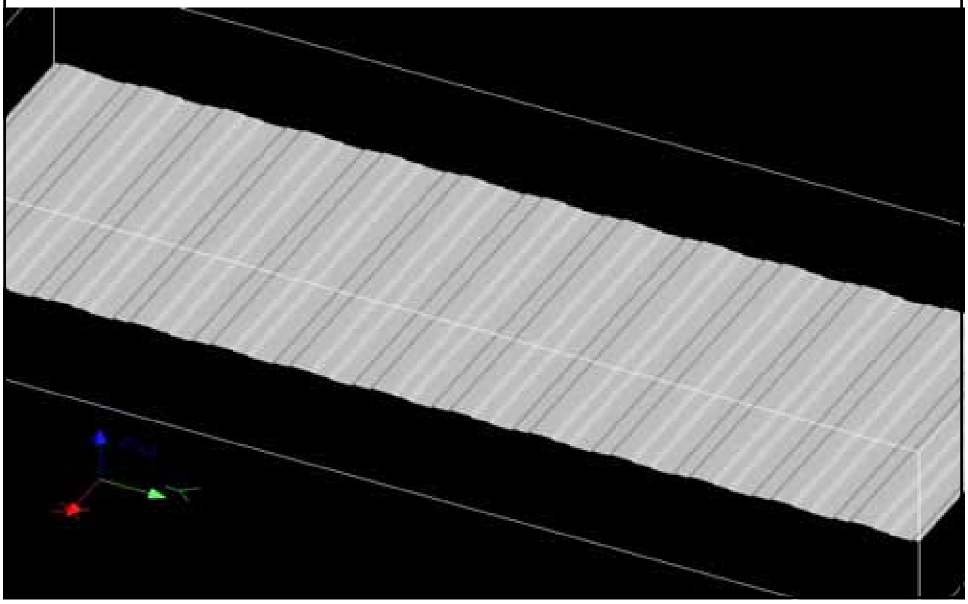

Velocity vector field (by the Earth Simulator)

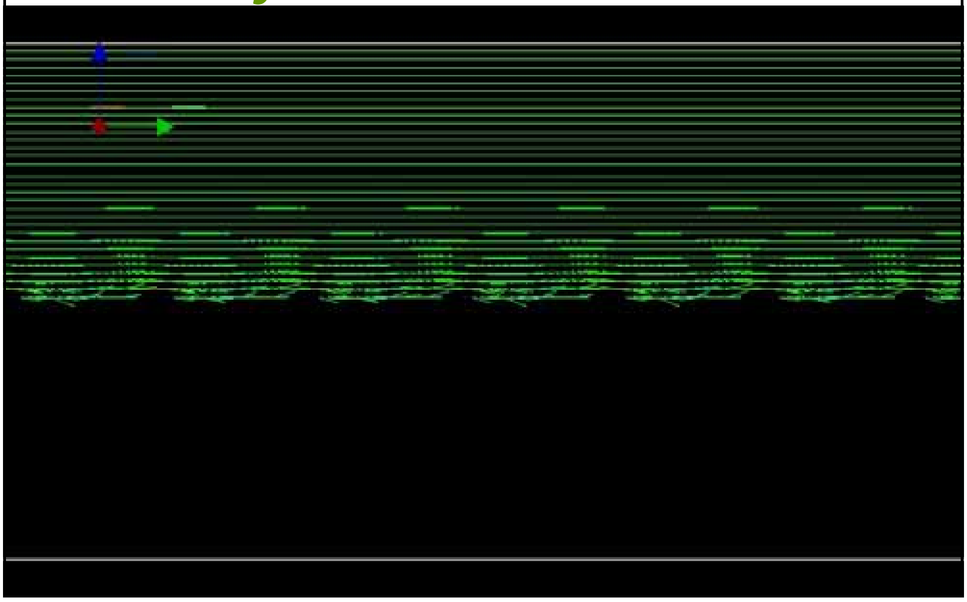

Toward large-scale simulation on the Earth Simulator

The current performance of our code on the Earth Simulator

Parallelization ratio	99.87%
Available nodes (8 processors/node)	100

Department of Energy Sciences, Tokyo Tech.

Current state of parallelism

Parallel speed up

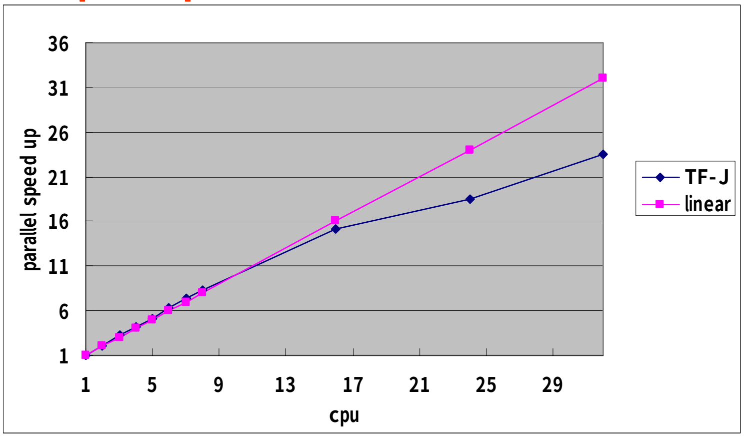

Powerful poisson solver — AMGCG —

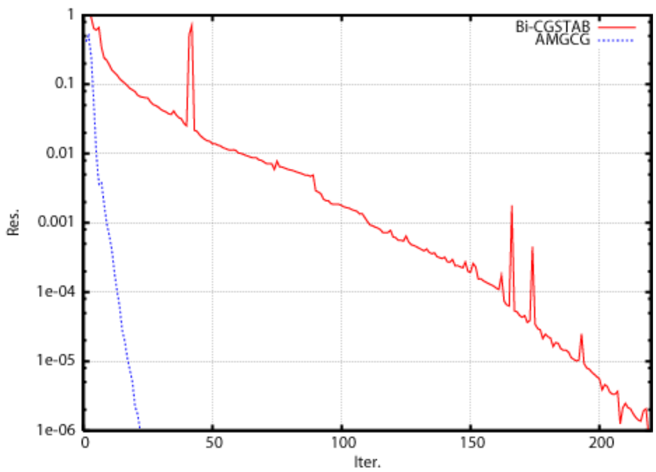

$$\partial_{xx} f + \partial_{yy} f + \partial_{zz} f = \sin(\pi x / L_x) \sin(\pi y / L_y) \sin(\pi z / L_z)$$

How fine mesh resolution we can get?

100 nodes : About 1,400,000,000 grids

→ DNS of 1m x 3 m x 0.7 m wave tank

512 nodes (max)

For example

→ DNS of 0.5 m x 20 m x 0.7 m wave tank

(assume the Kolmogorov scale = 1mm)

Summary

- The multi-phase flow simulation code including free-interface has been constructed.
- Robust and reasonable results have been obtained for free interface flows
- A suitable framework for wind-driven free interface simulation

Future work

- Further efforts for large-scale simulation on the Earth simulator. (Algebraic Multi Grid)
- "Real-case" simulations with validations through experiments
- Investigation of free-surface turbulence behavior by large scale simulations --- LES model ….
- Development and improvement of models for energy and material transfer on free surface

Solid-Fluid Interaction Analysis by Full Eulerian Formulation

Kenji Nakao
Shigenobu Okazawa
Masahiko Fujikubo

Hiroshima University

Outline

- Introduction
- Multi-Material Element Concept
- Present Computational Framework
- Computational Results
- Conclusions and Future Tasks

Outline

- Introduction
- Multi-Material Element Concept
- Present Computational Framework
- Computational Results
- Conclusions and Future Tasks

Lagrangian and Eulerian formulation

- Lagrangian Formulation
  →mesh moves with the material deformation

- Eulerian Formulation
  →mesh is fixed in space and material moves through the elements

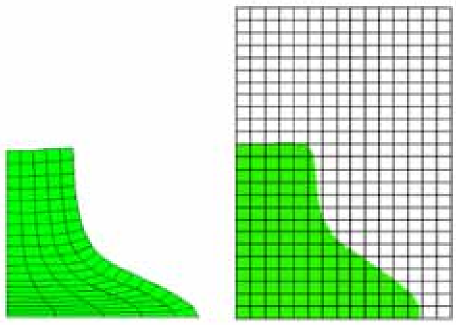

Lagrangian Formulation Eulerian Formulation

Solid Analysis → Lagrangian Formulation
Fluid Analysis → Eulerian Formulation

Conventional Solid-Fluid Interaction

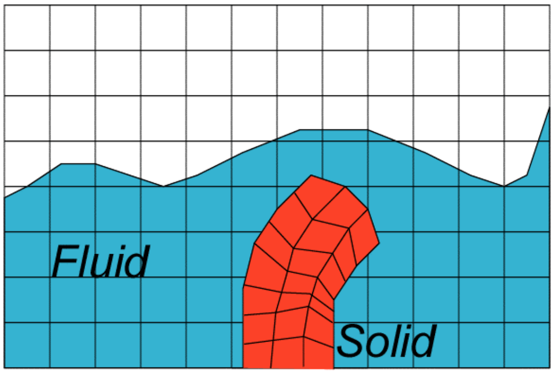

Lagrangian Solid
Eulerian Fluid

2 Solvers

Conventional Solid-Fluid Interaction

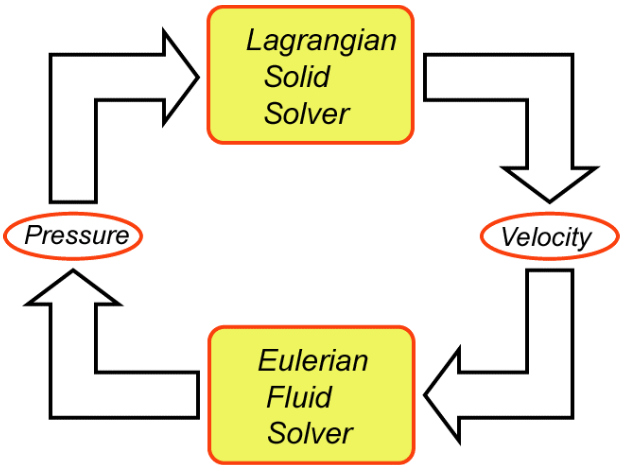

Conventional Solid-Fluid Interaction

Advantages:

- Tracking of solid interface
- Accuracy

Disadvantages:

- Large solid deformations
- Complex interaction algorithm

Present Solid-Fluid Interaction

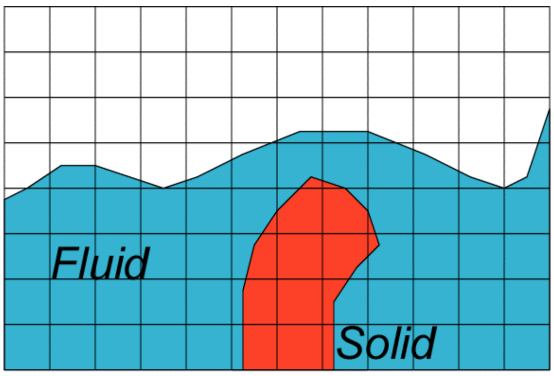

Eulerian Solid
Eulerian Fluid

only 1 Solver
Full Eulerian

Present Solid-Fluid Interaction

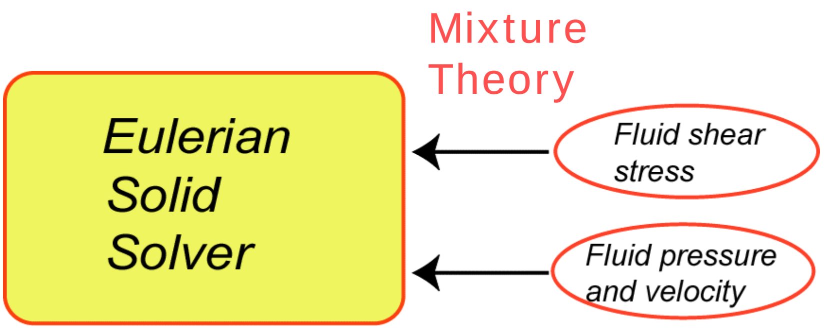

Structural Systems Laboratory HIROSHIMA UNIVERSITY

Present Solid-Fluid Interaction

Advantages:

- Interaction algorithm is simple because of simple mixture theory
- Large solid deformations
- easy extension by existing code

Disadvantage:

- Tracking of solid interface

Structural Systems Laboratory HIROSHIMA UNIVERSITY

Outline

- Introduction
- Multi-Material Element Concept
- Present Computational Framework
- Computational Results
- Conclusions and Future Tasks

Volume Fraction

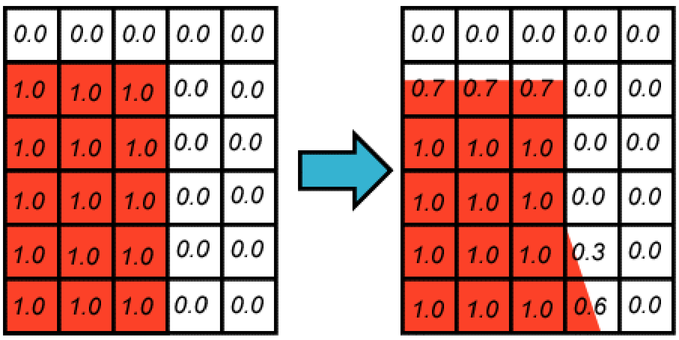

$\phi = 1.0$ → 100% filled
$\phi = 0.0$ → empty
$\phi < \phi_{min}$ → calculation is ignored

Multi-Material Element

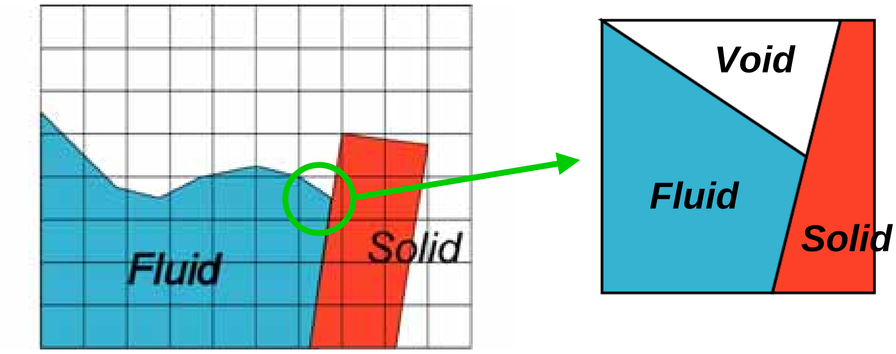

In contact surface,
→Eulerian element can have more than one material

Mixture Theory

Solid Stress

Solid elastic stress rate:

$$\dot{\boldsymbol{\sigma}} = \int_{\Omega} \mathbf{C}_s \mathbf{B} \boldsymbol{\upsilon} \, d\Omega$$

Constitutive matrix:

$$\mathbf{C}_s = \frac{E}{1-\nu^2} \begin{bmatrix} 1 & \nu & 0 \\ \nu & 1 & 0 \\ 0 & 0 & \frac{1-\nu}{2} \end{bmatrix}$$

Plastic corrector

Simulation of solid plasticity

Radial Return Method

Stress is returned to the yield surface

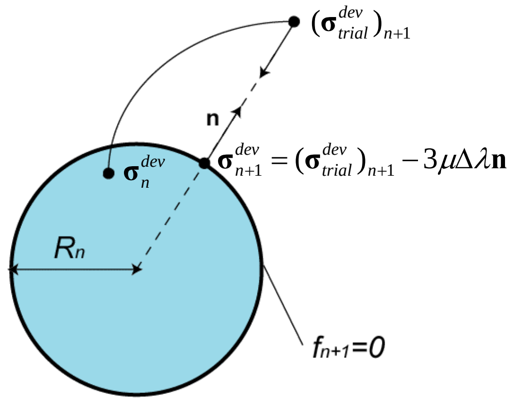

Fluid Stress

Fluid shear stress rate:

$$\dot{\boldsymbol{\tau}} = \int_{\Omega} \mathbf{C}_f \mathbf{B} \boldsymbol{\upsilon} \, d\Omega$$

Constitutive matrix:

$$\mathbf{C}_f = \mu \begin{bmatrix} 1 & -1 & 0 \\ -1 & 1 & 0 \\ 0 & 0 & 1 \end{bmatrix}$$

Structural Systems Laboratory HIROSHIMA UNIVERSITY

Mixture Theory

the strain rate $\dot{\boldsymbol{\varepsilon}} = \mathbf{B}\boldsymbol{\upsilon}$
is same for all material
in an element

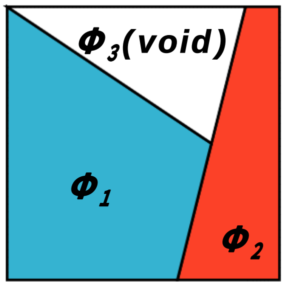

Element containing 2 materials

Including void

$$\sum_m \phi_m = 1$$

Structural Systems Laboratory HIROSHIMA UNIVERSITY

Mixture Theory

$\boldsymbol{\sigma}_{solid}$ $\boldsymbol{\tau}_{fluid}$

⇩

Average stresses
by material volume fraction

$$\bar{\boldsymbol{\sigma}} = \sum_m \boldsymbol{\sigma}_m \phi_m$$

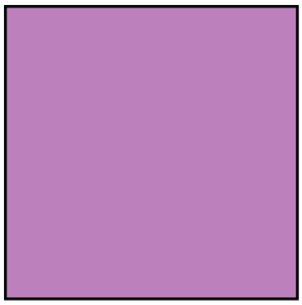

Mixed

Structural Systems Laboratory HIROSHIMA UNIVERSITY

Main Aspect of Mixture Theory

Same volumetric strain for all material:

Steel-Air Coupling
→The volumetric strain is too different

Steel-Water Coupling
→Difference is much less (both incompressible)

Outline

- Introduction
- Multi-Material Element Concept
- Present Computational Framework
- Computational Results
- Conclusions and Future Tasks

Present Computational Framework

Computational Framework → 2 Steps

Non-advective calculation

- calculation of solid and fluid variables by neglecting advective term

Advective calculation

- calculation of advection of mixed variables

Solid Analysis

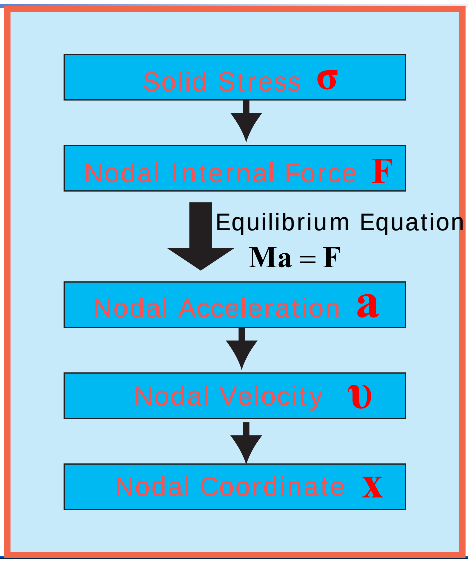

Fluid Analysis

Navier-Stokes Equation without Advective term

Momentum Equation: $\rho\dot{\boldsymbol{\upsilon}} + \nabla p = \mu\nabla^2\boldsymbol{\upsilon} + \rho\mathbf{g}$

Incompressibility Constrain Equation: $\nabla \cdot \boldsymbol{\upsilon} = 0$

Split in two equation

Neglecting the pressure term: $\rho\dot{\boldsymbol{\upsilon}} = \mu\nabla^2\boldsymbol{\upsilon} + \rho\mathbf{g}$

Containing only the pressure term: $\rho\dot{\boldsymbol{\upsilon}} = -\nabla p$

Fluid Analysis

Fractional Step Method

1. Intermediate velocity (no pressure)

$$\boldsymbol{\upsilon}_*^{n+1} = \boldsymbol{\upsilon}^n + \frac{\Delta t}{\rho}[\mu\nabla^2\boldsymbol{\upsilon}^n + \rho\mathbf{g}]$$

2. Pressure (consider the incompressibility constrain Eq.)

$$\nabla \cdot \boldsymbol{\upsilon}^{n+1} = \nabla \cdot \boldsymbol{\upsilon}_*^{n+1} - \frac{\Delta t}{\rho}\nabla \cdot \nabla p$$

$$\nabla^2 p = \frac{\rho}{\Delta t}[\nabla \cdot \upsilon_*^{n+1}]$$

3. Velocity correction (update)

$$\boldsymbol{\upsilon}^{n+1} = \boldsymbol{\upsilon}_*^{n+1} - \frac{\Delta t}{\rho}\nabla p$$

Present Solid-Fluid Interaction Analysis

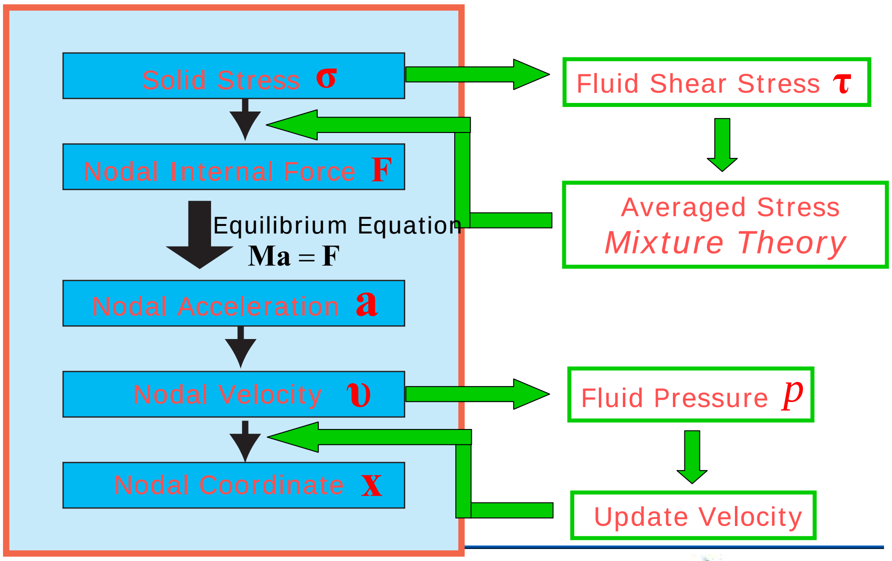

Structural Systems Laboratory HIROSHIMA UNIVERSITY

Advective Calculation

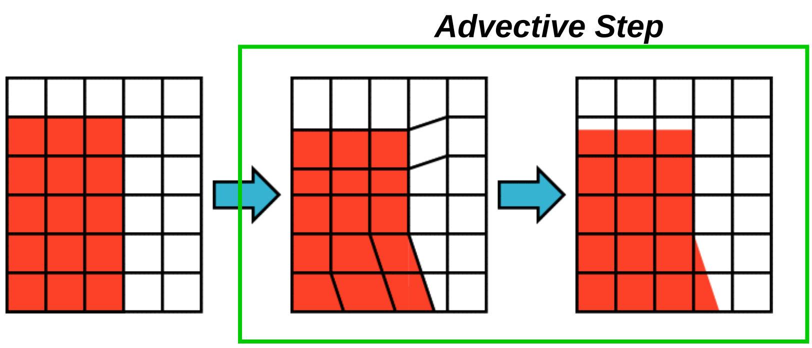

After Non-advective calculation

→the deformed mesh is re-meshed to the original place
→advection of mixed solution variables is calculated

Structural Systems Laboratory HIROSHIMA UNIVERSITY

Advection Algorithm

Advection of solution variables

$\boxed{\text{MUSCL method}}$

One-dimensional:

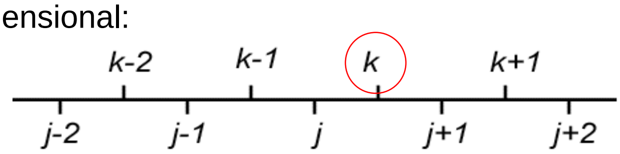

$$f_k^{+} = f_k^{-} + \frac{\Delta t}{\Delta x}(\Phi_j - \Phi_{j+1})$$

Structural Systems Laboratory HIROSHIMA UNIVERSITY

Outline

- Introduction
- Multi-Material Element Concept
- Present Computational Framework
- Computational Results
- Conclusions and Future Tasks

Structural Systems Laboratory HIROSHIMA UNIVERSITY

Ring Falling onto Fluid

Ring	
Density [kg/m³]	*500*
Young Modulus [MPa]	*0.05*
Poisson ratio [-]	*0.3*
Fluid	
Density [kg/m³]	*1000*
Dyn. Viscosity [N･s/m²]	*0.001*

Geometry [m×m]	*1.5×1.0*
Mesh Division [-]	*100×60*

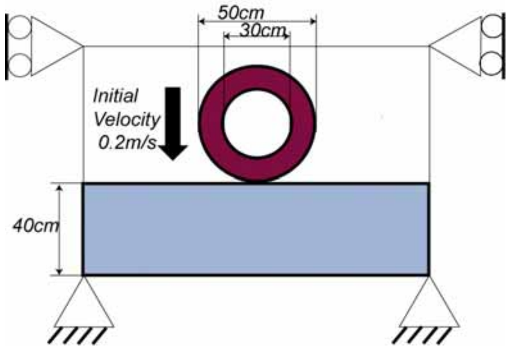

Computational Result

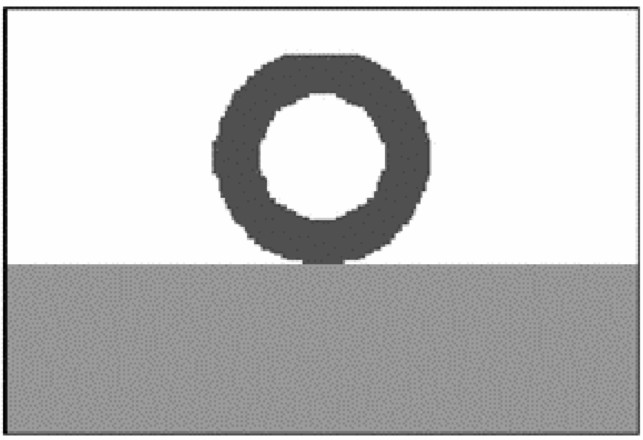

Dam break with elastic solid bar

Thick Bar (rubber)	
Density [kg/m³]	*1000*
Young Modulus [MPa]	*5*
Poisson ratio [-]	*0.45*
Fluid	
Density [kg/m³]	*1000*
Dyn. Viscosity [N･s/m²]	*0.001*

Geometry [m×m]	*0.6×0.4*
Mesh Division [-]	*60×40*

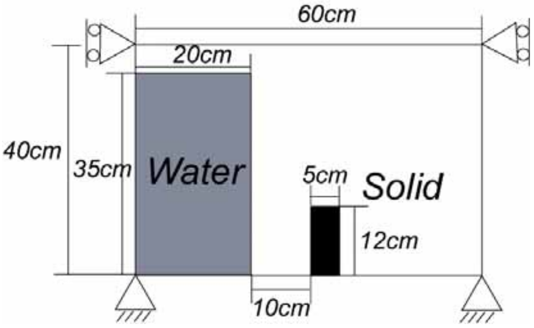

Structural Systems Laboratory   HIROSHIMA UNIVERSITY

Computational Result

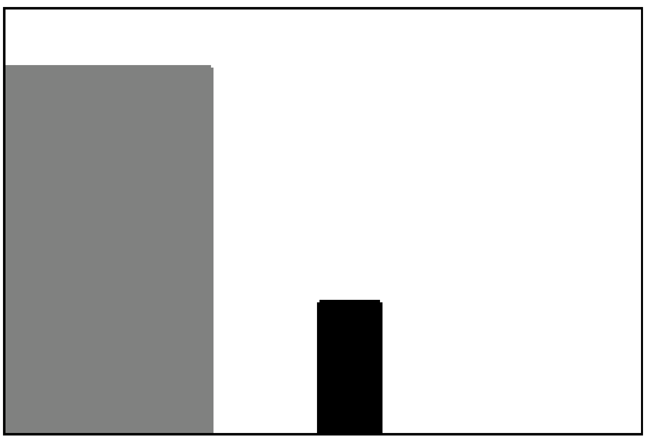

Structural Systems Laboratory   HIROSHIMA UNIVERSITY

Dam break with elasto-plastic solid bar

Thick Bar	
Density [kg/m³]	*1200*
Young Modulus [MPa]	*15*
Poisson ratio [-]	*0.3*
Yield Stress [MPa]	*0.1*
Fluid	
Density [kg/m³]	*1000*
Dyn. Viscosity [N・s/m²]	*0.001*

Geometry [m×m]	*0.6×0.4*
Mesh Division [-]	*60×40*

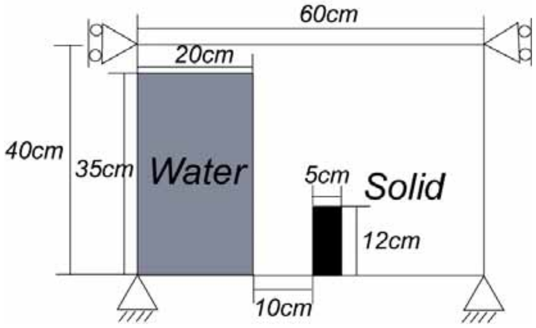

Computational Result

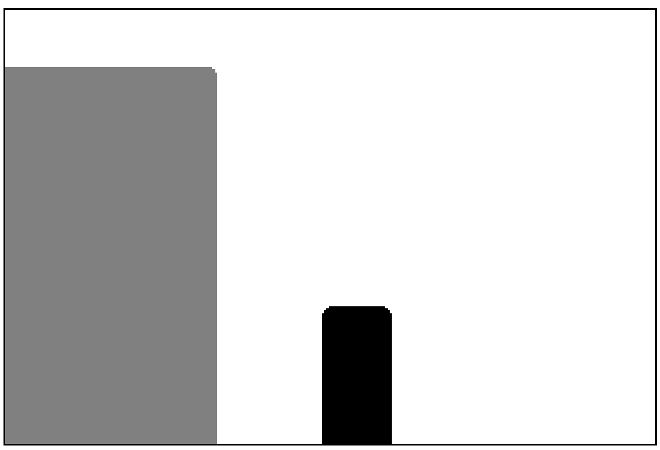

Outline

- Introduction
- Multi-Material Element Concept
- Present Computational Framework
- Computational Results
- Conclusions and Future Tasks

Conclusions

- An Eulerian finite element method is effective for flexible solid and fluid interaction problem by using the mixture theory.

- Existing Eulerian solid code can be simply extended to solid-fluid interaction.

Future Tasks

- Simulations with much larger solid deformation or with creation of new free surfaces after material separation
- Validation of present code by comparing with experiment or another simulation method (For example, Arbitrary Lagrangian Eulerian method or the particle method)

Thank you for your attention!

Manchester Metropolitan University

Centre for Mathematical Modelling and Flow Analysis

Computational Modelling of Free Surface Flows using a Surface Capturing Cartesian Cut Cell Method

Derek Causon and Clive Mingham

Centre for Mathematical Modelling and Flow Analysis

Manchester Metropolitan University
United Kingdom

Manchester Metropolitan University

Centre for Mathematical Modelling and Flow Analysis

Outline

- Wave overtopping simulation
- Cartesian cut cell method
- Surface capturing method
- Floating bodies and slamming
- Wave energy devices
- Future work

Manchester Metropolitan University

Centre for Mathematical Modelling and Flow Analysis

Acknowledgements

Funding for this visit to Japan was provided by the UK Foreign and Commonwealth Office (FCO)/British Embassy Japan Global Opportunities Fund (GOF):

- Wave overtopping
- Tsunami propagation
- Wave interaction with floating bodies

Manchester Metropolitan University

Centre for Mathematical Modelling and Flow Analysis

The VOWS Project

(**V**iolent **O**vertopping of **W**aves at **S**eawalls)

Aim:

To investigate the violent overtopping of seawalls and help engineers design sea defences.

Photo by G. Motyker, HR Wallingford

Manchester Metropolitan University

Centre for Mathematical Modelling and Flow Analysis

Experimental

Edinburgh, and Sheffield Universities

- 2D wave flume tests In Edinburgh.
- 3D wave basin tests at HR Wallingford.

Numerical

Manchester Metropolitan University (MMU)

- **AMAZON-CC** cut cell shallow water code
- **AMAZON-SC** surface capturing Navier Stokes code

Manchester Metropolitan University

Centre for Mathematical Modelling and Flow Analysis

VOWS: Numerical approach

- Use 1-D Shallow Water Equations to simulate wave flume and compare with experiments
- Use 2-D Shallow Water AMAZON-CC to *provide advice* for wave basin experiments
- Use AMAZON-SC to simulate violent wave overtopping

Manchester Metropolitan University

Centre for Mathematical Modelling and Flow Analysis

Edinburgh wave flume cross section

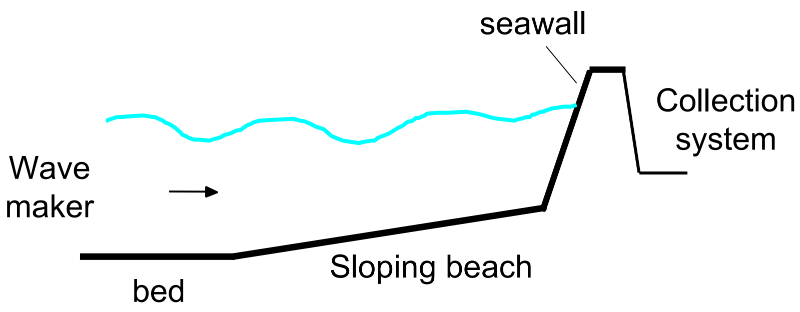

Shallow water simulations provided acceptable accuracy so go to wave basin

Manchester Metropolitan University

Centre for Mathematical Modelling and Flow Analysis

Experimental Investigation

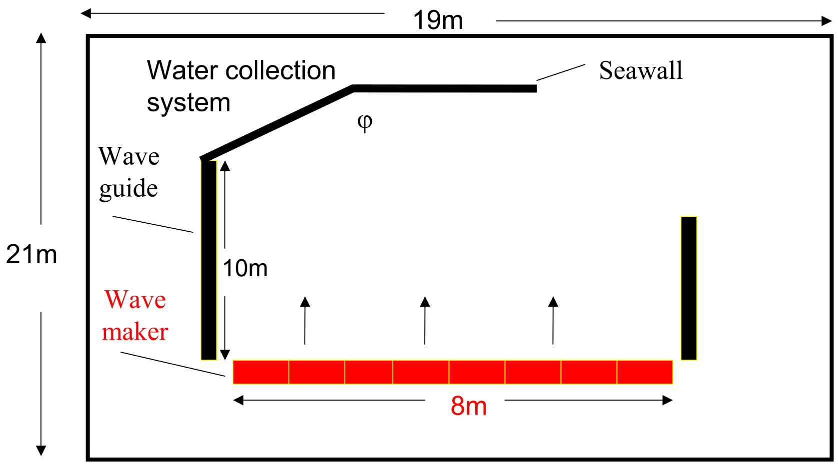

Schematic of HR Wallingford wave basin

Manchester Metropolitan University

Centre for Mathematical Modelling and Flow Analysis

Laboratory Experiments

- Wave maker: 2 blocks, 8, 0.5m units in each
- SWL: 0.425 - 0.525m
- Elbow angle j = 0, 45, 120°
- Vertical or 1:10 battered wall
- Wave Climate: Regular waves and JONSWAP: period 1.5s, wave height 0.1m
- Variable wave guide length 5 – 10m

Manchester Metropolitan University

Centre for Mathematical Modelling and Flow Analysis

Advice to Experimentalists

- Effect of gap between wave maker and wave guides - leakage
- Wave guide length to balance
  - Diffraction (around corners)
  - Reflection (from wall and sides)
- **Wave heights at seawall**
- **Where to expect overtopping**

Manchester Metropolitan University

Centre for Mathematical Modelling and Flow Analysis

Numerical Simulation of Wave Basin: AMAZON-CC

- Shallow Water Equations
  - provide a basic 2D (Plan) model of the wave basin and qualitative flow features (*but not strictly correct!*)
- Cartesian **C**ut **C**ell Method
  - **Automatic** boundary fitting mesh generation
  - **Moving** boundary to simulate wave maker
- Surface Gradient Method (SGM) is used for bed topography

Manchester Metropolitan University

Centre for Mathematical Modelling and Flow Analysis

Cut Cell Method

Input co-ordinates of solid boundary

solid boundary

Manchester Metropolitan University

Centre for Mathematical Modelling and Flow Analysis

Cut Cell Method

overlay Cartesian grid

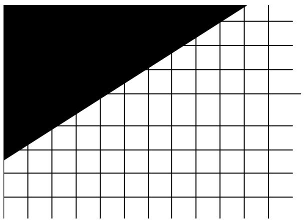

Manchester Metropolitan University

Centre for Mathematical Modelling and Flow Analysis

Cut Cell Method

Calculate where the solid boundary cuts through the background Cartesian mesh

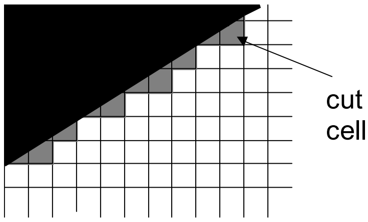

Boundary fitted mesh with cut cells

Manchester Metropolitan University

Centre for Mathematical Modelling and Flow Analysis

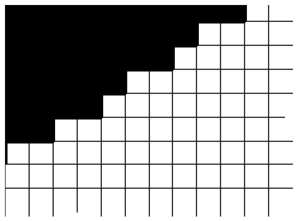

In contrast … the classical Cartesian grid …
uses a saw tooth representation of the boundary

Manchester Metropolitan University

Centre for Mathematical Modelling and Flow Analysis

Cut cells work for *any* domain

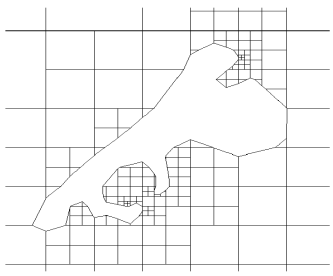

e.g. (adaptive) cut cell grid for an island geometry

Manchester Metropolitan University

Centre for Mathematical Modelling and Flow Analysis

Also work for *moving* bodies:

e.g. wave maker paddles

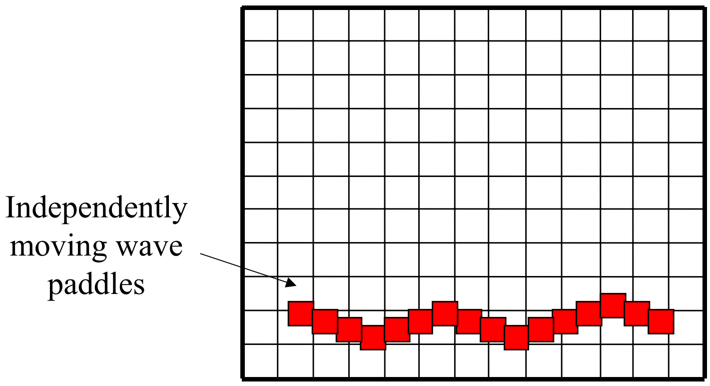

Manchester Metropolitan University

Centre for Mathematical Modelling and Flow Analysis

AMAZON-CC: numerical wave paddle using cut cells

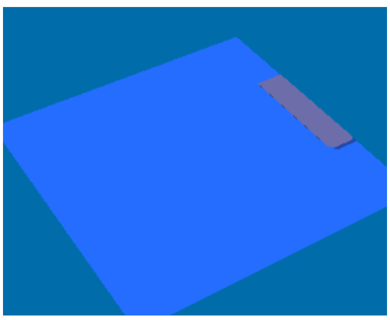

Manchester Metropolitan University

Centre for Mathematical Modelling and Flow Analysis

Numerical Wave basin

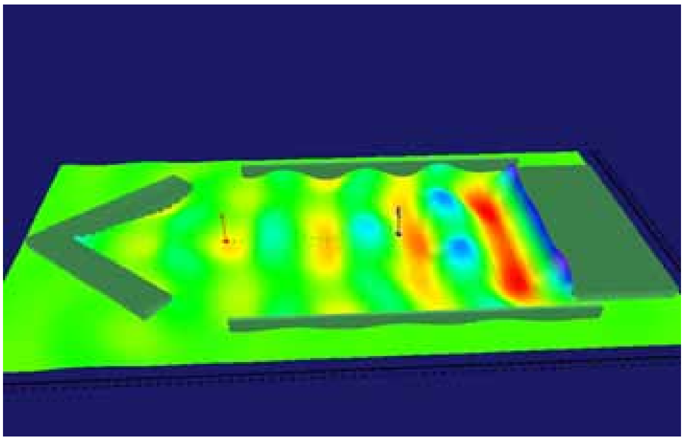

Wave interaction with a cranked sea wall geometry

Manchester Metropolitan University

Centre for Mathematical Modelling and Flow Analysis

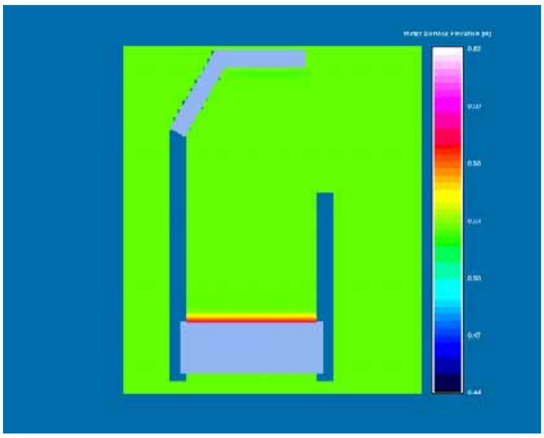

Numerical simulation of wave seawall interaction

Centre for Mathematical Modelling and Flow Analysis

Manchester Metropolitan University

AMAZON-SC: Numerical Wave Flume

- Two fluid (air/water), boundary conforming, time accurate, conservation law based, flow code utilising the surface capturing approach.
- Cartesian cut cells are used to boundary-fit coastal structures and bathymetry.

Centre for Mathematical Modelling and Flow Analysis

Manchester Metropolitan University

Multi-fluid Model

- Incompressible Navier-Stokes solver — Based on an artificial compressibility solver.
- Surface-capturing method
  - Treats the free surface as a contact discontinuity in the density field, allowing the use of modern high resolution "shock capturing" methods.
- Fully two phase approach which solves the flow equations in **both** air and water.

Manchester Metropolitan University

Centre for Mathematical Modelling and Flow Analysis

Governing equations

2D incompressible, Euler equations with variable density.

$$\frac{\partial}{\partial t}\iint_{\Omega}\mathbf{Q}\partial\Omega + \oint_{S}\mathbf{F}.\mathbf{n}\partial s = \iint_{\Omega}\mathbf{B}\partial\Omega$$

where

$$\mathbf{Q} = \begin{bmatrix}\rho & \rho u & \rho v & \dfrac{p}{\beta}\end{bmatrix}^T, \mathbf{F} = \mathbf{f}^I n_x + \mathbf{g}^I n_y, \mathbf{B} = \begin{bmatrix}0 & 0 & -\rho g & 0\end{bmatrix}^T$$

$$\mathbf{f}^I = \begin{bmatrix}\rho u & \rho u^2 + p & \rho uv & u\end{bmatrix}^T \text{ and } \mathbf{g}^I = \begin{bmatrix}\rho u & \rho uv & \rho v^2 + p & v\end{bmatrix}^T$$

β is the coefficient of artificial compressibility

Manchester Metropolitan University

Centre for Mathematical Modelling and Flow Analysis

Discretisation

- The equations are discretised using a **finite volume** formulation

$$\frac{\partial \mathbf{Q}_i V_i}{\partial t} = -\sum_{j=k(i)}\mathbf{F}_{ij}\Delta l_j + \mathbf{B}V_{ij} = -R(\mathbf{Q}_i)$$

Where $\mathbf{Q}_i$ is the average value of $\mathbf{Q}$ in cell i (stored at cell centres), V_i is the volume of the cell, $\mathbf{F}_{ij}$ is the numerical flux **across the interface** between cells i and j and and Δl_j is the length of cell side j.

Manchester Metropolitan University

Centre for Mathematical Modelling and Flow Analysis

Convective fluxes

- The convective flux ($\mathbf{F}_{ij}$) is evaluated using Roe's approximate Riemann solver.

$$\mathbf{F}_{ij}^{I} = \tfrac{1}{2}\left[\mathbf{F}^{I}\left(\mathbf{Q}_{ij}^{+}\right) + \mathbf{F}^{I}\left(\mathbf{Q}_{ij}^{-}\right) - \mathbf{R}\left|\Lambda\right|\mathbf{L}(\mathbf{Q}_{ij}^{+} - \mathbf{Q}_{ij}^{-})\right]$$

- To ensure *second order accuracy*, MUSCL reconstruction is used to get cell interface data

$$\mathbf{Q}(x,y) = \mathbf{Q}_{ij} + \Delta\mathbf{Q}_{ij}\cdot\mathbf{r}$$

where (x,y) is a point inside the cell ij, $\mathbf{r}$ is the coordinate vector of (x,y) relative to ij and $\Delta\mathbf{Q}_{ij}$ is a slope limited gradient.

Manchester Metropolitan University

Centre for Mathematical Modelling and Flow Analysis

Time discretisation

The implicit backward Euler scheme is used together with an artificial time variable *t* (to ensure a divergence free velocity field) and linearised RHS.

$$\left[I_m V + \frac{\partial R(\mathbf{Q}^{n+1,m})}{\partial \mathbf{Q}}\right]\left(\mathbf{Q}^{n+1,m+1} - \mathbf{Q}^{n+1,m}\right) =$$

$$-\left[I_{ta}\frac{\left(\mathbf{Q}^{n+1,m} - \mathbf{Q}^{n,m}\right)V}{\Delta t} + R\left(\mathbf{Q}^{n+1,m}\right)\right]$$

where $I_m = diag\left[\frac{1}{\Delta\tau} + \frac{1}{\Delta t} \quad \frac{1}{\Delta\tau} + \frac{1}{\Delta t} \quad \frac{1}{\Delta\tau} + \frac{1}{\Delta t} \quad \frac{1}{\Delta\tau}\right]$

The resulting system is solved using an approximate LU factorisation.

Manchester Metropolitan University

Centre for Mathematical Modelling and Flow Analysis

Computer Implementation

- A Jameson-type dual time iteration is used to eliminate τ at each real (outer) iteration.
- The code vectorises efficiently with simulations typically taking about three hours to run on an NEC SX6i deskside supercomputer.

Manchester Metropolitan University

Centre for Mathematical Modelling and Flow Analysis

Bench-Mark Test Cases

- Low amplitude sloshing (not shown)
- Collapsing water column with an obstacle
- Regular wave propagation

Manchester Metropolitan University

Centre for Mathematical Modelling and Flow Analysis

Collapsing water column flowing over an obstacle

Water flows to the right and inundates the obstacle then impacts on the right hand wall.

Displaced air escapes upwards and the water falls to the floor on the other side of the obstacle.

Comparisons with experiments conducted by Koshizuka et al. (1995).

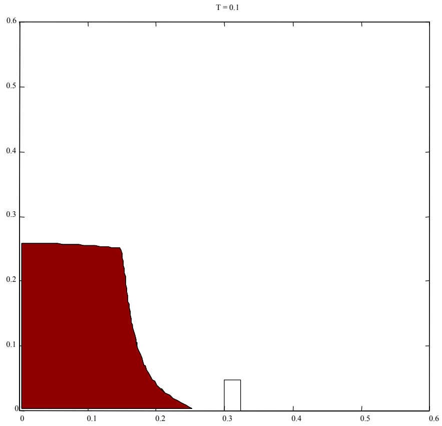

Manchester Metropolitan University

Centre for Mathematical Modelling and Flow Analysis

Collapsing water column flowing over an obstacle

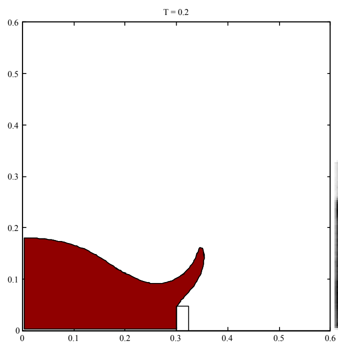

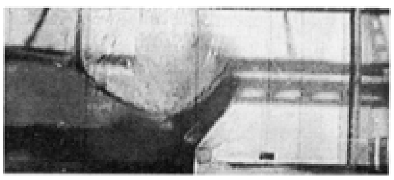

computation

experiment

Centre for Mathematical Modelling and Flow Analysis

Manchester Metropolitan University

Collapsing water column flowing over an obstacle

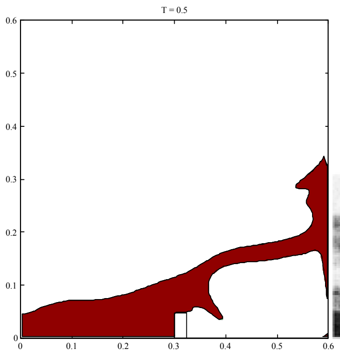

computation

experiment

Centre for Mathematical Modelling and Flow Analysis

Manchester Metropolitan University

Boundary Conditions

- **Seaward boundary** – a velocity controlled procedure is used to generate waves, velocities are either computed from linear wave theory using JONSWAP spectra or specified based on shallow water simulations.

- **Atmospheric boundary** – a constant atmospheric pressure gradient is applied. Spray and water passing out of this boundary are lost from the computation.

- **Landward boundary** – a solid wall boundary condition is used at the landward end of the domain.

- **Seawalls and beaches** – modelled using Cartesian cut cells.

Manchester Metropolitan University

Centre for Mathematical Modelling and Flow Analysis

VOWS Wave Flume experiments

- Experimental programme conducted in the 20m wave flume in Edinburgh and the 100m wave flume at UPC, Barcelona.

- Vertical and 10:1 battered walls tested (with/without berms and recurves) on a 1:10 beach, for impulsive wave conditions ($0.03<H^*<0.10$) using 1000 random waves.

•Water is 0.09m deep at the toe of the wall and the wall has a freeboard of 0.17m.

Manchester Metropolitan University

Centre for Mathematical Modelling and Flow Analysis

VOWS Test 1A

- Wave Climate: H_s=0.063, T_m=1.23
- Sea Wall: 10:1 batter, R_h=0.1296
- Wave Conditions: h*=0.0544
- Wave gauges, sampled at 100Hz, located 1.0, 2.0, 3.0, 4.25, 5.5, 6.75, 8.0 and 11.21 metres from the seawall.
- Wall fitted with an overtopping detector and a load cell.

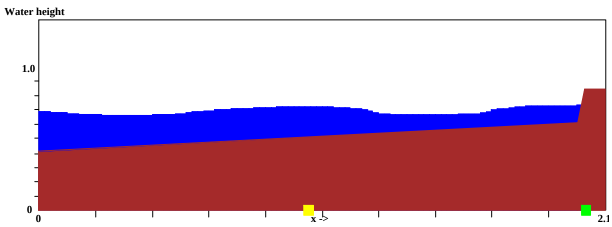

AMAZON-CC free surface simulation 2m from the seawall.

Manchester Metropolitan University

Centre for Mathematical Modelling and Flow Analysis

Seaward boundary conditions

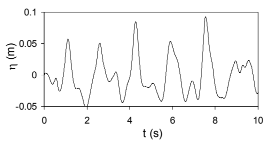

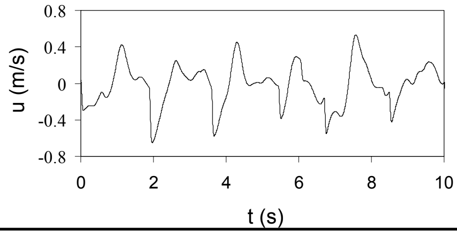

Surface elevation

- experimental wave gauge 2m from wall.

U Velocity

- Computed velocity from the Riemann invariant boundary condition of a shallow water simulation
- Applied uniformly to water column

Other variables

- p and v are extrapolated

Manchester Metropolitan University

Centre for Mathematical Modelling and Flow Analysis

AMAZON-SC simulation

- Overtopping event occurred 142 seconds into the experiment.
- Seaward boundary located 2m from wall.
- Landward boundary is transmissive.
- Assume: flat water for initial conditions.

Manchester Metropolitan University

Centre for Mathematical Modelling and Flow Analysis

Velocity vectors at t=2.75s

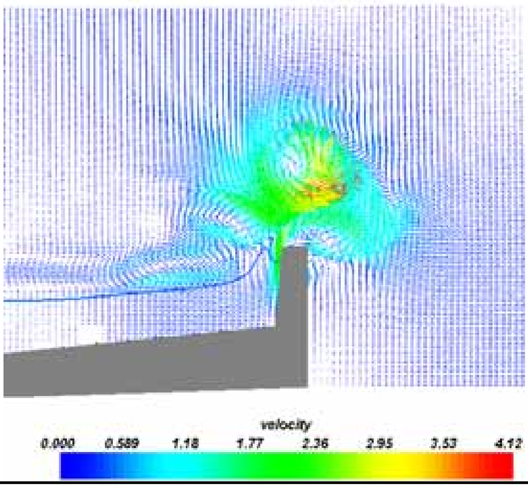

Manchester Metropolitan University

Centre for Mathematical Modelling and Flow Analysis

Water Entry of a Rigid Wedge

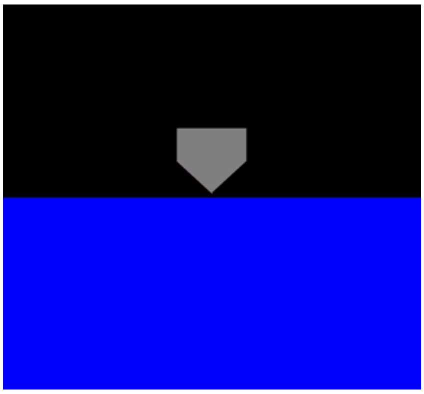

Rigid wedge moving at prescribed 1m/s with total immersion
AMAZON-SC

Manchester Metropolitan University

Centre for Mathematical Modelling and Flow Analysis

Water Entry of a Rigid Wedge

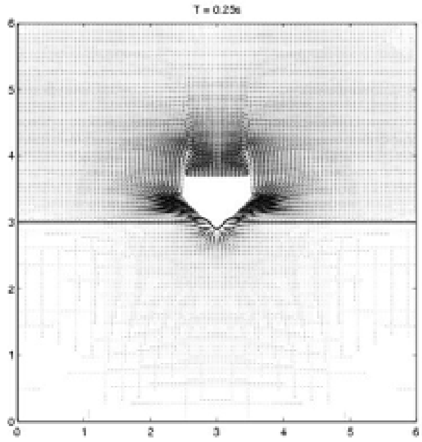

T = 0.25 s

Manchester Metropolitan University

Centre for Mathematical Modelling and Flow Analysis

Water Entry of a Rigid Wedge

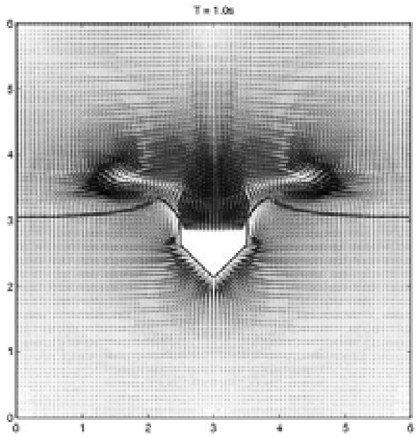

T = 1.0 s

Manchester Metropolitan University

Centre for Mathematical Modelling and Flow Analysis

Water Entry of a Rigid Wedge

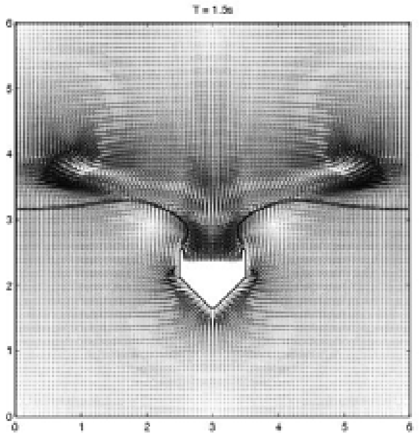

T = 1.5 s

Manchester Metropolitan University

Centre for Mathematical Modelling and Flow Analysis

Water Entry of a Rigid Wedge

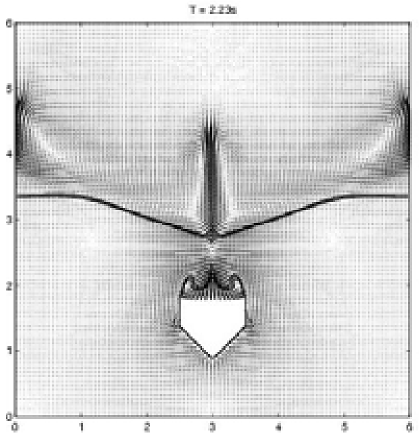

T = 2.23 s

Manchester Metropolitan University

Centre for Mathematical Modelling and Flow Analysis

Water Exit of a Rigid Wedge

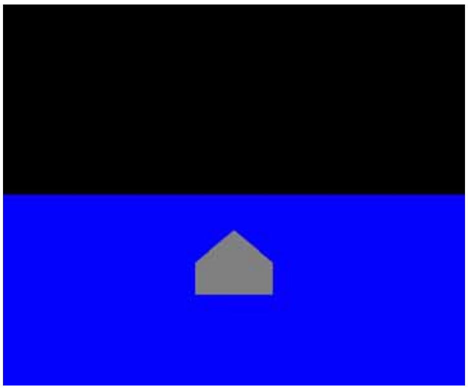

Rigid wedge moving up at prescribed 1m/s from water into air
AMAZON-SC

Manchester Metropolitan University

Centre for Mathematical Modelling and Flow Analysis

Wave Interaction with a Floating Body

- The floating body freely responds to the wave dynamics
- The body can undergo heave, sway and roll motions
- Flow conditions:

  Still water depth: H = 40 cm, Wave period : T = 1 second,
  Velocity of wave maker : U = -0.2 (1-e^(-5t)sin(2πt/T),
  Density of the square shaped body: ρ= 500 kg/m^3

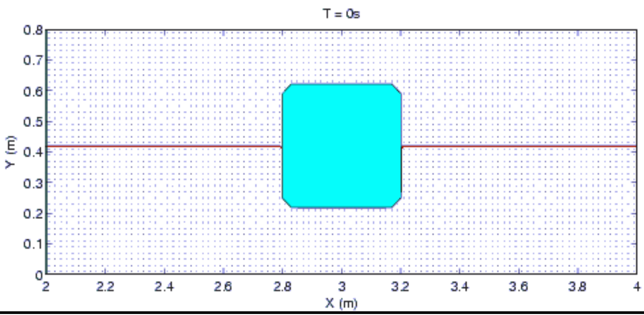

Manchester Metropolitan University

Centre for Mathematical Modelling and Flow Analysis

Preliminary 3D Results

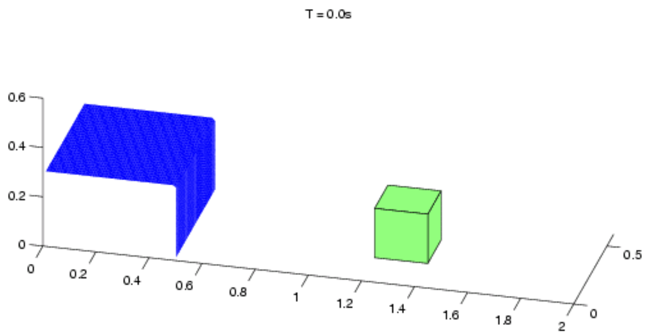

Dam break wave inundating a fixed box
AMAZON-SC3D

Manchester Metropolitan University

Centre for Mathematical Modelling and Flow Analysis

Wave Energy

Simulation of wave energy devices (with Queen's University, Belfast)

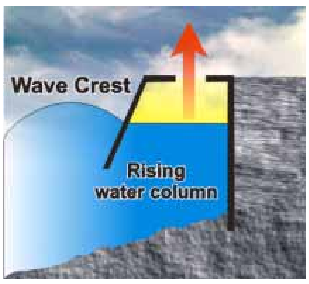

LIMPET: Oscillating Water Column (OWC)

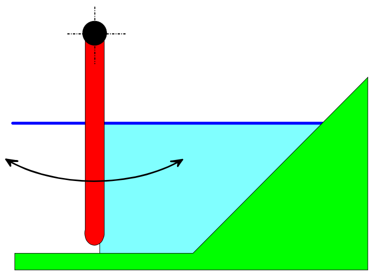

Oscillating Wave Surge Converter (OWSC)

Manchester Metropolitan University

Centre for Mathematical Modelling and Flow Analysis

Acknowledgements

Professor TJT Whittaker and Dr Matt Folley

School of Civil Engineering,
Queen's University of Belfast

Responsible for: Device design, laboratory experiments and full scale trials

Manchester Metropolitan University

Centre for Mathematical Modelling and Flow Analysis

Wave Energy

LIMPET:
500KW Station, **Islay**, **Scotland**.

First wave power station connected to the national grid, in the world.

Manchester Metropolitan University

Centre for Mathematical Modelling and Flow Analysis

Wave Energy

BRUICHLADDICH
ISLAY SINGLE MALT

LIMPET:
Supplies the town of **Portnahaven** and local industry.

Manchester Metropolitan University

Centre for Mathematical Modelling and Flow Analysis

Wave Paddle Test

Waves generated by numerical wave paddle using AMAZON-SC

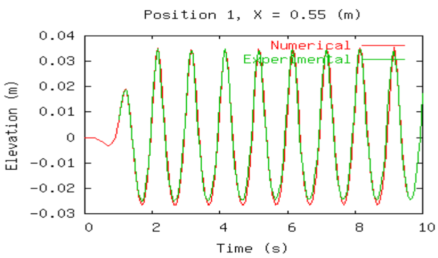

Comparison with laboratory data

Manchester Metropolitan University

Centre for Mathematical Modelling and Flow Analysis

LIMPET OWC Simulation

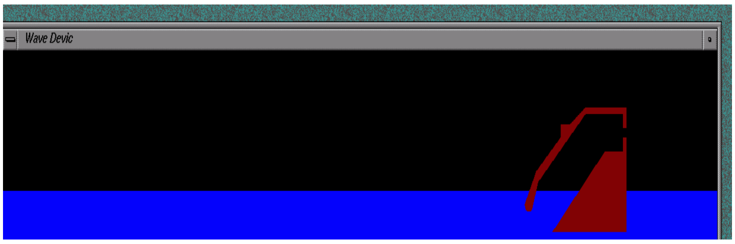

Simulation of waves interacting with LIMPET using AMAZON-SC

Manchester Metropolitan University

Centre for Mathematical Modelling and Flow Analysis

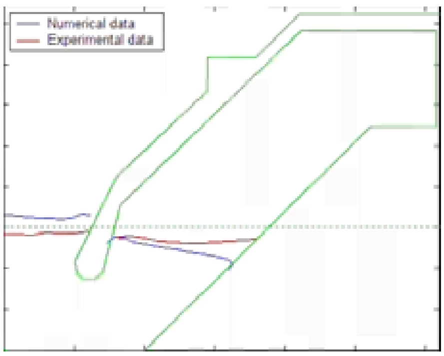

LIMPET: Comparison of experimental and simulated free surfaces

Manchester Metropolitan University

Centre for Mathematical Modelling and Flow Analysis

Oscillating wave surge converter (OWSC)

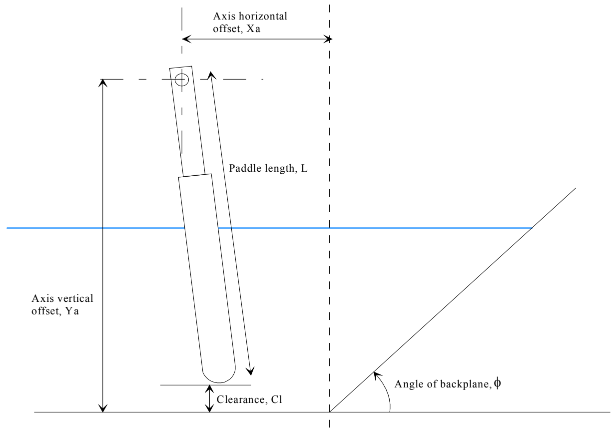

Manchester Metropolitan University

Centre for Mathematical Modelling and Flow Analysis

The Vane as a Wave Maker

Vane with *prescribed* motion in air and water using AMAZON-SC

Manchester Metropolitan University

Centre for Mathematical Modelling and Flow Analysis

The Vane as a Wave Maker

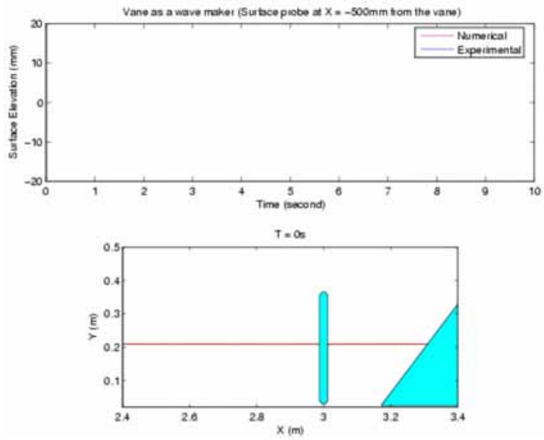

Animation showing velocity vectors and free surface position around the vane

Manchester Metropolitan University

Centre for Mathematical Modelling and Flow Analysis

OWSC Device Modelling using AMAZON-SC

The motion of the vane is derived from the forces exerted on it by the surrounding water.

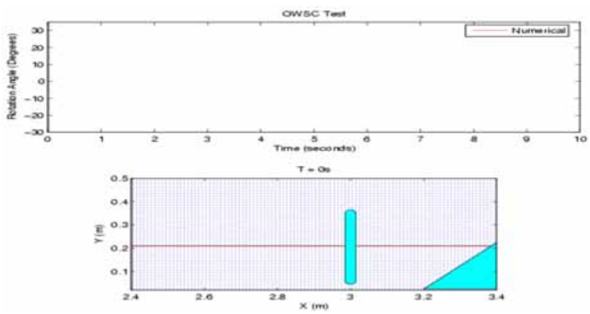

Manchester Metropolitan University

Centre for Mathematical Modelling and Flow Analysis

OWSC Device Modelling using AMAZON-SC

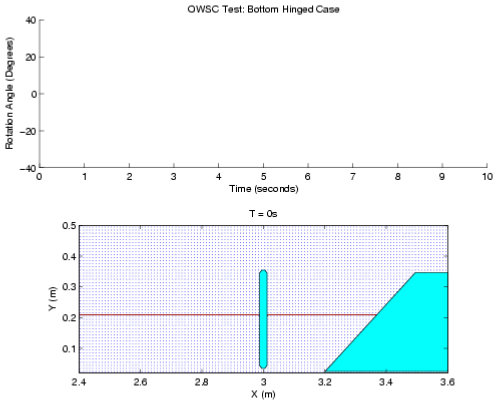

Manchester Metropolitan University

Centre for Mathematical Modelling and Flow Analysis

Future Work

- Extend AMAZON-SC to 3D and adaptive mesh refinement on high performance computers
- Apply AMAZON-CC to tsunami modelling
- Develop solvers for sediment transport and scour
- Apply AMAZON-SC to deck slam and greenwater overtopping

Manchester Metropolitan University

Centre for Mathematical Modelling and Flow Analysis

Further Details:

- http://www.docm.mmu.ac.uk/cmmfa/
- http://www.docm.mmu.ac.uk/cmmfa/project/vows.html
- http://www.owsc.ac.uk/

Manchester Metropolitan University

Centre for Mathematical Modelling and Flow Analysis

Thank you for your Attention

RIAM Symposium *7-8, November, 2006*

Comparison of Different CIP-Based Interface Capturing Methods for Sloshing Computation

Changhong HU （RIAM, Kyushu University）

CFD Model

- CFD Method for Extreme Nonlinear hydrodynamics
  - Flow solver
    - FS Method
    - Turbulence modeling
    - Fast solution method for Poisson Eq.
  - Inner interface treatment
    - Interface capturing method for free surface
      - CIP with Sharpness enhancement
      - CIP-CSL3
      - THINC
      - Surface tension modeling
    - Cartesian grid method for solid body
      - Particle method
      - Adaptive grid refinement

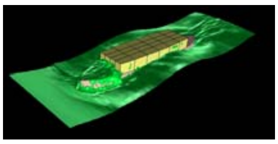

RIAM-CMEN **C**omputation **M**ethod for **E**xtremely **N**onlinear **H**ydrodynamics

A Perfect Interface Capturing Scheme

- A scheme that should be conservative and can guarantee a sharp and non-oscillatory interface

Numerous techniques have been present to

- Improve conservation of the scheme
- Limit the diffusiveness of low order schemes
- Minimize the instability of high order schemes

CIP method and its late developments seem to be a promising interface capturing scheme to satisfy these requirements

Interface Capturing Method for RIAM-CMEN

$$\frac{\partial \phi_1}{\partial t} + u_i \frac{\partial \phi_1}{\partial x_i} = 0$$

Solved by CIP based method

Sharpness enhancement

Function Transformation

$\Phi = \Phi(\phi_1)$

$$\frac{\partial \Phi}{\partial t} + u_i \frac{\partial \Phi}{\partial x_i} = 0$$

Profile modification

CIP-CSL3

THINC

- $\Phi(\phi_1) = \tan\left[(1-\varepsilon)\pi(\phi_1 - 0.5)\right]$
- $\Phi(\phi_1) = 0.5 + \alpha(\phi_1 - 0.5)$

CIP based Interface Capturing Methods for Comparison

(1) Original CIP	➢ CIP
(2) CIP/Tangent Transformation	➢ CIP-TT
(3) CIP/Linear Transformation	➢ CIP-LT
(4) CIP-CSL3	➢ CIP-CSL3
(5) THINC	➢ THINC

(1) Original CIP

1-D Advection equation $\frac{\partial \phi}{\partial t} + u\frac{\partial \phi}{\partial x} = 0$

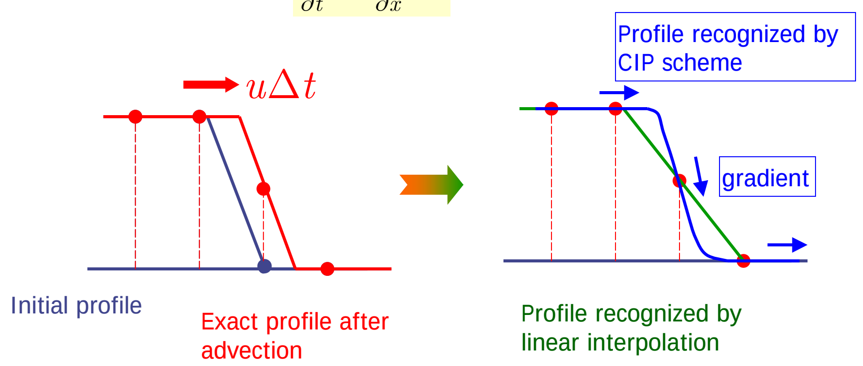

Use both ϕ and $\phi_x = \partial\phi/\partial x$ for advection calculation

$$\frac{\partial \phi_x}{\partial t} + u\frac{\partial \phi_x}{\partial x} = -\frac{\partial u}{\partial x}\phi_x$$

Additional equation

(1) Original CIP - *continue*

Profile inside a cell can be reconstructed by the four constraints

$$F_i^n(x) = a_i(x - x_i)^3 + b_i(x - x_i)^2 + c_i(x - x_i) + d_i$$

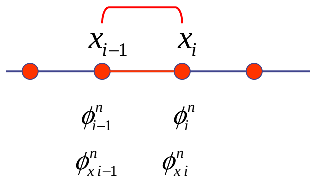

4 unknown coefficients

4 Constrained conditions

Semi-Lagrangian Scheme

$$\begin{cases} \phi_i^{n+1} = \phi^n(x_i, \Delta t) = F^n(x_i - u\Delta t) \\ \phi_{x i}^{n+1} = \dfrac{d\phi^n(x_i, \Delta t)}{dx} = \dfrac{dF^n(x_i - u\Delta t)}{dx} \end{cases}$$

High-order scheme can be obtained using Less grid points

(2) CIP-TT : CIP/Tangent Transformation

$$\frac{\partial \phi}{\partial t} + u_i \frac{\partial \phi}{\partial x_i} = 0$$

$$F(\phi) = \tan[s\pi(\phi - 0.5)]$$

$$\frac{\partial F(\phi)}{\partial t} + u_i \frac{\partial F(\phi)}{\partial x_i} = 0$$

$$\phi = arc\tan F(\phi)/s\pi + 0.5$$

At Interface

ϕ rapid change

$F(\phi)$ regular behavior

better spatial resolution

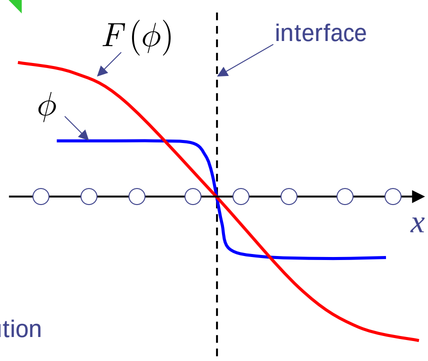

(3) CIP-LT : CIP/Linear Transformation

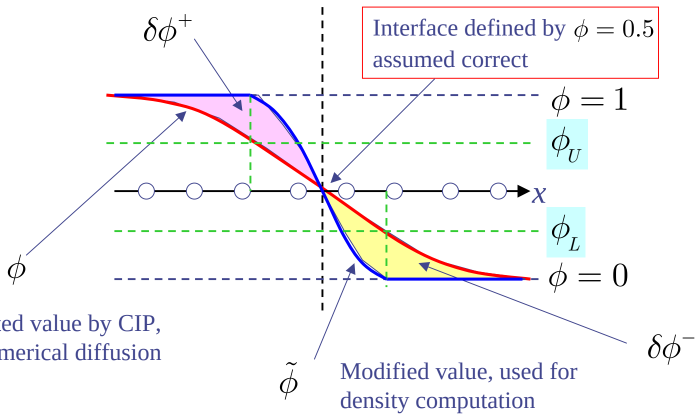

$$\tilde{\phi} = \begin{cases} 1.0 & if\ \phi \ge \phi_U \\ 0.0 & if\ \phi \le \phi_L \\ 0.5 + \alpha(\phi - 0.5) & if\ \phi_L < \phi < \phi_U \end{cases}$$

$$\alpha = \begin{cases} 0.5/(0.5 - \phi_L) & if\ \phi < 0.5 \\ 0.5/(\phi_U - 0.5) & if\ \phi \ge 0.5 \end{cases}$$

satisfy $\sum(\delta\phi^+ + \delta\phi^-) = 0$

(4) CIP-CSL3 : Conservative Semi-Lagrangian scheme with 3rd-order polynomial function

- Using cell averaged value as additional constraint to reconstruct profile

Conservative form :

$$\frac{\partial \phi}{\partial t} + \frac{\partial (u\phi)}{\partial x} = \phi \frac{\partial u}{\partial x}$$

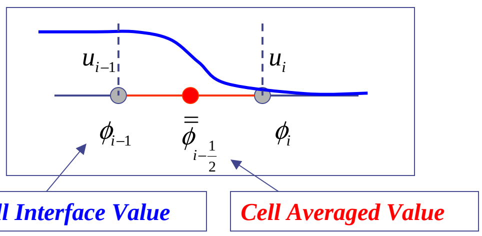

Volume Integrated Average

$$\frac{\bar{\bar{\phi}}^{n+1}_{i-1/2} - \bar{\bar{\phi}}^{n}_{i-1/2}}{\Delta t} + \frac{1}{\Delta x}(u_i\phi_i - u_{i-1}\phi_{i-1}) = 0$$

Conservation guaranteed scheme

Surface Integrated Average

$$\frac{\partial \phi}{\partial t} + u\frac{\partial \phi}{\partial x} = 0$$

Determined by interpolation method

(4) CIP-CSL3 - *continue*

Cubic interpolation function

$$\Phi^n(x) = a_m(x - x_m)^3 + b_m(x - x_m)^2 + c_m(x - x_m) + d_m$$

approximate interpolation function of ϕ

4 unknown coefficients

3 Constrained conditions

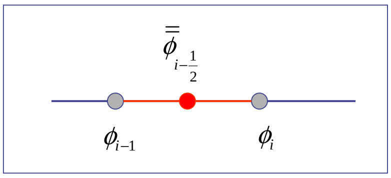

The 4th constrained condition : **Slope of profile** $\lambda_{m+\frac{1}{2}}$ Free parameter!

provides us a way to reduce numerical diffusion **and to** suppress numerical oscillation **by modifying the interpolation function**

(5) THINC (Tangent of Hyperbola for INterface Capturing)

- Similar concept to CIP-CSL3

1-D case

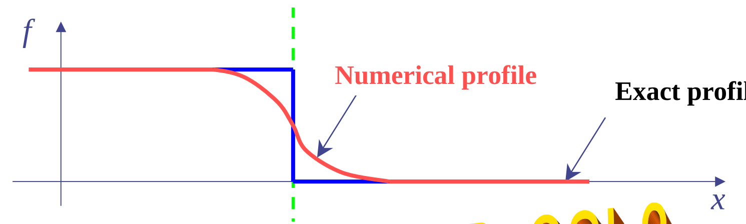

Cubic interpolation function $\Phi_m(x) = a_m(\ldots (x - x_m) + d_m$

CIP-CSL3

Hyperbolic tangent function $\Phi_m(x) = \frac{\alpha}{2}\{1 \ldots \}$

THINC

Test Example: A Tank Sloshing Experiment

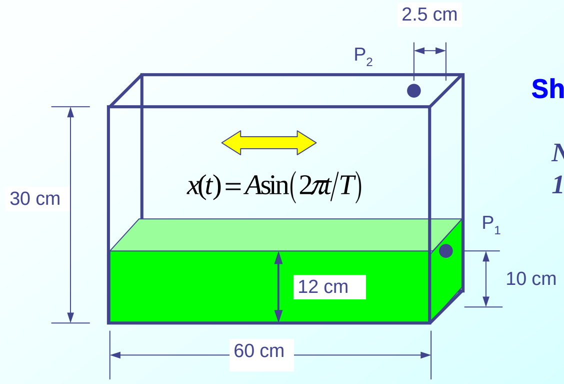

Shallow Water Sloshing

Natural period between
1.3 sec - 1.4sec

A=5cm T = 1.30 sec

Computation
Uniform mesh: 200 x 100

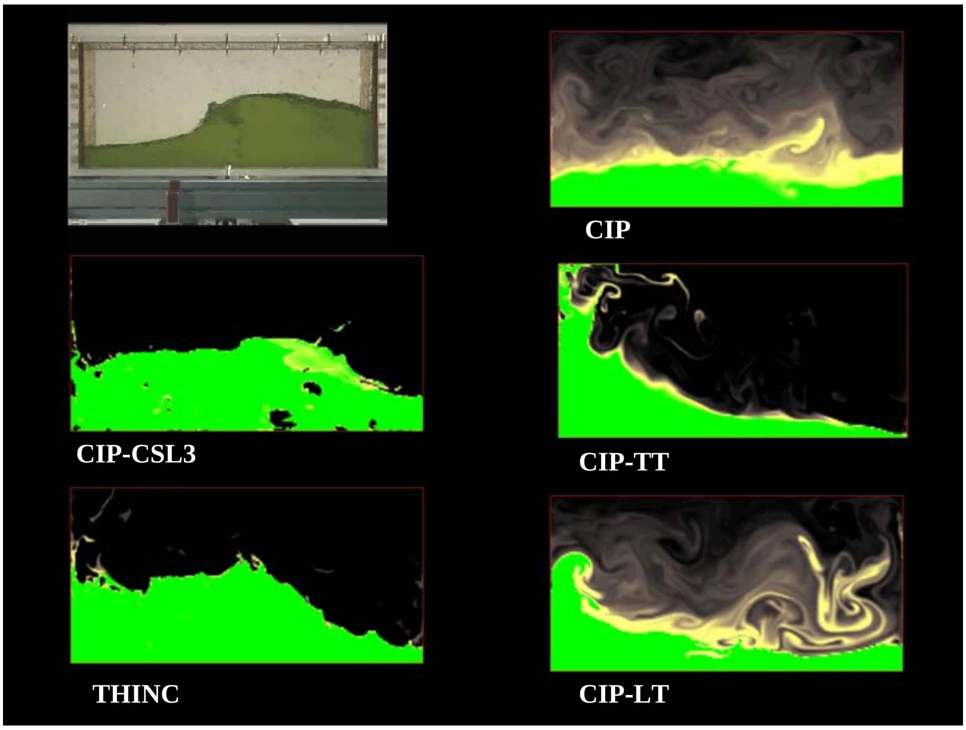

Comparison of Free Surface

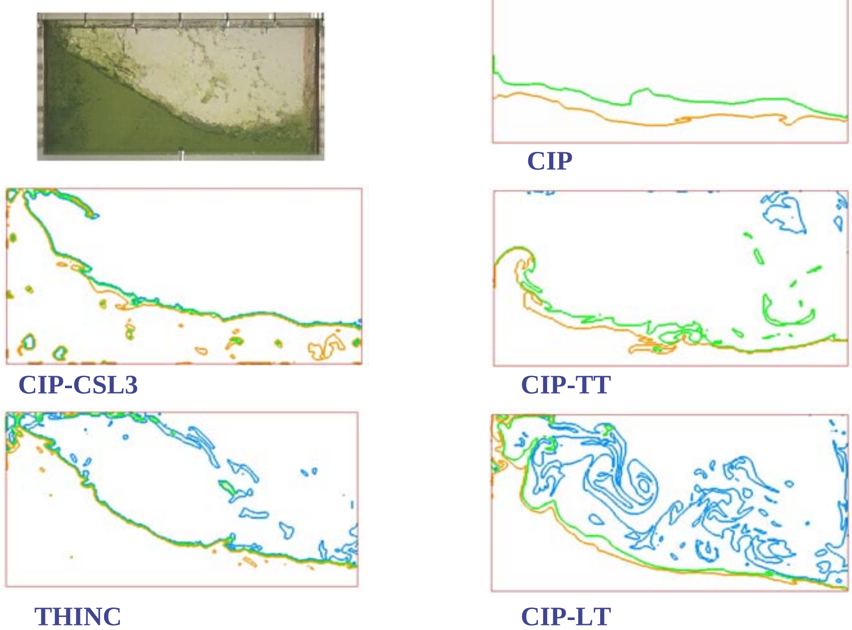

Comparison of Mass Conservation

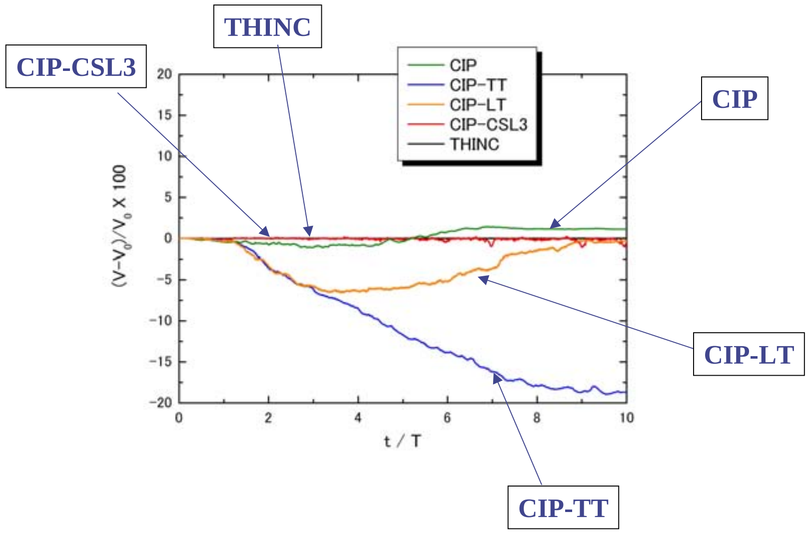

Pressure at Side Wall

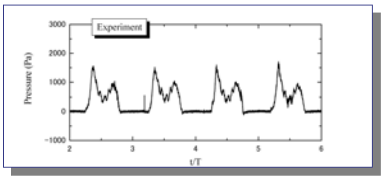

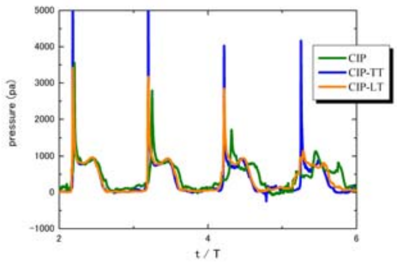

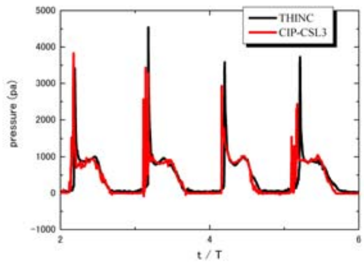

Pressure at Roof

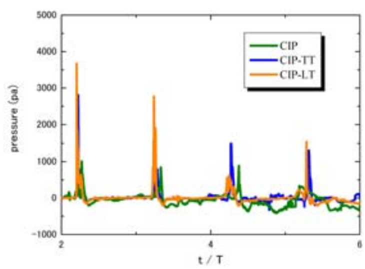

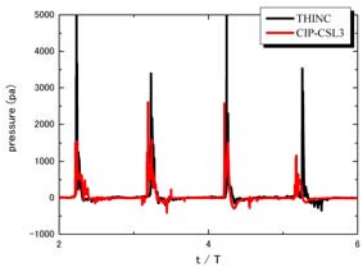

CONCLUSION

Sharpness preservation

THINC = CIP-CSL3 > CIP-TT > CIP-LT > CIP

Mass conservation

THINC > CIP-CSL3 >> CIP > CIP-LT > CIP-TT

Simplicity in Scheme

CIP > CIP-TT > CIP-LT >> THINC > CIP-CSL3

Numerical Simulation of Flow and Motion of Underwater Vehicle with Mechanical Pectoral Fin Devices

Hiroyoshi Suzuki, Naomi Kato

**Graduate School of Engineering,
Osaka University,
Osaka, Japan**

Background

- It is promising to use the pectoral fins as propulsion devices and /or control devices for an underwater vehicle(UV) from the view -point of its maneuverability.

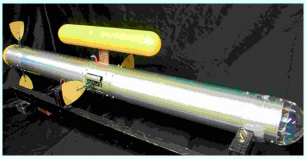

- The optimum design for an underwater vehicle varies depending on factors such as the missions and the environments, and it requires considerable cost and time to develop such optimum vehicle on the basis of experiments.
- We began to develop a numerical motion simulator for an underwater vehicle equipped with mechanical pectoral fins.

Objective

- To investigate hydrodynamic characteristics of the mechanical pectoral fin device.
- To develop a CFD-based motion simulator which consisted from a CFD code and an equation of motion solver.
- To simulate basic motions of the UV using above simulator.

Mechanical Pectoral Fin Device -BIRDFIN

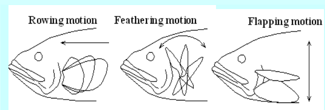

Motion of Pectoral Fin

$$\begin{cases} \phi_R = \phi_{R0} - \phi_{RA} \cdot \cos(\omega_{fin} \cdot t) \\ \phi_{FE} = \phi_{FE0} - \phi_{FEA} \cdot \cos(\omega_{fin} \cdot t + \Delta\phi_{FE}) \\ \phi_{FL} = \phi_{FE0} - \phi_{FEA} \cdot \cos(\omega_{fin} \cdot t + \Delta\phi_{FL}) \end{cases}$$

ϕ_R : *Rowing angle,*

ϕ_{FE} :*Feathering angle*

ϕ_{FL} :*Flapping angle*

Definitions of fin motion

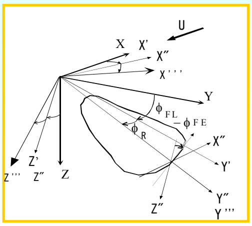

Coordinate system

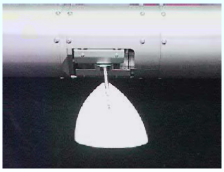

Mechanical pectoral fin device

Motion Pattern of Pectoral Fin

Drag-based swimming mode

Rowing motion of pectoral fins forming a high angle in relations to the horizontal axis of the fish body

Lift-based swimming mode

Flapping motion of pectoral fins forming a small angle to the horizontal axis of the fish body

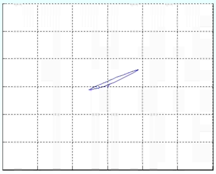

Numerical Methods/Conditions -BIRDFIN

Numerical Methods

- Overlapping grid method
- Discretization : 12pts. Finite analytic method
- V-P coupling : PISO type 1step procedure
- Unsteady method: dual-time-stepping (pseudo time iteration)

Conditions

•Uniform flow

•Rn =20,000 (=UC/ν;Reynolds number)

•K =4 (= $2\pi fC/U$;Reduced Frequency)

U=0.251m/s、f=2Hz(T=0.5sec)

C:Chord length(0.08m)

•Fin shape: asymmetrical

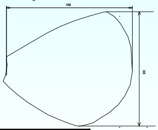

•Angular parameter

ϕ_{R0}	ϕ_{RA}	ϕ_{FE0}	ϕ_{FEA}	$\Delta\phi_{FE}$	ϕ_{FLA}	$\Delta\phi_{FL}$
0°	0°	-90°	30°	30°	30°	0,30,60,90°

Computational Grids

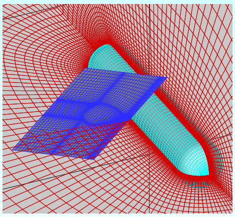

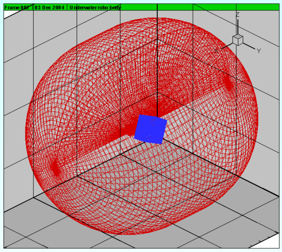

- Grid topology, Number of grids and Minimum grid spacing
  - Grid system around the body(Main solution domain): O-O type, 80×61×63, 0.0001(on the body)
  - Grid system around the fin(Sub solution domain) : H-H type , 57×49×42, 0.001(on the fin)

Computed Fin Motions

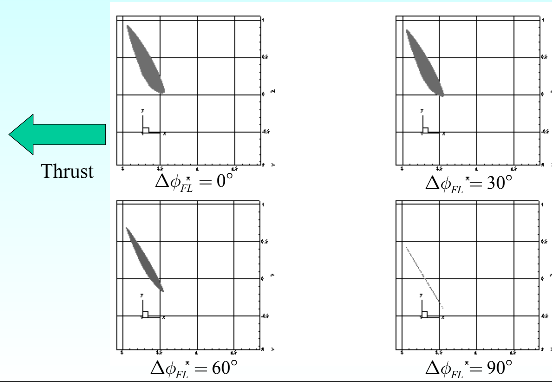

Computational Results

1.Time-averaged Hydrodynamic Force Coefficients

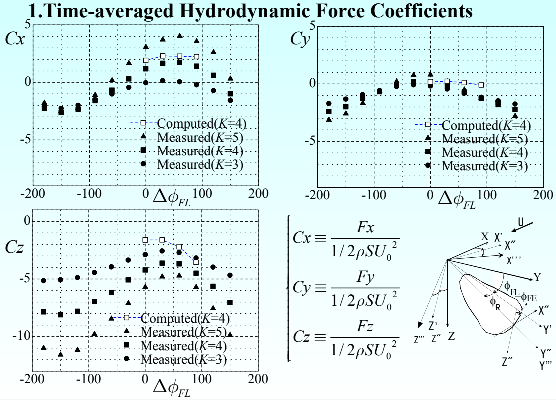

$$Cx \equiv \frac{Fx}{1/2\rho S U_0^2}, \quad Cy \equiv \frac{Fy}{1/2\rho S U_0^2}, \quad Cz \equiv \frac{Fz}{1/2\rho S U_0^2}$$

Computational Results $\Delta\phi_{FL}=0°$

2.Time-varied Hydrodynamic Force Coefficients

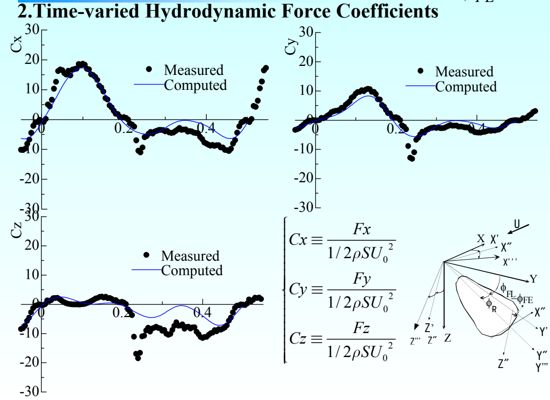

$$Cx \equiv \frac{Fx}{1/2\rho S U_0^2}, \quad Cy \equiv \frac{Fy}{1/2\rho S U_0^2}, \quad Cz \equiv \frac{Fz}{1/2\rho S U_0^2}$$

Computational Results $\Delta\phi_{FL}=0°$

3.Pressure distributions on the fin surface

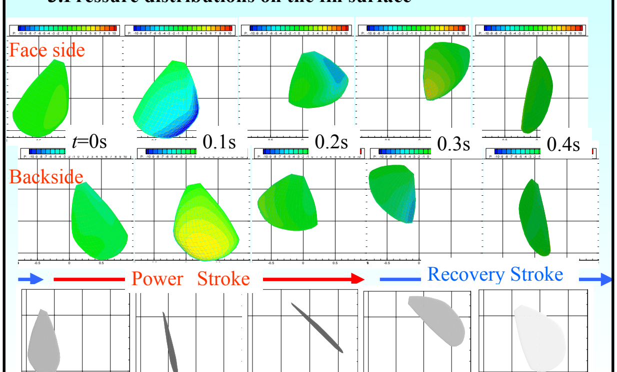

Computational Results $\Delta\phi_{FL}=0°$

5.Vorticity and Pressure distribution near/on the fin surface

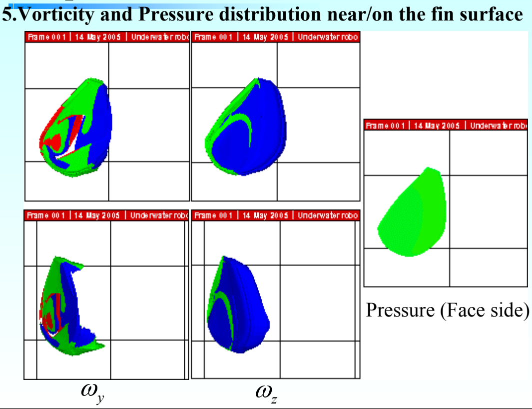

Flow Visualization

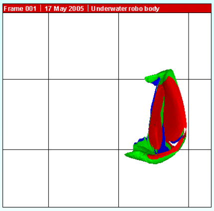

ω_y

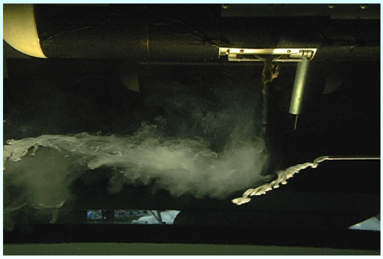

Underwater Vehicle "PLATYPUS"

Specifications of PLATYPUS

- Length: 1.36 m
- Diameter: 0.12 m
- Weight: 14.5 Kgf
- CPU, Attitude Sensors
- Motion Sensors of BIRDFIN
- Force Sensors on BIRDFIN
- Acoustic Localizing Device

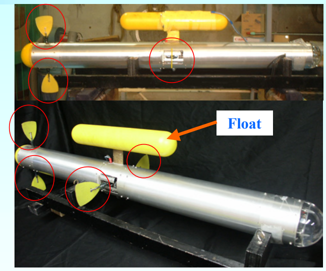

Specification of the Fin

Chord length of 0.1 m

Span of 0.008m

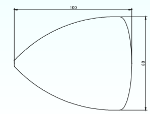

Computational Grids(PLATYPUS)

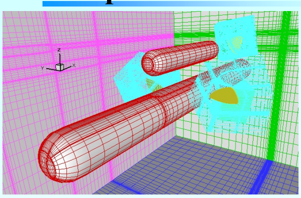

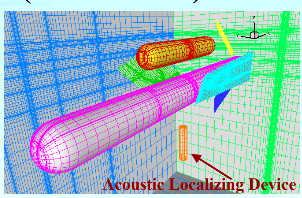

Hydrodynamic force computation　　Motion simulation

- Grid topology, Number of grids and Minimum grid spacing
  - Grid system around the fuselage with float(Main solution domain)
    - For Hydrodynamic force computation
      - » H-H type, 95×69×71, 0.0001(on the fuselage and the float)
    - For Motion Simulation
      - » H-H type, 126×69×95, 0.0001(on the fuselage and the float)
  - Grid system around the each fin (Sub solution domain) :
    - » H-H type , 49×49×32, 0.001(on the fin)

Computational Conditions

-Hydrodynamic Force Computation/motion Simulation

Numerical Methods: Same as the method for BIRDFIN

Conditions

Hydordynamic force Computation

- Rn =10,000 (=UC/ν;Reynolds number)
- K =4 (= $2\pi fC/U$;Reduced Frequency)
- U=0.0125m/s、f=1Hz(T=1.0sec)

•Fin shape: symmetrical

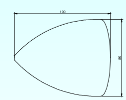

Motion Simulation

- Rn =20,000　•BG=0mm,24.8mm
- K =4

Angular parameters

Hydrodynamic force computation　Motion simulation

	ϕ_{R0}	ϕ_{RA}	ϕ_{FE0}	ϕ_{FEA}	$\Delta\phi_{FE}$	ϕ_{FLA}	$\Delta\phi_{FL}$	$\Delta\phi_{FL}$
Drag-based	0°	0°	-90°	30°	30°	30°	0,60°	0°
Lift-based	30°	30°	30°	30°	90°	20°	0,60°	60°

Computational Results

-Time-averaged Hydrodynamic Force Coefficients per fin

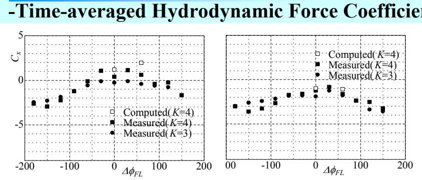

(a) Drag-based swimming mode

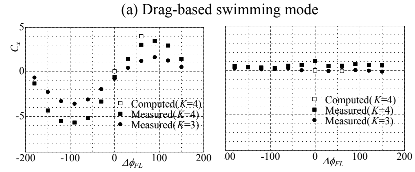

(b) Lift-based swimming mode

$$Cx \equiv \frac{Thrust/4}{1/2\rho S U_0^2}$$

$$Cy \equiv \frac{Fy/4}{1/2\rho S U_0^2}$$

$\Delta\phi_{FL}$:the phase differences between rowing and flapping motion

Simulation of Motion (Governing Eqs.)

Navier-Stokes Equation (fluid)

in body-fixed coordinate system

$$\begin{cases} \dfrac{\partial \mathbf{u}}{\partial t} + (\mathbf{u} \bullet \nabla)\mathbf{u} = -\nabla p + \dfrac{1}{Rn}\Delta \mathbf{u} + \boxed{\mathbf{K}} \\ \quad \mathbf{K} = -2\boldsymbol{\omega} \times \mathbf{u} - \boldsymbol{\omega} \times (\boldsymbol{\omega} \times \mathbf{r}) - \dfrac{d\boldsymbol{\omega}}{dt} \times \mathbf{r} - \dfrac{d\mathbf{V}}{dt} \\ \nabla \bullet \mathbf{u} = 0 \end{cases}$$

Equation of Motion

in body-fixed coordinate system

$$\begin{cases} m\left(\dfrac{d^*}{dt}\mathbf{V} + \boldsymbol{\omega} \times \mathbf{V}\right) = \mathbf{F} \\ \dfrac{d^*}{dt}(\mathbf{I}_0 \bullet \boldsymbol{\omega}) + \boldsymbol{\omega} \times (\mathbf{I}_0 \bullet \boldsymbol{\omega}) = \mathbf{G} \end{cases}$$

K : Body force which represents the effect of motion of the vehicle such as a Coriolis force
r :the position vector in body-fixed coordinate system
ω :the angular velocity vector of the vehicle
V :the velocity of the center of gravity of the vehicle
F :the hydrodynamic forces acting on the vehicle
G :the moment acting of the vehicle
$\mathbf{I}_0$:the inertia tensor oh the vehicle about body-fixed coordinate system

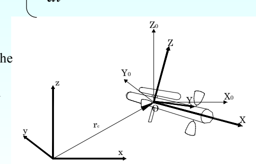

Space-fixed, Translation, Body-fixed coordinate system

Coordinate System

Motion in Experiment (Lift-based swimming mode)

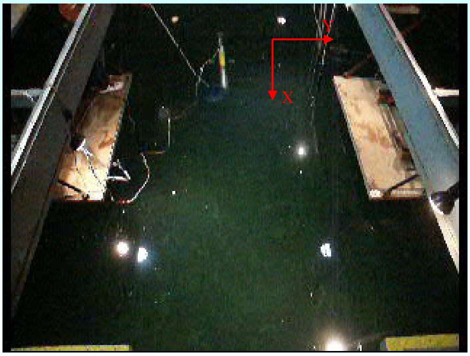

Computational Results BG=0mm

– Motion simulation (Lift-based swimming mode)

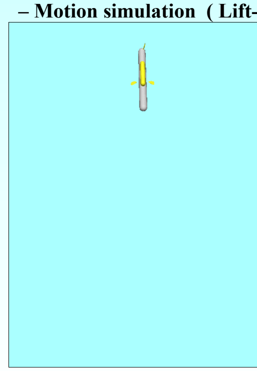

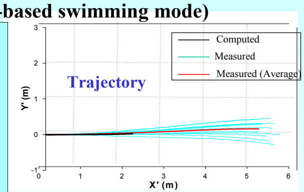

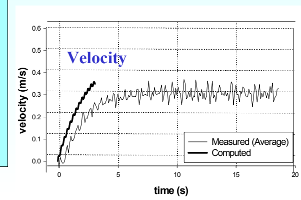

Motion in experiment (Drag-based swimming mode)

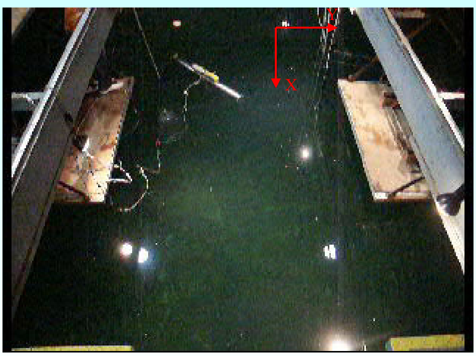

Computational Results BG=0mm

–Motion simulation (Drag-based swimming mode)

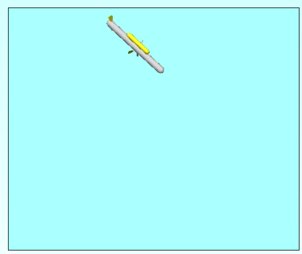

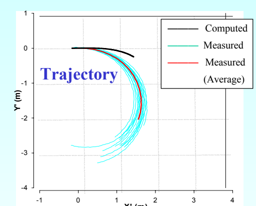

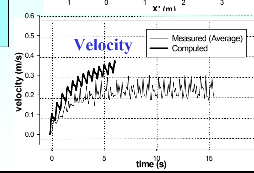

Computational Results(drag-based Swimming Mode)

-Difference of BG(— BG=24.8mm,— BG=0mm)

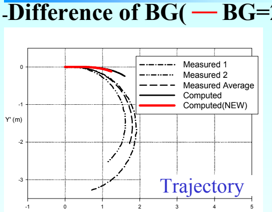

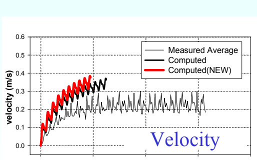

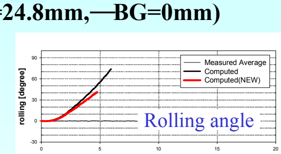

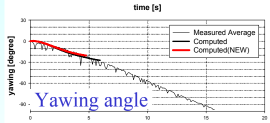

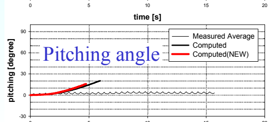

Summary(1/2)

1. An unsteady, multi-block, overlapping grid Navier-Stokes equation solver was developed and applied to solve the unsteady flow around a mechanical pectoral fin and UV named PLATYPUS.
2. The computed time-averaged and time-varied hydrodynamic force coefficients showed good agreement with the experimental results.
3. The variations in hydrodynamic force coefficients due to the phase differences could be resolved.
4. It was confirmed that the pressure distribution on the fin is closely related to the vortex phenomena in the flow field from the flow visualization and computational results.

Summary(2/2)

5. The simulations of motion of the UV were carried out.
6. The simulated and measured motions showed a similar tendency.
7. The computed velocities of the underwater vehicle were overestimated because of the overestimation of the thrust and the underestimation of the drag.
8. Stability was not sufficient in the computation, Some problems may occur in the computational code.

Future Plan

Improvement of the motion simulator

- Stability
- Computational accuracy
- Speed-up of CPU time

Numerical Prediction of Wave Loads and Ship Structural Response in Heavy Seas

Ould el Moctar, Department Fluid Dynamics

2006-12-08

Germanischer Lloyd

Contents

- **Motivation**
- **Part 1: Prediction of slamming loads**
- **Part 2: Prediction of sectional loads incl. whipping effects**
- **Part 3: Shipboard routing assistance system: decision support for ship operation in heavy seas**

Motivation (1)
Assessment of the structural design

- Extreme <u>sectional loads</u> for global strength analysis
- <u>Maximum slamming pressure</u> for local strength analysis
- <u>Water on deck</u> induced loads
- Whipping effects

Motivation (2)
Assessment of ship sea keeping

- Extreme <u>ship motions</u>
- Likelihood of <u>parametric rolling</u>
- Extreme <u>accelerations</u>

International RIAM Symposium in Kyushu University 2006-12-08 No. 5 Germanischer Lloyd

International RIAM Symposium in Kyushu University 2006-12-08 No. 6 Germanischer Lloyd

International RIAM Symposium in Kyushu University 2006-12-08 No. 7 Germanischer Lloyd

International RIAM Symposium in Kyushu University 2006-12-08 No. 8 Germanischer Lloyd

Part 1: Prediction of Slamming Loads

Properties of flow around hull under slamming conditions

- Strongly nonlinear behaviour
- 3D effects
- Flow separations
(knuckle, convex parts of section, bulbous bow)
- Air trapping
- Disturbed flow (free surface deformation)
- Compressibility

Computational Procedure for Slamming Loads

Linear computation of relative normal velocity (RNV) for different loading and wave conditions using 3D seakeeping code

⇓

Long-term calculation of RNV envelope curves, determination of equivalent design waves for each plate field using statistic tool

⇓

Non-linear, time domain computation of motions and slamming loads using RANSE coupled with 6DoF

Criteria used for selection of "slamming" design wave: worst but realistic scenario!

- **Maximum relative normal velocity between hull plate field and wave**
- **Vertical acceleration on bridge ≤ 9.81m/²**
- **No propeller racing**
- **Maximum wave height = λ_W/ 10**

Sample of Design Wave Selection based on linear GL PANEL Computations

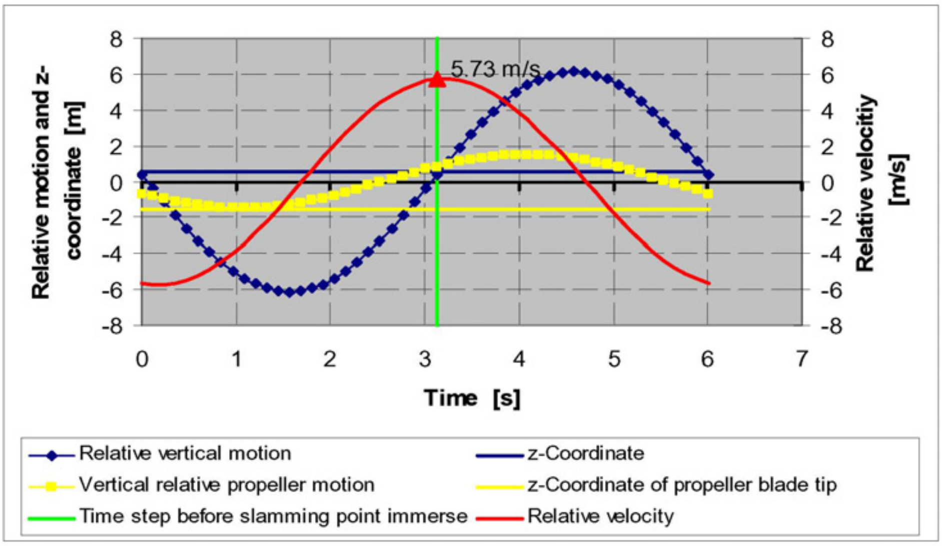

It is important to define the appropriate design wave: Influence of wave length

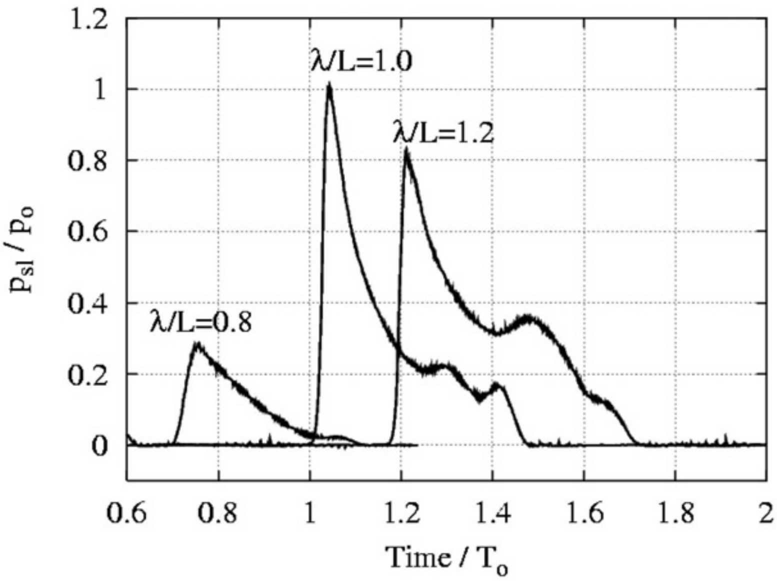

It is important to define the appropriate design wave: Influence of wave height and ship speed

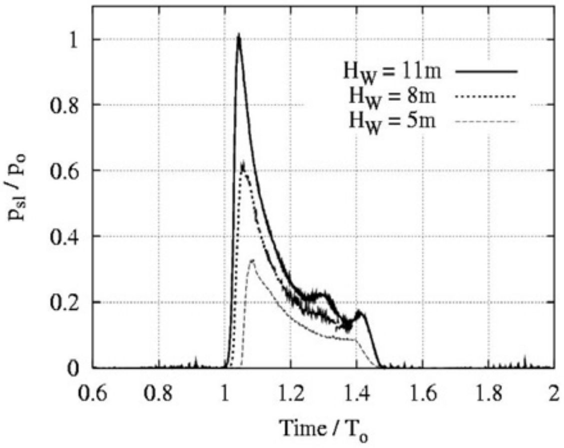

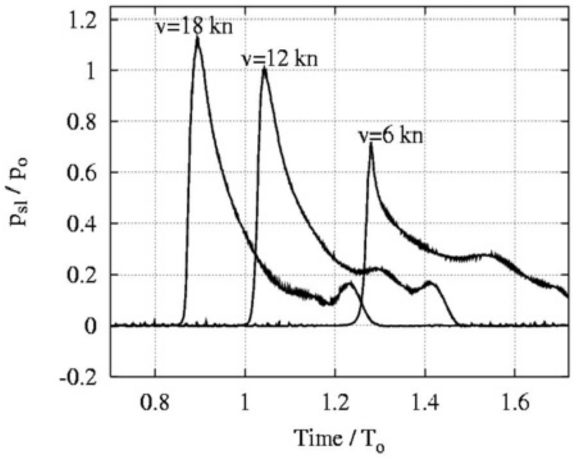

Used RANSE-solver

- **Conservation equations are solved using FV-method**
  - mass
  - momentum
- **Transport equation for volume of fluid function**
- **Transport equations for turbulence variables**

Generation and damping of waves

- **prescribe velocity (Airy or Stokes waves) at the inlet boundary**
- **Use fine grids and 2nd order approximation at inlet and around the hull (avoid wave damping)**
- **Use coarse grid and first order approximation near outlet (wave damping)**

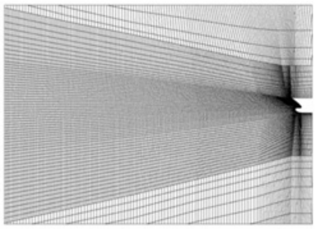

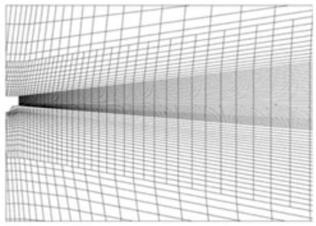

Coupling of RANSE and equations of motion

$$\frac{d(m\vec{v})}{dt} = \vec{f} \qquad \frac{d(I \cdot \vec{\omega})}{dt} = \vec{M}$$

- **explicit**
  - accurate enough for moderate accelerations
- **implicit**
  - recommended for large accelerations
  - more robust
  - time consuming

Realisation of ship motions

- **Moving the entire grid**
  - additional space conservation equation has to be solved
  - robust
  - fine grid is required in the free surface area
- **Static grid and moving free surface**
  - body forces are added to source terms of the momentum equations
  - time consuming
  - robust
- **Overlapping grid**
  - not robust
  - time consuming

Test case 1: RoRo Ferry MS DEXTRA

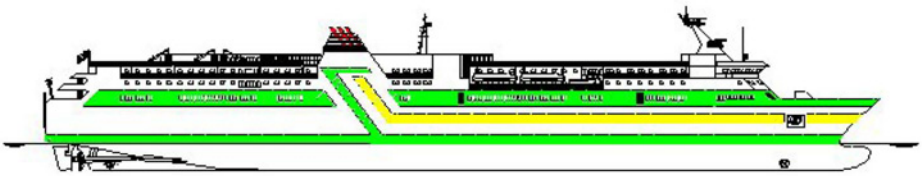

Ship main data:

L_{PP} = 173.0 m

B = 26.0 m

T = 6.5 m

Δ = 16800 t

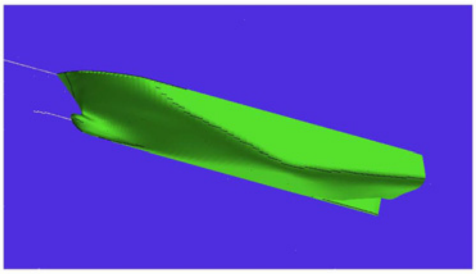

Ship velocity [kn]	Wave height [m]	Wave frequency [1/s]	Wave direction [°]
26	7.3	0.60	180 (Head waves)

MS DEXTRA

Pressure sensor locations

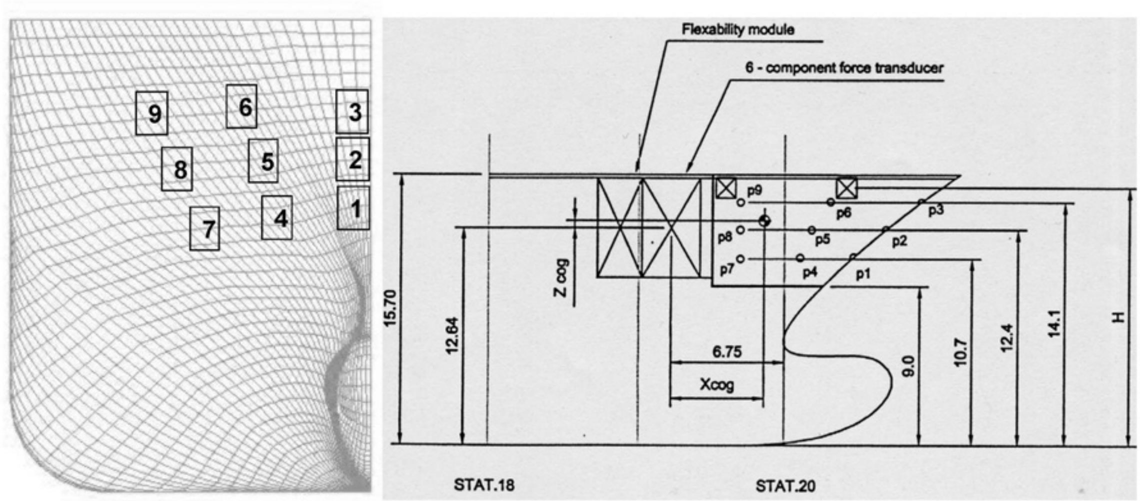

Monohull 3 L=250 m v=26 kts H=5m (head waves)

Time histories of bow door pressures

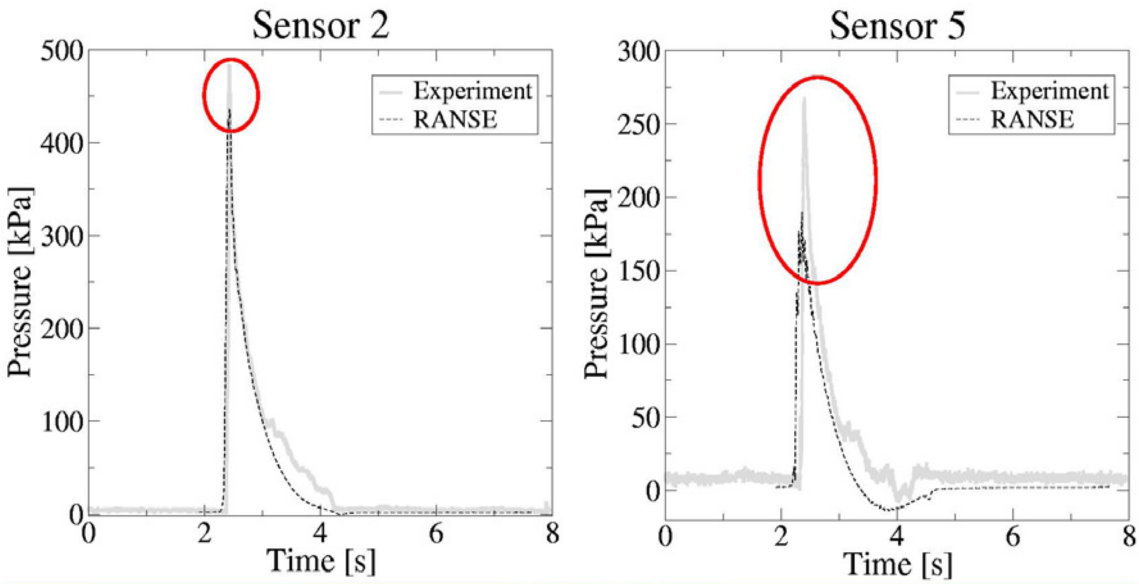

Test case 2: Mega Yacht

Ship main data:

L_{PP} = 70.0 m

B = 15.0 m

T = 5.0 m

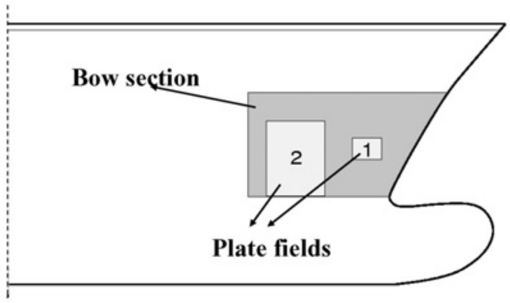

HSVA test case	Ship velocity [kn]	Wave height [m]	λ / L_{PP}	Wave direction [°]
Run 1	14.0	3.5	1.0	180
Run 2	14.0	3.5	1.2	180
Design wave condition	10.7	7.0	1.2	180

Monohull 1

Time history of forces and pressures

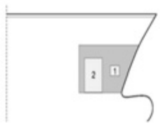

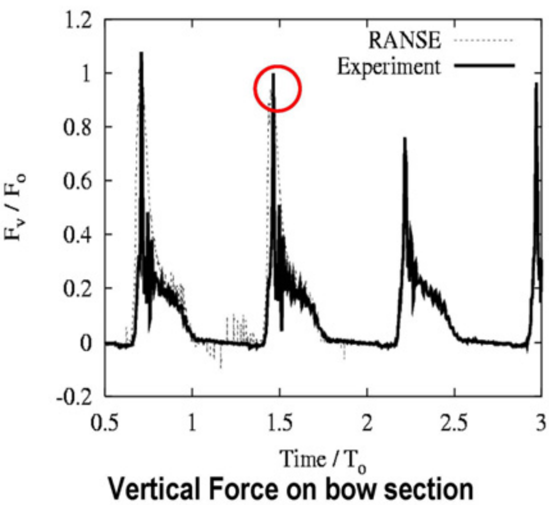

Vertical Force on bow section

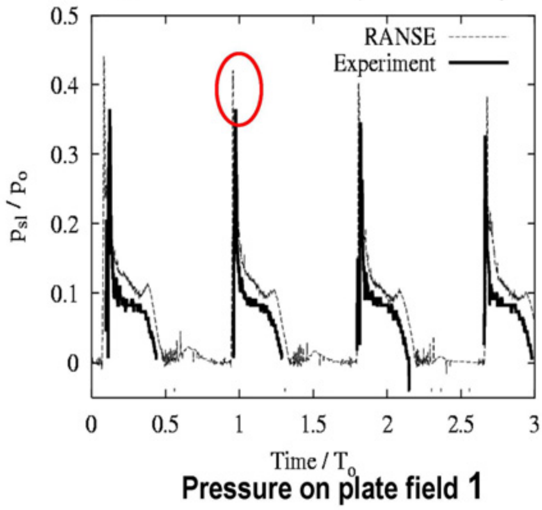

Pressure on plate field 1

Slamming forces acting on larger areas can be predicted accurately enough, pressure on smaller areas are meaningless for structural design!

Design wave conditions for bow flare slamming

Ship velocity v_s	6 kn
Wave direction Φ	180°
Wave length λ_W	95.0 m
Wave height H_W	9.5 m
λ_W / L_{PP}	1.16

Summary of Part 1

- Accounting for strong nonlinearities associated with slamming loads impelled to use RANS
- Slamming forces acting on larger areas can be predicted accurately enough using RANS
- Pressure on smaller areas are meaningless for structural design and can hardly be predicted accurately
- Potential flow codes and statistical tools can be used to define the appropriate design waves
- Computational procedure is used for standard applications

Part 2: Prediction of Sectional Loads

Computational Procedure for Sectional Loads

<u>Linear computation</u> of wave loads for different loading and wave conditions using 3D seakeeping code

⇩

Long-term calculation of wave load envelope curves, determination of equivalent <u>design waves</u> for each section using statistic tool

⇩

Non-linear, time domain computation of motions and wave loads incl. slamming and water on deck for each design wave using <u>RANSE</u>

⇧⇩

Time domain calculation of hull girder strength using <u>FEM</u>

⇩

Computed, rule based and full scale measured (if available) values are compared

Methods & Tools Used in Computational Procedure

- **Frequency-domain 3D panel code GL PANEL**
- **Linear statistic tool GL STAT**
- **RANS & VoF Equations are solved by COMET**
- ***Stokes & Airy waves are generated at the inlet boundary using GL WAVE***
- ***Nonlinear equations of motions (6 DOF) are solved and coupled with COMET using GL MOT***
- ***Mapping from RANS to FEM using GL MAP***
- *Finite Element Code ANSYS*

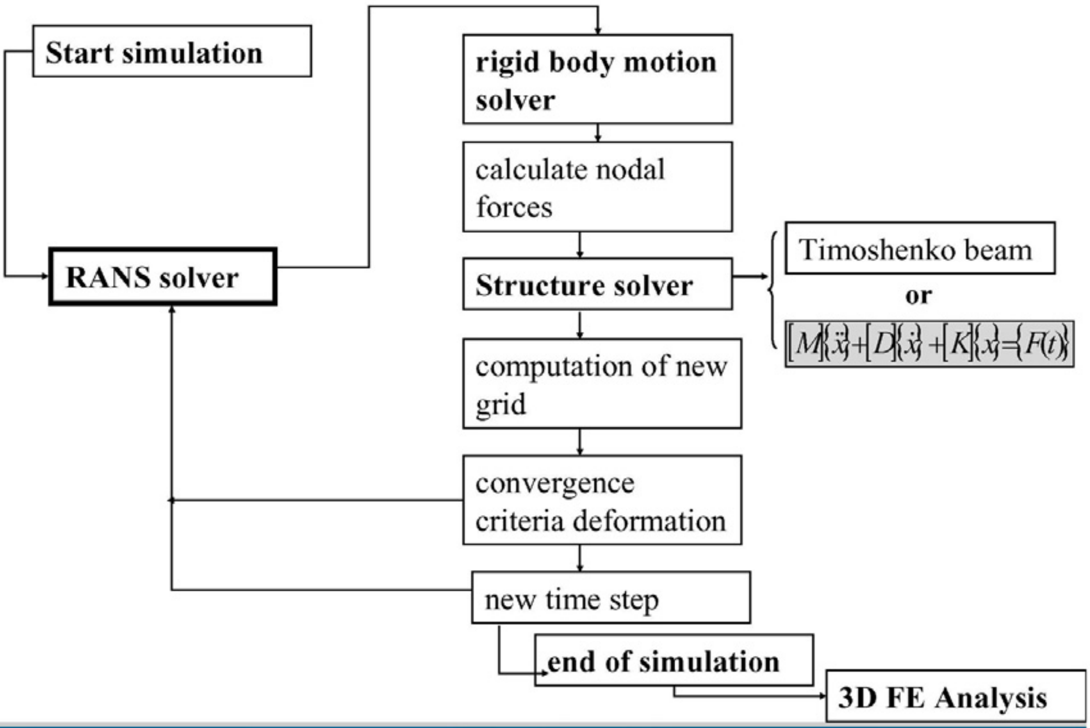

13,000TEU: RANS Analysis

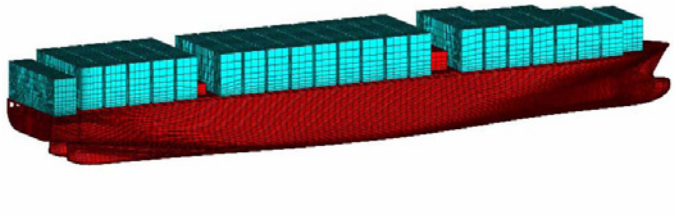

Ship length [m]	382
Breadth [m]	54.2
Draught [m]	15
Speed [kts]	26

- Number of elements: 1.1 mil. / 2.5 mil. cells
- Time step: 0.01 seconds
- Ship motions: moving entire grid
- Inlet boundary: Stokes waves

13,000 TEU: Load Case 1

Ship speed [kn]	1/3v 1/2v 2/3v v
Draught [m]	15.0
Wave length [m]	400
Wave height [m]	19
Wave direction [°]	180 (head waves)

13,000 TEU: Ship accelerations in extreme waves are moderate!

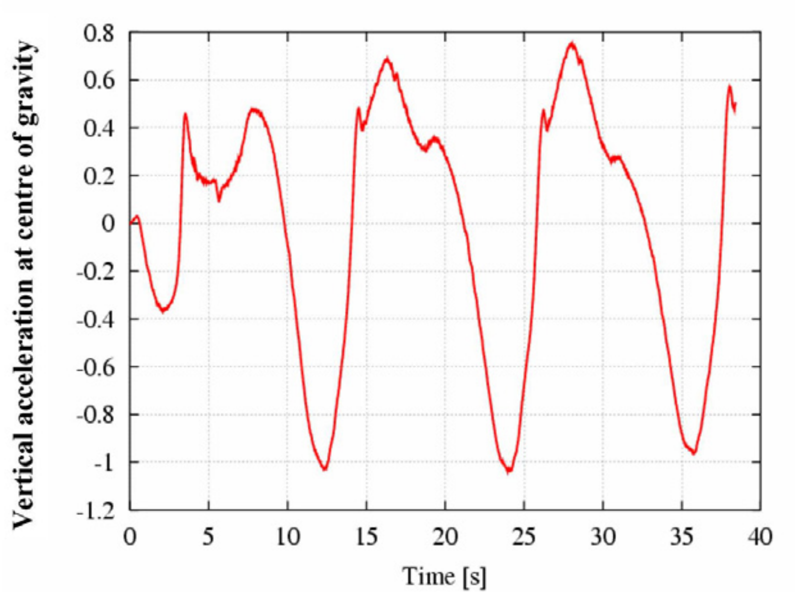

13,000 TEU: Ship motions in extreme waves are moderate!

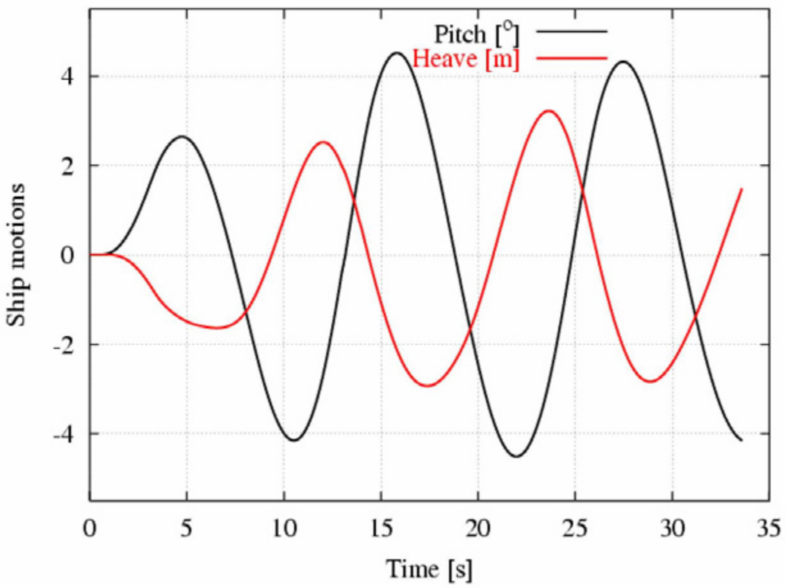

13,000 TEU: Wave loads incl. slamming and water on deck

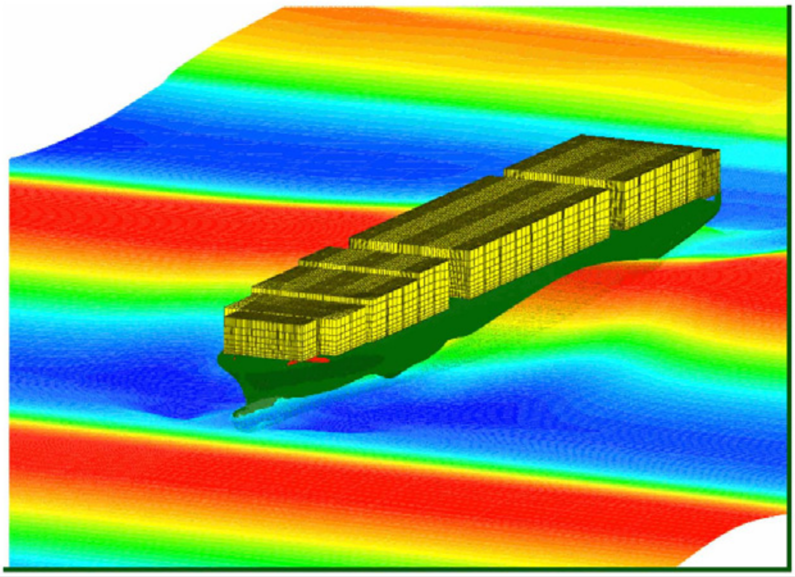

Wave Length 400m **Wave Height 19 m** **Ship Speed 17kts**

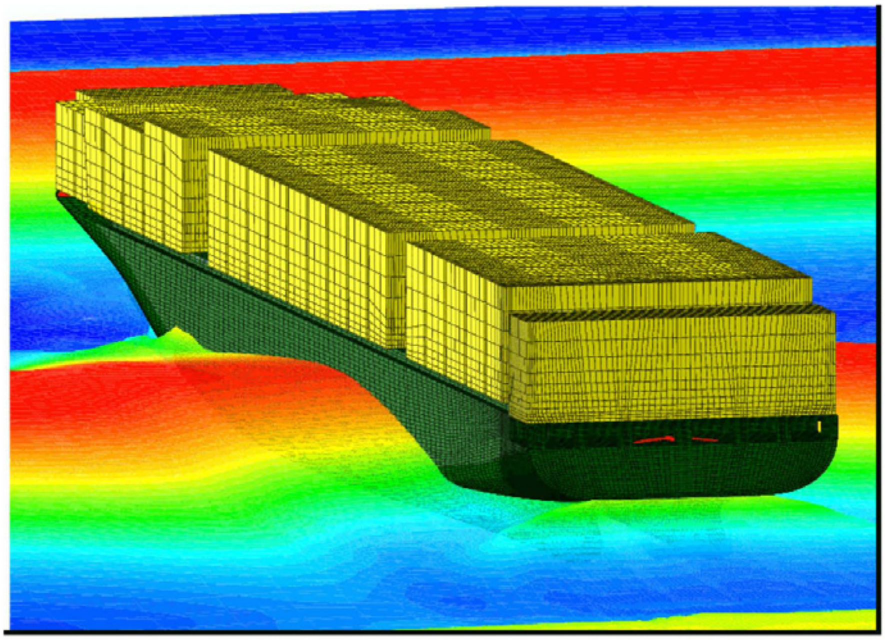

Wave Length 400m **Wave Height 19 m** **Ship Speed 17kts**

13,000 TEU: Wave loads incl. slamming and water on deck

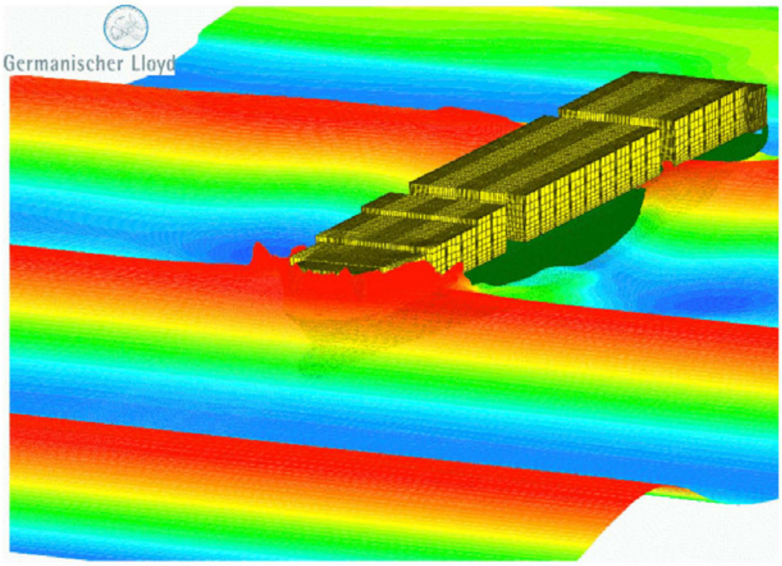

Wave Length 300m **Wave Height 30 m** **Ship Speed 6kts**

13,000 TEU: Computed time history of pressure distribution

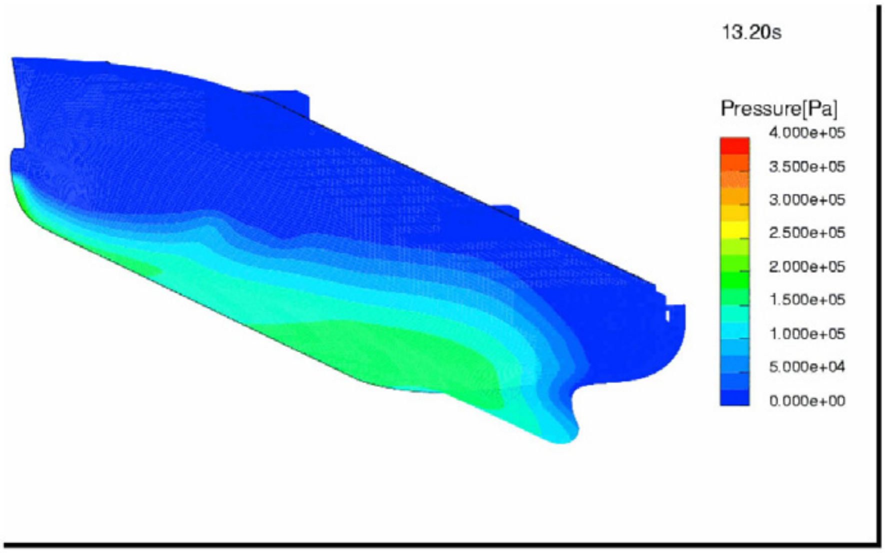

Wave Length 400m **Wave Height 19 m** **Ship Speed 17kts**

13,000 TEU: Envelopes of vertical bending moments for mid ship design wave conditions at 1/3 ship speed

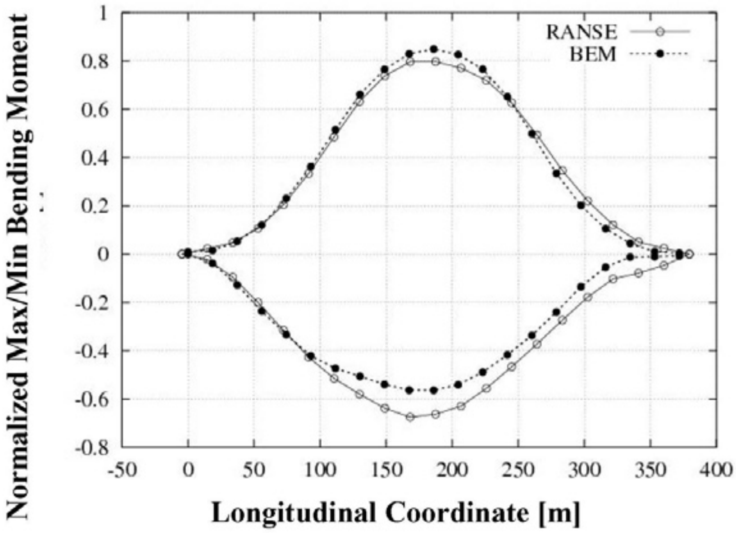

For low ship speed BEM and RANS computed sectional loads agree fairly!

13,000TEU: Envelopes of vertical bending moments for mid ship design wave conditions at 2/3 ship speed

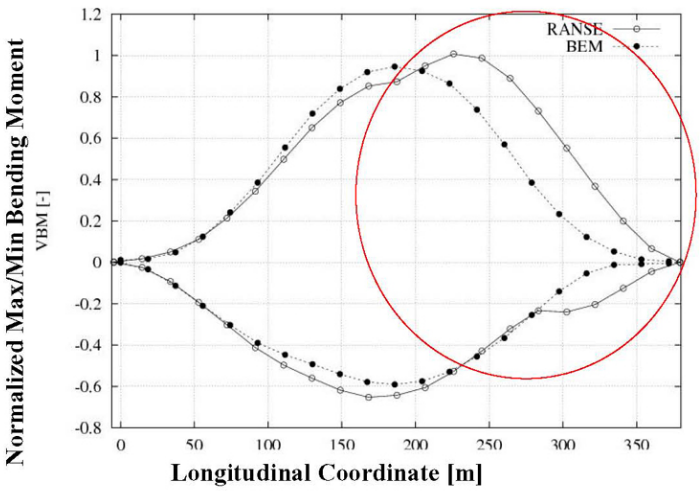

Larger deviations between BEM and RANS computed sectional loads due to slamming and water on deck

13,000 TEU: Time History of Equivalent Stress Distribution

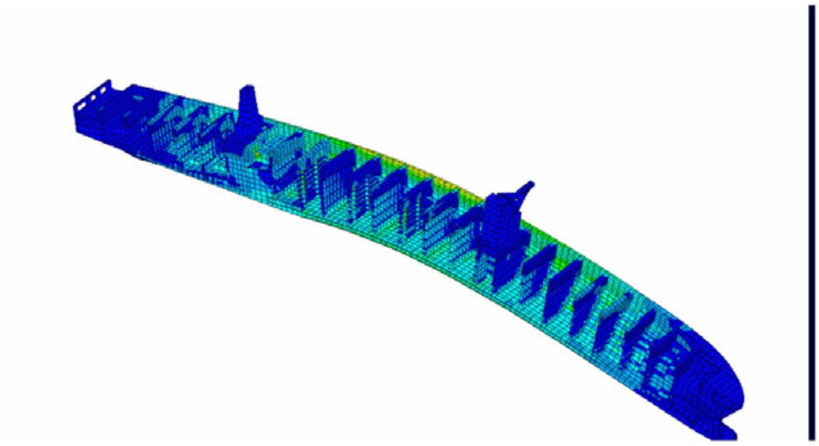

Relative Deflection was computed to be about 1m
Stress level is below yield stress !

Wave-Piercing Trimaran Earthrace

The Earthrace project challenges to break the world record for circumnavigating the globe in 65 days, while using bio-diesel.

L [m]	23.9
B [m]	7.9
T [m]	0.91
Speed [kts]	25/50
Fn	0.9/1.7

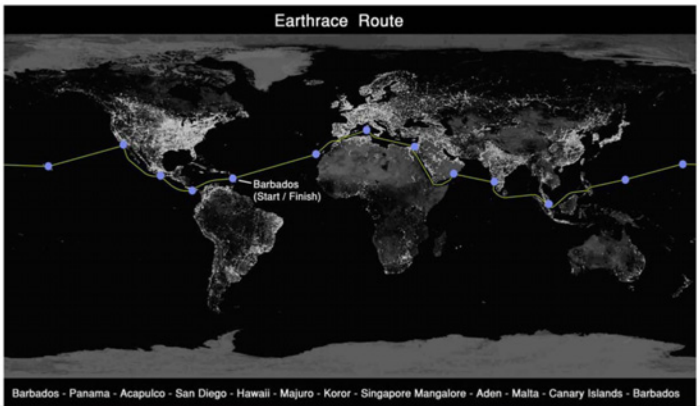

EARTHRACE: Different scenarios were investigated using RANS+6DoF, BEM were not suitable to compute motions and loads

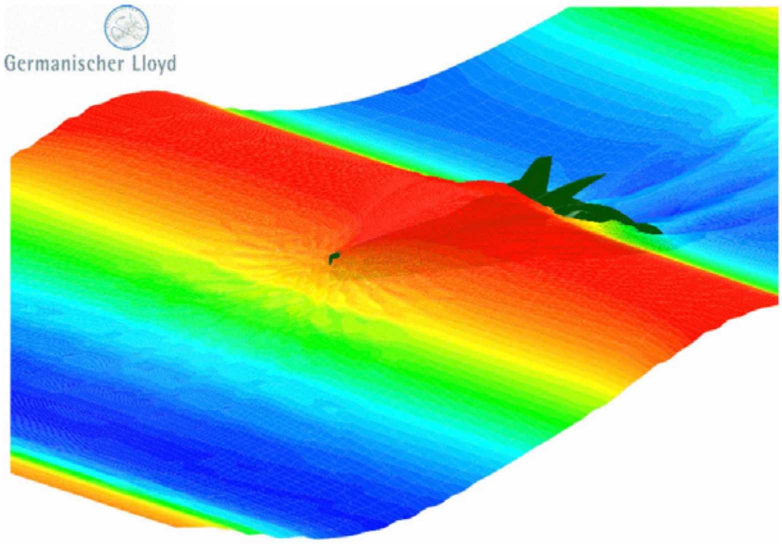

Computed ship motions in head waves

Summary of Part 2

- **Due to high computational time RANS can only be used for selected wave conditions. Selection is based on linear BEM and statistic tool**
- **RANS and BEM computed vertical sectional loads agree favorably for low ship speeds**
- **Coupling RANSE with Timoshenko beam equations was an effective and useful way to assess structure deformation in extreme wave conditions**
- **Elastic amplification of VBM at midship was appr. 20%**

Part 3: Shipboard routing assistance system

Objectives

An onboard system to support decision-making of the navigator

- to reduce the risk for ship damage and cargo loss by identifying and avoiding effects of extreme wave situations
- to enable active route planning

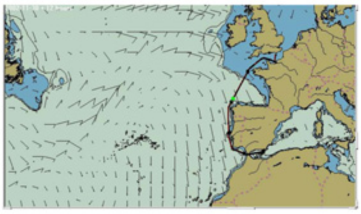

Basic Concept of SRA System

Actual mass distribution from loading computer

\+

Hydrodynamic characteristics from pre-calculated database

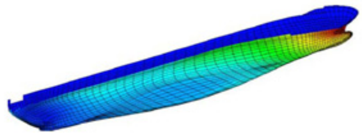

\+

Seaway: measured, forecasted or observed

→

On-board Computation of Ship Responses and Display on Bridge

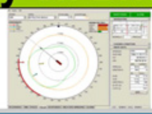

Thank you for your attention

Numerical Analysis on Dynamics of Pinch-Off in Immiscible Liquid/Liquid Jet Systems

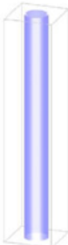

"Analyses of Strongly Nonlinear Flows around Moving Boundaries"

Dec. 7-8 2006

RIAM Kyushu University

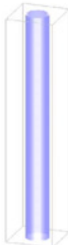

School of Eng. Chihiro Inoue
Univ.of Tokyo Toshinori Watanabe
Univ.of Tokyo Takehiro Himeno

Department of Aeronautics and Astronautics

The Beauty of Droplets

Ref: ひとしずくの水-A DROP OF WATER
ウォルター・ウィック／林田康一訳
あすなろ書房

What is Pinch-Off ?

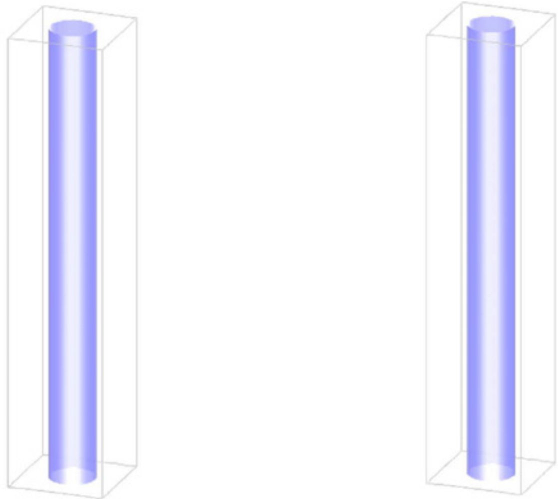

With Surface Tension *Without Surface Tension*

Inertia , Surface Tension, Viscosity, Gravity

Classification of Liquid Disintegration

Interaction between Liquid and Gas

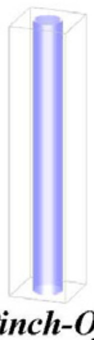

Pinch-Off

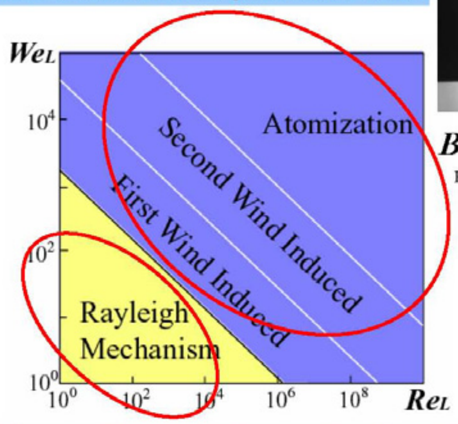

Breakup of Liquid Sheet

Ref, http://www.photron.co.jp/index.html

- Automobile
- Gas Turbine
- Rocket Engine
- Waterfall
- Rain etc.

➢No complete theory has yet been developed to describe these processes.

➢An in-depth understanding of Pinch-Off will lead us to provide desirable atomization systems.

Objectives

- To clarify detailed flow field in Pinch-Off by developed numerical method, *CIP-LSM*.
- Especially, focusing on structures inside liquid jets, which are difficult to observe experimentally.

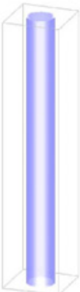

Numerical method, CIP-LSM

Comparison with Experiments

What happens inside Liquid Jet??

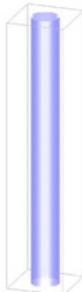

Numerical Method for Free-Surface Flows

CIP-LSM …… **CCUP** scheme coupled with **LSM**

To capture the surface configuration, curvature and normal vector distinctly

→ **Multi-interface Advection and Reconstruction Solver (MARS)** …Kunugi (1997)

→ **Level Set Method (LSM)** …Sussman (1994)

To estimate surface tension and wetting phenomena adequately

→ **Continuum Surface Force (CSF) model** …Blackbill (1992)

To solve both gas phase and liquid phase together in a domain.

→ **CIP Coupled Unified Procedure (CCUP)** …Yabe (1991)

↓

CCUP , LSM and CSF model were combined and modified, to be applicable to generalized curved-linear coordinate system in three-dimensional domain. …Himeno (1997)

Convection Algorithm of MARS was included to improve volume conservation of CIP-LSM. …Himeno (2002)

ref. *AIAA-2001-3822*

Numerical Method: TCUP (Thermo CIP-CUP)

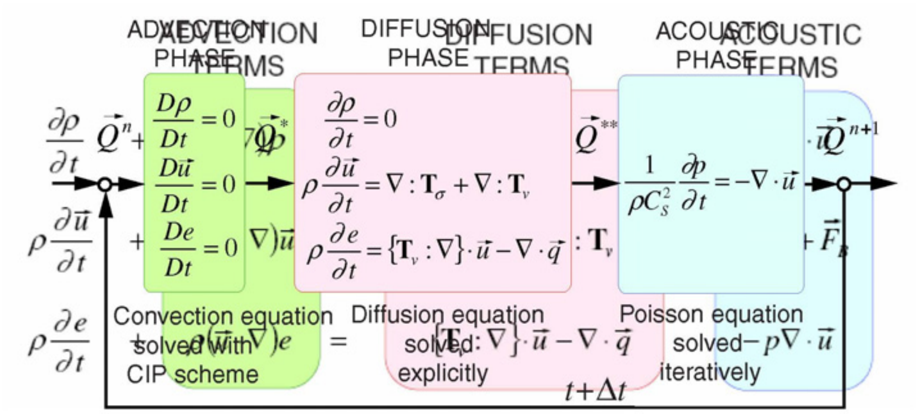

Computation of Navier-Stokes eq.

Ref: T.Himeno et.al., JSME int. j. Ser. B, vol.47, No.4, (2004)

Numerical Method : CIP-LSM

Distance Function for Capturing Surface Shapes

Rising bubble in a cylinder

Distance function ϕ from moving interface was generated.

From the distribution of ϕ

Normal Vector

$$\vec{n}_S = \frac{\nabla\phi}{|\nabla\phi|}$$

Curvature

$$\kappa = \nabla\cdot\vec{n}_S = \nabla\cdot\left(\frac{\nabla\phi}{|\nabla\phi|}\right)$$

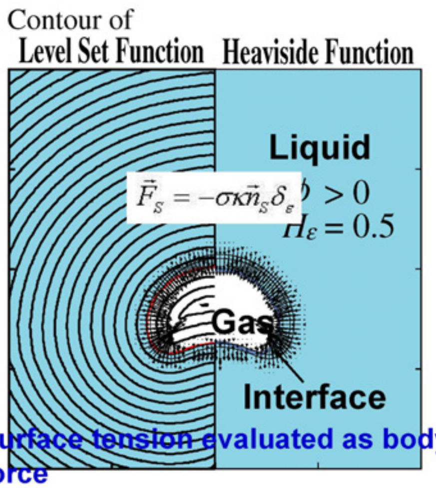

Surface tension evaluated as body force

Numerical Method : MARS (Kunugi, 1994)

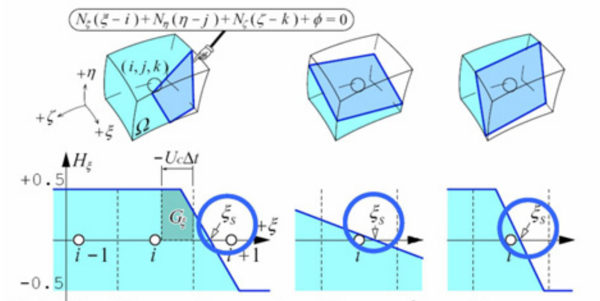

VOF is interpolated with a piecewise linear function

→ Flux is calculated as integration of $H_\xi\ H_\eta\ H_\zeta$

Volume Fraction

$$\frac{H_V}{J} = \int_\Omega H_S dV = \int_{k-1/2}^{k+1/2}\int_{j-1/2}^{j+1/2}\int_{i-1/2}^{i+1/2} H_S \frac{d\xi d\eta d\zeta}{J}$$

Area Fraction

$$\frac{H_\xi}{J} = \lim_{\Delta\xi \to 0}\left\{\frac{1}{\Delta\xi}\int_{k-1/2}^{k+1/2}\int_{j-1/2}^{j+1/2}\int_{\xi-\Delta\xi/2}^{\xi+\Delta\xi/2} H_S \frac{d\xi d\eta d\zeta}{J}\right\}$$

→ **Approximation** $\quad H_\xi = \max\{-0.5, \min[0.5, H'_\xi(\xi - \xi_S)]\}$

MARS+LSM=CIP-LSM (Himeno, 2003)

Volume conservation by MARS, Precise surface shapes by LSM

Surface Plane $\quad N_\xi(\xi - i) + N_\eta(\eta - j) + N_\zeta(\zeta - k) + \phi = 0$

Heaviside function as color function

$$\begin{cases} H_S = 0.5 & (\text{if } \phi > 0 \text{ : liquid}) \\ H_S = 0.0 & (\text{if } \phi = 0 \text{ : Interface}) \\ H_S = -0.5 & (\text{if } \phi < 0 \text{ : Gas}) \end{cases}$$

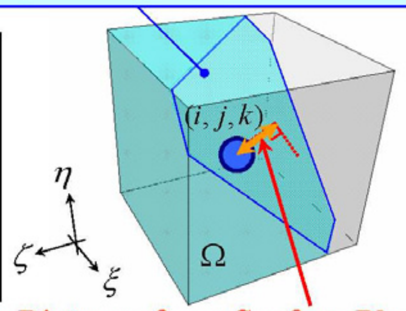

ϕ : Distance from Surface Plane

$$H_V = \frac{1}{J}\int_\Omega H_S dV$$

Introduce VOF

$$H_V \cong \frac{\phi}{|N_\xi| + |N_\eta| + |N_\zeta|}$$

Clipping LS near interface

$$H'_\xi \cong \frac{N_\xi}{|N_\eta| + |N_\zeta|}$$

Gradient of Surface

(Himeno, 2003)

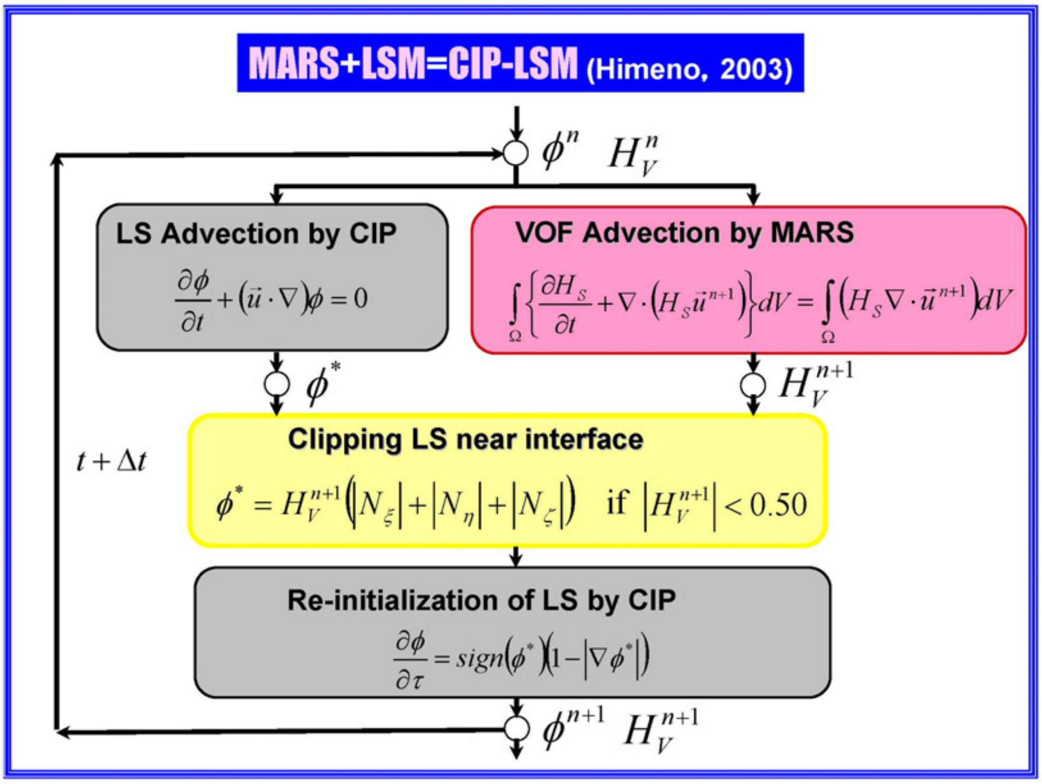

Sloshing Prediction in a Small Vessel

Comparison and Correlation

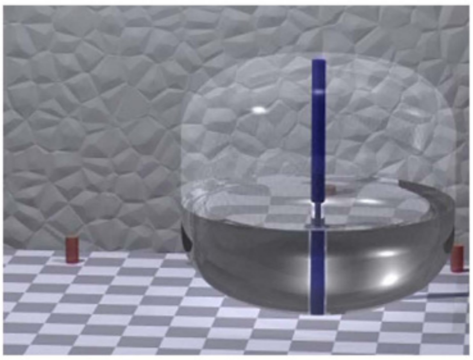

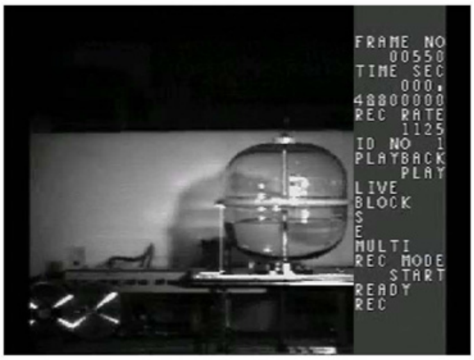

The numerical results with droplets are visualized with the technique of ray-tracing, and compared with the corresponding experiment at the same frame rate.

Though the bubbles and droplets smaller than the grid scale could not be captured, it is possible to say that liquid motion be well simulated.

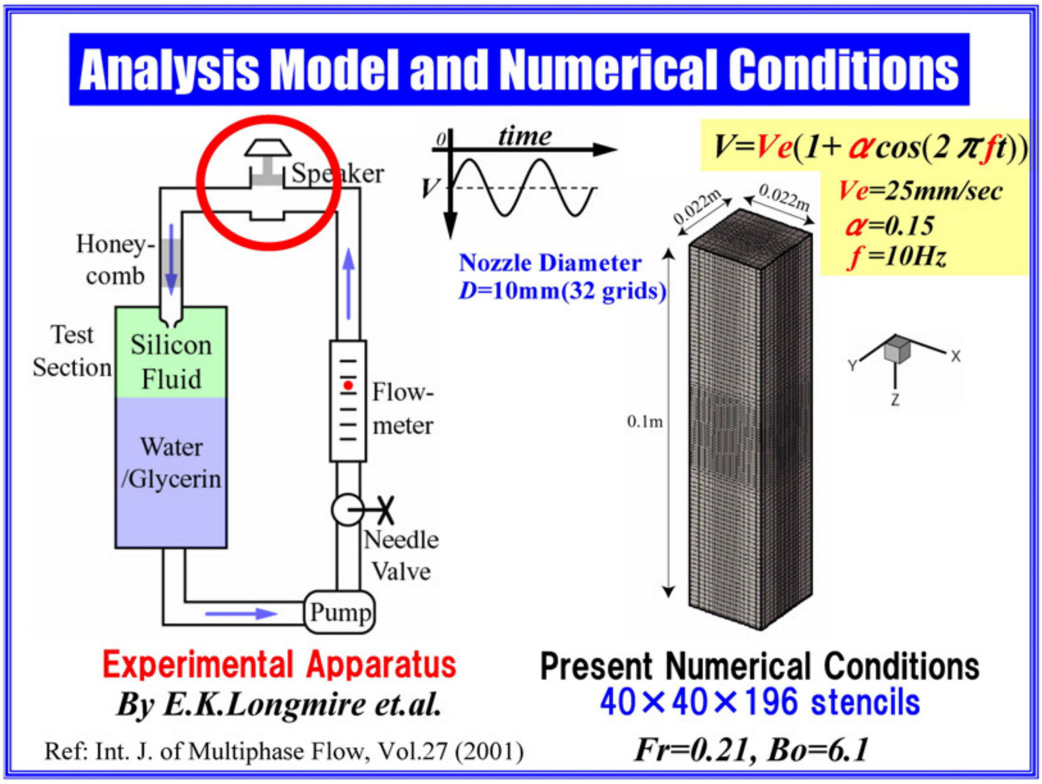
Analysis Model and Numerical Conditions
time
V
Speaker
Honey-
comb
Test
Section
Silicon
Fluid
Water
/Glycerin
Flow-
meter
Needle
Valve
Pump
Nozzle Diameter
D=10mm(32 grids)
0.022m
0.022m
0.1m
V=Ve(1+αcos(2πft))
Ve=25mm/sec
α=0.15
f=10Hz
Experimental Apparatus
By E.K.Longmire et.al.
Ref: Int. J. of Multiphase Flow, Vol.27 (2001)
Present Numerical Conditions
40×40×196 stencils
Fr=0.21, Bo=6.1

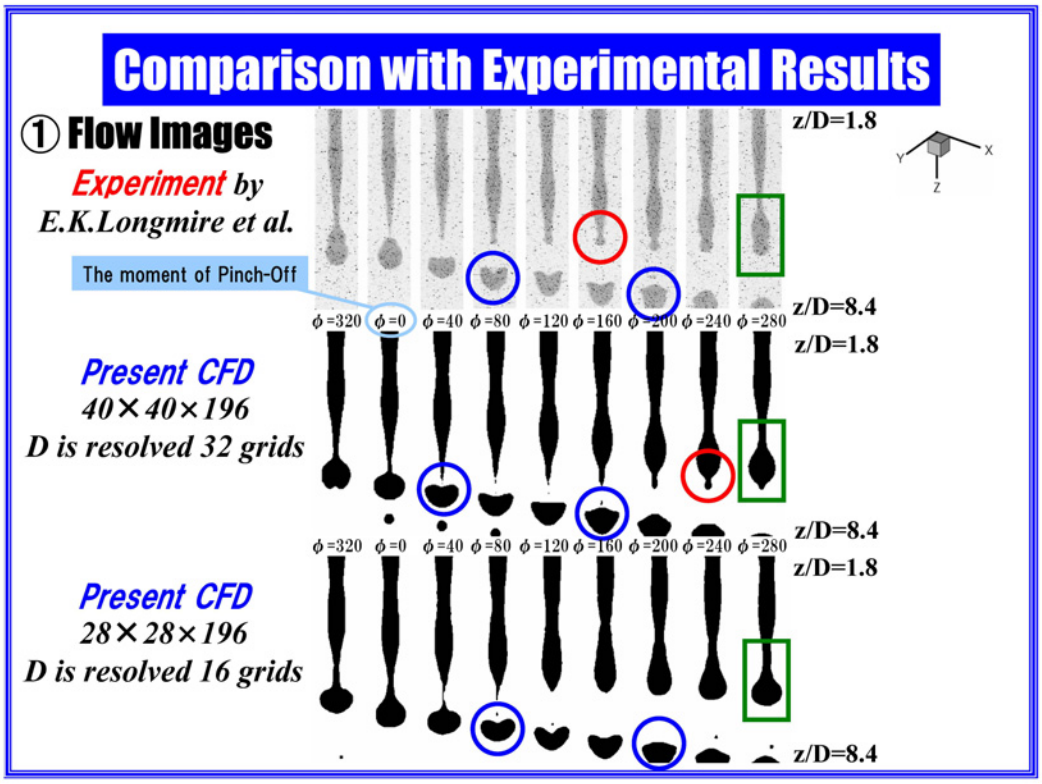
Comparison with Experimental Results
① Flow Images
Experiment by
E.K.Longmire et al.
The moment of Pinch-Off
z/D=1.8
z/D=8.4
φ=320 φ=0 φ=40 φ=80 φ=120 φ=160 φ=200 φ=240 φ=280
Present CFD
40×40×196
D is resolved 32 grids
Present CFD
28×28×196
D is resolved 16 grids

Comparison with Experimental Results

② Velocity distribution

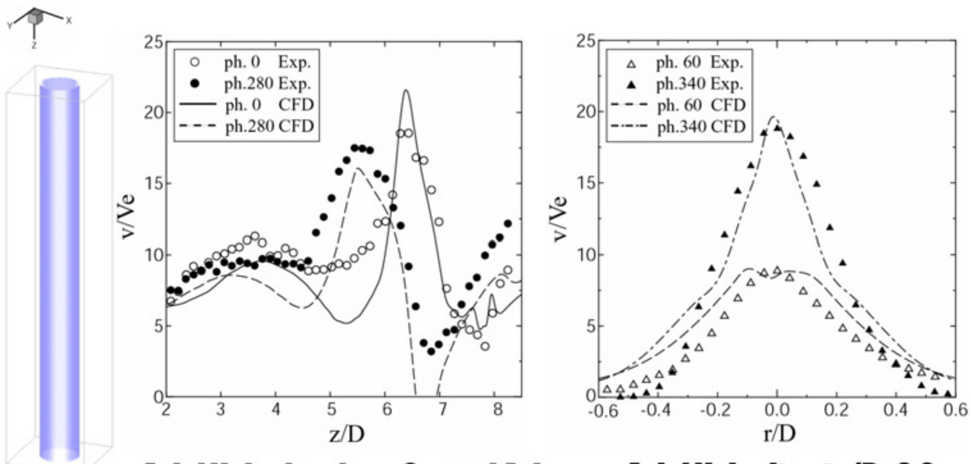

Axial Velocity along Central Axis (ϕ =0, 280 deg)

Axial Velocity at z/D=6.0 (ϕ =60, 340 deg)

40×40×196 stencils (D=32Δ)

Configuration and Structure of Liquid Jet

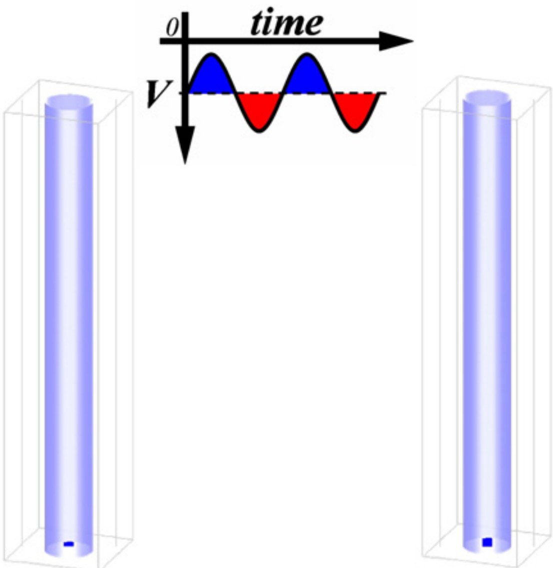

__With__ Surface Tension *__Without__ Surface Tension*

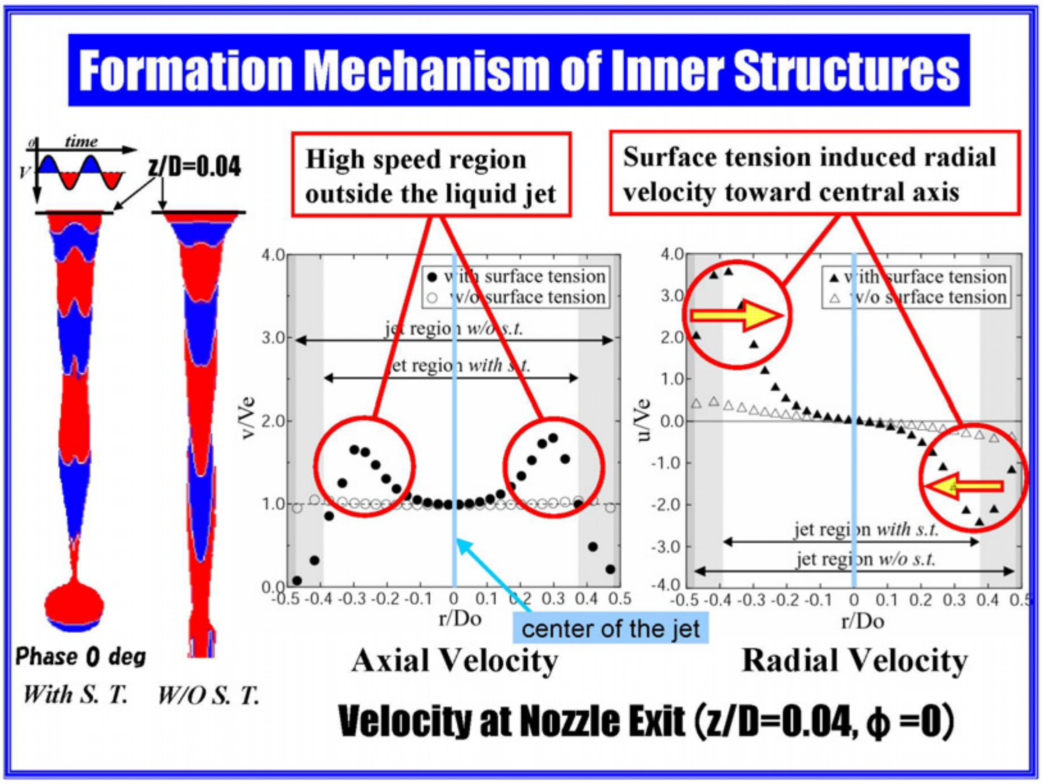
Formation Mechanism of Inner Structures
time
z/D=0.04
High speed region outside the liquid jet
Surface tension induced radial velocity toward central axis
with surface tension
w/o surface tension
jet region w/o s.t.
jet region with s.t.
v/Ve
u/Ve
r/Do
center of the jet
Phase 0 deg
With S. T.
W/O S. T.
Axial Velocity
Radial Velocity
Velocity at Nozzle Exit (z/D=0.04, ϕ =0)

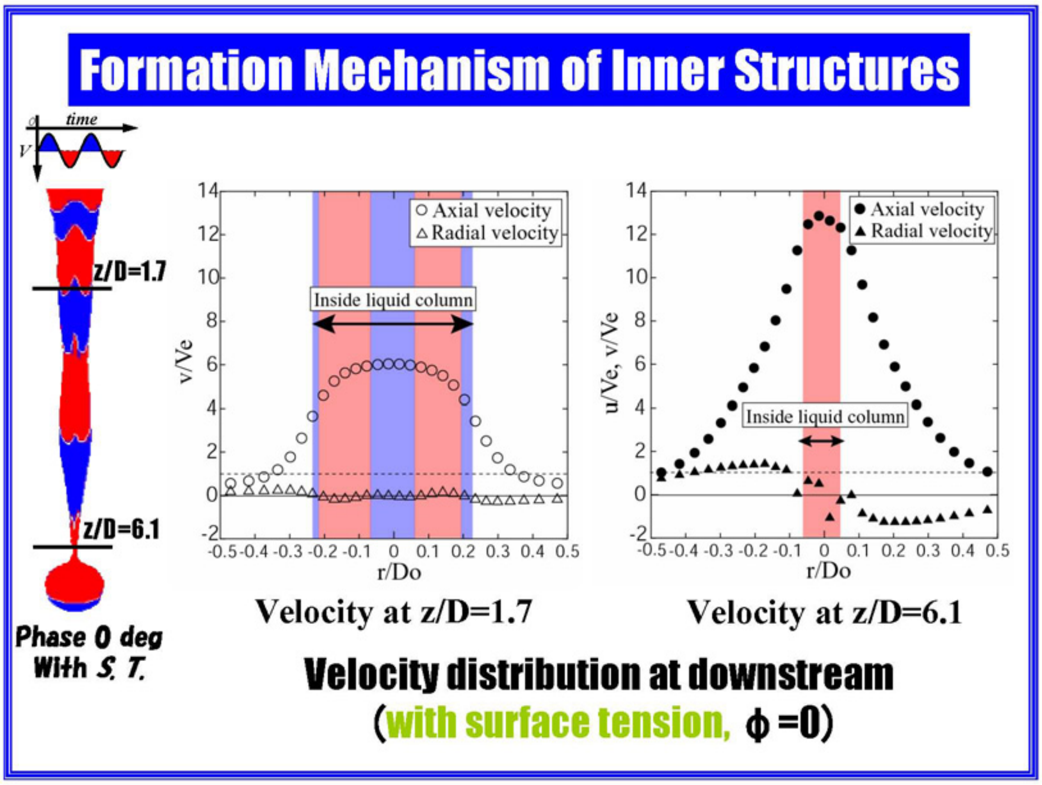
Formation Mechanism of Inner Structures
time
z/D=1.7
z/D=6.1
Axial velocity
Radial velocity
Inside liquid column
v/Ve
u/Ve, v/Ve
r/Do
Phase 0 deg
With S. T.
Velocity at z/D=1.7
Velocity at z/D=6.1
Velocity distribution at downstream
(with surface tension, ϕ =0)

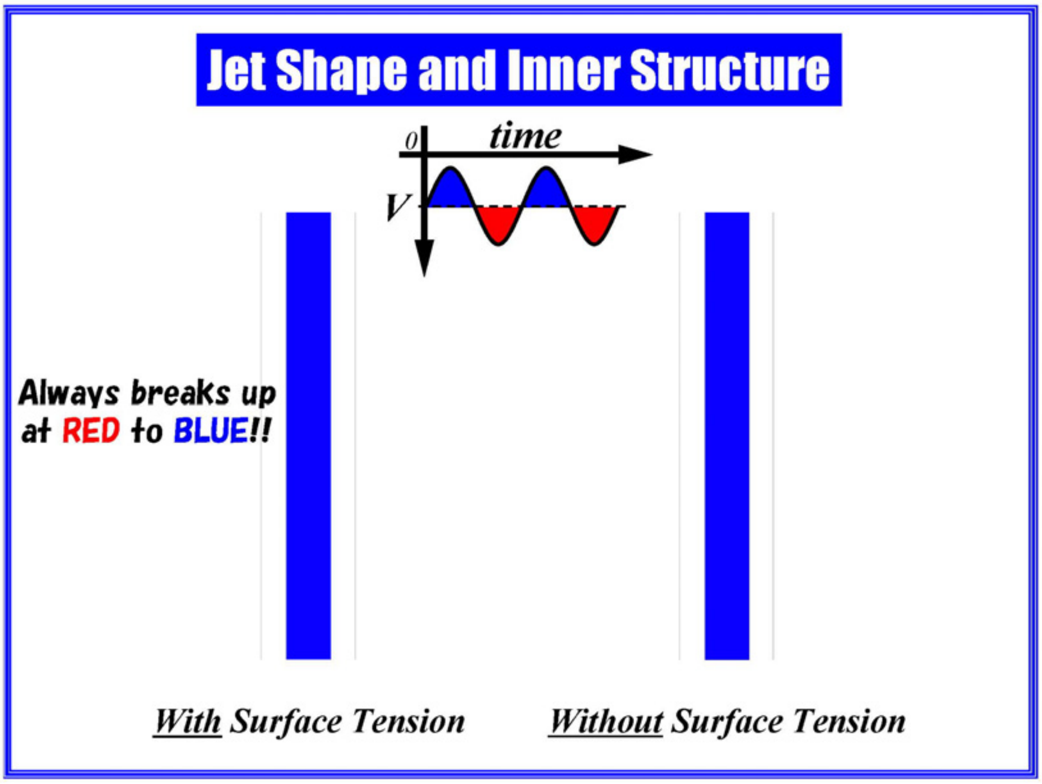
Jet Shape and Inner Structure
0
time
V
Always breaks up
at RED to BLUE!!
With Surface Tension
Without Surface Tension

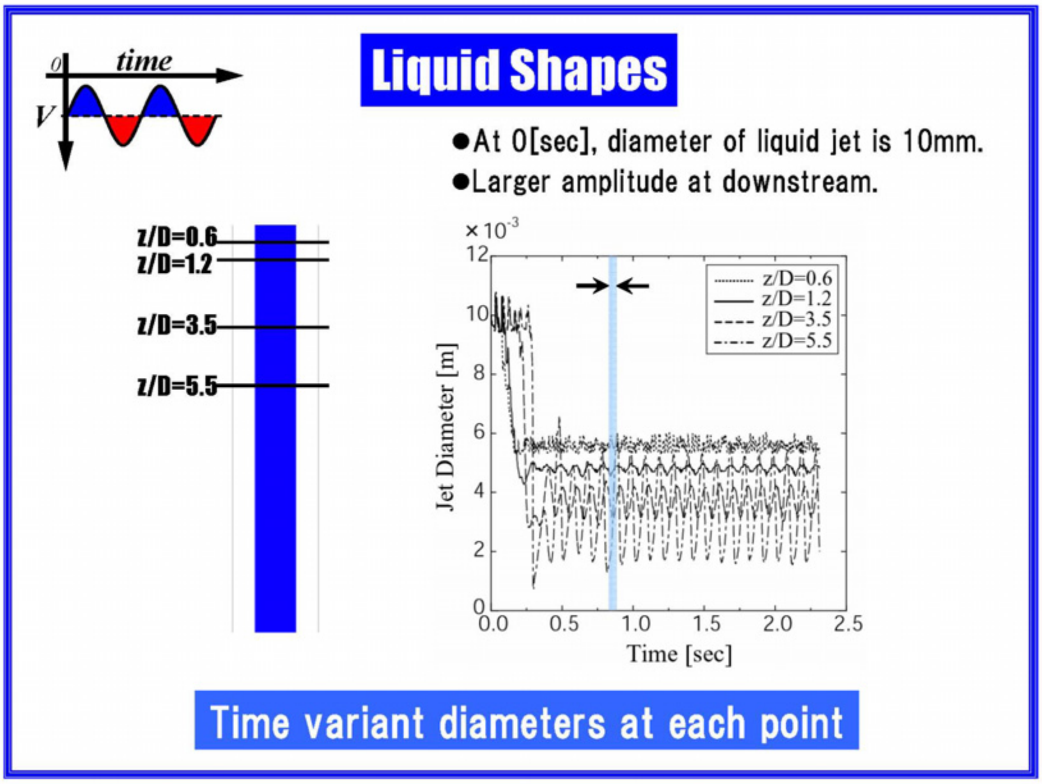
Liquid Shapes
0
time
V
●At 0[sec], diameter of liquid jet is 10mm.
●Larger amplitude at downstream.
z/D=0.6
z/D=1.2
z/D=3.5
z/D=5.5
×10^-3
12
10
8
6
4
2
0
Jet Diameter [m]
0.0
0.5
1.0
1.5
2.0
2.5
Time [sec]
z/D=0.6
z/D=1.2
z/D=3.5
z/D=5.5
Time variant diameters at each point

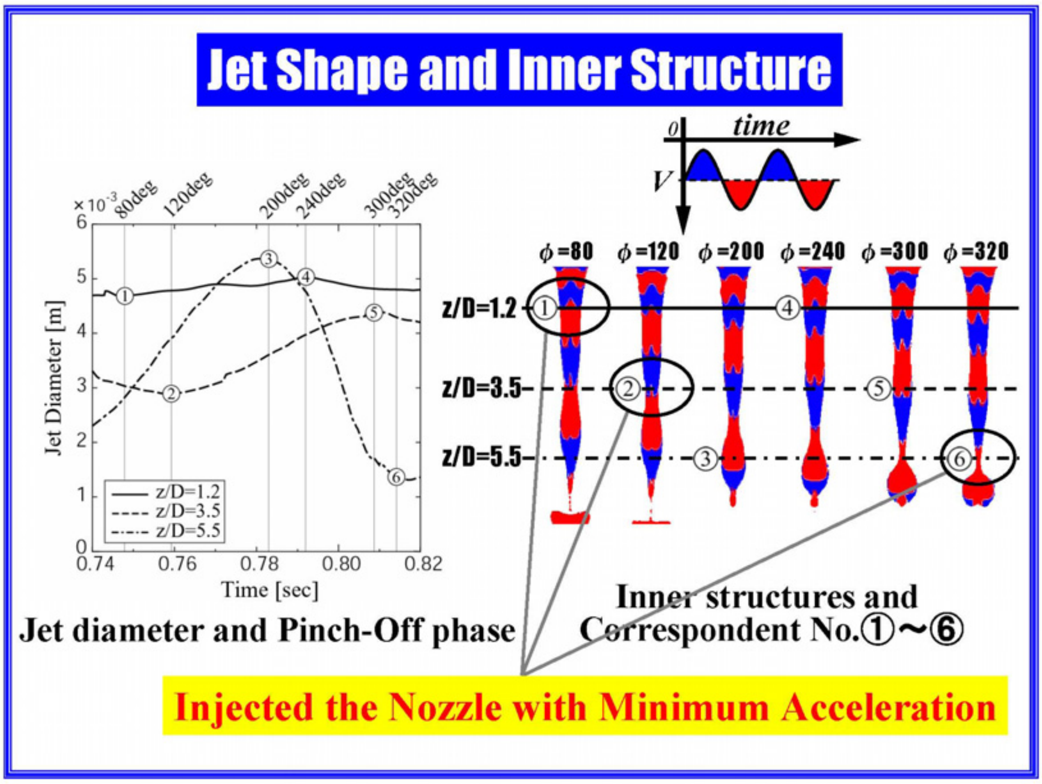

Jet Shape and Inner Structure
time
0
V
×10⁻³
80deg
120deg
200deg
240deg
300deg
320deg
Jet Diameter [m]
Time [sec]
z/D=1.2
z/D=3.5
z/D=5.5
φ=80 φ=120 φ=200 φ=240 φ=300 φ=320
Jet diameter and Pinch-Off phase
Inner structures and Correspondent No.①～⑥
Injected the Nozzle with Minimum Acceleration

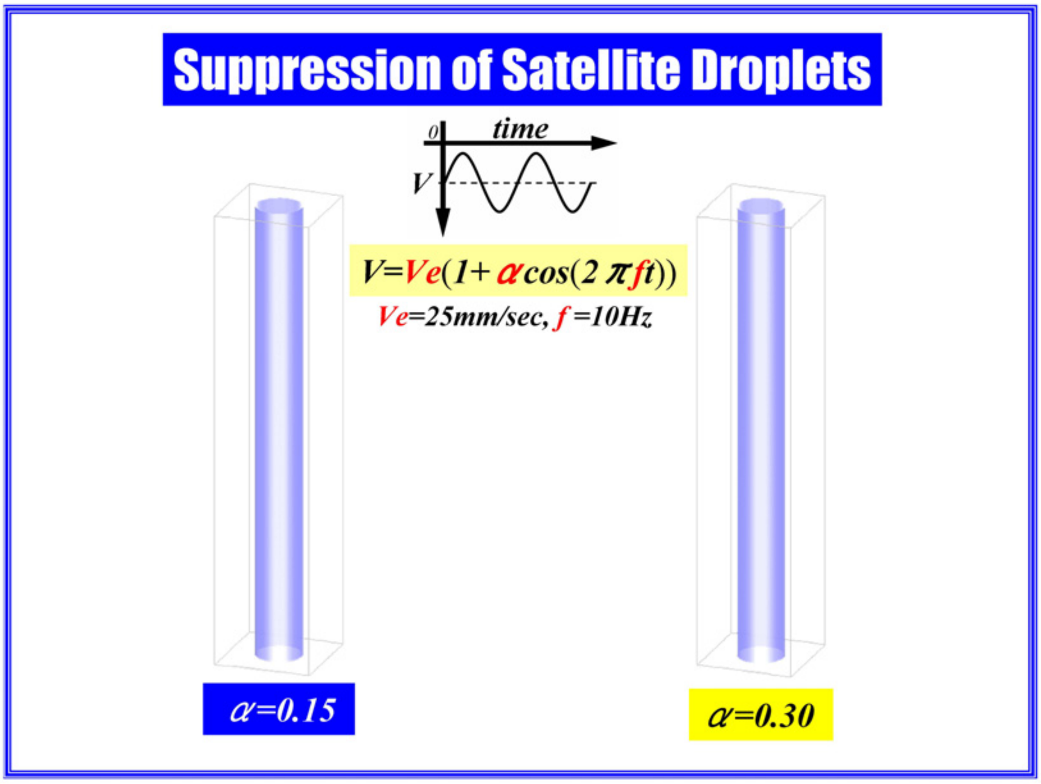

Suppression of Satellite Droplets
time
0
V
V=Ve(1+αcos(2πft))
Ve=25mm/sec, f=10Hz
α=0.15
α=0.30

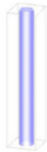

Conclusions

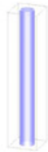

①CIP-LSM can evaluate inertia force, viscous force, gravity and surface tension adequately, and **it has potential to simulate and predict liquid disintegration phenomena**, where surface tension is predominant.

②**Surface tension at the nozzle exit** induces radial velocity toward central axis and constructs structures inside liquid jets.

③The jet Pinch-Off occurs at fluid element **injected with the minimum acceleration**.

Future Works

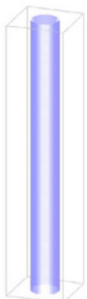

Pinch-Off

Breakup of Liquid Sheet

Atomization

Favorite Fountain

和田倉噴水公園

Wadakura Fountain Park in Tokyo, Japan

Close to Tokyo-Station

Liquefaction Analysis by Numerical Simulation Based on Fluid-Particle Interaction

S. Moriguchi and T. Aoki

Tokyo institute of Technology , Japan

Introduction

Before liquefaction → During liquefaction → Recovery from liquefaction

(Earthquake occurrence)

Shear force works in the ground

Decreace volume of geomaterial

Lateral spread of liquefied ground

Increase of pore water pressure → Dissipation of pore water pressure

Possible to describe behavior of ground using numerical simulation.

Difficult to simulate behavior of ground using numerical simulation.

Traditional method for liquefaction analysis

Continuum mechanics + Constitutive models + FEM (Finite different method)
+ Blot's two phase mixture theory + Concept of effective stress

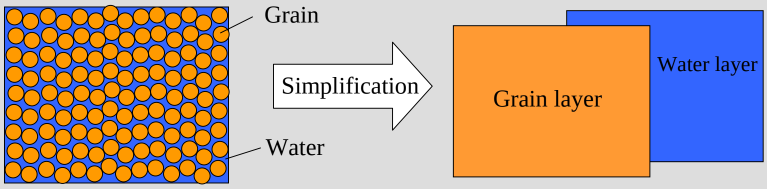

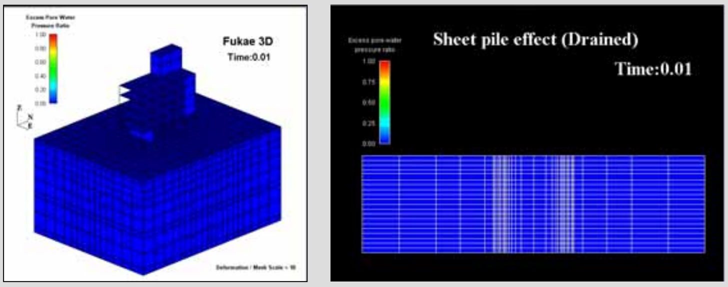

Problems

Constitutive model can not describe continuum behavior from before liquefaction to after liquefaction.
FEM can not describe large deformation. (Large deformation of liquefied ground)

Objective of this study

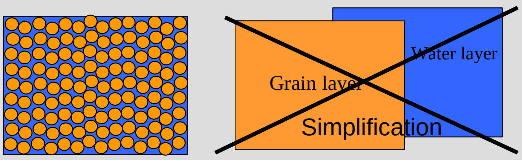

Without FEM.
Without constitutive model.
Based on fluid-particle interaction.

CFD (Computational Fluid dynamics) : Behavior of pore fluid (water and air)

+

DEM (Distinct Element method) : Behavior of soil grain

+

Immersed boundary method : Fluid-particle interaction

+

Parallel computation

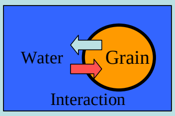

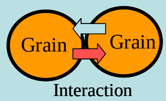

To develop new numerical method for liquefaction problem.

Numerical method for fluid

Fluid = Water + Air

< Equations >

Navier-Stokes Equation

$$\frac{\partial \mathbf{u}}{\partial t} + (\mathbf{u} \cdot \nabla)\mathbf{u} = -\frac{1}{\rho}\nabla p + \frac{\mu}{\rho}\nabla^2 \mathbf{u} + \mathbf{F}$$

Equation of continuity

$$\nabla \cdot \mathbf{u} = 0$$

Advection equation of density function

$$\frac{\partial \phi}{\partial t} + (\mathbf{u} \cdot \nabla)\phi = 0$$

$\mathbf{u}$: Velocity vector
ρ : Density p : Pressure
μ : Viscosity coefficient
ϕ : Density function
(Density function for water)

Advection part — $\frac{\mathbf{u}^{**} - \mathbf{u}^{n}}{\Delta t} = -(\mathbf{u} \cdot \nabla)\mathbf{u}$ ← Cubic Lagrange method

↓

Viscous term and external force term — $\frac{\mathbf{u}^{*} - \mathbf{u}^{**}}{\Delta t} = \frac{\mu}{\rho}\nabla^2 \mathbf{u} + \mathbf{F}$ ← FDM + Runge-Kutta method

↓

Pressure term (Poisson equation) — $\frac{\mathbf{u}^{n+1} - \mathbf{u}^{*}}{\Delta t} = -\frac{1}{\rho}\nabla p$ $\nabla \cdot \mathbf{u}^{n+1} = 0$ ← FDM + Implicit calculation

↓

Advection calculation for density function — $\frac{\phi^{n+1} - \phi^{n}}{\Delta t} = -(\mathbf{u} \cdot \nabla)\phi$ ← Cubic Lagrange method

↓

Update density and viscosity

$$\rho = \rho_w \phi + \rho_a (1-\phi)$$
$$\mu = \mu_w \phi + \mu_a (1-\phi)$$

ρ_w : Density of water μ_w : Viscosity of water
ρ_a : Density of air μ_a : Viscosity of air

Cubic Lagrange (CUL) method

Cubic interpolation + Semi Lagrange

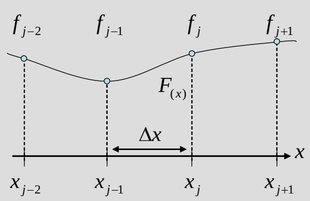

Cubic interpolation function

$$F_{(x)} = ax^3 + bx^2 + cx + f_j$$

Restraint condition

$$F_{(\Delta x)} = f_{j+1} \quad F_{(-\Delta x)} = f_{j-1} \quad F_{(-2\Delta x)} = f_{j-2}$$

$$a = (f_{j+1} - 3f_j + 3f_{j-1} - f_{j-2})/6\Delta x^3$$
$$b = (f_{j+1} - 2f_j + f_{j-1})/2\Delta x^2$$
$$c = (2f_{j+1} + 3f_j - 6f_{j-1} + f_{j-2})/6\Delta x$$

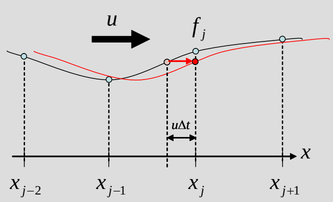

Time integration : Semi Lagrange

$$f_j^{n+1} = F_{(-u\Delta t)} = a(-u\Delta t)^3 + b(-u\Delta t)^2 + c(-u\Delta t) + f_j$$

Surface treatment

Surface treatment using tangent function (Yabe and Xiao, 1993)

$$\frac{\partial \phi}{\partial t} + (\mathbf{u} \cdot \nabla)\phi = 0 \quad \rightarrow \quad \frac{\partial H}{\partial t} + (\mathbf{u} \cdot \nabla)H = 0 \qquad H_{(\phi)} = \tan\left[\pi(\phi - 0.5)\right]$$

H : Transformed density function

Zalesak's problem

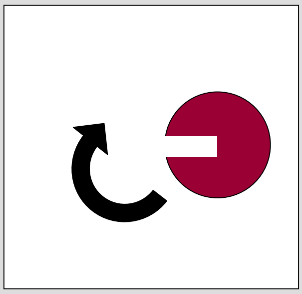

Cubic Lagrange method

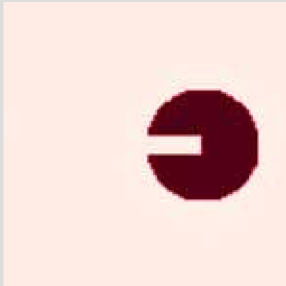

Cubic Lagrange method
+
Surface treatment

Numerical method for particle

DEM (Distinct Element method)

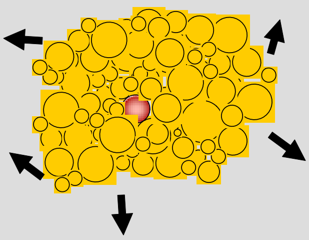

Interparticle force

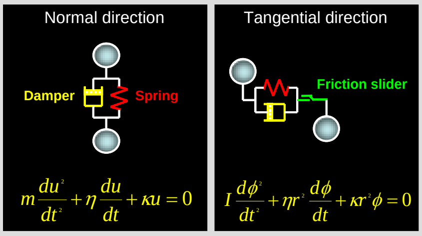

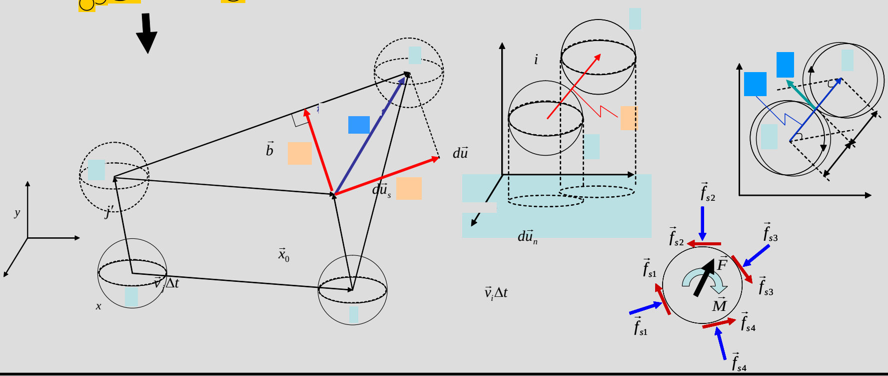

Fluid-particle interaction

Concept of immersed boundary method

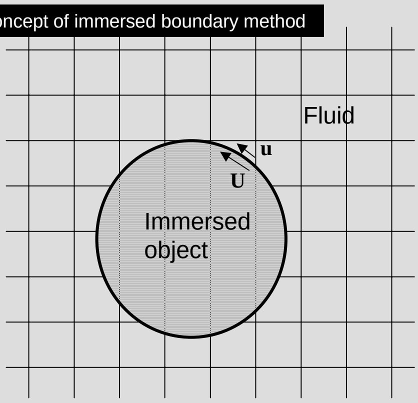

Basic idea

Peskin(1972,1977)
Blood flow simulation with complex elastic boundary

$\mathbf{u}$: velocity of fluid at surface
$\mathbf{U}$: velocity of object at surface

$$\mathbf{U} \neq \mathbf{u}^n$$

$$\Downarrow$$

$$\frac{\partial u}{\partial t} + (\mathbf{u} \cdot \nabla)\mathbf{u} = -\nabla p + \nu \nabla^2 \mathbf{u} + \boxed{\mathbf{F}}$$

Additional body force

$$\Downarrow$$

$$\mathbf{U} = \mathbf{u}^{n+1}$$

IB
- Feedback forcing method ････**Goldstein et al.(1993)** **Saiki and Biringen (1996)**
- Direct forcing method ････ ････ **Mohd-Yusof(1997)**

Feedback forcing method

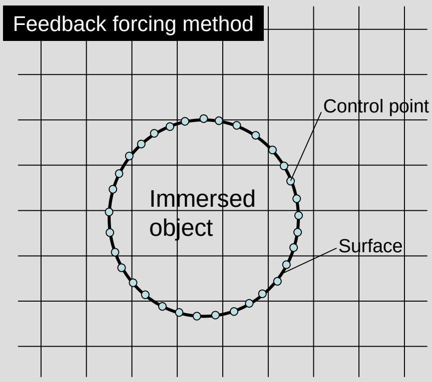

● Calculation grid (Eulerian point)
○ Control point (Lagrangean point)

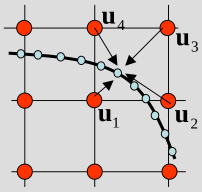

$$\mathbf{u}_s = \sum_{i=1}^{4} W_i \mathbf{u}_i$$

W weighting function

$\mathbf{u}_s$: velocity of fluid at surface

Estimation of body force $\mathbf{F}_s = \alpha \int_0^t (\mathbf{u}_s - \mathbf{U}_s) dt + \beta (\mathbf{u}_s - \mathbf{U}_s)$

$\mathbf{F}_s$: Body force at surface α, β : Negative parameter

Distribution of body force
From control points to calculation grids

$$\mathbf{F}_{ij} = \frac{1}{N_s} \sum_{n=1}^{N_s} W_{i,j} \mathbf{F}_{s(n)}$$

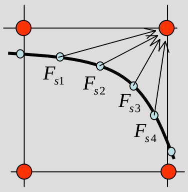

Direct forcing method

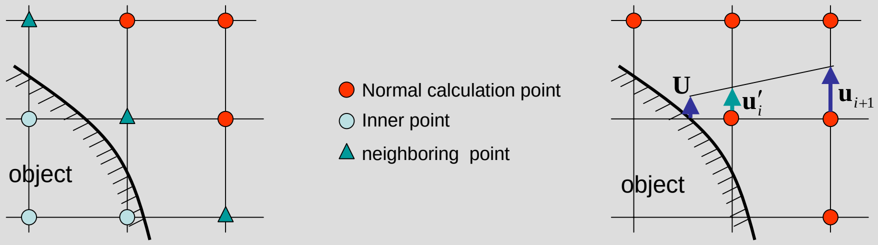

Estimation of body force

$$\frac{u^{n+1}-u^n}{\Delta t} = RHS + \mathbf{F}$$

※ $RHS = -\nabla p + \nu\nabla^2\mathbf{u} - (\mathbf{u}\cdot\nabla)\mathbf{u}$

$$\Rightarrow \frac{u'-u^n}{\Delta t} = RHS + \mathbf{F} \Rightarrow \mathbf{F} = -RHS + \frac{u'-u^n}{\Delta t}$$

$$\begin{cases} \mathbf{F} = -RHS + \dfrac{u'-u^n}{\Delta t} & \text{on neighboring point} \\ \mathbf{F} = 0 & \text{elsewhere} \end{cases}$$

Modified Direct forcing method (Balaras, 2004)

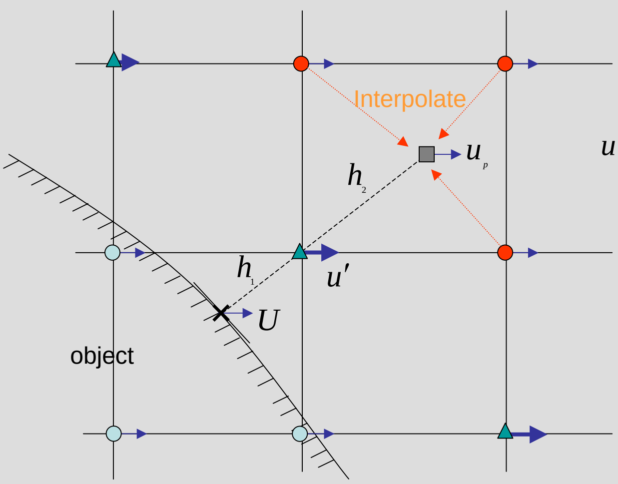

$$u' = \frac{(u_p - U)}{h_1 + h_2} h_1 + U$$

- Normal calculation point
- Inner point
- neighboring point
- Virtual point

Karman vortex simulation using immersed boundary method

Mesh size	$\Delta x, \Delta y$	0.1 m
Number of mesh	$Nx \times Ny$	100×50
Raynolds number	Re	300

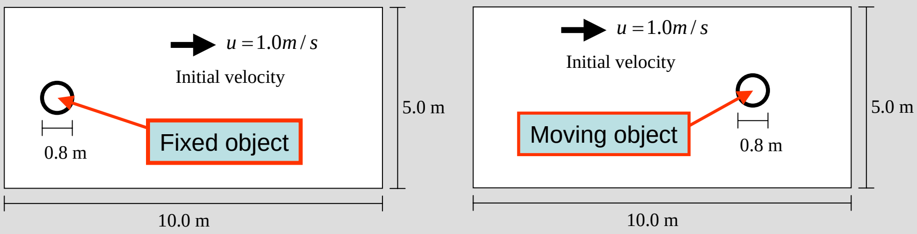

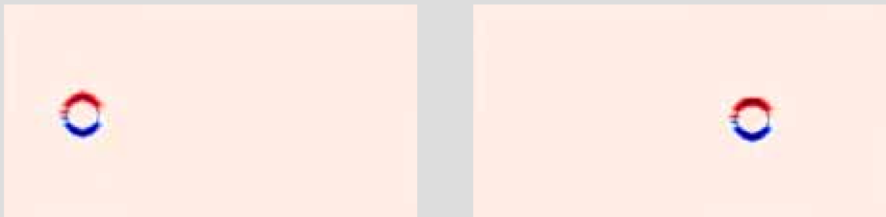

Two phase flow simulation using immersed boundary method

ϕ : Density function for water

ϕ_o : Density function for object

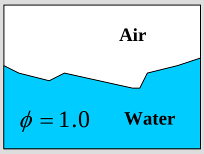

$$\frac{\partial \phi}{\partial t} + (\mathbf{u} \cdot \nabla)\phi = 0$$

$$\rho = \rho_w \phi + \rho_a (1 - \phi)$$

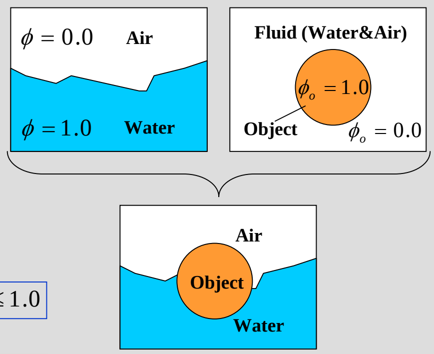

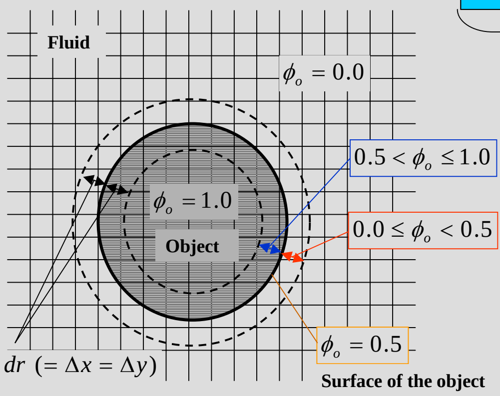

$$\rho_{fluid} = \rho_w \phi + \rho_a (1 - \phi)$$

$$\rho = \rho_o \phi_o + \rho_{fluid} (1 - \phi_o)$$

ρ_w : Density of water

ρ_a : Density of air

ρ_o : Density of object

Interaction between water and one particle

Mesh size	$\Delta x, \Delta y$	0.01 m
Number of mesh	$Nx \times Ny$	100×100
Density (Air)	ρ_a	1.2 kg/m^3
(Wtaer)	ρ_w	1000.0 kg/m^3
Gravity acceleration	g	9.8 m/s^2

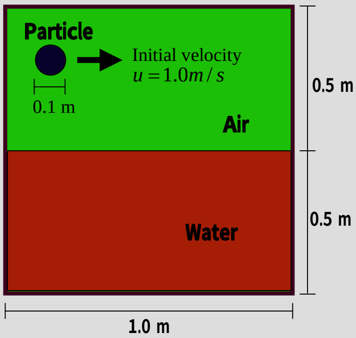

Density of particle 500.0 kg/m3 Density of particle 1200.0 kg/m3

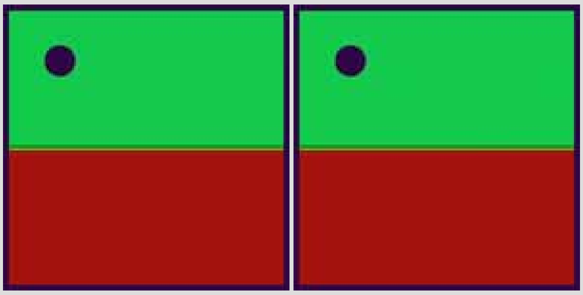

Interaction between water and particles

Mesh size	$\Delta x, \Delta y$	0.005 m
Number of mesh	$Nx \times Ny$	200×200
Density (Air)	ρ_a	1.2 kg/m^3
(Wtaer)	ρ_w	1000.0 kg/m^3
Gravity acceleration	g	9.8 m/s^2

Density of particles 500.0 kg/m3 Density of particles 1500.0 kg/m3

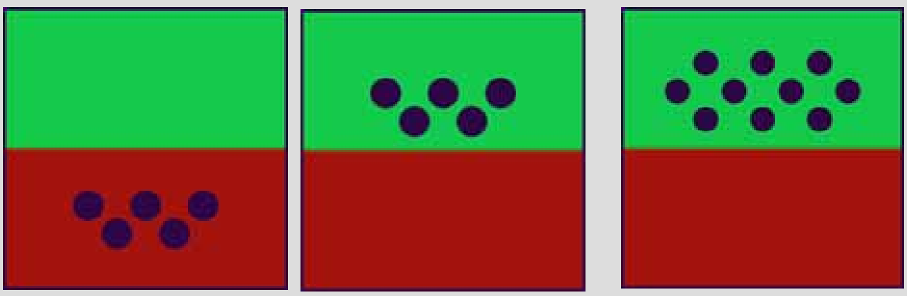

Conclusion

- **New numerical framework for liquefaction analysis**
  - Behavior of pore fluid is solved CFD.
  - Behavior of soil grain are solved DEM.
  - Interaction is described by using immersed boundary method.

～ **Future study** ～

- Parallel computing
- Validation

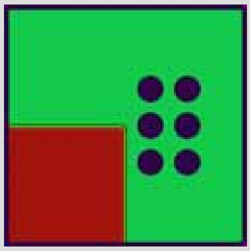

Tank you for your kind attention.

International RIAM Symposium, December 8, 2006
Analyses of Strongly Nonlinear Flows around Moving Boundaries

Numerical simulation method for free surface flows using the Boltzmann equation

Yoshiki Nishi
Research Institute for Applied Mechanics
Kyushu University

1

CFD approach for the seakeeping problems

(1) Objective of numerical simulations

●Free surface,

●Hydrodynamic force, and

●Floating body motion.

(2) Current CFD approaches

■Finite Difference Method (FDM), and Finite Volume Method (FVM),

■Multi-moment methods (CIP-based methods etc.), and

■Particle methods (MPS, SPH etc.).

Governing equation: Navier-Stokes equation, continuity equation

Computational procedure: MAC algorithm, or its family

2

The Boltzmann equation

$$\boxed{\frac{\partial f}{\partial t} + \mathbf{e} \bullet \nabla f = \left(\frac{\partial f}{\partial t}\right)_{Collision}}$$

f : *Velocity distribution function*

$\mathbf{e}$: *Velocity vector of molecular kinetics*

Macroscopic view

Microscopic view

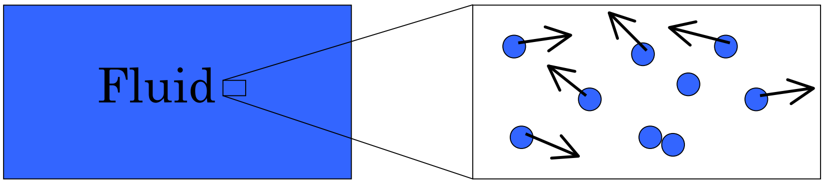

Governed by N-S equation

Governed by the Boltzmann equation

3

Theoretical relation between molecular kinetics and fluid dynamics

(1) $\frac{\partial f}{\partial t} + \mathbf{e} \bullet \nabla f = \left(\frac{\partial f}{\partial t}\right)_{Collision}$

(2) $\langle \Psi \rangle (\mathbf{x}, t) = \frac{\int \Psi(\mathbf{e}, \mathbf{x}, t) f(\mathbf{e}, \mathbf{x}, t) d^3\mathbf{e}}{n(\mathbf{x}, t)}$ $\cdots$ *Ensemble average of* Ψ

(3) $n(\mathbf{x}, t) \equiv \int f(\mathbf{e}, \mathbf{x}, t) d^3\mathbf{e}$ $\cdots$ *Total molecular number*

$\int (1) d^3\mathbf{e}$

0th-order moment

$\int (1)\mathbf{e}\, d^3\mathbf{e}$

1st-order moment

$$\boxed{\frac{\partial \rho}{\partial t} + \nabla \bullet (\rho \mathbf{v}) = 0}$$

Continuity equation

$$\boxed{\frac{\partial \rho \mathbf{v}}{\partial t} + \nabla \bullet (\rho \mathbf{v}\mathbf{v}) = -\nabla p + \nabla \Pi}$$

Navier-Stokes equation

4

Previous works and current status of the Boltzmann method

(1) Basic research (theory of statistical physics, or chemical physics)

reviewed by Chen and Doolen (1998); Luo (2000)

(2) Application to engineering problems

✓Two-phase flow simulations

Air bubble deformation, and upwelling (e.g. Inamuro et al., 2004; Takada et al., 2001)

Boiling water (e.g. Yang et al., 2000)

✓Deformation of metal materials due to solidification, melting, and foaming (e.g., Korner et al., 2005)

5

Motivation of the present research

➔ Development of a Boltzmann equation based-numerical method for ocean engineering problems that can be comfortably used in practical engineering societies (industrial societies).

■Simplicity of the form of the Boltzmann equation $\frac{\partial f}{\partial t} + \mathbf{e} \bullet \nabla f = \left(\frac{\partial f}{\partial t} \right)_{Collision}$

●Linearity of translation (advection) term

●There are only two terms: translation and collision

■Simplicity of the algorithm: Lattice Boltzmann Method (LBM)

●Translation term: perfect shifting semi-Lagrangian procedure

●Collision term: Single relaxation time (τ) model (BGK model)

$$f_i(\mathbf{x} + \mathbf{e}_i \Delta t, t + \Delta t) = f_i(\mathbf{x}, t) - \frac{\left(f_i(\mathbf{x}, t) - f_i^{eq}(\mathbf{x}, t) \right)}{\tau}$$

$f_i^{eq}(\mathbf{x}, t) \cdots$ *Local equilibrium distribution function*

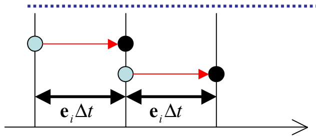

6

Local equilibrium distribution function

$$f^{eq}(e,\mathbf{x},t) = n(\mathbf{x},t)\frac{|\mathbf{e}|^2}{2\pi\sigma^2}\frac{|\mathbf{e}|}{\sqrt{2\pi}\sigma}\exp\left(-\frac{(\mathbf{e}-\mathbf{v})^2}{2\sigma^2}\right)$$

$$\sigma^2 \equiv \frac{p}{\rho}$$

Normal distribution with the mean $\mathbf{v}$ and dispersion σ^2

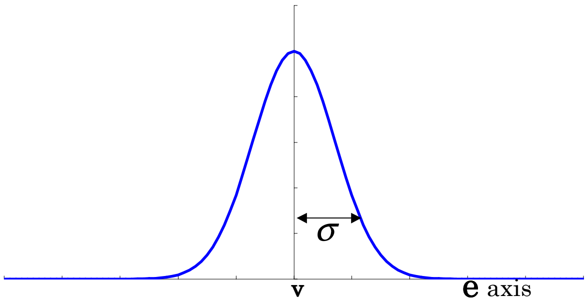

7

Dynamic boundary condition

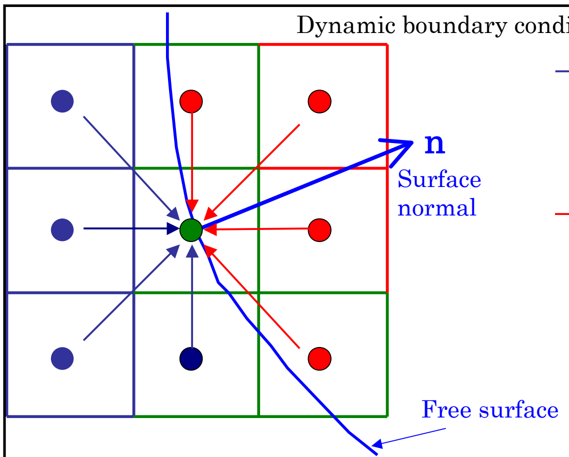

From water to interface (known by translation)

Known $f_i(\mathbf{x},t)$

From air to interface (unknown by translation)

Unknown $f_i(\mathbf{x},t)$

Water pressure at an interface cell

$$F_\alpha/\Delta S = -\left[\overset{\text{Known}}{\sum_{i,\mathbf{n}\cdot\mathbf{e}_i>0} f_i(\mathbf{x},t)}(e_{i,\alpha}-v_\alpha)(\mathbf{e}_i-\mathbf{v})\bullet\mathbf{n} + \overset{\text{Unknown}}{\sum_{i,\mathbf{n}\cdot\mathbf{e}_i\le 0} f_i(\mathbf{x},t)}(e_{i,\alpha}-v_\alpha)(\mathbf{e}_i-\mathbf{v})\bullet\mathbf{n}\right]$$

|| Dynamic boundary condition

Atmospheric pressure near the interface cell

$$p^{atm} n_\alpha = \sum_i f_i^{eq}(\mathbf{x},t)(e_{i,\alpha}-v_\alpha)(\mathbf{e}_i-\mathbf{v})\bullet\mathbf{n}$$

$$\overset{\text{Unknown}}{f_i(\mathbf{x},t)} = f_i^{eq}(p^{atm},\mathbf{v}) + f_{\bar{i}}^{eq}(p^{atm},\mathbf{v}) - \overset{\text{Known}}{f_{\bar{i}}(\mathbf{x},t)}, \quad \mathbf{n}\bullet\mathbf{e}_i \le 0, \ \mathbf{e}_i = -\mathbf{e}_{\bar{i}}$$

8

Free surface capturing

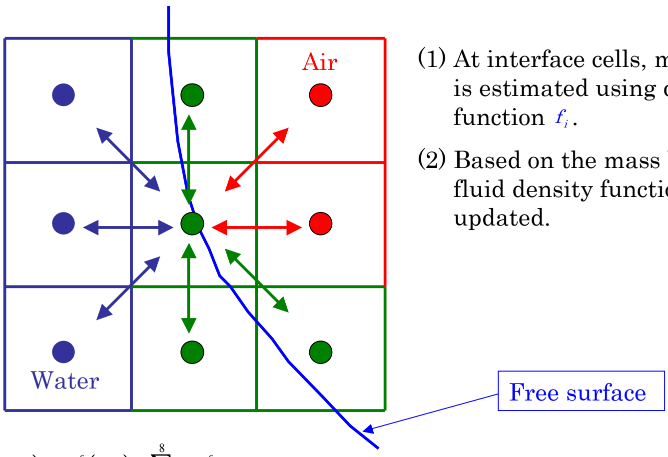

(1) At interface cells, mass budget is estimated using distribution function f_i.

(2) Based on the mass budget, fluid density function ϕ_i is updated.

$$\phi^f(\mathbf{x}, t+\Delta t) = \phi^f(\mathbf{x}, t) + \sum_{i=1}^{8} \Delta\phi_i^f$$

$$\Delta\phi_i^f \begin{cases} = f_{\bar{i}}(\mathbf{x}+\mathbf{e}_i\Delta t,\, t) - f_i(\mathbf{x},\, t) \; \textit{if upstream cell is fluid} \\ = \{f_{\bar{i}}(\mathbf{x}+\mathbf{e}_i\Delta t,\, t) - f_i(\mathbf{x},\, t)\}\phi^f(x+1/2\,\mathbf{e}_i\Delta t,\, t) \; \textit{if upstream cell is interface} \\ = 0 \quad \textit{if upstream cell is atmosphere} \end{cases}$$

9

Incorporation of solid body

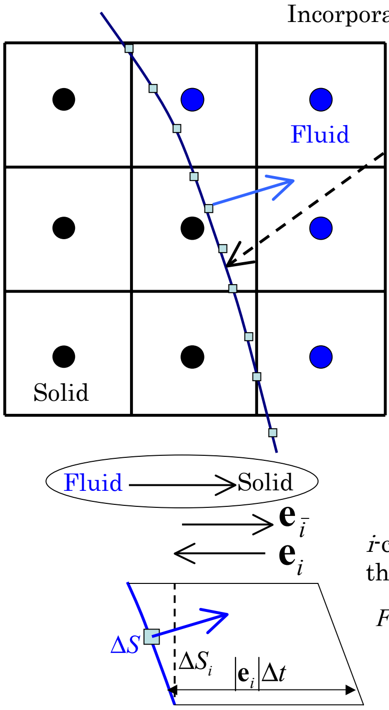

Immersed boundary method (proposed originally by Peskin, 1977)

Immersed (embedded) boundary

Solid → Fluid

Approximate No-slip condition using the local equilibrium distribution function

$$f_i(\mathbf{x}, t, \mathbf{v}) \cong f_i^{eq}(\mathbf{x}, t, \mathbf{v}_{body})$$

Direct forcing in the framework of molecular kinetics

i-component force exerted on the solid surface element

$$F_i = -(f_{\bar{i}} e_{\bar{i}} + f_i e_i)\Delta S_i n \bullet \frac{\mathbf{e}_i}{|\mathbf{e}_i|}\mathbf{e}_i, \quad n \bullet \mathbf{e}_i < 0$$

10

Flow chart of computational procedure

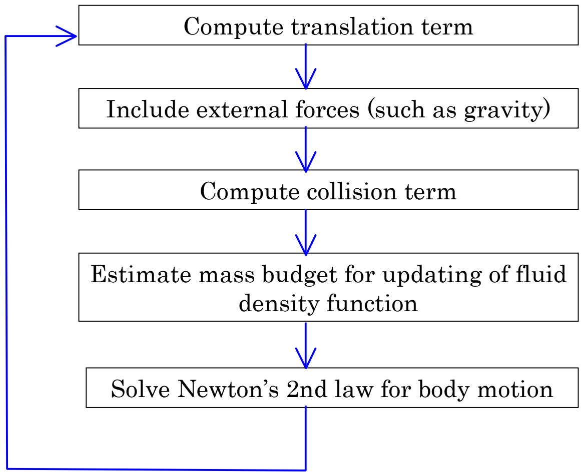

11

Advection test for the check of the code using the Boltzmann method

$$\frac{\partial \phi}{\partial t} + \mathbf{v} \bullet (\nabla \phi) = 0$$

Velocity **v** is given as no-shear rotational flow.

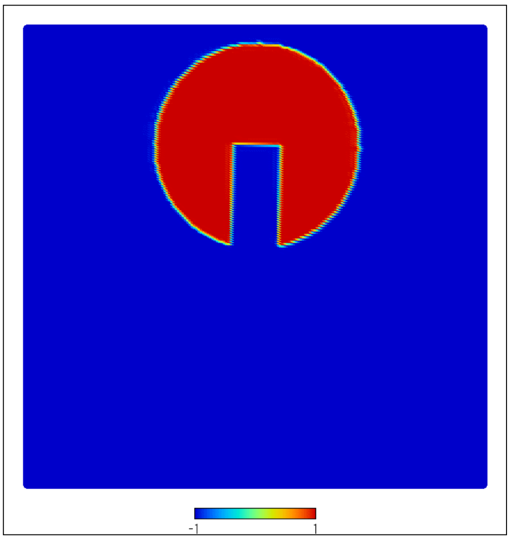

12

Water mass deformation in gravity field 1

Free fall of water ball

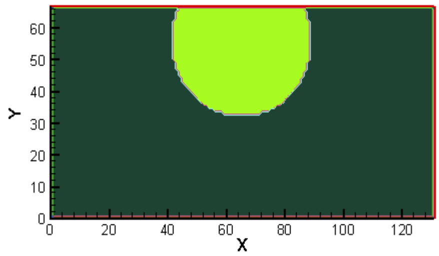

13

Water mass deformation in gravity field 2

Dam breaking

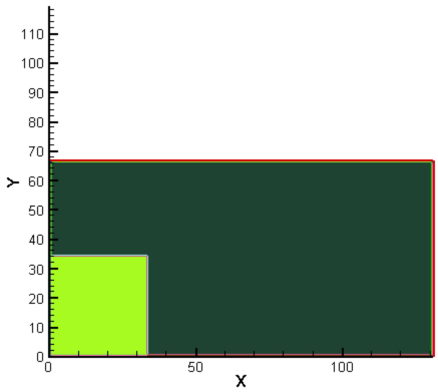

14

Water entry of a light body with a simple shape

Specific gravity: 0.5

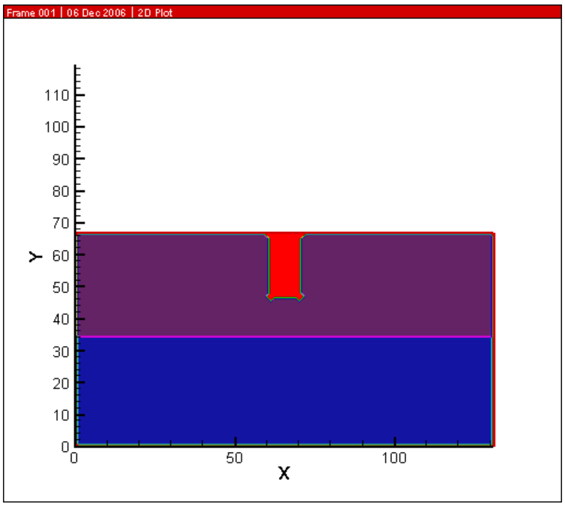

15

Piston-type wavemaker

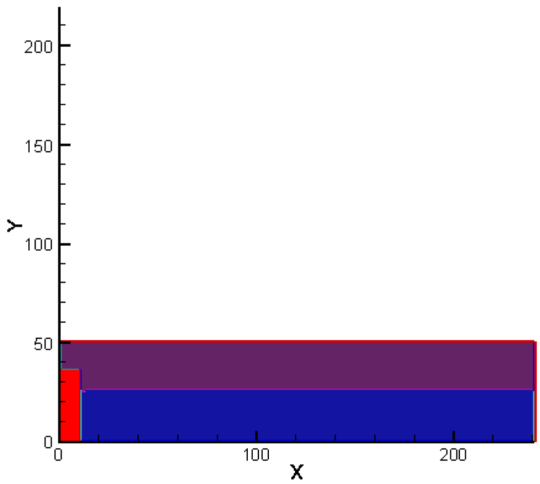

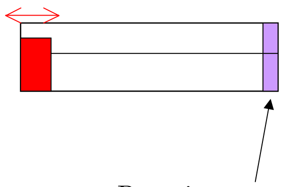

16

Forced oscillation of a circle-shape body

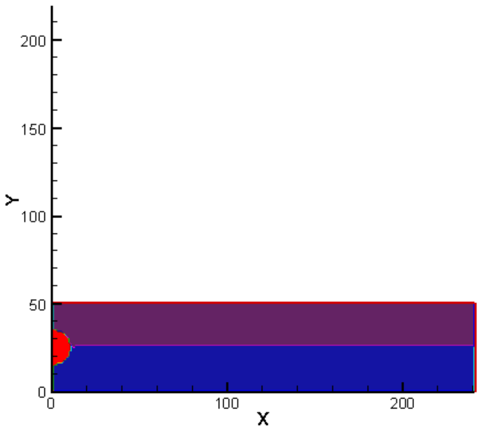

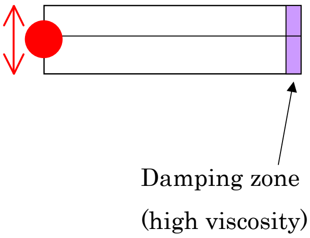

17

Propulsive ellipse body

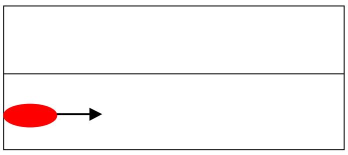

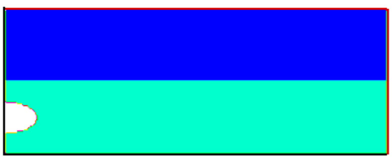

18

Concluding remarks

(1) From the standpoint of practical engineering, the present research has begun to develop a Boltzmann equation-based numerical method for free surface flows.

(2) Several 2-D simple cases have been simulated, which has confirmed that the present new method performs acceptably as a first step.

(3) Future works

to make respects of current technical difficulties clear,

to check the quantitative validity in cases of 2-D simple problems, and

to extend 3-D computation.

A practical tool!

Thank you for your attentions.

19

Representation of stress tensor using ensemble averages

$$\rho\left\langle\left(e_\alpha-v_\alpha\right)\left(e_\beta-v_\beta\right)\right\rangle=p\delta_{\alpha\beta}+\Pi_{\alpha\beta}$$

$$f(\mathbf{x},t)=f^{eq}(\mathbf{x},t)+f'(\mathbf{x},t)$$

Analytical form

$$\begin{cases} p\delta_{\alpha\beta}=\rho\left\langle\left(e_\alpha-v_\alpha\right)\left(e_\beta-v_\beta\right)\right\rangle^{eq} \\ \Pi_{\alpha\beta}=\rho\left\langle\left(e_\alpha-v_\alpha\right)\left(e_\beta-v_\beta\right)\right\rangle' \end{cases}$$

Discretized form

$$\begin{cases} p\delta_{\alpha\beta}=\sum_{i=0}^{N} f_i^{eq}\left(e_\alpha-v_\alpha\right)\left(e_\beta-v_\beta\right) \\ \Pi_{\alpha\beta}=\sum_{i=0}^{N} f_i'\left(e_\alpha-v_\alpha\right)\left(e_\beta-v_\beta\right) \end{cases}$$

20

External force (gravity)

$$f_i(\mathbf{x}+\mathbf{e}_i\Delta t, t+\Delta t) = f_i(\mathbf{x}, t) - \frac{\left(f_i(\mathbf{x}, t) - f_i^{eq}(\mathbf{x}, t)\right)}{\tau} + \underline{F_i \Delta t}$$

$$\rho\mathbf{v} = \sum_{i=0}^{N} \mathbf{e}_i f_i + \frac{\Delta t}{2}\mathbf{F}$$

$$F_i = \left(1 - \frac{1}{2\tau}\right)\omega_i \left[\frac{\mathbf{e}_i - \mathbf{v}}{c_s^{\ 2}} + \frac{\mathbf{e}_i \bullet \mathbf{v}}{c_s^{\ 4}}\mathbf{e}_i\right] \bullet \mathbf{F}$$

$$\begin{cases} \mathbf{F} : \textit{External force} \\ F_i : \textit{Forcing term in the Boltzmann equation} \end{cases}$$

21

Macroscopic variables

$$\rho = \sum_{i=0}^{N} f_i \quad \text{Fluid density}$$

$$\rho\mathbf{v} = \sum_{i=0}^{N} f_i \mathbf{e}_i \quad \textit{Momentum of fluid flow}$$

Discretized directions of molecular motion

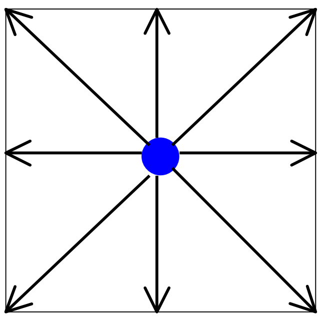

22

Ensemble average

Operation which relates microscopic variables to macroscopic variables

$$\overbrace{\langle\Psi\rangle}^{\text{Macroscopic}}(\mathbf{x},t)=\frac{\int \overbrace{\Psi(\mathbf{e},\mathbf{x},t)}^{\text{Microscopic}} f(\mathbf{e},\mathbf{x},t)\,d^3\mathbf{e}}{\int f(\mathbf{e},\mathbf{x},t)\,d^3\mathbf{e}} \cdots \textit{Ensemble average}$$

Ensemble averages of momentum

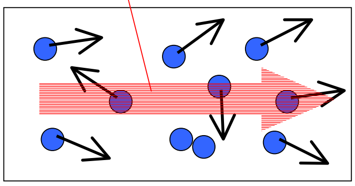

23

Wall boundary

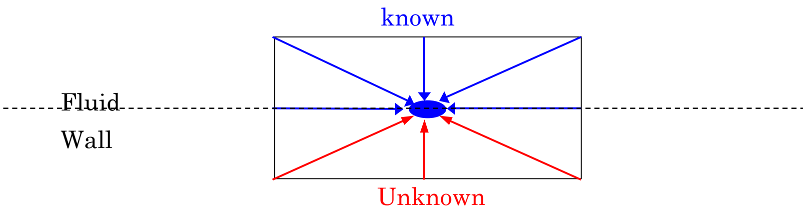

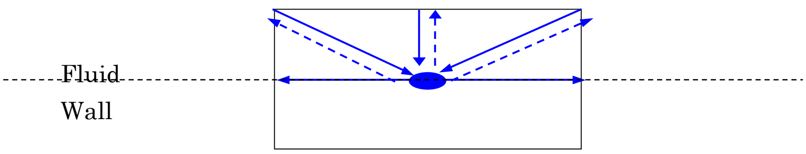

- Bounce-back ⟶ No-slip
- Light reflection ⟶ Free-slip

24

1

Momentum Conservative Sharp Interface Cartesian Grid Method for Free-Surface Flow

National Maritime Research Institute, Japan
Kenji Takizawa

2

Motivation 1

- I was using…
  - Non-conservative scheme (CIP)
  - Semi-Lagrangian scheme
  - But…
- We are interested in …
  - Impulse than Impact
  - High Reynolds number
  - More and more accuracy

Motivation 2 (IDO-CF)

- We are developing new scheme.
  - Conservation scheme
  - High accuracy
  - Euler method
- Apply to free-surface problem
  - Keep conservation
  - Keep the accuracy
  - The research started at this year.

Sharp interface concept

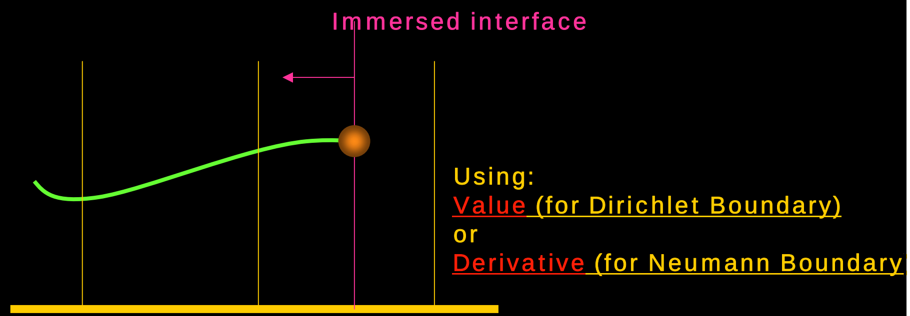

•Using interface properties

•Reconstruct only fluid part → Conserve

5

Sharp interface concept

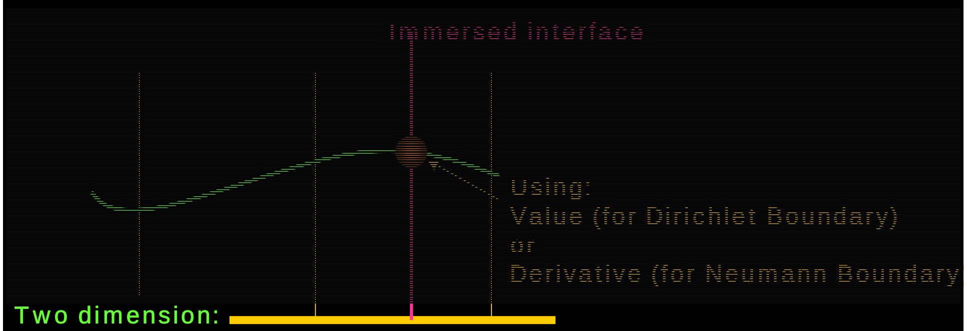

x direction: using 1 dimensional scheme

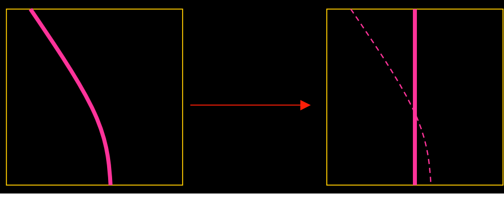

6

About IDO-CF $\phi(x, y)$

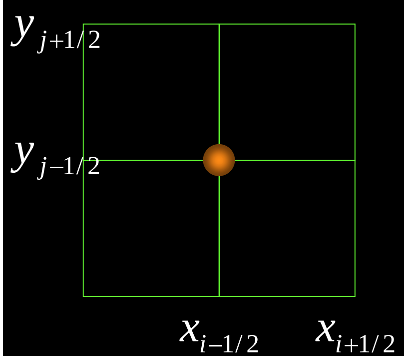

4 kind variables (Moment)

Point Value

$$\boxed{\phi_{i-1/2,j-1/2} = \phi\left(x_{i-1/2}, y_{j-1/2}\right)}$$

$$\phi_{i,j-1/2} = \frac{1}{\Delta x}\int_{x_{i-1/2}}^{x_{i+1/2}} \phi\left(x, y_{j-1/2}\right) dx$$

$$\phi_{i-1/2,j} = \frac{1}{\Delta y}\int_{y_{j-1/2}}^{y_{j+1/2}} \phi\left(x_{i-1/2}, y\right) dy$$

$$\phi_{i,j} = \frac{1}{\Delta x \Delta y}\int_{y_{j-1/2}}^{y_{j+1/2}}\int_{x_{i-1/2}}^{x_{i+1/2}} \phi(x, y)\, dxdy$$

7

About IDO-CF $\phi(x,y)$

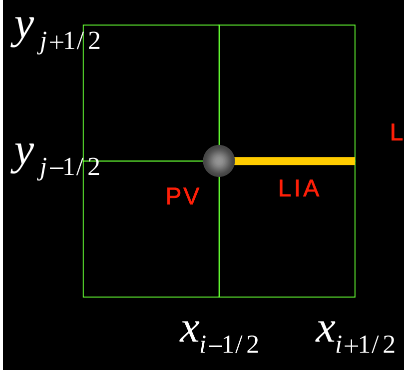

4 kind variables (Moment)

$$\phi_{i-1/2,j-1/2} = \phi\left(x_{i-1/2}, y_{j-1/2}\right)$$

Line Integrate Average

$$\boxed{\phi_{i,j-1/2} = \frac{1}{\Delta x}\int_{x_{i-1/2}}^{x_{i+1/2}} \phi\left(x, y_{j-1/2}\right)dx}$$

$$\phi_{i-1/2,j} = \frac{1}{\Delta y}\int_{y_{j-1/2}}^{y_{j+1/2}} \phi\left(x_{i-1/2}, y\right)dy$$

$$\phi_{i,j} = \frac{1}{\Delta x \Delta y}\int_{y_{j-1/2}}^{y_{j+1/2}}\int_{x_{i-1/2}}^{x_{i+1/2}} \phi(x,y)dxdy$$

8

About IDO-CF $\phi(x,y)$

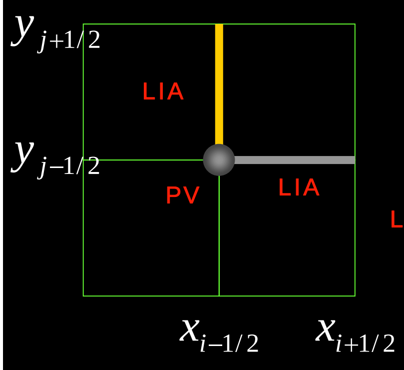

4 kind variables (Moment)

$$\phi_{i-1/2,j-1/2} = \phi\left(x_{i-1/2}, y_{j-1/2}\right)$$

$$\phi_{i,j-1/2} = \frac{1}{\Delta x}\int_{x_{i-1/2}}^{x_{i+1/2}} \phi\left(x, y_{j-1/2}\right)dx$$

Line Integrate Average

$$\boxed{\phi_{i-1/2,j} = \frac{1}{\Delta y}\int_{y_{j-1/2}}^{y_{j+1/2}} \phi\left(x_{i-1/2}, y\right)dy}$$

$$\phi_{i,j} = \frac{1}{\Delta x \Delta y}\int_{y_{j-1/2}}^{y_{j+1/2}}\int_{x_{i-1/2}}^{x_{i+1/2}} \phi(x,y)dxdy$$

9

About IDO-CF $\phi(x,y)$

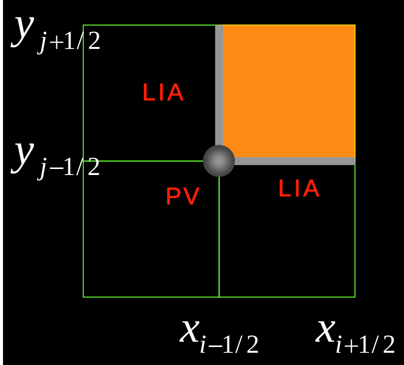

4 kind variables (Moment)

$$\phi_{i-1/2,j-1/2} = \phi\left(x_{i-1/2}, y_{j-1/2}\right)$$

$$\phi_{i,j-1/2} = \frac{1}{\Delta x}\int_{x_{i-1/2}}^{x_{i+1/2}} \phi\left(x, y_{j-1/2}\right)dx$$

$$\phi_{i-1/2,j} = \frac{1}{\Delta y}\int_{y_{j-1/2}}^{y_{j+1/2}} \phi\left(x_{i-1/2}, y\right)dy$$

Surface/Volume Integrate Average

$$\boxed{\phi_{i,j} = \frac{1}{\Delta x \Delta y}\int_{y_{j-1/2}}^{y_{j+1/2}}\int_{x_{i-1/2}}^{x_{i+1/2}} \phi(x,y)dxdy}$$

10

About IDO-CF $\phi(x,y)$

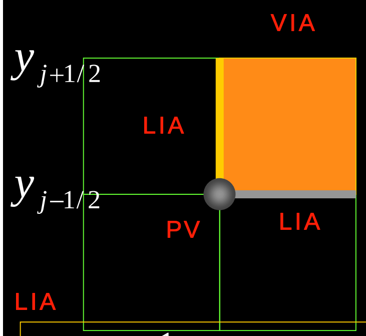

Moments are only two types.

LIA

$$\boxed{\phi_{i-1/2,j} = \frac{1}{\Delta y}\int_{y_{j-1/2}}^{y_{j+1/2}} \phi\left(x_{i-1/2}, y\right)dy}$$

VIA

$$\boxed{\phi_{i,j} = \frac{1}{\Delta x}\int_{x_{i-1/2}}^{x_{i+1/2}}\left[\frac{1}{\Delta y}\int_{y_{j-1/2}}^{y_{j+1/2}} \phi(x,y)dy\right]dx}$$

PV

$$\phi_{i-1/2,j-1/2} = \phi\left(x_{i-1/2}, y_{j-1/2}\right)$$

LIA

$$\phi_{i,j-1/2} = \frac{1}{\Delta x}\int_{x_{i-1/2}}^{x_{i+1/2}} \phi\left(x, y_{j-1/2}\right)dx$$

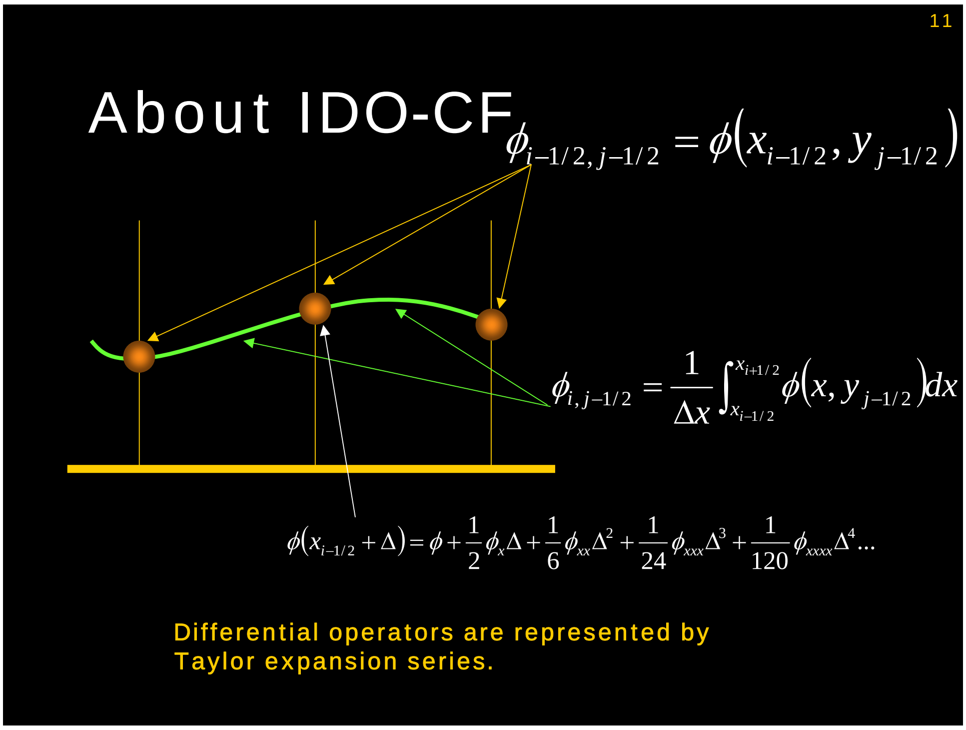
11
About IDO-CF
$\phi_{i-1/2,j-1/2} = \phi(x_{i-1/2}, y_{j-1/2})$
$\phi_{i,j-1/2} = \frac{1}{\Delta x}\int_{x_{i-1/2}}^{x_{i+1/2}} \phi(x, y_{j-1/2})dx$
$\phi(x_{i-1/2} + \Delta) = \phi + \frac{1}{2}\phi_x\Delta + \frac{1}{6}\phi_{xx}\Delta^2 + \frac{1}{24}\phi_{xxx}\Delta^3 + \frac{1}{120}\phi_{xxxx}\Delta^4 ...$
Differential operators are represented by
Taylor expansion series.

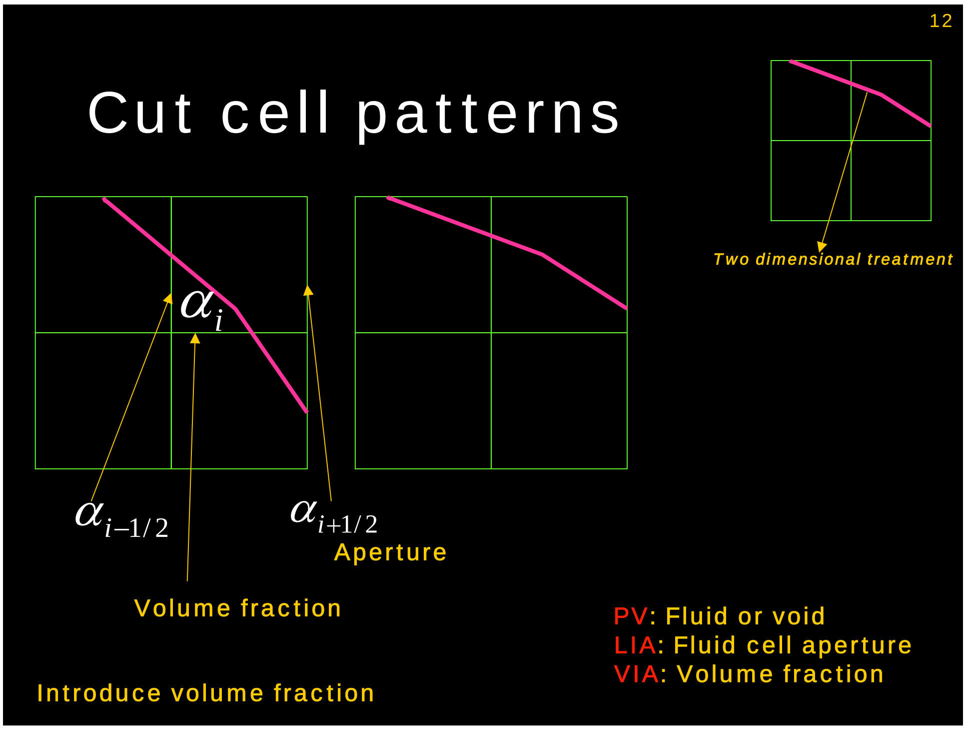
12
Cut cell patterns
α_i
$\alpha_{i-1/2}$
$\alpha_{i+1/2}$
Aperture
Volume fraction
Two dimensional treatment
PV: Fluid or void
LIA: Fluid cell aperture
VIA: Volume fraction
Introduce volume fraction

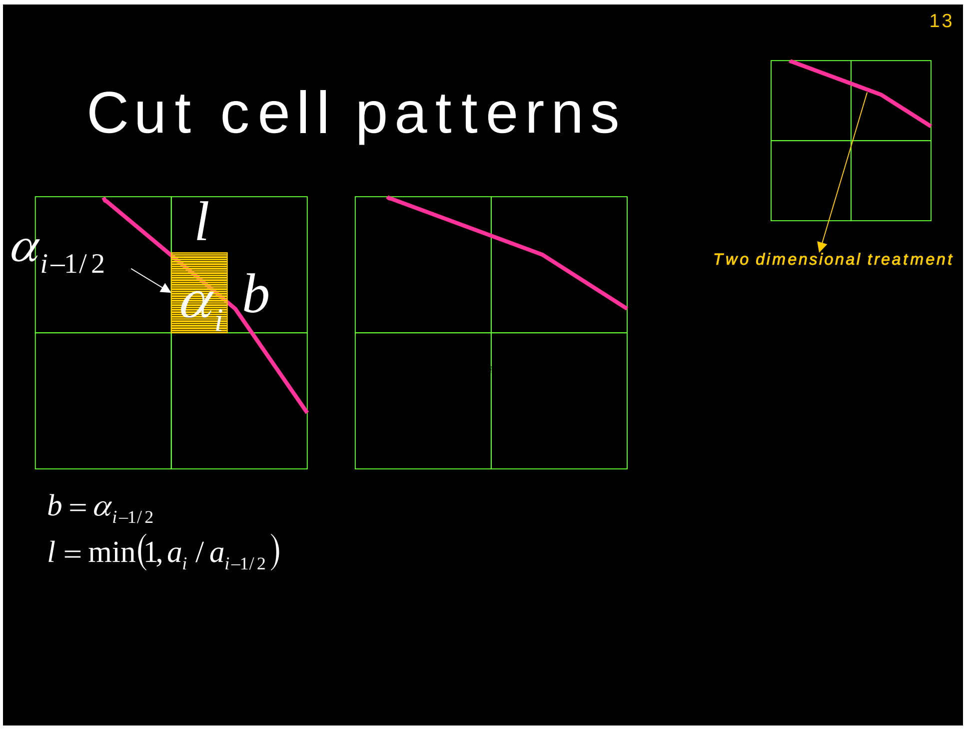
13
Cut cell patterns
l
$\alpha_{i-1/2}$
α_i
b
Two dimensional treatment
$b = \alpha_{i-1/2}$
$l = \min(1, a_i / a_{i-1/2})$

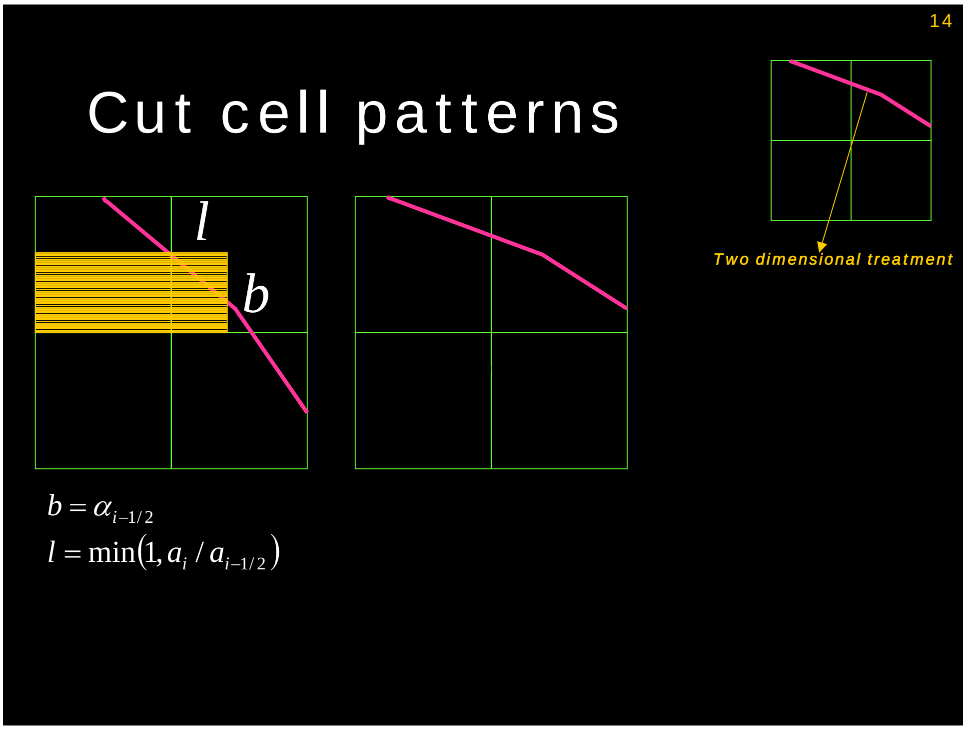
14
Cut cell patterns
l
b
Two dimensional treatment
$b = \alpha_{i-1/2}$
$l = \min(1, a_i / a_{i-1/2})$

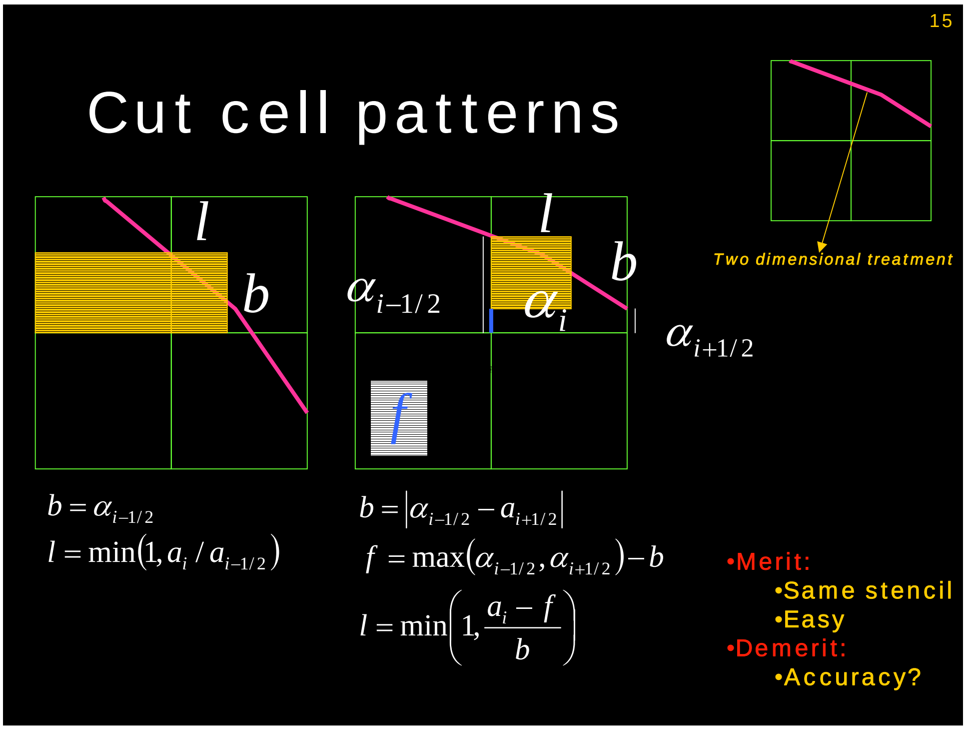
15
Cut cell patterns
l
b
$\alpha_{i-1/2}$
α_i
$\alpha_{i+1/2}$
f
Two dimensional treatment
$b = \alpha_{i-1/2}$
$l = \min(1, a_i / a_{i-1/2})$
$b = |\alpha_{i-1/2} - a_{i+1/2}|$
$f = \max(\alpha_{i-1/2}, \alpha_{i+1/2}) - b$
$l = \min\left(1, \frac{a_i - f}{b}\right)$
•Merit:
•Same stencil
•Easy
•Demerit:
•Accuracy?

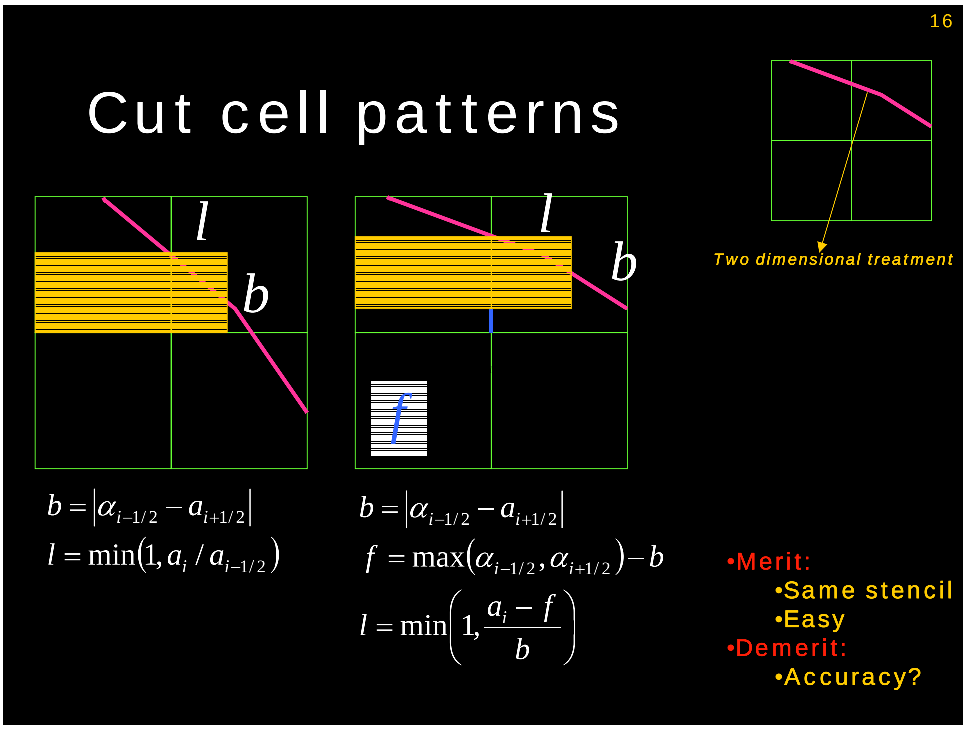
16
Cut cell patterns
l
b
f
Two dimensional treatment
$b = |\alpha_{i-1/2} - a_{i+1/2}|$
$l = \min(1, a_i / a_{i-1/2})$
$b = |\alpha_{i-1/2} - a_{i+1/2}|$
$f = \max(\alpha_{i-1/2}, \alpha_{i+1/2}) - b$
$l = \min\left(1, \frac{a_i - f}{b}\right)$
•Merit:
•Same stencil
•Easy
•Demerit:
•Accuracy?

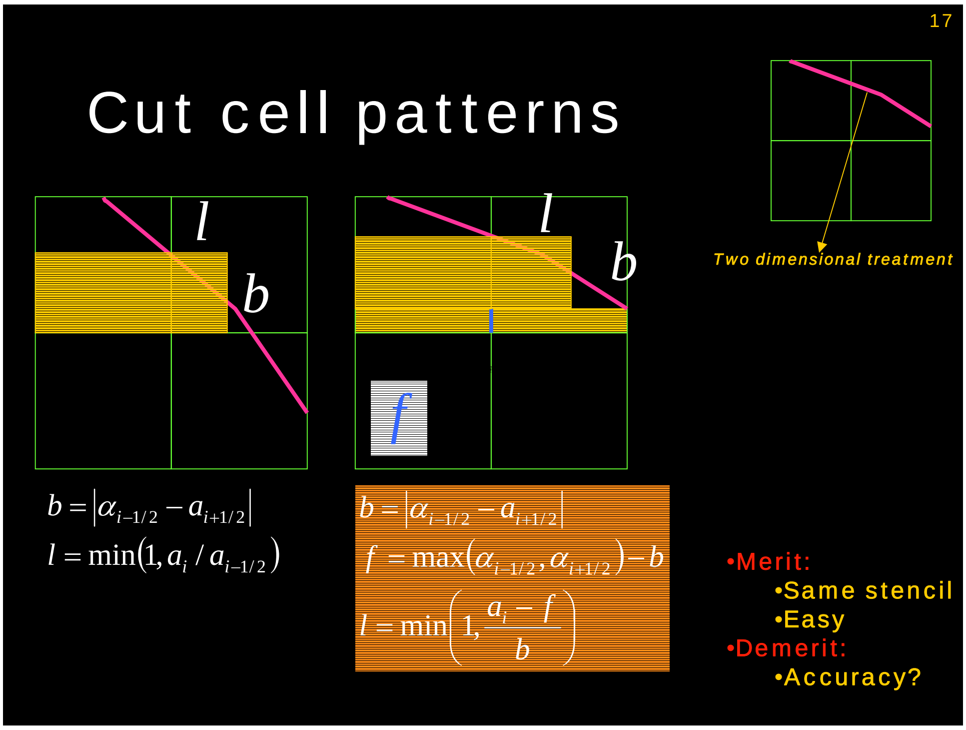
17
Cut cell patterns
Two dimensional treatment
l
b
l
b
f
$b=|\alpha_{i-1/2}-a_{i+1/2}|$
$l=\min(1,a_i/a_{i-1/2})$
$b=|\alpha_{i-1/2}-a_{i+1/2}|$
$f=\max(\alpha_{i-1/2},\alpha_{i+1/2})-b$
$l=\min\left(1,\frac{a_i-f}{b}\right)$
•Merit:
•Same stencil
•Easy
•Demerit:
•Accuracy?

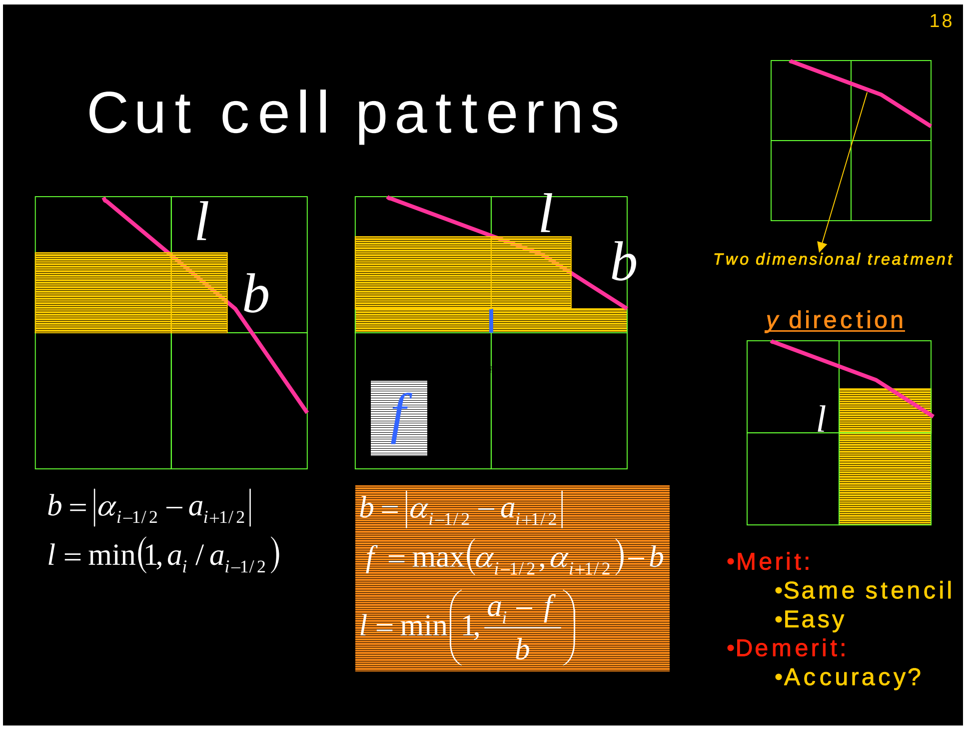
18
Cut cell patterns
Two dimensional treatment
y direction
l
l
b
l
b
f
$b=|\alpha_{i-1/2}-a_{i+1/2}|$
$l=\min(1,a_i/a_{i-1/2})$
$b=|\alpha_{i-1/2}-a_{i+1/2}|$
$f=\max(\alpha_{i-1/2},\alpha_{i+1/2})-b$
$l=\min\left(1,\frac{a_i-f}{b}\right)$
•Merit:
•Same stencil
•Easy
•Demerit:
•Accuracy?

Complex boundary

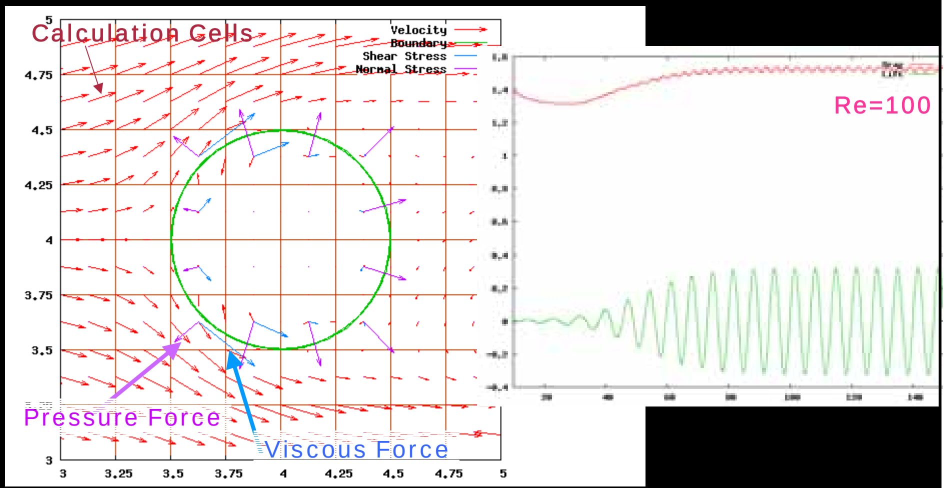

Interface Exchange Flux

Force directions are reasonable.

Moving boundary

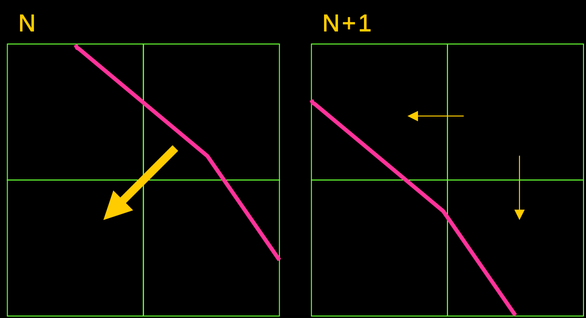

$\alpha_{i,j} = 0.3 \dashrightarrow \alpha_{i,j} = 0$

Must $\phi_{i,j}^{n+1} \to 0$

$$\frac{\alpha_{i,j}\phi_{i,j}^{n+1} - \alpha_{i,j}\phi_{i,j}^{n}}{\Delta t} + \frac{\left(\alpha_{i+1/2,j}u_{i+1/2,j}\phi_{i+1/2,j} - \alpha_{i-1/2}u_{i-1/2,j}\phi_{i-1/2,j}\right)}{\Delta x} + \ldots = 0$$

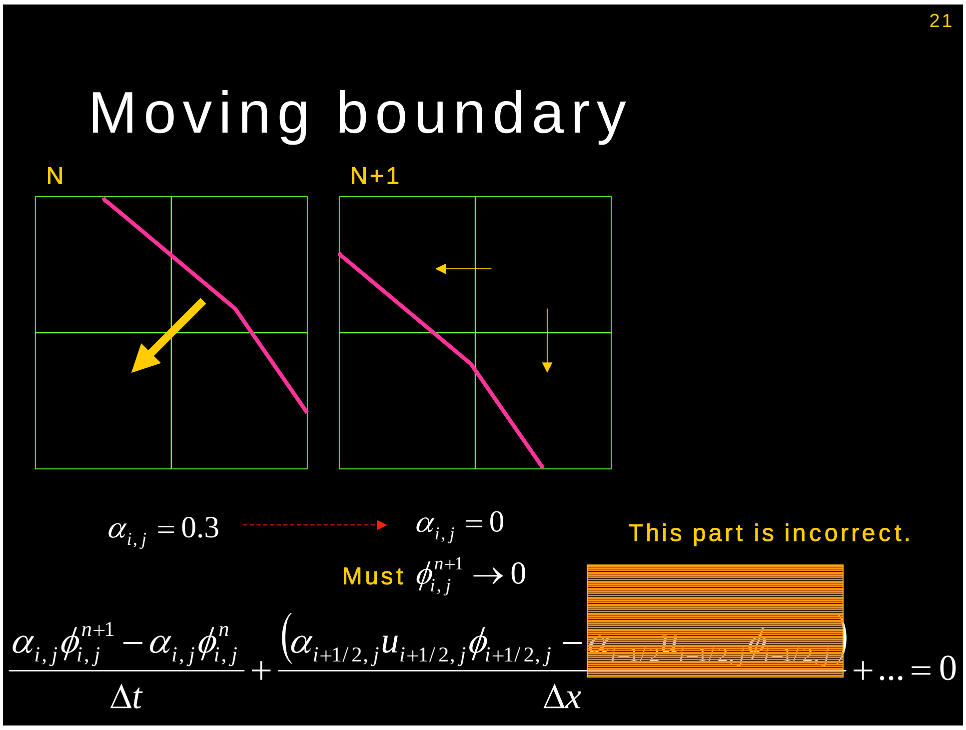
21
Moving boundary
N
N+1
$\alpha_{i,j}=0.3$
$\alpha_{i,j}=0$
Must $\phi_{i,j}^{n+1}\to 0$
This part is incorrect.
$\frac{\alpha_{i,j}\phi_{i,j}^{n+1}-\alpha_{i,j}\phi_{i,j}^{n}}{\Delta t}+\frac{\left(\alpha_{i+1/2,j}u_{i+1/2,j}\phi_{i+1/2,j}-\alpha_{i-1/2,j}u_{i-1/2,j}\phi_{i-1/2,j}\right)}{\Delta x}+\ldots=0$

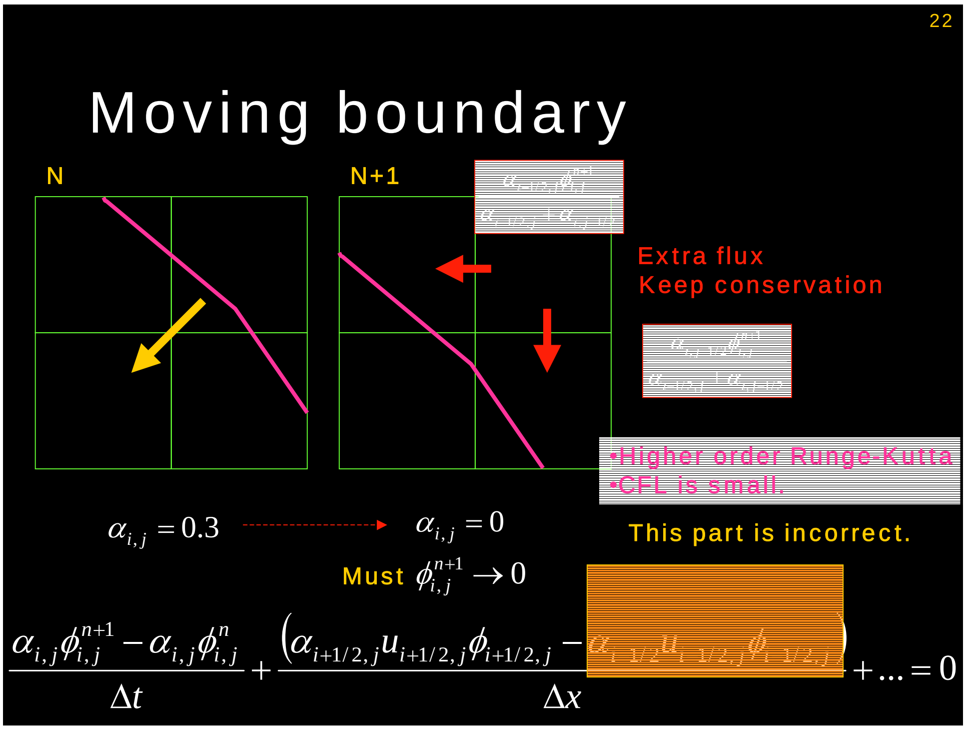
22
Moving boundary
N
N+1
Extra flux
Keep conservation
•Higher order Runge-Kutta
•CFL is small.
$\alpha_{i,j}=0.3$
$\alpha_{i,j}=0$
Must $\phi_{i,j}^{n+1}\to 0$
This part is incorrect.
$\frac{\alpha_{i,j}\phi_{i,j}^{n+1}-\alpha_{i,j}\phi_{i,j}^{n}}{\Delta t}+\frac{\left(\alpha_{i+1/2,j}u_{i+1/2,j}\phi_{i+1/2,j}-\alpha_{i-1/2,j}u_{i-1/2,j}\phi_{i-1/2,j}\right)}{\Delta x}+\ldots=0$

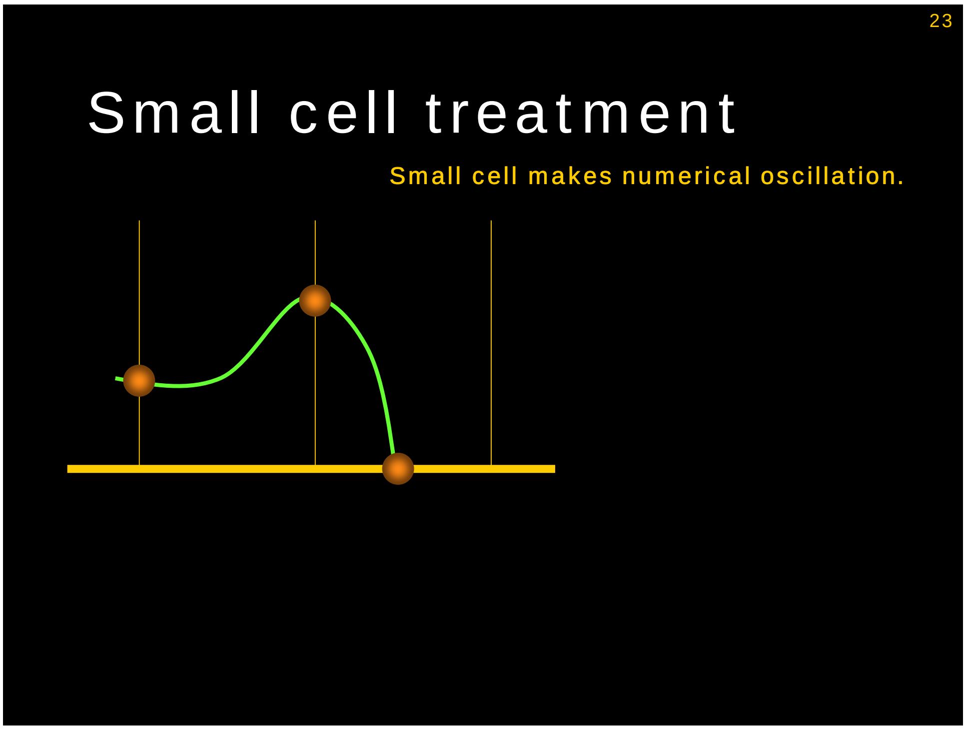
23
Small cell treatment
Small cell makes numerical oscillation.

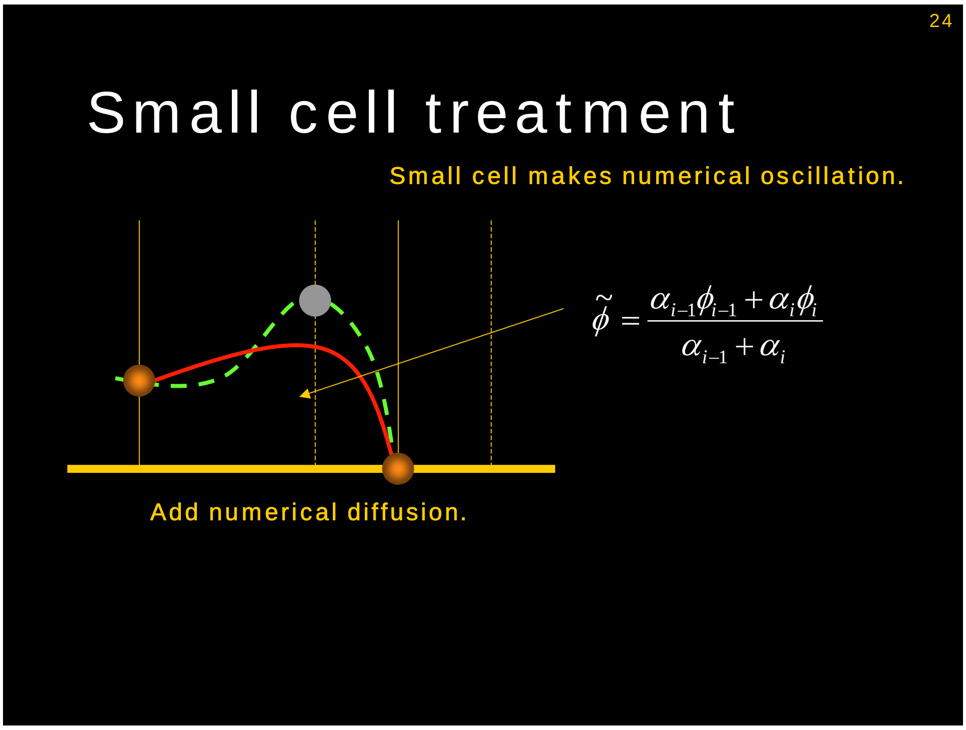
24
Small cell treatment
Small cell makes numerical oscillation.
$\tilde{\phi} = \dfrac{\alpha_{i-1}\phi_{i-1} + \alpha_i \phi_i}{\alpha_{i-1} + \alpha_i}$
Add numerical diffusion.

25

Small cell treatment

Small cell makes numerical oscillation.

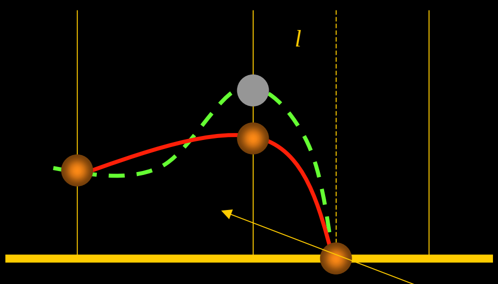

$$\tilde{\phi} = \frac{\alpha_{i-1}\phi_{i-1} + \alpha_i\phi_i}{\alpha_{i-1} + \alpha_i}$$

Add numerical diffusion.

$$\phi^*_{i-1} = \frac{\Delta x}{\Delta x(1+l)} \int_{x_{i-3/2}}^{x_{i-1/2}} \tilde{\phi}(\xi)\, d\xi$$

26

Small cell treatment

Small cell makes numerical oscillation.

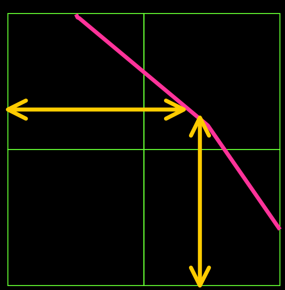

Iteration method

$$\phi_i^{m+1} = \phi_i^m + (\Delta_x\phi + \Delta_y\phi)\delta$$

When $\delta = 0.25$,

$(1-\delta)^{36}=0.001$

27

Single phase

Free-Surface

$$\frac{\partial u}{\partial x}+\frac{\partial v}{\partial y}=0$$

$$\frac{\partial u}{\partial t}+\frac{\partial uu}{\partial x}+\frac{\partial vu}{\partial y}+\frac{\partial P}{\partial x}=0$$

$$\frac{\partial v}{\partial t}+\frac{\partial uv}{\partial x}+\frac{\partial vv}{\partial y}+\frac{\partial P}{\partial y}=0$$

$$\frac{\partial \alpha}{\partial t}+U\frac{\partial \alpha}{\partial x}+V\frac{\partial \alpha}{\partial y}=0$$

28

Single phase

Free-surface

$$\boxed{\frac{\partial u}{\partial x}+\frac{\partial v}{\partial y}=0}$$

$$\frac{\partial u}{\partial t}+\frac{\partial uu}{\partial x}+\frac{\partial vu}{\partial y}+\boxed{\frac{\partial P}{\partial x}}=0$$

$$\frac{\partial v}{\partial t}+\frac{\partial uv}{\partial x}+\frac{\partial vv}{\partial y}+\boxed{\frac{\partial P}{\partial y}}=0$$

$$\frac{\partial \alpha}{\partial t}+U\frac{\partial \alpha}{\partial x}+V\frac{\partial \alpha}{\partial y}=0$$

Pressure Poisson's equation

$$\boxed{\frac{\partial^2 P}{\partial x^2}+\frac{\partial^2 P}{\partial y^2}=\frac{\partial}{\partial x}\frac{\partial u^*}{\partial t}+\frac{\partial}{\partial y}\frac{\partial v^*}{\partial t}}$$

29

Single phase

Free-surface

$$\frac{\partial u}{\partial x}+\frac{\partial v}{\partial y}=0$$

$$\frac{\partial u}{\partial t}+\frac{\partial uu}{\partial x}+\frac{\partial vu}{\partial y}+\frac{\partial P}{\partial x}=0$$

$$\frac{\partial v}{\partial t}+\frac{\partial uv}{\partial x}+\frac{\partial vv}{\partial y}+\frac{\partial P}{\partial y}=0$$

$$\frac{\partial \alpha}{\partial t}+U\frac{\partial \alpha}{\partial x}+V\frac{\partial \alpha}{\partial y}=0$$

Pressure Poisson's equation

$$\frac{\partial^2 P}{\partial x^2}+\frac{\partial^2 P}{\partial y^2}=\frac{\partial}{\partial x}\frac{\partial u^*}{\partial t}+\frac{\partial}{\partial y}\frac{\partial v^*}{\partial t}$$

Interface moving velocity

Fluid velocity

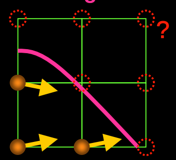

Ghost fluid method

$U_0=u$

$V_0=v$

Initial guess

$$\frac{\partial U}{\partial \tau}+(1-\alpha)\mathbf{n}\cdot\nabla U=0$$

$$\frac{\partial V}{\partial \tau}+(1-\alpha)\mathbf{n}\cdot\nabla V=0$$

$\Delta y=0.0125\lambda$ 30

Stokes wave $2a/\lambda=0.02$

Wave steepness

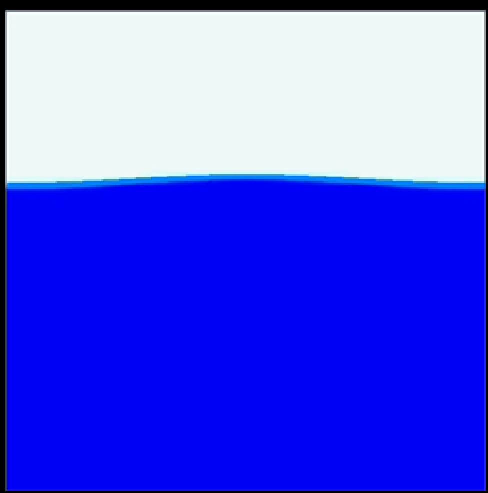

Rigid wave

Periodic condition, Initial condition is 4th order Stokes wave

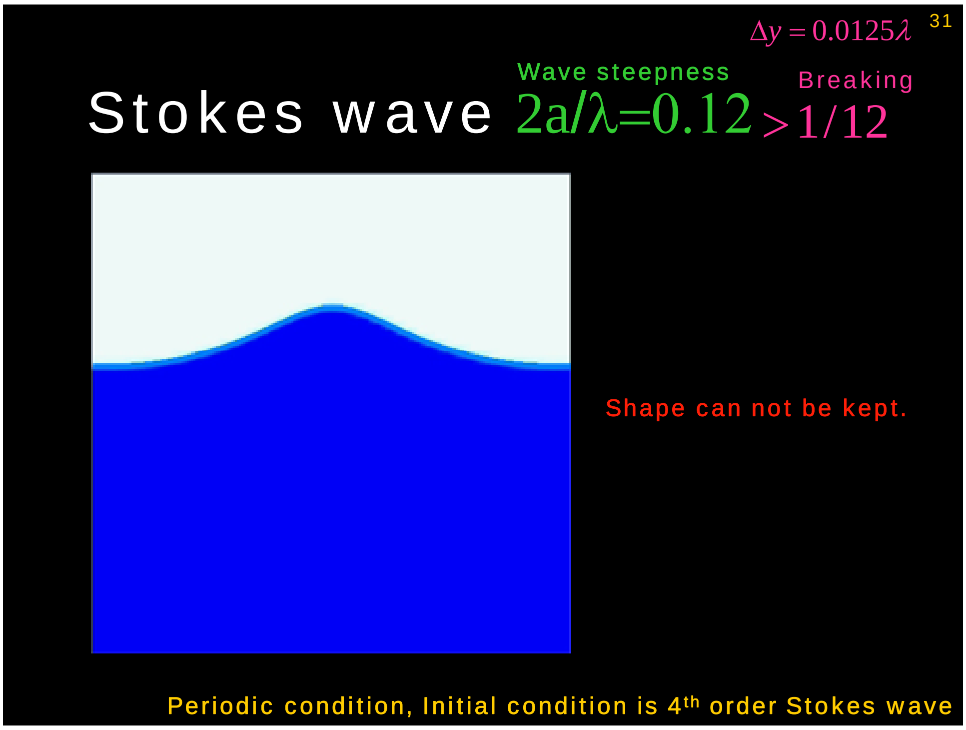

$\Delta y = 0.0125\lambda$
31
Stokes wave
Wave steepness
$2a/\lambda=0.12 > 1/12$
Breaking
Shape can not be kept.
Periodic condition, Initial condition is 4th order Stokes wave

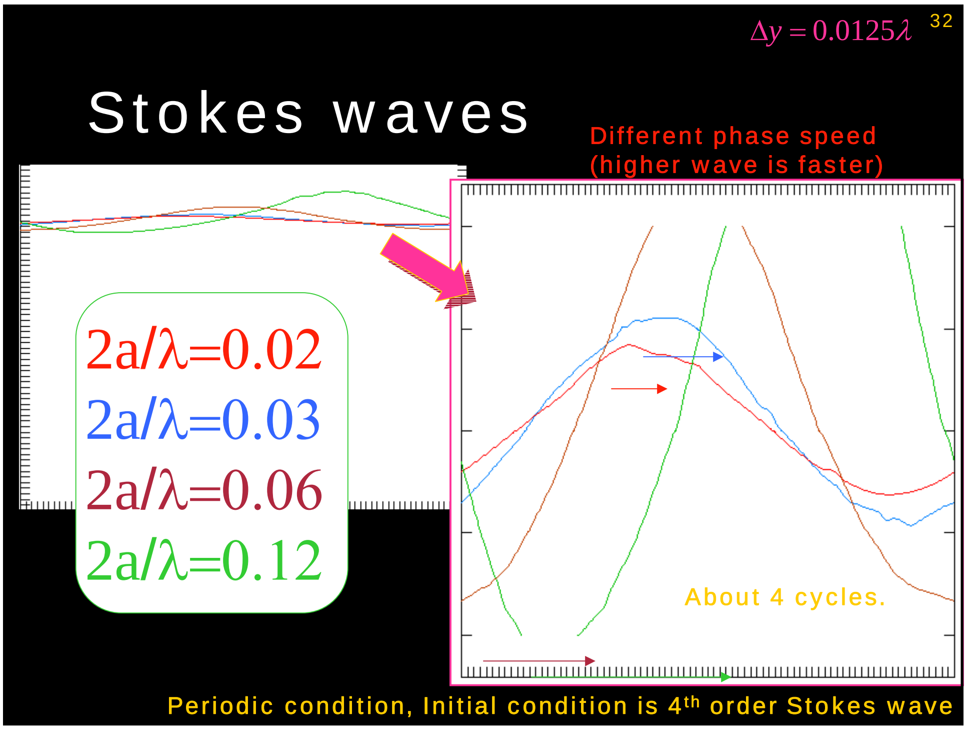

$\Delta y = 0.0125\lambda$
32
Stokes waves
Different phase speed
(higher wave is faster)
$2a/\lambda=0.02$
$2a/\lambda=0.03$
$2a/\lambda=0.06$
$2a/\lambda=0.12$
About 4 cycles.
Periodic condition, Initial condition is 4th order Stokes wave

33

$\Delta y = 0.0125\lambda$

Higher

Wave steepness

Stokes wave $2a/\lambda=0.18$

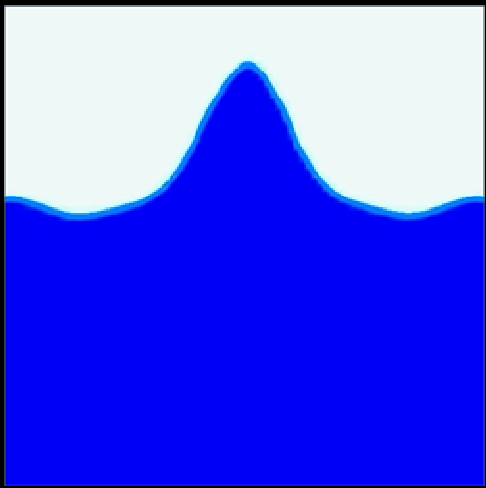

Plunging breaker

Periodic condition, Initial condition is 4th order Stokes wave

34

Summary/Future direction

- Developments:
  - Immersed boundary treatment for IDO-CF
  - Moving boundary treatment
- Next:
  - Fluid-structure interaction with free-surface
  - Three dimensions
  - Adaptive/Local mesh refinement

35

36

Difference with Ghost fluid method

- Conservation
- Implicit construction
- Smallest stencil

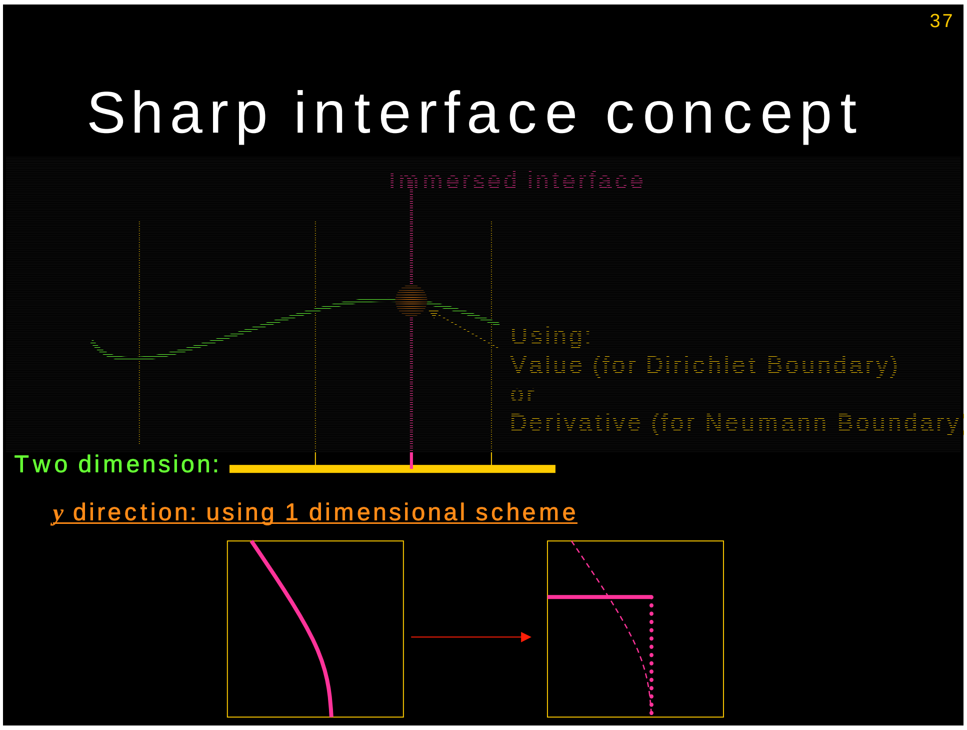
37
Sharp interface concept
Immersed interface
Using:
Value (for Dirichlet Boundary)
or
Derivative (for Neumann Boundary)
Two dimension:
y direction: using 1 dimensional scheme

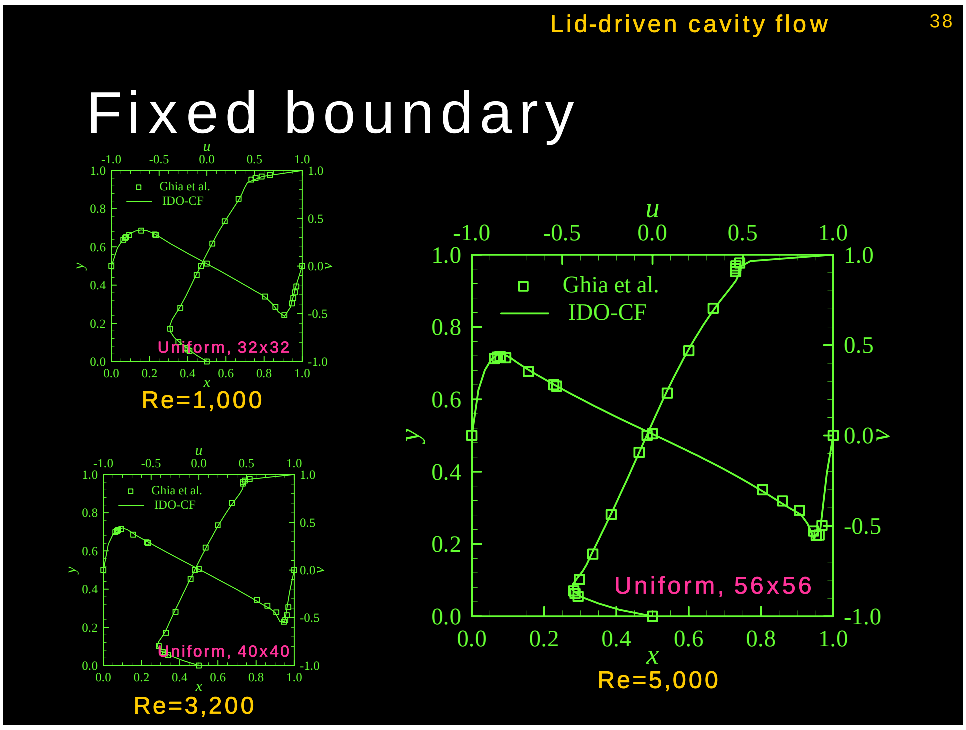
Lid-driven cavity flow
38
Fixed boundary
Ghia et al.
IDO-CF
Uniform, 32x32
Re=1,000
Uniform, 40x40
Re=3,200
Uniform, 56x56
Re=5,000

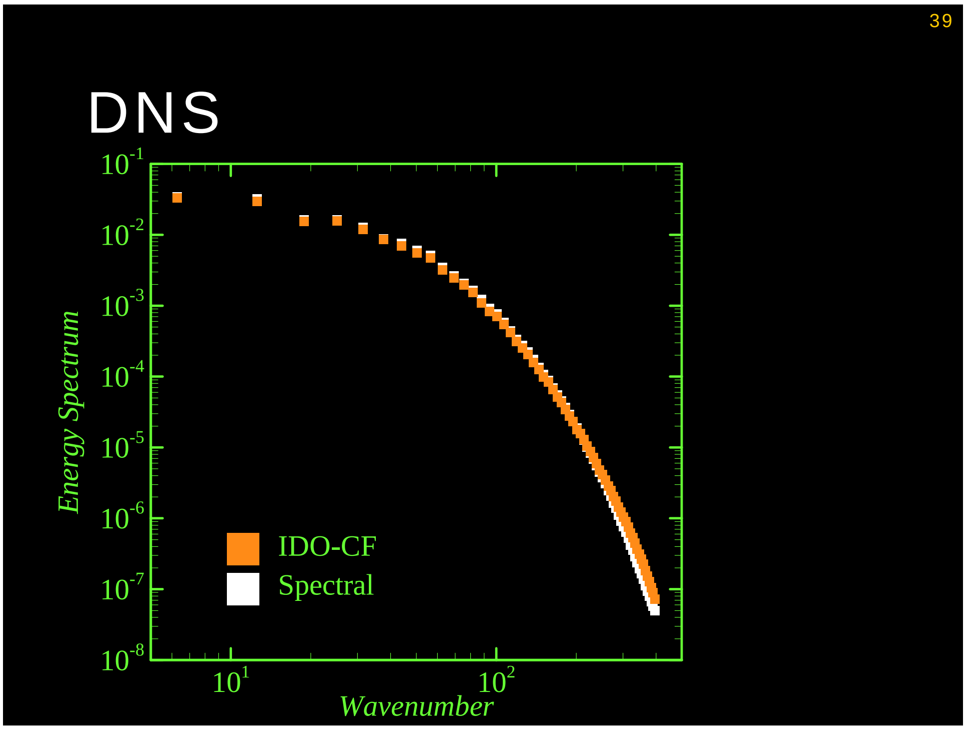
39
DNS
Energy Spectrum
Wavenumber
10^-1
10^-2
10^-3
10^-4
10^-5
10^-6
10^-7
10^-8
10^1
10^2
IDO-CF
Spectral

A Computing Method for the Flow Analysis around a Prismatic Planing-Hull

Hajime KIHARA
National Defense Academy of Japan
Yokosuka / Japan

Strongly Nonlinear Problem

- Impact jet
  - **High pressure on planing-surface**
  - **Hydrodynamic impact in waves**
- Large deformation of free surface
  - **Spray & splash generation at a bow**
  - **Breaking waves and their behavior after breaking**
  - **Cavity hollow behind a transom stern**
  - **Rooster tail in wake**
- Liquid breakup & coalescence
  - **Spray**
  - **Splash**
  - **Breaking waves**
- Two-phase flow
  - **Air-liquid interface**
  - **?**

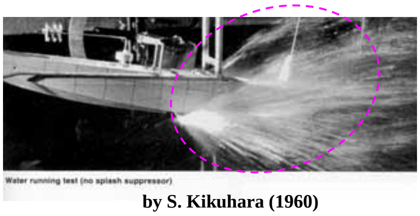

by S. Kikuhara (1960)

How much is the BEM effective as analysis tool ?

- ✓ VOF
- ✓ CIP
- ✓ SPH
- ✓ MPS
- ✓ …

- BEM + α ?
- Hybrid approach ?

A Planing-Hull Wave Problem

- Prismatic hull with uniform wedge section
- Steadily planing with a trim angle τ & an advanced speed U
- Potential flow

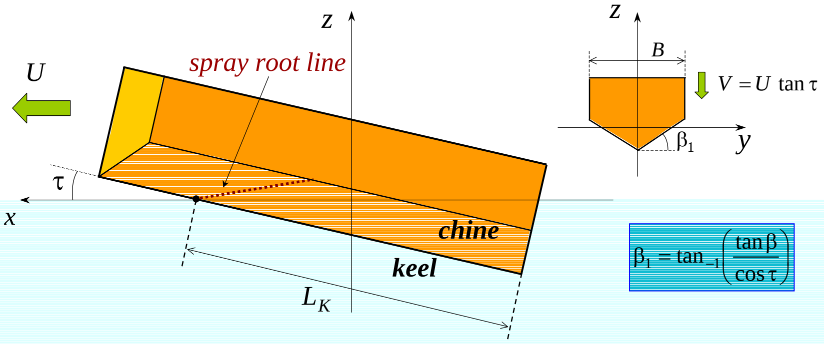

(x, y, z) : Earth fixed coordinate system

Mathematical Formulation (1)

- Steady wave-making problem

ϕ : disturbance -velocity potential

$$[L] \quad \frac{\partial^2\phi}{\partial X^2}+\frac{\partial^2\phi}{\partial Y^2}+\frac{\partial^2\phi}{\partial Z^2}=0 \qquad \cdots(1)$$

$$[H] \quad \frac{\partial\phi}{\partial n}=Un_X=U\sin\tau\cos\beta \qquad \cdots(2)$$

$$[K] \quad -U\frac{\partial\zeta}{\partial X}+\frac{\partial\phi}{\partial X}\frac{\partial\zeta}{\partial X}+\frac{\partial\phi}{\partial Y}\frac{\partial\zeta}{\partial Y}-\frac{\partial\phi}{\partial Z}=0 \quad \text{on} \quad Z=\zeta \qquad \cdots(3)$$

$$[D] \quad -U\frac{\partial\phi}{\partial X}+\frac{1}{2}\left\{\left(\frac{\partial\phi}{\partial X}\right)^2+\left(\frac{\partial\phi}{\partial Y}\right)^2+\left(\frac{\partial\phi}{\partial Z}\right)^2\right\}+g\zeta=0 \quad \text{on} \quad Z=\zeta \qquad \cdots(4)$$

$[R]$

(X, Y, Z) : Coordinate system moving constant speed U

Mathematical Formulation (2)

- Slender body approximation & Coordinate transformation

$$\frac{\partial}{\partial X} \ll \frac{\partial}{\partial Y}, \frac{\partial}{\partial Z} \quad \cdots(5) \quad , \qquad \frac{\partial}{\partial t} = -U\frac{\partial}{\partial X} \quad \cdots(6)$$

- Initial-boundary value problem near a ship

$$[L] \quad \frac{\partial^2 \phi}{\partial y^2} + \frac{\partial^2 \phi}{\partial z^2} = 0 \qquad \cdots(7)$$

$$[H] \quad \frac{\partial \phi}{\partial N} = U \tan\tau \cos\beta_1 = V\cos\beta_1 \quad \cdots(8)$$

$$[K] \quad \frac{\partial \zeta}{\partial t} + \frac{\partial \phi}{\partial y}\frac{\partial \zeta}{\partial y} - \frac{\partial \phi}{\partial z} = 0 \quad \text{on} \quad z = \zeta \quad \cdots(9)$$

$$[D] \quad \frac{\partial \phi}{\partial t} + \frac{1}{2}\left\{\left(\frac{\partial \phi}{\partial y}\right)^2 + \left(\frac{\partial \phi}{\partial z}\right)^2\right\} + g\zeta = 0 \quad \text{on} \quad z = \zeta \qquad \cdots(10)$$

$$[I] \quad \phi = \overline{\phi}, \quad \zeta = \overline{\zeta} \quad \text{at} \quad t = 0 \qquad \cdots(11)$$

(y, z) : Earth fixed coordinate system

Mathematical Formulation (3)

- IBVP of ϕ_t for pressure computation

$$[L] \quad \frac{\partial^2 \phi_t}{\partial y^2} + \frac{\partial^2 \phi_t}{\partial z^2} = 0 \qquad \cdots(12)$$

$$[H] \quad \frac{\partial \phi_t}{\partial N} = \frac{\partial \phi}{\partial N}\frac{\partial^2 \phi}{\partial s^2} - \frac{\partial \phi}{\partial s}\frac{\partial^2 \phi}{\partial s \partial N} \qquad \cdots(13)$$

[N : normal derivative on yz-plane]

$$[F] \quad \phi_t = -\frac{1}{2}\left\{\left(\frac{\partial \phi}{\partial y}\right)^2 + \left(\frac{\partial \phi}{\partial z}\right)^2\right\} - g\zeta \quad \text{on} \quad z = \zeta \qquad \cdots(14)$$

$$[I] \quad \phi_t = \overline{\phi}_t, \quad \text{at} \quad t = 0 \qquad \cdots(15)$$

- Bernoulli equation

$$p = -\rho\left[\phi_t + \frac{1}{2}\left\{\left(\frac{\partial \phi}{\partial y}\right)^2 + \left(\frac{\partial \phi}{\partial z}\right)^2\right\} + gz\right] \quad \text{on} \quad \text{body}$$

Outlines of Solution Procedures

BEM based 2D+T approach

- Time Domain Computation
  - ✓ Description of steady wave-making problem by the earth fixed coordinate system
- Solution method of BVP using BEM
  - ✓ Using linear isoparametric elements for discretization
  - ✓ Introducing double nodes on corner points
  - ✓ Evaluating element integration analytically
  - ✓ Excluding the bottom boundary by using a mirror image
  - ✓ Imposing rigid wall condition on a vertical boundary far away from a body
- Computation of moving boundary
  - ✓ MEL(Mixed Eulerian Lagrangian) scheme
  - ✓ Time integration scheme by RK4
  - ✓ Control of nodal density for high resolution

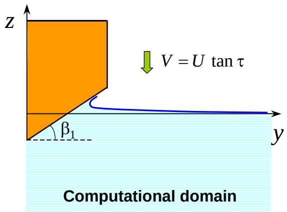

What is difficult in BE analysis ?

- Numerical description of liquid jet
  - Singularity on the intersection
  - Barrier of expression by continuous fluid domain
- Liquid breakup
  - Jet flow ⇒ Potential theory
    - ✓1-D flow
    - ✓Shallow water approximation
  - Air-liquid two-phase flow
- Liquid detachment from a body
  - Fluid ejection at chine or knuckle
  - Fluid ejection from curved surface

by C.Lugni et al.(2005)

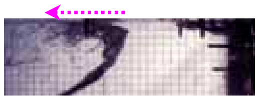

by O.F.Rognebake et al.(2005)

by S. Kikuhara (1960)

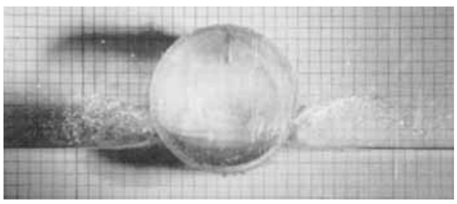

by M. Greenhow & W.M. Lin (1983)

Artificial liquid breakup (1)

- Jet ejection on the hull bottom (Case : V=1.08m/s, B=0.126m, β=25°)

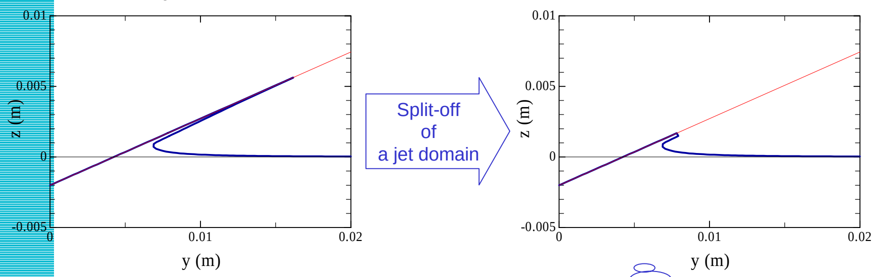

✓ **Numerical instability on HS in the jet**
⇨ **Small negative pressure**

✓ **Geometric description of thin layer**
⇨ **Comp. break by contact**

✓ **Jet domain growth**
⇨ **Increase of comp. loads**

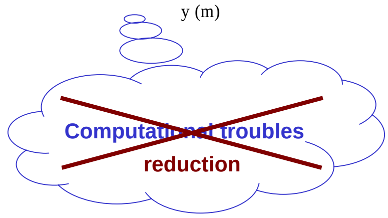

Domain-Decomposition of the jet domain

- Rational D.D. using BEM
  - ✓ **Valid everywhere in the fluid domain in principle**
  - ✓ **Rationally able to compute potential & its flux on the interface boundary**

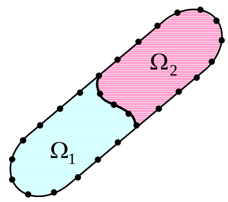

- Practical D.D. based on shallow water approximation
  - ✓ **Restricted within the jet domain**
  - ✓ **Approximately able to interpolate potential & its flux on the interface boundary**

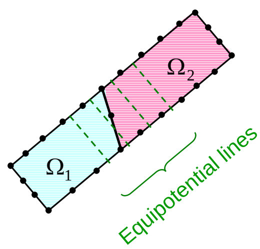

Artificial liquid breakup (2)

- Splash ejection at the chine (Case : V=1.08m/s, B=0.126m, β=25 °)

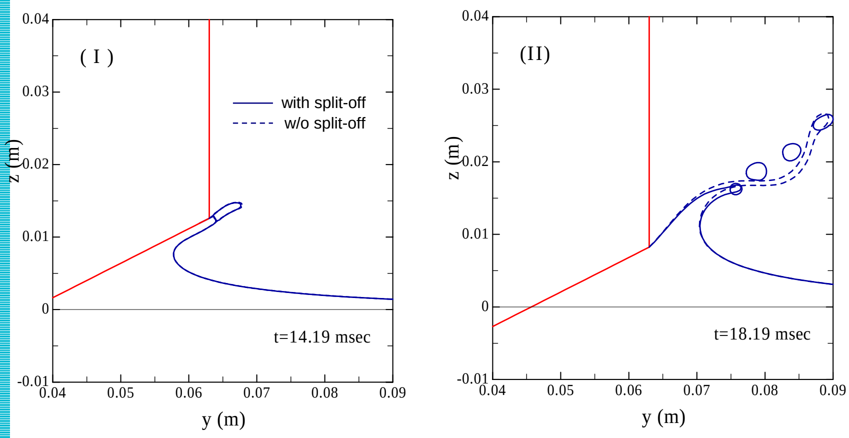

Computation of flying droplets

- Motion simulation of droplets
  - A domain filled with fluid perfectly
  - Assuming the potential flow
  - Approach by the MEL based BEM with Dirichlet condition
  - Consideration of surface tension

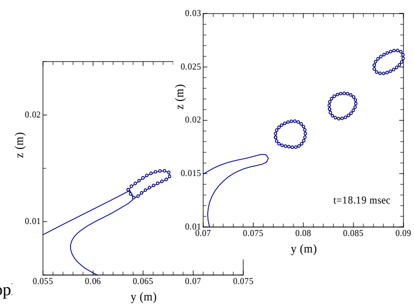

$$[L] \quad \frac{\partial^2 \phi}{\partial y^2} + \frac{\partial^2 \phi}{\partial z^2} = 0 \qquad \text{in} \quad \Omega_{\text{drop}}$$

$$[K] \quad \frac{\partial \zeta}{\partial t} + \frac{\partial \phi}{\partial y}\frac{\partial \zeta}{\partial y} - \frac{\partial \phi}{\partial z} = 0 \quad \text{on} \quad \Gamma_{\text{droplet}}$$

Surface tension term

$$[D] \quad \frac{\partial \phi}{\partial t} + \frac{1}{2}\left\{\left(\frac{\partial \phi}{\partial y}\right)^2 + \left(\frac{\partial \phi}{\partial z}\right)^2\right\} + g\zeta + \nu\kappa + \mu\phi = 0 \quad \text{on} \quad \Gamma_{\text{droplet}}$$

Artificial damping term

$$[I] \quad \phi = \overline{\phi}, \quad \zeta = \overline{\zeta} \quad \text{on} \quad \Gamma_{\text{droplet}} \quad \text{at} \quad t = t_{\text{eject}}$$

Numerical simulation by the BEM-2D+T

- Simulated free surface near the bow of a prismatic planing-hull

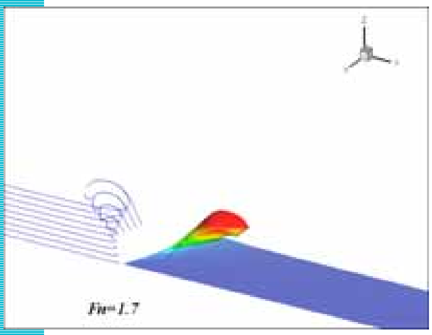

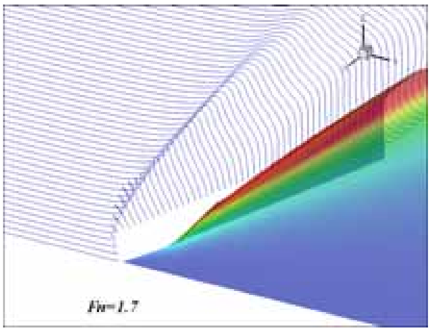

- Spray is described just like a continuous fluid sheet.
- Spray blister is artificially split-off.

Comparison with experiments (1)

Experiments (2D)

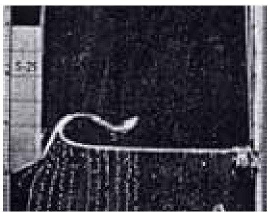

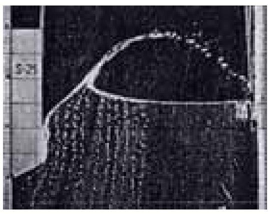

Computations

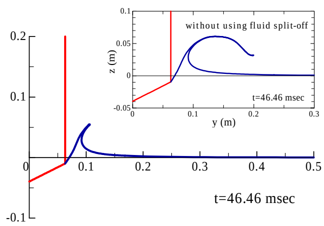

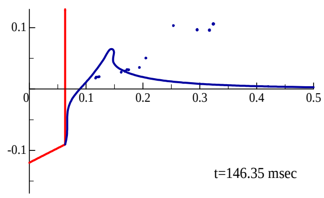

by S. Kikuhara (1960) （case : V=0.85m/s, B=0.126m, β=25°）

Comparison with experiments (2)

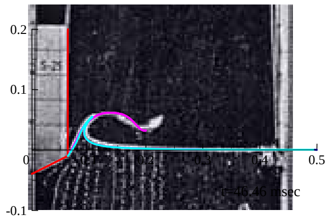

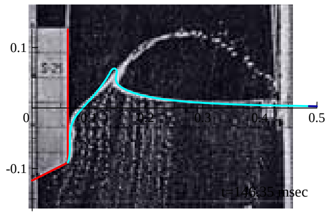

Simulated spray generation

- Whisker spray

  ✓ too much decay
  for horizontal velocity
  ?

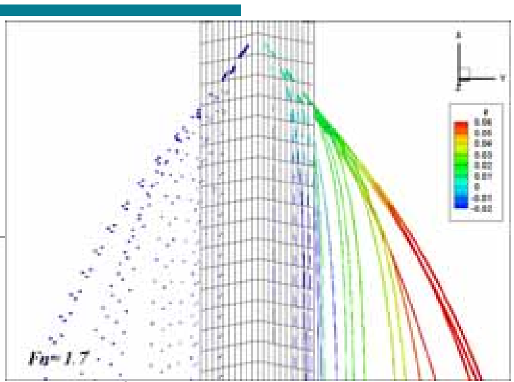

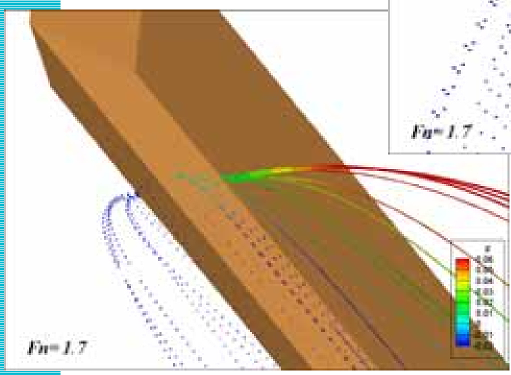

（Fn=1.7, V=1.08m/s, B=0.126m, β=25°）

- Spray blister

Projectile paths of spray blister

- Comparison of the numerical model with the point mass model

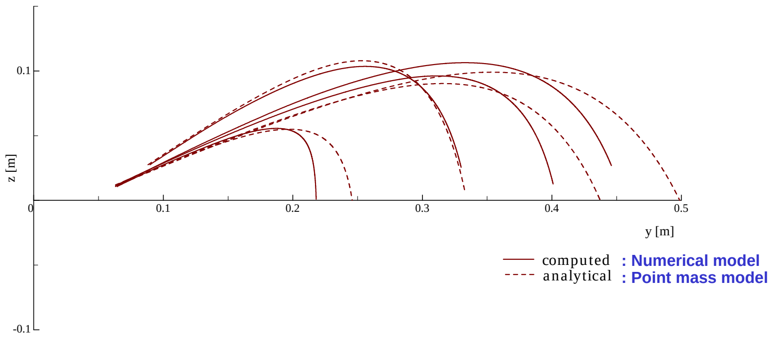

Numerical model : The MEL based BEM computation

Point mass model : $m\dot{\boldsymbol{v}} = -\frac{1}{2} C_D \, \rho_a \left| \boldsymbol{v} \right| \boldsymbol{v} \;\; d + \boldsymbol{K}$ $\quad [\boldsymbol{K} = (0, -mg) : \text{conservative force}]$

Pressure distribution on the hull bottom

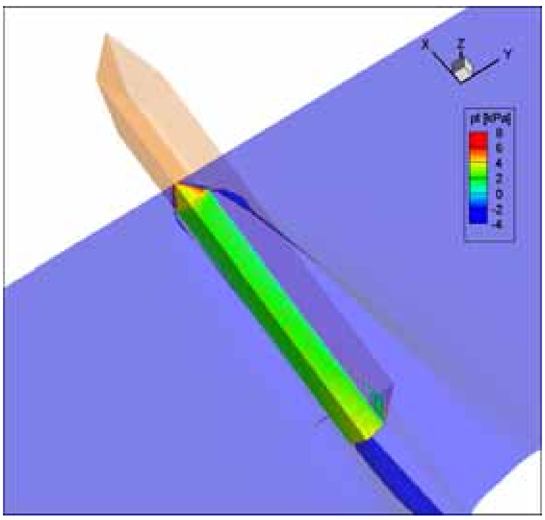

Looking up the hull bottom in water（Fn=1.7, V=1.08m/s, B=0.126m, β=25°）

3D-View

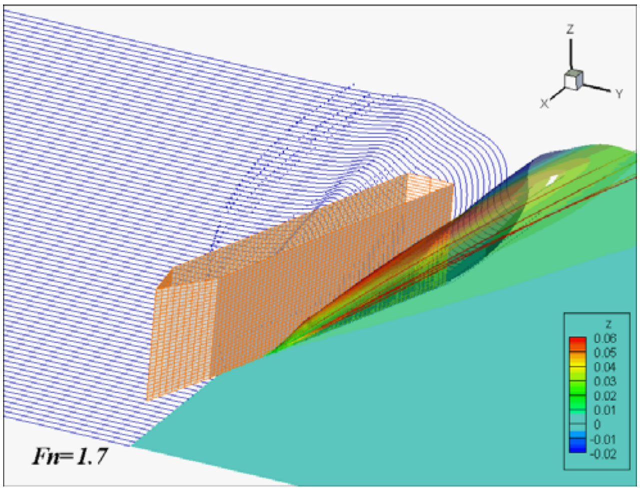

Hull dimension	:	**L_k= 1.0 m, B=0.126 m**	;	**Step size**	:	**$\Delta x = L_k$ / 20,000**
Domain size	:	**W=10.0 m, h=5.0 m, L=1.5 L_k**	;	**CPU Time**	:	**about 2.6 hours for 1 L_k length**
Node numbers	:	**Totally 350 (NH = 31, NF=261)**	;			

Concluding remarks

Availability of the potential based computation to strongly nonlinear problems was investigated by using the BEM in the study.

- ✓ A computational method by the BEM based 2D+T could be developed.
- ✓ Numerical simulation including the spray and splash ejection by a prismatic planing-hull could be conducted practically.
- ✓ The artificial liquid breakup of the jet flow was proposed for the robust and long term computation.
- ✓ More detailed studies are necessary for realistic simulation of the fragmented fluid.

In the future, following studies are necessary :

- The investigation from a viewpoint of energetic conservation
- Consideration of the attitude change of a hull in running

Symposium on Analyses of Strongly Nonlinear Flows
around Moving Boundaries
Fukuoka, Japan, 7-8 December 2006

CFD simulation of resistance and seakeeping performance for multi-hull vessels

Yohei Sato
National Maritime Research Institute

ABSTRACT

A numerical method for the prediction of hydrodynamic performance of a trimaran vessel is developed and it is validated through the comparison with experiments. The unsteady Reynolds-averaged Navier-Stokes equations are solved with the density function for the free surface treatment. The multi-block grid system is used to cope with the complicated geometry around a practical trimaran vessel with a long bulb and a transom stern. Using this method, flows around a trimaran vessel are simulated in steadily towed conditions. In order to evaluate seakeeping performance, the motion simulations in incident waves are carried out with heave, roll and pitch motions being set free. The experiments are conducted for the condition of steady straight condition and the drag, the attitude and the transverse wave profiles are measured. The experimental and numerical data, especially the transverse wave profiles, agrees well. Thus, the availability of the present method is demonstrated by these simulations.

I. INTRODUCTION

The demand of fast sea transportation has increased in the past two decades. About 50 percent of fast ferries are currently catamarans and they are satisfactorily making services. However, some shortcomings are recognized for catamarans, such as high acceleration due to the excessive amount of TKM value. With this background the footlight is shed on the trimaran of which TKM is in between monohull and catamaran. Besides, several experimental studies and numerical resistance tests reveal the superior property of low wave making resistance.

The estimation of the wave induced motion and load of a trimaran vessel is essential for the ride comfort and for the structural design. The full scale measurement test was conducted for RV Triton by Renilson et al. (2004), a 126m trimaran capable of 40 knots at 500 ton deadweight was constructed by Austal Ships in 2005 and several tank tests and numerical simulations for the seakeeping performance have been recently carried out. However, large ship motions in rough weather including slamming are not investigated satisfactorily. In order to prevent injury accidents and breakage of a vessel, it is necessary to predict wave induced motion and wave impact load more quantitatively.

For the seakeeping characteristics, numerical simulation is obviously useful because it is almost impossible to measure the motions of advancing ship in beam or oblique waves in an ordinary tank. Therefore, the ship motion problem has been mostly treated by the technique of theoretical fluid dynamics with the postulation that a velocity potential exists. Since the important part of ship motion in waves is liner, this approach has provided a lot of useful information for the prediction of ship motion. However, it cannot be applied to motion which includes nonlinear properties, such as large-amplitude motions, motions with a wave impact load (slamming) and capsizing. Besides, the disadvantage of the theoretical methods seems to be amplified for the cases of multi-hulls. To resolve these problems, the technique of computational fluid dynamics (CFD) can be very useful.

The objective of this study is to establish a numerical method for predicting resistance and seakeeping performance of multi-hull vessels by CFD technique.

II. NUMERICAL METHOD

The present numerical method is based on the WISDAM-Vmotion method which was developed by Sato et al. (1999). This method was extended to overlapping grid system, WISDAM-X, which is explained in the previous part of this paper and it is actually used as a design tool for the purpose of reducing added wave resistance. In this study, the WISDAM-V method is modified into a multi-block grid system in order to cope with the complicated configuration of a multi-hull vessel.

The governing equations are the three-dimensional, time-dependent, incompressible RANS equations and the continuity equation. The density-function method is used for the implementation of the free-surface condition.

In order to compute flow around a moving ship, a body-fixed coordinate system is employed. The grid system which is fixed to the ship is translated and rotated in accordance with the motion of a ship as shown in Figure 1. The trajectory and the attitude of the ship are defined in the space-fixed coordinates system.

The incident waves are assumed to be sinusoidal in infinitely deep water. The generation of incident waves is implemented by setting the velocities and the wave height explicitly on the inflow boundary.

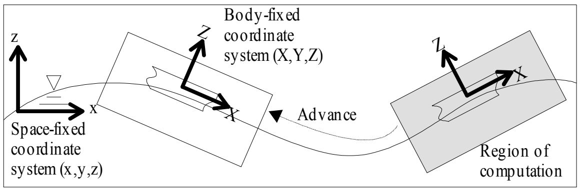

Fig. 1: Moving, body-fixed coordinate system.

III. PREDICTION OF RESISTANCE PERFORMANCE

The accuracy of the present method of resistance performance is examined by comparison with towing tank experiment.

The resistance test is performed on three trimaran vessels at the towing tank of the University of Tokyo. Drag, trim, sinkage as well as the transverse wave profile at 0.2×Lpp aft from AP section are measured. The trimaran vessels, named TRI A1-1, TRI A1-3 and TRI A3-1 consist of same main hull named MAIN and side hull named SIDE-A. The difference between them is the position of the side hull with respect to the main hull which is depicted in Figure 2. The principal particulars of MAIN and SIDE-A are shown in Table 1. MAIN has a practical hull form with a (DSB type, double step bulb) long bulb and a transom stern. The Lpp of SIDE-A is half length of MAIN.

The computational grids are generated by using the grid generating software Gridgen®. The number of grid point for the half model is about 850,000. The computational grid of TRI A1-1 is shown in Figure 3. By using the multi block method, the vertical transom stern is shaped accurately without any deformation from CAD data.

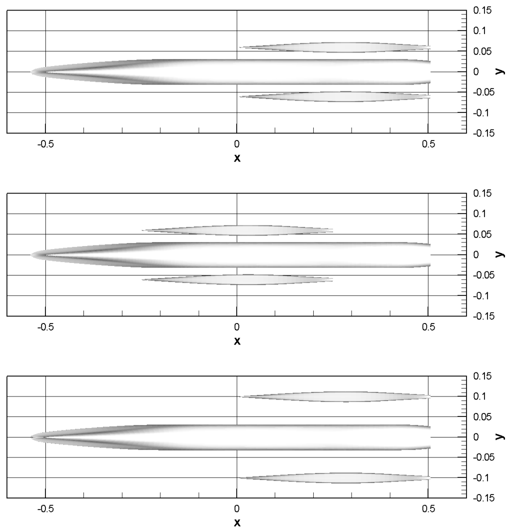
Fig. 2: Definition sketch of TRI A1-1(top), TRI A1-3(middle) and TRI A3-1(bottom).

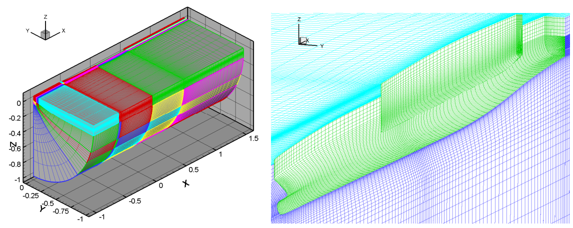
Fig. 3: Computational grid system of TRI A1-1.

Table 1: Principal paticulars of main and side hulls.

	Lpp [m]	B [m]	d [m]	Volume [m^3]
MAIN	203.2	12.7	5.0	6,137
SIDE-A	101.6	5.1	2.5	604

A. Fixed Trim and Sinkage Condition

As the first step of the resistance performance test, calculations of fixed trim and sinkage condition are conducted. The trim and sinakge of the computations are set in accordance with the results of tank test.

The computed pressure drag and the measured residual drag are shown in Figures 4 and 5, respectively. They agree qualitatively and quantitatively well.

The measured and computed transverse wave profiles of TRI A1-1 advancing at Froude number 0.41 are shown in Figure 6. The computed wave height is smaller than the measurement in the area away from the center line (y=0). This is mainly due to the coarse grid spacing in the far field. However, the measured and computed wave profiles agree satisfactorily well in the near field.

From these results, it can be concluded that the resistance performance of trimaran vessels, which is effected by the interactions between hulls are well computed by the WISDAM-XI code.

B. Free Trim and Sinkage Condition

In order to use the CFD code as a design tool, it is

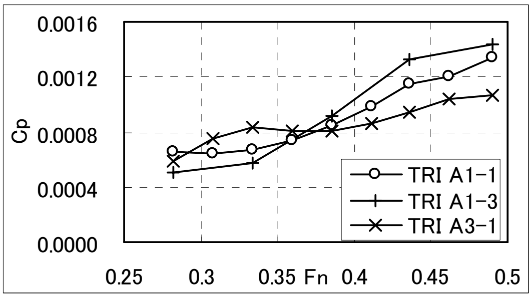

Fig. 4: Computed pressure drag.

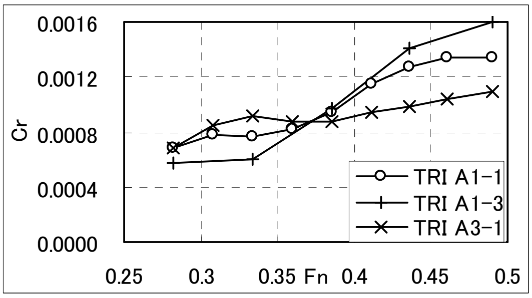

Fig. 5: Measured residual drag.

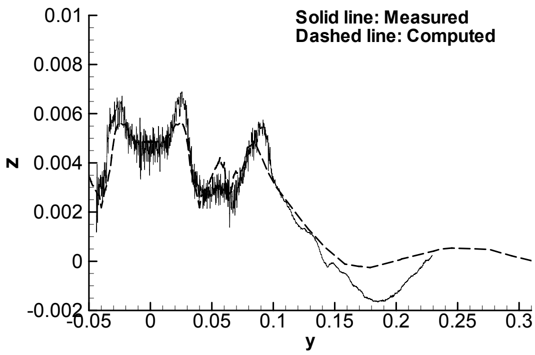

Fig. 6: Measured and computed transverse wave profile of the TRI-A1 vessel. (Fn=0.41, 0.2xLpp aft from AP section)

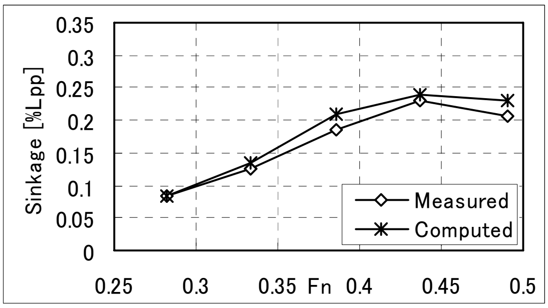

Fig. 7: Comparison of computed and measured sinkage.

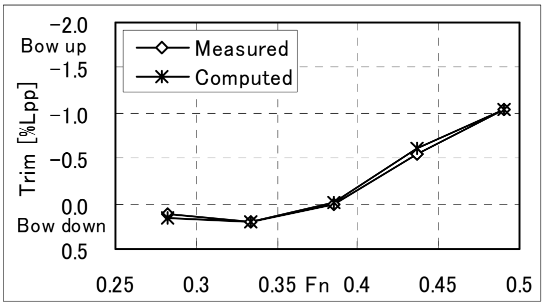

Fig. 8: Comparison of computed and measured trim.

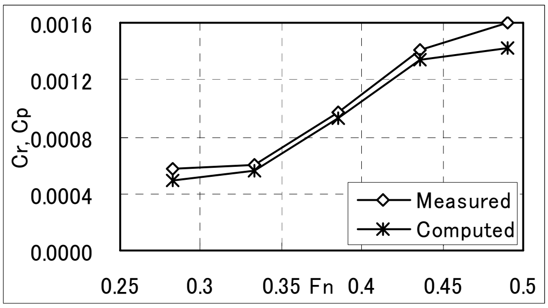

Fig. 9: Comparison of computed pressure drag and measured residual drag.

necessary to predict not only resistance but also trim and sinkage, because a resistance performance of a fast ship is seriously affected by the attitude.

Calculations on trim free and sinkage condition are conducted with TRI A 1-3. In these computations, trim and sinakge are obtained by solving the motion equation.

The results of sinkage, trim and drag are shown in Figures 7 to 9, respectively. The computed results agree satisfactory well with the measured data.

It can be said that the WISDAM-XI code can be used as a design tool of a hull form of multi-hull vessels.

IV. PREDICTION OF SEAKEEPING PERFORMANCE

To assess the accuracy of predicting seakeeping performance of the WISDAM-XI code, the roll motion tests in beam waves without advance speed are performed with a mono hull, a catamaran and a trimaran vessel and compared with the results of tank test. Followed by this test, ship motion simulations with advance speed in regular arbitrary waves are performed on the same ships.

The principal particular of the mono hull, the catamaran and the trimaran vessel which are called MONO, CAT and TRI, respectively is shown in Table 2.

The displacement of these ships is set at the same value. The principal particulars of the demi-hull of CAT, the main hull and the side hull of TRI are shown in Table 3. The longitudinal positions of main hull's AE (aft end) and side hull's AE of TRI are set at the same position. The design speed of MONO is 30 knot, while that of CAT and TRI is 35 knot for the practical design with respect to required engine power. The scale ratio of tank test model is 0.0126. The tank test model CAT and TRI are shown in Figures 10 and 11, respectively. Neither bilge keel nor foil is attached to the model.

A. Roll motion in Regular Beam Waves

Simulations of roll motion in beam waves without advance speed are conducted on MONO, CAT and TRI.

Roll damping force model

Free roll simulations are executed and they are compared with the tank test results in order to check the damping coefficient of roll motion. Large discrepancy is noted on the roll damping coefficient of MONO, while good agreement is obtained in CAT and TRI case. It can be considered that the reason of such discrepancy on MONO is caused by the underestimation of viscous damping force. Roll damping force consists of wave damping force and viscous damping force. In case of MONO, the wave damping force is relatively small, thus the ratio of viscous damping force is relatively large. On the other hand, the wave damping force of CAT and TRI play a dominant role due to the large radiation wave generated by demi-hull or side hull. The accuracy of viscous damping force calculated by CFD is insufficient, because the viscous force depends on turbulence modeling and grid spacing. In order to obtain viscous force in sufficient accuracy, a fine grid and a proper turbulence model should be employed. However it is difficult to use such a fine grid for the motion simulation, thus artificial roll damping force is added so as to coincident with the experimental damping coefficient. The damping force which is proportional to the roll angular velocity is added to the motion equation of ship. By using this model, the roll damping coefficient of MONO is tuned so as to agree with the experimental results.

Condition of computation

Four modes of motion, sway, heave, roll and pitch, are set free and the others are restricted.

The amplitude of the beam incident wave is 1.0×10^{-2} for all simulation cases. The wave length is set longer than 0.5L.

Grid parameters are set according to the result of wave generating test of the WISDAM-XI code. It is noted that more than 40 grids are required in a wave advance direction for one wave length in order to simulate wave propagation with sufficient degree of accuracy. In the vertical direction, more than 3 grids

Table 2: Principal particulars of mono hull, catamaran and trimaran vessel.

Name of ship		MONO	CAT	TRI
Lpp	[m]	152.4	170.3	208.8
B	[m]	19.0	31.1	40.8
d	[m]	5.3	5.3	5.1
Displacement	[ton]	7,500	7,500	7,500
Wetted Surface Area	[m^2]	2,926	4,145	4,246
TKM	[m]	13.6	55.4	17.7
GM	[m]	0	45	4

Table 3: Principal particulars of demi-hull of CAT, main and side hull of TRI.

Name of ship		CAT	TRI	
Name of hull		DEMI	MAIN	SIDE
Lpp	[m]	170.3	208.8	104.4
B	[m]	8.5	13.1	2.6
d	[m]	5.3	5.1	2.6
Displacement	[ton]	3,750	6,828	336

Fig. 10: Tank test model CAT.

Fig. 11: Tank test model TRI.

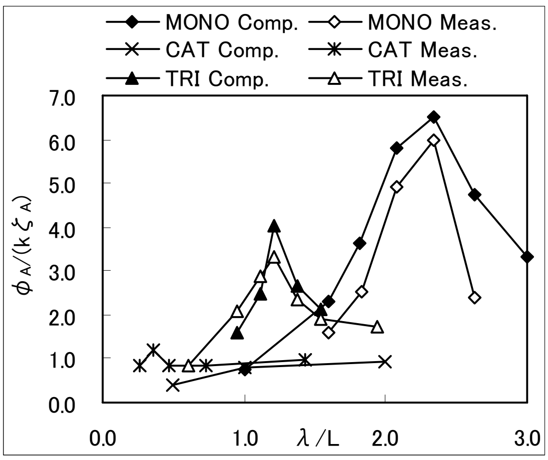

Fig. 12: Comparison of computed and measured roll motion amplitude.

points are required for half wave height.

The number of grid points is 1.4×10^6 for MONO, 1.6×10^6 for CAT and 2.9×10^6 for TRI. The minimum grid spacing on the hull is 1.0×10^{-3} and the maximum grid spacing in vertical direction in the vicinity of the free surface is 5.0×10^{-3}.

Tank test

Roll motion experiments are performed on these three ships at the rolling tank of the University of Tokyo. The roll angle is measured by using a fiber optic gyro.

Results and discussion

The computed and measured results of roll amplitude are shown in Figure 12. In case of MONO and TRI, the computed results agree well with the measured results. The wave length of the peak is accurately calculated while the roll amplitude is slightly overestimated.

B. Moving Conditions in Regular Incident Waves

The seakeeping simulations of MONO, CAT and TRI are conducted for the purpose of understanding the characteristics of seakeeping performance of multi-hull vessels.

Condition of computation

The condition of simulation is as follows.

- Advance speed of MONO is 30 knot, while that of CAT and TRI is 35 knot.
- Sway, heave, roll and pitch motions are set free and other modes of motions are restricted.
- The regular incident wave is from five directions, head wave (χ=180°), oblique head wave (χ=150°), beam wave (χ=90°), oblique follow wave (χ=30°) or follow wave (χ=0°).

The condition of computation and parameters for the incident wave are shown in Table 4 and 5, respectively.

Table 4: Condition of computation.

Froude number	0.399[*1], 0.441[*2], 0.398[*3]
Reynolds number	1.0×10^6

[*1] : MONO, [*2]: CAT1, [*3]: TRI C1-1

Table 5: Parameters of incident wave.

Wave length [m]	50, 100, 150, 75[*], 125[*]
Amplitude of incident wave, ζ_a [L]	1.0×10^{-2}
Direction of incident wave, χ [deg.]	180, 150, 90, 30, 0

[*]: Only for χ= 180 and 150 degree.

Results and discussion

The computed time history and time-sequential drawing of ship motion of MONO is shown in Figure 13. It is noted that the stable cyclic condition is obtained. Since the wave direction is 150°, the roll amplitude is relatively small, about 0.25°, and mean heel angle, about -0.75°, is observed. In the same way, the results of CAT and TRI are shown in Figures 14 and 15. The ship motion and large deformation of free surface can be simulated by the WISDAM-XI code. Non liner free surface around the bulbous bow is realized as shown in Figure 13 (II) and the bow bottom sometimes appears in the air as depicted in Figure 15 (III).

Comparison of heave, roll, pitch amplitude and vertical acceleration are made between three types of ship in Figures 16-a to 16-d.

In the head or oblique head wave conditions, heave, pitch amplitude and vertical acceleration of CAT are significantly larger than those of MONO and TRI, especially when the wave length is long. The vertical acceleration of CAT exceeds 0.2 G, while that of TRI is less than half of CAT.

In the follow or oblique follow wave conditions, obvious difference between the characteristics of three vessels is not well observed due to the limited time of computation.

In beam wave conditions, roll amplitude of CAT is large in short incident wave length condition and TRI is large in long wave length. This tendency is similar to the roll simulation without advance speed which is depicted in Figure 12.

The seakeeping performance of the mono hull, the catamaran and the trimaran vessel are predicted by WISDAM-XI, and it may safe to say that the motion and acceleration characteristics of trimaran hull have some advantages over other two hulls.

V. CONCLUSIONS

The newly developed-versions of the WISDAM code is described with a lot of computed results of practical application. The method has been proved to be useful for the prediction of hydrodynamic performance of high-speed multi-hull vessels.

REFERENCE

Renilson,M., Scrace, R., Johnson, M. and Richardsen, C., "Trials to measure the Hydrodynamic performance of RV Triton," Proc. Int. Conf. Design & Operation of Trimaran Ships, 2004, pp.5-18.

Sato, Y., Miyata, H. and Sato, T., "CFD Simulation of 3-dimensional motion of a ship in waves: application to an advancing ship in regular heading waves," J. Marine Science and Tech., Vol. 4, No. 3, 1999, pp. 108-116.

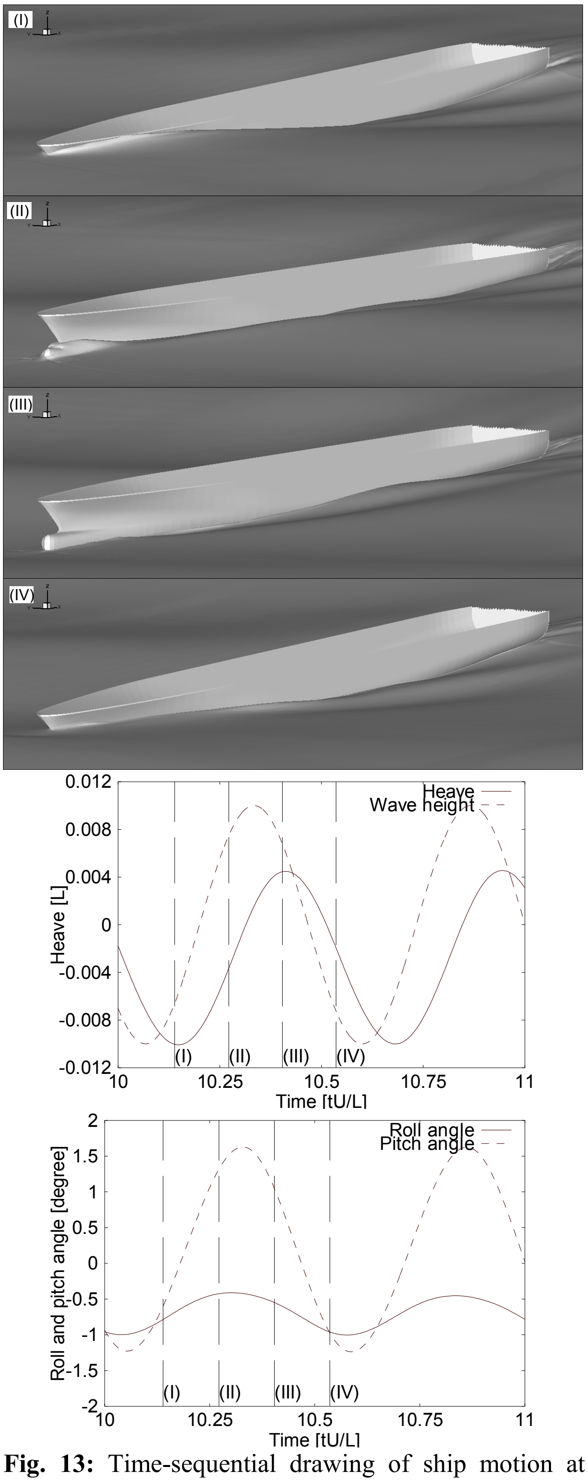

Fig. 13: Time-sequential drawing of ship motion at every 1/4 encounter period (top), time history of incident wave height at center of gravity, heave motion (middle), roll and pitch angle (bottom).
(Ship: MONO, Fn=0.40, χ=150°, λ/L=0.98, ζ_A/L =0.01)

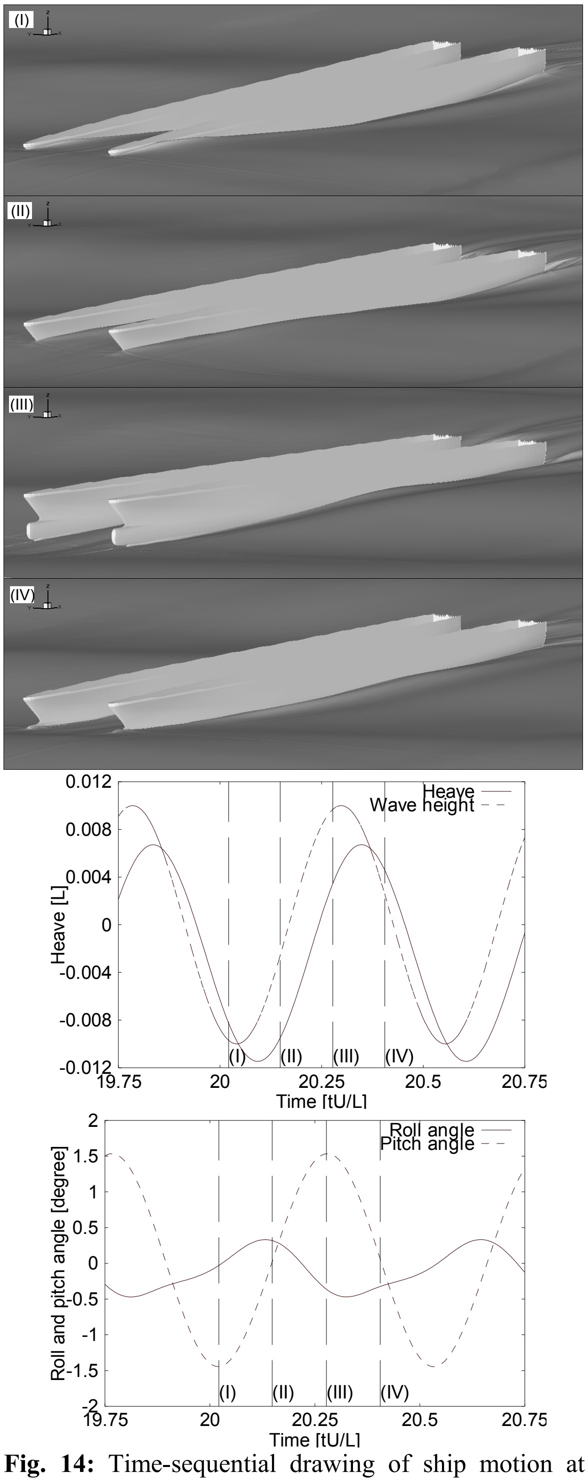

Fig. 14: Time-sequential drawing of ship motion at every 1/4 encounter period (top), time history of incident wave height at center of gravity, heave motion (middle), roll and pitch angle (bottom).
(Ship: CAT, Fn=0.44, χ=150°., λ/L=0.88, ζ_A/L =0.01)

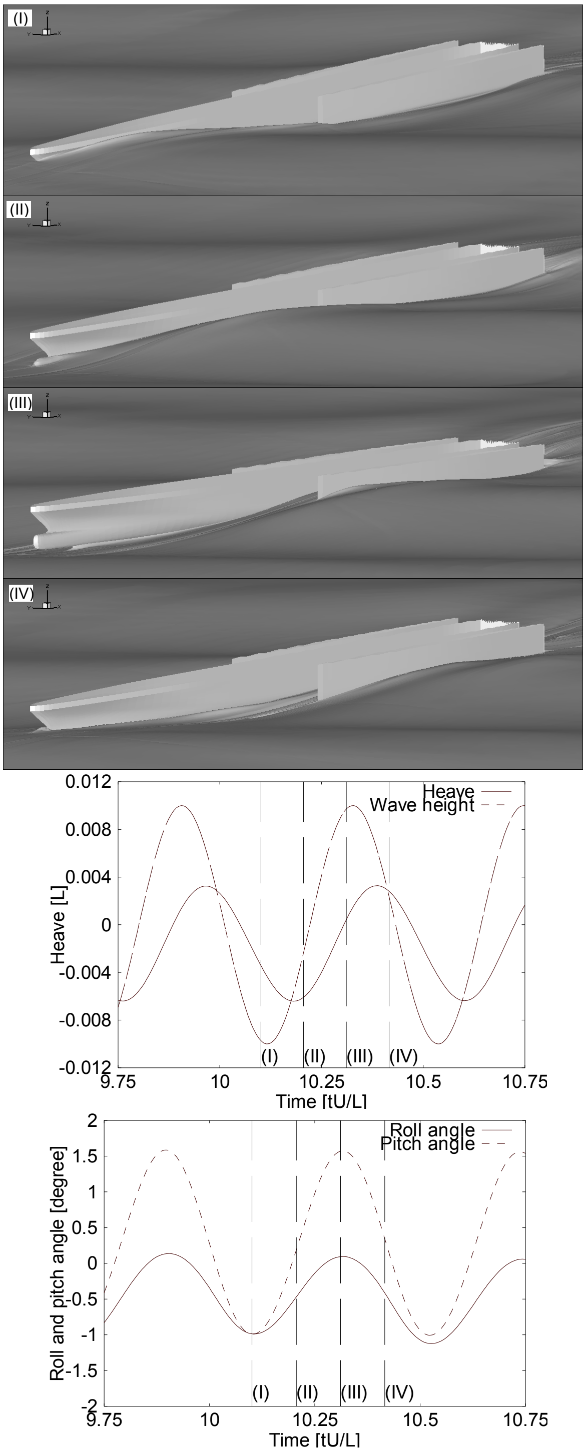

Fig. 15: Time-sequential drawing of ship motion at every 1/4 encounter period (top), time history of incident wave height at center of gravity, heave motion (middle), roll and pitch angle (bottom).
(Ship: TRI, Fn=0.40, χ=150°, λ/L=0.72, ζ_A/L =0.01)

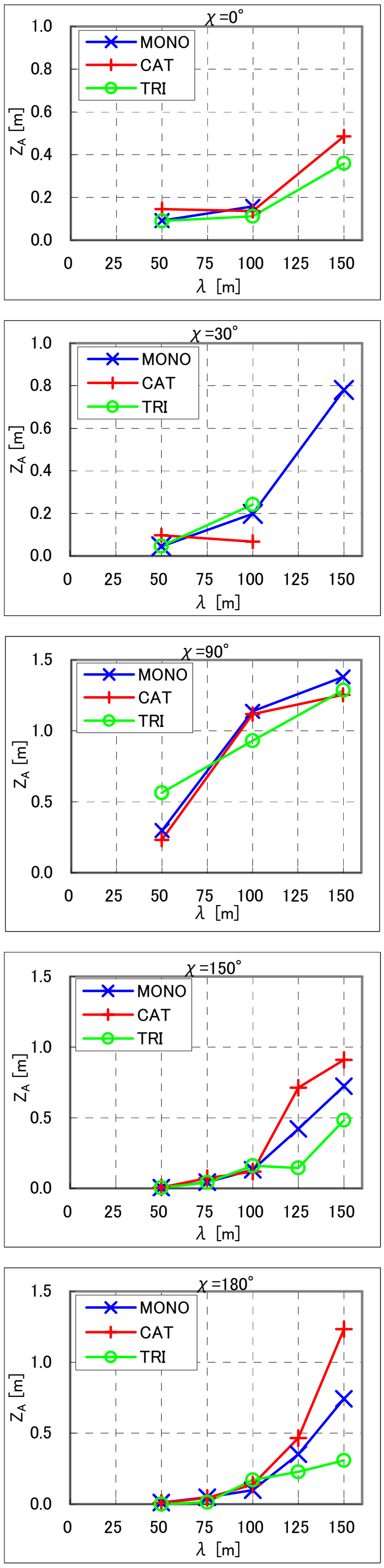

Fig. 16-a: Comparison of heave motion amplitude. (ζ_A=1.5m)

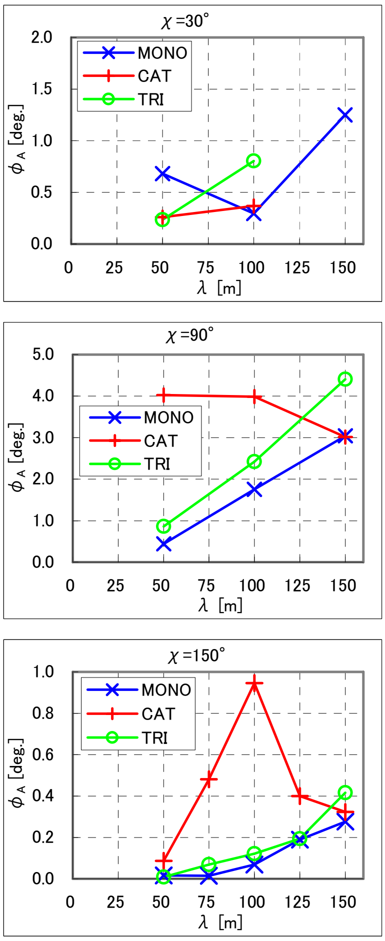

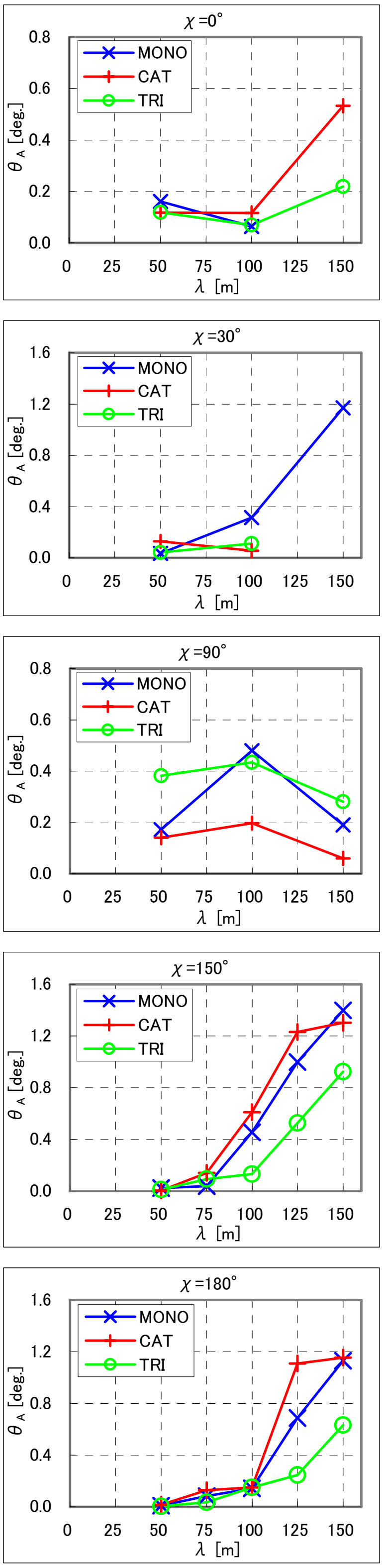

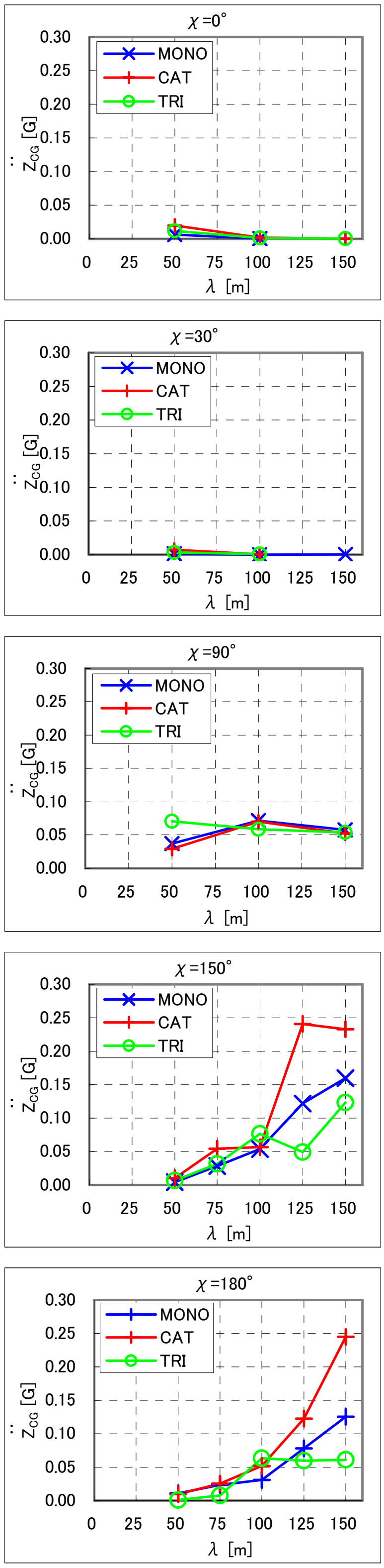

Fig. 16-b: Comparison of roll motion amplitude. (ζ_A=1.5m)

Fig. 16-c: Comparison of pitch motion amplitude. (ζ_A=1.5m)

Fig. 16-d: Comparison of vertical acceleration amplitude at center of gravity. (ζ_A=1.5m)

Int. Workshop on Analyses of Strongly Nonlinear Flows around Moving Boundaries,
Kasuga, JAPAN, 7-8 Dec., 2006.

CFD simulation of Diffraction Flow Fields about a Blunt Ship in Oblique Waves

H. Orihara

Technical Research Center, Universal Shipbuilding Corporation
1-3 Kumozukokan-cho, Tsu-city, Mie 514-1113, JAPAN
Email : orihara-hideo@u-zosen.co.jp

Summary

CFD simulations have been carried out of flows about a blunt ship advancing in regular oblique waves. Unsteady RANS code called WISDAM-X is employed. The characteristics of diffraction waves in the vicinity of an advancing ship are studied numerically. The computed results show that the features of diffracted waves vary significantly with the wave-incident angle and that the hull surface pressures due to the wave diffraction increases in the case of head waves. The effect of diffraction of incident waves on added resistance is also discussed.

Introduction

In recent years, there have been growing interests in ship performance in a seaway and development hull forms with fine performance in actual sea environment as well as in smooth water in an attempt to reduce the environmental load and running cost of ship in operation.

In order to achieve this goal, it is of crucial importance to reduce the added resistance in waves, which is the component of fluid resistance acting on a ship due to the interaction with encountered waves, since the waves have predominant effect among the elements of actual sea environment, e.g. wind, waves, current. For large ocean-going ships, such as tankers and bulk carriers (which is usually longer than 200m), particular attention has been given to the reduction of added resistance in shooter wave range, that is, in the cases where the wave length (λ) to ship length (L) ratio (λ/L) is smaller than unity, since most of the waves encountered in a seaway are in these range for the larger ships. In shorter waves, it is well known that the diffraction of incident waves about an advancing ship is mainly responsible for the occurrence of added resistance and that the added resistance increases considerably in oblique waves.

Despite the importance of added resistance characteristics in oblique waves, the details of the characteristics of the diffraction waves and the mechanism of occurrence of added resistance have not yet been fully elucidated. This may be principally due to the difficulty of detailed measurements of unsteady flow fields around moving ships in waves, and very limited data of the diffraction flow fields are available as yet. Consequently, further detailed understanding of flow physics has been requested for the progress of diffraction wave mechanics and its application to practical purposes.

The purpose of this paper is to study the mechanism of diffraction waves about an advancing ship in deep water by means of CFD simulations. CFD simulation methods have an advantage that it can directly simulate nonlinear flow fields without any simplification of mathematical formulation and can offer local unsteady flow structures, i.e. wave height, pressure and velocity distributions. As a representative of actual ocean going ship, SR221C tanker model is used. CFD simulations are performed in short waves range for a range of wave directions. Following the brief description of CFD simulation method, simulation results are presented and discussed in the following section. Concluding remarks are given at the end of the paper.

CFD Simulation Method

In the present study, WISDAM-X code is employed for flow simulations. The code, developed by Orihara and Miyata[1)] for simulating flows about a freely moving ship with advancing speed, is based on the solution of incompressible Reynolds-Averaged Navier-Stokes equations in the framework of overlapping (or overset) grid system. The accuracy of the WISDAM-X method has been examined by the comparison with the experimental results for a practical hull forms (see Orihara and Miyata[1], Sato et al[2]). It has shown that the degree of agreement with the experiments is quite satisfactory with respect to motion amplitudes and added resistance in regular waves. The effectiveness of the WISDAM-X method as a design tool has also examined by applying the method to the problem of reducing the added resistance of a medium-speed tanker in regular heading waves (see Orihara and Miyata[1]). Since the details of the computational procedure of the WISDAM-X method are explained in Orihara and Miyata[2], they are described here only briefly in this paper.

In the WISDAM-X code, RANS equation and the continuity equation are solved in the overlapping grid system as shown in Fig. 1 using finite-volume descretization. The free-surface treatment is based on the density-function method[3), 4)] (DFM), which is a kind of front capturing method and treats the time-historical evolution of the free surface by solving the transport equation of the scalar variable called density function. The motion of a ship is simultaneously solved by combining the equation of motion of the ship body with the flow computation. Employing these simple formulations with the coupling of flow solution and ship motion, the large amplitude ship motion can be treated in the straightforward manner. The incident waves are realized by specifying wave orbital velocity components and waves height at the inflow and side boundaries, as schematically shown in Fig. 2.

Results and Discussion

The calculations are conducted on the overlapping grid system consisting of the inner and outer grids. The numbers of grid points allocated for the grids is 133×30×179 and 141×81×101 for the inner and the outer grids, respectively. To prevent the occurrence of unrealistic wave reflection at the boundaries of the computational grid, the locations of the down-stream and side boundaries of the outer grid are located at distances of 2L and 3L from the center of the hull, respectively.

The calculations are conducted in regular waves over a range of wave direction from 180^o(head) to 90^o(beam) with an interval of 30^o at Fn=0.15 and Re=1.0×10^6. The length and amplitude of incident waves are kept constant for all the cases at $\zeta_A/L=0.01$ throughout the present study. The ship motion is realized in four-degree-of-freedom, i.e. heave, pitch, roll and surge modes. The flow is accelerated to a steady advancing condition during the computational time T=0.0 to T=4.0, where T is made dimensionless with respect to (L/U_0). The wave computation starts at T=8.0 and continued until T=20.0.

Three sets of time evolutions of computed wave-height contour maps are shown in Fig. 3 for the cases of wave angles (χ) of 120^o, 150^o, 180^o, $\lambda/L=0.5$. Wave height contours are shown at an interval of 1/4 of the encounter period ($\boldsymbol{T_e}$). The time-sequential variation of the diffraction wave formation is very remarkable in one cycle of wave encounter. From these figures, it is seen that diffraction of incident waves become significant as the wave angle is changed from head to beam condition. The diffraction processes can be clearly seen in the case of $\chi=120^o$. In the weather-side of the hull, the wave reflection on the hull is intensified with the decrease of direction of the incident waves and very steep waves which has the maximum height greater than two times of that of the incident waves are generated around the bow and propagated towards the stern-quartering direction. It is also noted that the elevated wave formation and the depressed wave formation in the vicinity of the bow show very similar configuration each other. For the case of $\chi=120^o$, the contour maps at 1/16Te and 5/16Te resemble well with those at 9/16Te and 13/16Te, if the sign of wave elevation is reversed. This implies that the location of the maximum slope, positive or negative, does not change in wave encounter cycles. This feature of wave formation is very similar to the principal characteristics of unsteady FSSWs discovered by Miyata[5] for the case of a series of wedge models advancing in regular head waves, and exemplifies the occurrence of unsteady FSSWs in oblique wave conditions.

Three sets of time-evolutions of hull-surface pressure distributions on the weather- and leeward -side of the hull are shown in Fig. 4 for the cases of $\chi=120^o$ and 180^o. Instantaneous pressure distributions are shown at an interval of 1/4 of the encounter period ($\boldsymbol{T_e}$) at the same instants as shown in Fig. 3. The time-sequential variations of the hull surface pressures are very remarkable in one cycle of wave encounter. From these figures, it can be clearly seen that quite large values of pressure are generated on the weather-side bow flare part of the model in oblique wave conditions. The generation of such large pressures has very close relationship with the diffraction wave process as shown in the case of χ =120° at Te = 9/16. It is also shown in Fig. 4 is that the variation of lee-side surface pressures in the case of 120° is attenuated remarkably compared to that in the case of 180°. This may be due to the shielding effect of ship hull and consistent with the occurrence of large wave drift forces in short oblique waves.

The computed time-evolution of velocity vector field is shown in Fig. 5 for χ =120° at an interval of 1/4 of T_e in the same manner as Fig. 3. The velocity vectors on the transverse plane normal to the ship's longitudinal axis at x/L = 0.45 (approximately 0.05L aft of the bow) are drawn in the figure. It is noted that the noticeable secondary flows are generated at 9/16 in the vicinity of the hull with a very steep wave profile, which is similar to spilling breaker in appearance.

Added pressure distributions on the hull are shown in Fig. 6 for the case of λ/L = 0.5 in wave directions of 120°, 150°, 180°, where time-averaged pressures excluding the steady component is drawn. Since the integration of these pressures yields the added resistance in waves, it is equivalent to the distribution of the added resistance on the hull. In Fig. 6, it appears that the added pressures confined to the relatively narrow areas near the wave profiles on the hull and increased significantly in the weather side of the hull with the decrease of the wave direction (χ). Thus, it can be considered that the occurrence of the added resistance in oblique wave is mainly due to reflection of incident waves above the still water level in the similar way as the case of head waves and that the added pressures acting on the weather-side of the hull are mainly responsible for the increase in the added resistance in oblique waves.

Concluding Remarks

CFD simulation has been conducted of flows about a blunt ship advancing in regular oblique waves using unsteady RANS-code WISDAM-X. The detailed characteristics of diffraction waves in the vicinity of an advancing ship are studied based on the computed flow structures including surface wave-height contours, hull-surface pressures and velocity distributions. The computed results show that the structures of diffracted waves system vary significantly with the wave-incident angle and that the hull surface pressures due to the wave diffraction increases in the case of head waves. It is shown that the variation in the formation of diffraction wave system causes a significant increase in the added pressures on the weather side of the hull and results in the increased added resistance in short oblique waves.

Reference

1) Orihara, H., Miyata, H. :" Evaluation of added resistance in regular incident waves by computational fluid dynamics motion simulation using an overlapping grid system ", Journal of Marine Science and Technology, Vol. 8, No. 2, pp. 47-60, 2003.
2) Sato, Y., Orihara, H., Miyata, H. :" Practical application of two CFD codes for ship motions in arbitrary waves ", Proc. Symp. Naval Hydrodynamics, Rome, Italy, 2003.
3) Miyata, H., Katsumata, M., Lee, Y.G. and Kajitani, H., "A Finite-Difference Simulation Method for Strongly Interacting Two-Phase Flow," Journal of The Society of Naval Architects of Japan, Vol. 163, pp. 1-16., 1988.
4) Miyata, H., Kanai, A., Kawamura, T. and Park, J-C. :" Numerical simulation of three-dimensional breaking waves ", Journal of Marine Science and Technology, Vol. 1, No. 4, pp. 183-197, 1996.
5) Miyata, H., Kanai, M., Yoshiyasu, N., Furuno, Y. :" Diffraction waves about an advancing wedge model in deep water ", Journal of Ship Research, Vol. 34, No. 2, pp. 105-122, 1990.

Int. Workshop on Analyses of Strongly Nonlinear Flows around Moving Boundaries,
Kasuga, JAPAN, 7-8 Dec., 2006.

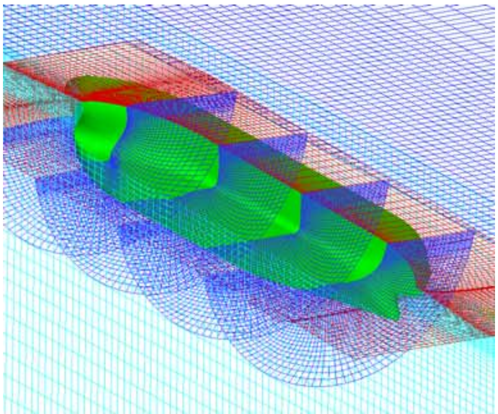

Fig. 1 Close-up view of overlapping computational grid system for SR221C tanker model .

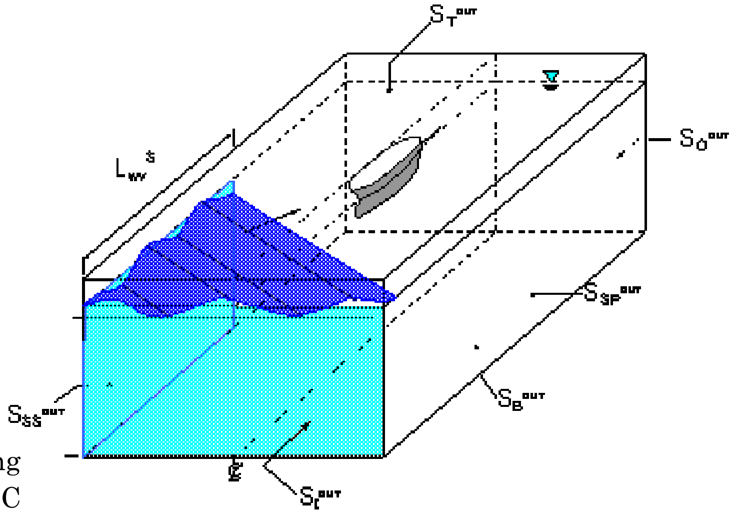

Fig. 2 Schematic sketch of treatment of incident waves for oblique waves.

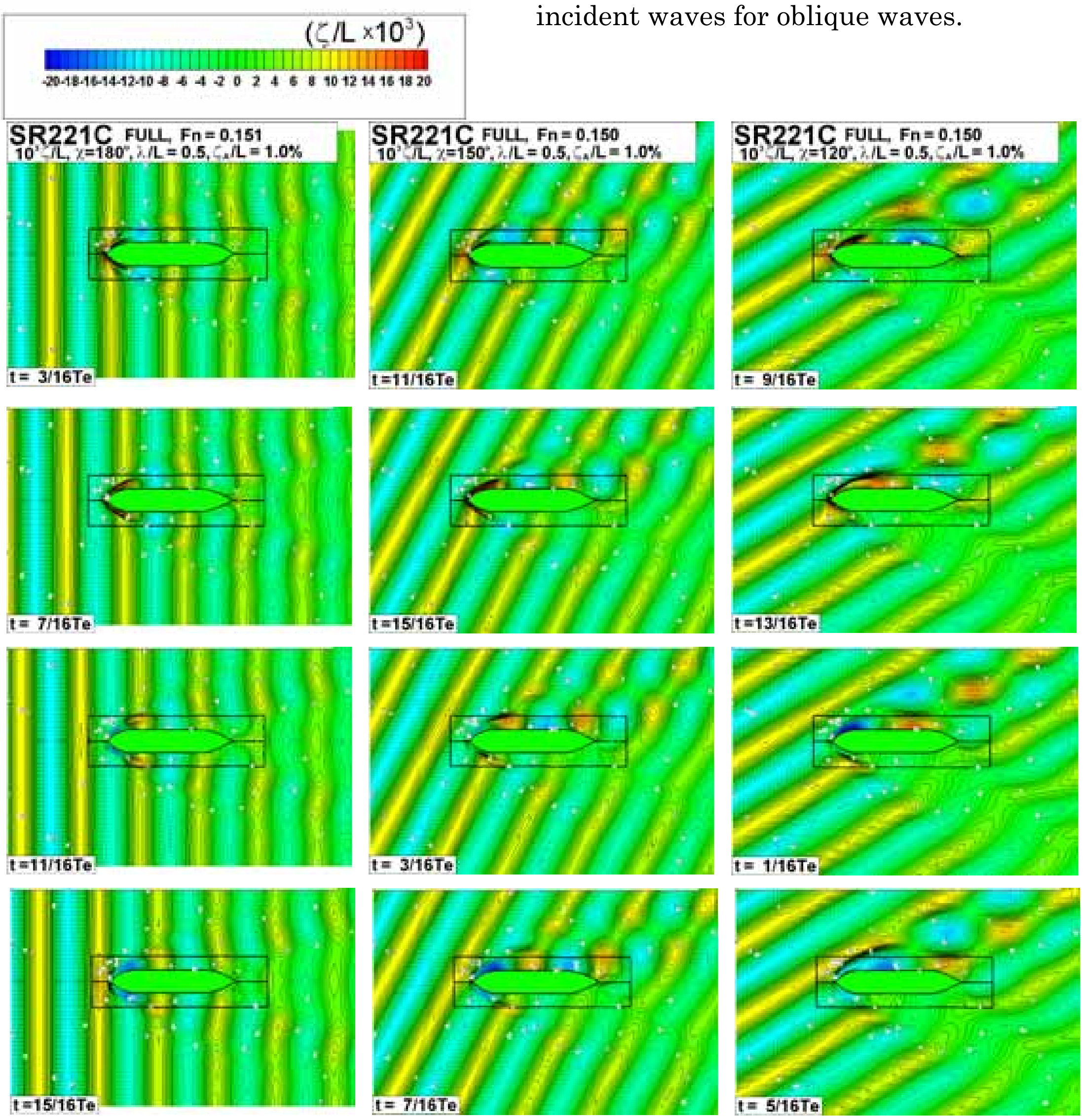

Fig. 3： Time-evolutions of computed wave-height contour maps about a SR221C tanker at Fn=0.150 in waves of λ/L=0.5, χ=120, 150, 180 deg. and ζ_A/L=0.01. The interval of the contours is 0.001L, contours of positive value are drawn in solid lines and those of negative value are drawn in dotted lines.

Int. Workshop on Analyses of Strongly Nonlinear Flows around Moving Boundaries,
Kasuga, JAPAN, 7-8 Dec., 2006.

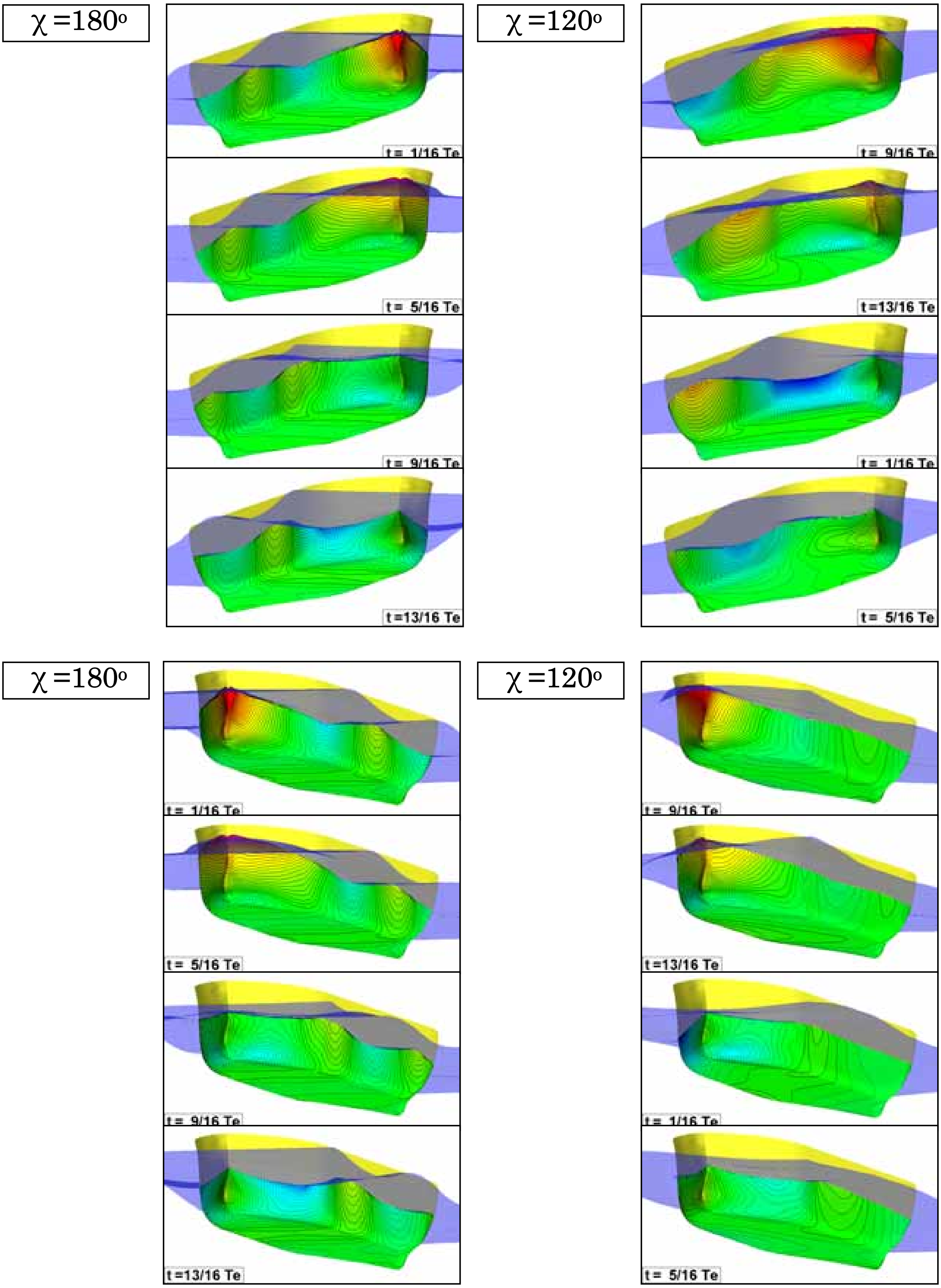

Fig. 4 : Comparison of time-evolutions of computed hull-surface pressures on a SR221C tanker running at Fn=0.15 in waves of λ/L=0.5, χ=120, 180 deg. and ζ_A/L=0.01. The interval of the contours is 0.001 ρU^2, contours of positive value are drawn in solid lines and those of negative value are drawn in dotted lines.

Int. Workshop on Analyses of Strongly Nonlinear Flows around Moving Boundaries,
Kasuga, JAPAN, 7-8 Dec., 2006.

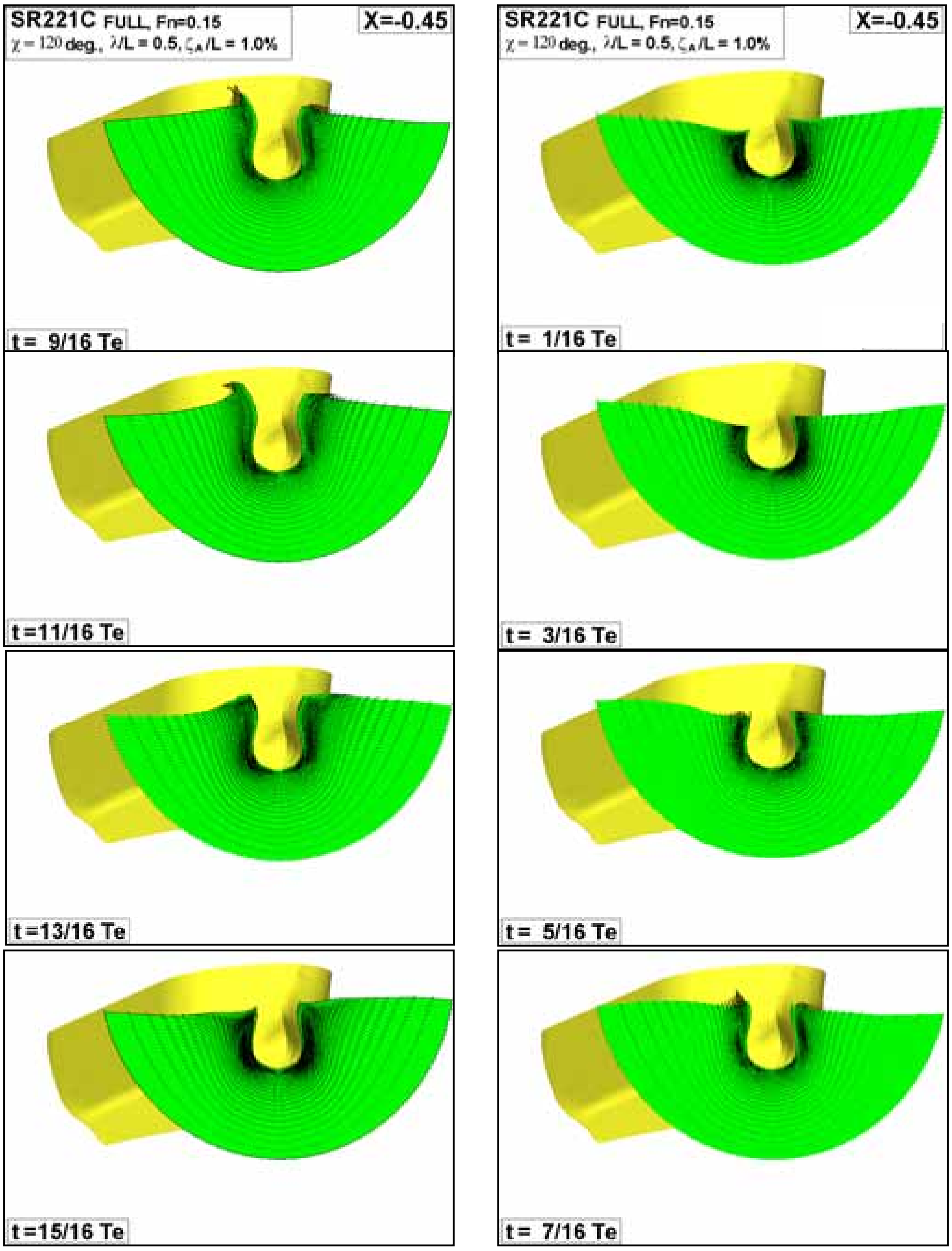

Fig. 5 : Time-evolutions of velocity vectors on a transverse plane at x/L=-0.45 around a SR221C tanker running at Fn=0.15 in waves of $\lambda/L=0.5$, $\chi=120$ deg. and $\zeta_A/L=0.01$.

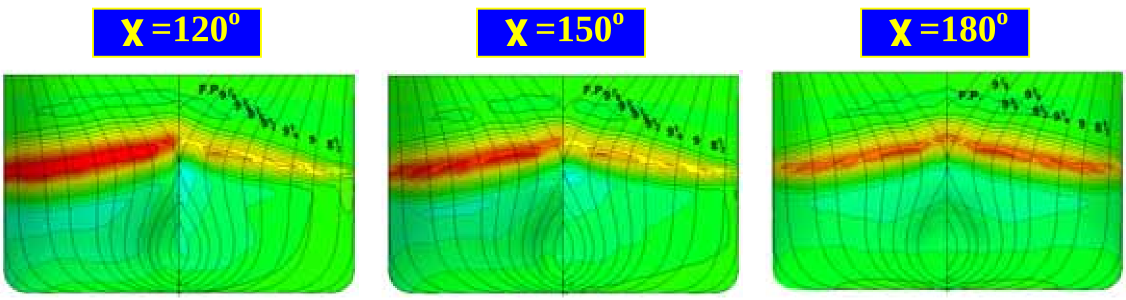

Fig. 6 : Comparison of computed time-averaged hull-surface added pressure distributions on a SR221C tanker running at Fn=0.15 in waves of $\lambda/L=0.5$, $\chi=120$, 150, 180 deg. and $\zeta_A/L=0.01$.

応用力学研究所研究集会報告　18 特 1－1

移動境界まわりの強非線形流れ解析

日時：2006 年 12 月 7 日～8 日
場所：応用力学研究所 6 階 W601 号室

発行　九州大学応用力学研究所
研究代表者　青木 尊之
所内担当　力学専門部会・柏木　正